THE
PHYSICAL REVIEW

A journal of experimental and theoretical physics established by E. L. Nichols in 1893

SECOND SERIES, VOL. 73, No. 4 FEBRUARY 15, 1948

Range of Ra$-\alpha-$Be Neutrons in Water*

J. H. RUSH
Department of Physics, Duke University, Durham, North Carolina
(Received October 10, 1947)

Radial distributions of Ra$-\alpha-$Be neutrons about an approximate point source in water were determined by means of indium foil activations. Values for migration area (M^2) derived from the data are: For all activating neutrons, 54.7 cm^2; for indium resonance neutrons, 45.4 cm^2.

STANDARDIZATION of a set of indium foils involved mapping the distribution of both total and indium-resonance activations about an approximate point source of neutrons in water. The same data can be used to evaluate the mean-square distance $\langle r^2\rangle$ and the migration area ($M^2=\langle r^2\rangle/6$) in water.

The saturated activity (A_s) of a foil irradiated at radius (r) from a point source of neutrons is a function $f(r)$ of the radius and can be determined experimentally. The total neutron flux at energies which activate the foil is proportional to the space integral $\langle A_s\rangle$ of the saturated activity:

$$\langle A_s\rangle=4\pi\int_0^\infty A_s r^2 dr.$$

The mean square $\langle r^2\rangle$ of the migration distance of a neutron, i.e., the distance from the source to the point at which the neutron is captured, is then:

$$\langle r^2\rangle=6M^2=\frac{\int_0^\infty A_s r^4 dr}{\int_0^\infty A_s r^2 dr}.$$

EXPERIMENTAL DETAILS

Supports for source and foil holder were set up on a 4 ft.×4 ft. cylindrical galvanized steel tank (Fig. 1). The aluminum source cup was suspended from three supports on the angle iron rim of the tank by 0.016 inch steel piano wire; each wire was fixed in a bead which rested in a conical socket clamped to the tank rim. One of the wires was attached to a cord fastened to the tank rim, so that the time of beginning or ending an irradiation could be controlled within one second by slipping the support wire in or out through a slot in the socket, causing the source to swing into or away from the central position. A lead counterweight of about 1 lb, suspended 30 cm below the source on a $\frac{1}{8}$-inch aluminum rod, held the system taut.

Each foil holder was carried on the end of a $\frac{3}{16}$-inch aluminum tube held radial to the source

* This report is based on work performed in 1945, under Contract No. W-7405-eng-39 for the Manhattan Project, and the information covered therein will appear in Division IV of the Manhattan Project Technical Series as part of the contribution of the Clinton Laboratories.

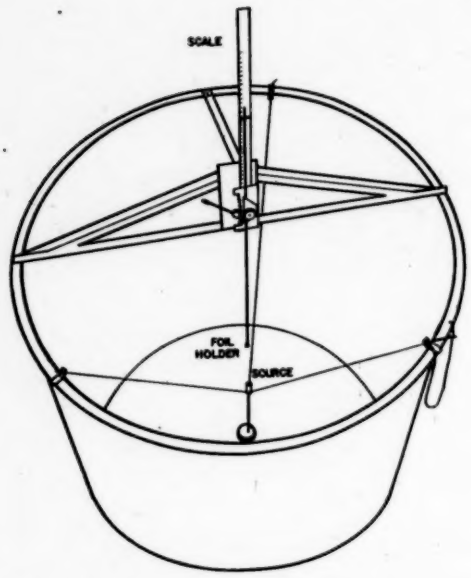

FIG. 1. Apparatus used in determining range of Ra$-\alpha-$Be neutrons in water.

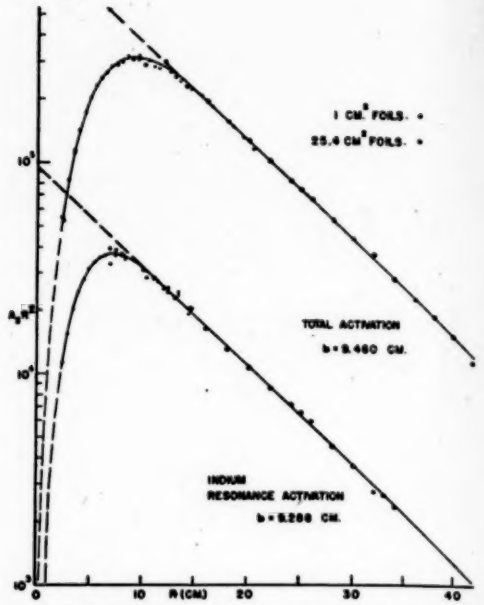

FIG. 2. Spherical space distribution ($A_s r^2$) of neutron flux from 0.5 g Ra$-\alpha-$Be source in water, using indium detectors.

in a movable clamp mounted on a rigid truss of 1-inch angle iron bolted to the rim of the tank; by this means the support for both foil and source was made a rigid structural unit. The aluminum tube could be quickly clamped at the approximate position desired, as indicated by a flag moving on a meter stick fixed to the support; and the clamp itself was mounted on a ratchet having about 2-cm vertical travel. By means of this mechanism, settings of (r) were easily reproducible to about 0.02 cm.

The various foil holders will be described in turn. The source was 0.5 g of radium with 3 g of beryllium in the form of a $\frac{9}{16}$-inch$\times\frac{9}{16}$-inch cylinder inside a brass cylinder $\frac{7}{8}$-inch long$\times\frac{11}{16}$-inch o.d. (Clinton Labs. source No. 3). Earlier calibration of this source had indicated a strength of 5.17×10^6 neutrons/sec.

Measurements were made with a set of about 500 indium foils, approximately 1 cm$\times$1 cm$\times$0.005 inch. No individual calibrations were used, as few foils deviated from the mean by more than 2 percent. A different, randomly selected foil was used for each irradiation, and the resulting data smoothed graphically.

The effective distance of the "point source" from the zero on the meter stick was determined by taping 10 foils at 3-cm intervals to a $\frac{3}{16}$-inch aluminum tube which was offset so as to pass vertically about 5 cm to one side of the source, and irradiating such a set at each of three successive positions 1 cm apart vertically. The axis of symmetry of the resulting activity curve, 80 cm below the top of the tank, was taken as the level of the source ($r=0$).

The holder used for small foils consisted of a stirrup-shaped strip of 0.005-inch aluminum weighing 0.19 g fixed to the end of a $\frac{3}{16}$-inch aluminum tube with Plicene cement; a projection from the base of the stirrup was folded back on itself to form a 1-cm² envelope to receive the foil, holding it normal to the radius from the source and about 3 cm beyond the end of the tube. Overlapping covers of cadmium were made to slip over the loaded holder, encasing the foil in a 0.04-inch shield without disturbing its position.

Activations of the small foils beyond 15- to 20-cm radius were too low for reliable counting. Rather than increase the source strength, it was decided to extend the range of the measurements with larger foils (4$\times$6.35 cm) of the same thickness as the small ones; and to normalize the two portions of the curve empirically by taking overlapping data. One holder consisted of two plates of $\frac{1}{16}$-inch Lucite between which the foil was placed, the other of two plates of 0.015-inch

cadmium, the upper plate in each case being cemented to the end of the supporting aluminum tube. The error caused by the variable value of (r) over a large flat foil was compensated by calculating a corrected radius (r') to the center of the foil such that half the area of the foil should be located at a lesser radius than the desired value (r). A setting corresponding to (r') was then made on the apparatus, and the value (r) recorded for that irradiation. A set of 8 calibrated large foils was used.

Two corrections to the small-foil data were made. By attaching to the holder first one and then two strips of aluminum duplicating the holder in both shape and weight, together with duplicate sections of tubing adjacent to the holder, it was found that an augmentation of about 1 percent in activity resulted from each addition. Data taken with the aluminum holder should, therefore, be corrected by a factor of 0.99 to give the "free foil" value. Addition of one and then two duplicate coverings of cadmium to the large cadmium holder (the small holder not being used here because of mechanical difficulties) indicated a decrease of about 4 percent for each 0.015-inch layer. The corresponding decrement for the small-foil holder of 0.04-inch cadmium is thus 0.11; and the resulting correction to the observed cadmium ratio is $(0.99 \times 0.89 = 0.88)$. The graph (Fig. 2) is based on corrected values.

RESULTS

Figure 2 is a plot of $(A_s r^2)$ in arbitrary units against (r). The cadmium ratio C.R. (A_s total/A_s in Cd) rises sharply until, around 14-cm radius, it becomes a slowly-increasing exponential. Representative values are:

r_{cm}:	2	5	8	12	16	24	34
C.R.;	4.7	6.4	8.1	10.8	11.4	11.6	11.9

Relaxation lengths (b) derived from the curves, Fig. 2, (defined by: $A_b = A_0/e$) are:

Curve I (uncovered foils): $b = 9.46$ cm.
Curve II (Cd-covered foils): $b = 9.29$ cm.

The space integrals of $(A_s r^2 dr)$ and $(A_s r^4 dr)$ were evaluated by formal integration over the exponential region of $(A_s r^2)$, assuming exponential decrease without limit, and by Simpson's rule over the remainder. Results are:

$$\langle r_T^2 \rangle = \frac{4\pi \int_0^\infty A_T r^4 dr}{4\pi \int_0^\infty A_T r^2 dr} = \frac{2.107 \times 10^{10}}{6.42 \times 10^7} = 328 \text{ cm}^2$$

$$\langle r_{In}^2 \rangle = 1.853 \times 10^9 / 6.811 \times 10^6 = 272 \text{ cm}^2,$$

where $\langle r_T^2 \rangle$ and $\langle r_{In} \rangle$ are the "second moments" indicated by total and by indium resonance activation, respectively. The corresponding migration areas are:

$$M_T^2 = r_T^2/6 = 54.7 \text{ cm}^2$$
$$M_{In}^2 = \tau_{In} = 45.4 \text{ cm}^2,$$

where (τ_{In}) is the "age" of indium resonance neutrons in water.

If the previously reported value for diffusion length (L) in water of 2.88 cm[1] and the above value for (M_T^2) are inserted in the equation $M^2 = L^2 + \tau_{thermal}$ the result is $\tau_{th} = 46.4$ cm^2 and $\tau_{th} - \tau_{In} = 1.0$ cm^2.

This result is comparable to the value 0.6 cm^2 previously reported.[2]

Comparable determinations of $\langle r^2 \rangle$ reported by Auger, Munn, and Pontecorvo[3] are:

$\langle r_{In}^2 \rangle = 278$ cm^2
$\langle r_T^2 \rangle$ (Dy detectors) $= 330$ cm^2.

A memorandum from Anderson[4] gives $\langle r_{In}^2 \rangle = 288$ cm^2.

I should like to acknowledge particularly the assistance of A. Weinberg and H. Jones, in connection with the theoretical background and some details of the experiment.

[1] S. Allison *et al.*, Project Report C-82.
[2] Project Handbook IV E 8.
[3] P. Auger, A. M. Munn, and B. Pontecorvo, Can. J. Research **A25**, 143–56 (1947).
[4] H. L. Anderson, Report N-1708.

Neutron and Gamma-Ray Yields from Deuterons on Carbon

CARL L. BAILEY,* GEORGE FREIER, AND JOHN H. WILLIAMS
Department of Physics, University of Minnesota, Minneapolis, Minnesota
(Received November 3, 1947)

Observations on the yield of neutrons and gamma-rays from carbon bombarded with deuterons of discrete energies between 0.85 and 3.25 Mev are reported. The yield of neutrons per unit solid angle at 0° and 90° is given in absolute terms. Resonances for the formation of the compound nucleus N^{14} exhibit features such as: varied widths of resonances, shifts in energy between gamma-ray and neutron resonances, exclusion of neutron resonances by gamma-ray resonances and *vice versa*, and the strong forward asymmetry of the neutron yield.

1. INTRODUCTION

INVESTIGATIONS of the yields of neutrons from the reaction

$$D^2+C^{12}\rightarrow(N^{14})\rightarrow N^{13}+n^1, \qquad (1)$$

and gamma-rays from the competing reaction

$$D^2+C^{12}\rightarrow(N^{14})\rightarrow C^{13*}+H^1 \qquad (2)$$
$$C^{13*}\rightarrow C^{13}+h\nu$$

have been made by the Rice Institute group[1–4] and at the University of Minnesota.[5]

These early researches established the nature of these reactions and showed a number of resonances for the production of neutrons and gamma-rays. The present paper reports an extension of these studies to higher deuteron energies and an investigation of the angular dependence of the yield of neutrons from reaction (1). In reference 1, the neutron yield in the forward direction was measured as a function of deuteron energy up to 2 Mev, whereas in reference 5 essentially the total yield, averaged over all angles, was observed up to 2.75 Mev. The partial disagreement between these two results suggested that the neutron reaction is asymmetric; therefore, it was decided to investigate the yield of neutrons in two directions, namely, 0° and 90°, in the laboratory system of coordinates.

2. APPARATUS

Deuterons whose energy was controlled to the order of 0.2 percent were furnished by the Minnesota electrostatic generator. This accelerator has been modified since it was first described[6] and a report of these improvements is forthcoming. The energy of the deuterons was controlled and measured by electrostatic analysis of the diatomic ion beam. The energy scale was normalized by assuming that the threshold of the Li(p,n) reaction is 1.86 Mev.[7,8]

Thin carbon targets were made by slowly depositing soot from a gas flame onto thin tantalum plates. With a little practice it was found possible to produce uniform deposits of any thickness desired up to 60-kev stopping power. In practice, several different targets were used with thicknesses from 20 to 60 kev to cover the range of bombarding energies. To prevent carbon from residual vapors in the accelerating tube being added to the target during ion bombardment, and also to prevent absorption of D_2, we heated these targets electrically throughout the time of the observations. Under these conditions the yield of neutrons could be duplicated from day to day to within an accuracy of a few percent.

As is common to all experiments with deuteron accelerators, a background of neutrons and gamma-rays exists as a result of deuterium absorbed on diaphragms and other surfaces. In order to measure this background, the heated

* Now at Concordia College, Moorhead, Minnesota.
[1] W. E. Bennett and T. W. Bonner, Phys. Rev. **58**, 183 (1940).
[2] T. W. Bonner, E. Hudspeth, and W. E. Bennett, Phys. Rev. **58**, 185 (1940).
[3] W. E. Bennett, T. W. Bonner, E. Hudspeth, H. T. Richards, and B. E. Watt, Phys. Rev. **59**, 781 (1941).
[4] W. E. Bennett and H. T. Richards, Phys. Rev. **71**, 565 (1947).
[5] C. L. Bailey, M. Phillips, and J. H. Williams, Phys. Rev. **62**, 80 (1942).
[6] J. H. Williams, L. H. Rumbaugh, and J. T. Tate, Rev. Sci. Inst. **13**, 202 (1942).
[7] R. O. Haxby, W. E. Shoupp, W. E. Stephens, and W. H. Wells, Phys. Rev. **58**, 1035 (1940).
[8] A. O. Hanson and D. L. Benedict, Phys. Rev. **65**, 33 (1947).

tantalum backing of the carbon target was mounted on a tapered ground joint, so that it could be turned over to present a clean tantalum surface to the deuteron beam. It was found necessary to make many alternate observations of the background count to be subtracted from the total count, since the background effect varied considerably with time and other operating conditions.

The neutrons were detected by means of a "long counter" of the type described by A. O. Hanson and J. L. McKibben.[9] These authors have shown that the sensitivity of this detector is constant to within a few percent for neutrons of energies from 23 kev to 3 Mev. A further advantage of this counter is the side and back shielding, so that only those neutrons which enter its front face are detected.

The gamma-rays were detected by a thick wall Geiger counter encased in a two-inch thick lead shield which had a $\frac{1}{2}$-inch square window cut out on the side facing the carbon target. It seems reasonable to attribute the gamma-rays to reaction (2) where the energy of excitation of the intermediate C^{13} nucleus is 3.15 Mev. Even at deuteron energies of 7 Mev there seems to be[10] only one further excited state of C^{13}, at 3.95 Mev. We can therefore expect the gamma-ray energy to be approximately constant over the range of deuteron energies reported here and consequently the yield as measured by a Geiger counter will be a true representation of the relative gamma-ray yield as a function of deuteron energy.

The geometrical arrangement of the detectors with respect to the carbon target is shown in Fig. 1. The angular definition of the neutron detector is difficult to estimate. The efficiency for detecting a neutron depends on the distance between the central axis of the counter and the point of impact of the neutron on the front paraffin surface of the counter in an unknown way. A rough estimate of this efficiency gives the angular definition as $\pi/16$ steradians for the geometry employed in these experiments. The angular definition of the gamma-ray counter is of little importance since the gamma-rays are

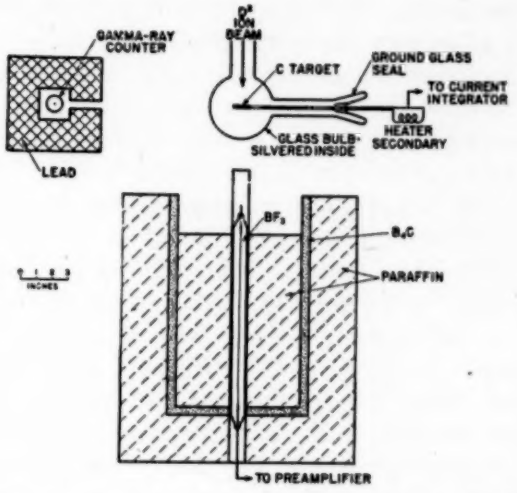

FIG. 1. Geometrical arrangement of gamma-ray detector at 90° and neutron detector at 0°.

expected to be emitted in a spherically symmetrical fashion. This expectation has been checked approximately by observations at 0° and 90°.

The possibility of gamma-rays being generated by absorption of neutrons in the massive paraffin block and then being detected by the Geiger counter was eliminated by removing the paraffin during a test run. Similarily, the contribution of neutrons scattered from the lead into the neutron detector was found to be negligible.

3. PROCEDURE

With the geometry shown in Fig. 1, simultaneous readings of the neutrons detected at 0° with respect to the direction of the deuterons and of the gamma-rays at 90° were made. The number of such counts was recorded for a given total charge of deuterons striking alternately the carbon covered face of the target and the clean surface. Since the time for these observations was on the average the same, the difference between them could be attributed to the yield from the thin carbon alone. Since the neutrons and gamma-rays were observed simultaneously, there was no uncertainty in the relative voltages at which resonance maxima occurred in the respective yields from reactions (1) and (2).

When the geometry of the neutron counter was changed from 0° to 90°, the solid angle subtended at the target was kept constant and,

[9] A. O. Hanson and J. L. McKibben, Phys. Rev. **72**, 673 (1947).
[10] K. M. Guggenheimer, H. Heitler, and C. F. Powell, Proc. Roy. Soc. **A190**, 196 (1947).

consequently, the relative neutron yield at these two laboratory angles was observed directly.

To obtain the absolute value for the efficiency of reaction (1) we measured the neutron flux by counting fissions from a thin layer of normal uranium. This thin target, surface density 0.40 mg/cm², was prepared by spraying uranyl nitrate on a platinum plate and reducing the compound to U_3O_8 by heating. This uranium foil was fastened to the negative high voltage electrode of a simple parallel-plate ionization chamber which was covered with cadmium, 0.020 inch thick. When the chamber was placed in the flux of 0° neutrons, tests showed that the number of background fissions in U^{235} due to the presence of thermal and epethermal neutrons was neglible. For these observations the deuteron energy was 2.8 Mev, so that the neutron energy was 2.5 Mev. In order to calculate a value for the neutron yield from the thin carbon target, we have assumed[11,12] that the fission cross section of U^{238} for 2.5-Mev neutrons is 0.5×10^{-24} cm², 0.5 barn, that the masses of C^{12} and U^{238} on the target and foil could be determined by weighing the tantalum and platinum disks before and after deposition of the soot and U_3O_8, respectively, and that the ion beam contained only D^+ ions with no H_2^+ contamination. This last assumption should introduce a negligbly small error, less than 1 percent, since the ion source was operated with 99 percent pure D_2O for more than 100 hours before these observations were made. The cross section for reaction (1) was thus found to be $1.4\pm0.4\times10^{-26}$ cm² per unit laboratory solid angle in the forward direction at a deuteron energy of 2.8 Mev. The uncertainties in the weights of the uranium foil and carbon target were the principal sources of error in this determination.

The above cross section for the $C^{12}(d,n)N^{13}$ reaction is subject to the assumption that the contribution to the neutron flux from the $C^{13}(d,n)N^{14}$ reaction can be neglected; this contribution is negligible for the present measurement, at least up to 2-Mev deuteron energy.[4]

[11] R. Ladenburg, M. H. Kanner, H. H. Barschall, and C. C. vanVoorhis, Phys. Rev. **56**, 168 (1939).
[12] N. Bohr and J. H. Wheeler, Phys. Rev. **56**, 426 (1939).

4. RESULTS

The observations are shown in Fig. 2. The neutron yield curves are given to an absolute scale determined by the fission method described above. The gamma-ray yield curve is plotted to an arbitrary scale, but the earlier results of Bennett and co-workers[3] indicate that the yield of gamma-rays and neutrons at 0° is about equal for a deuteron energy of 1.6 Mev.

A comparison, with respect to the structure of the resonance peaks, of the 0° neutron curve and the gamma-ray curve with those of the Rice Institute group[1,2] shows good agreement. The present results do not confirm the existence of a resonance for reaction (1) at 1.15 Mev. A comparison with the earlier results obtained in this laboratory[5] is difficult because the early observations measured a yield averaged roughly over all angles. A common feature is the decline in the 90° neutron curve of Fig. 2, and the diminishing yield of neutrons for a bombarding deuteron energy of 2.3 Mev shown in Fig. 1 of reference 5.

5. DISCUSSION

Although a detailed interpretation of these results is not possible at the present time, it seems worth while to emphasize some features which present evidence for the complexity of these nuclear reactions, and may be common to (d,n) and (d,p) reactions in this energy region and range of atomic numbers.

The true widths of the resonances for the formation of the compound nucleus, N^{14}, are probably only slightly less than those shown in Fig. 2 with the exception of the gamma-ray resonance at 1.43 Mev. This particular resonance has been studied in some detail by Bennett and co-workers.[3] For the 11- to 14-Mev range of excitation energy of the compound nucleus, N^{14}, presented here, the widths of the resonance energies vary by at least an order of magnitude from 10 to more than 100 kev.

A more puzzling feature of these observations is disclosed by a study of the relative positions of the 1.80- and 2.96-Mev resonances for 0° neutrons and the 1.75- and 2.90-Mev resonances for gamma-rays. It seems reasonable to attribute the first pair (1.80 Mev and 1.75 Mev), of these resonances to a common excited state of the N^{14}

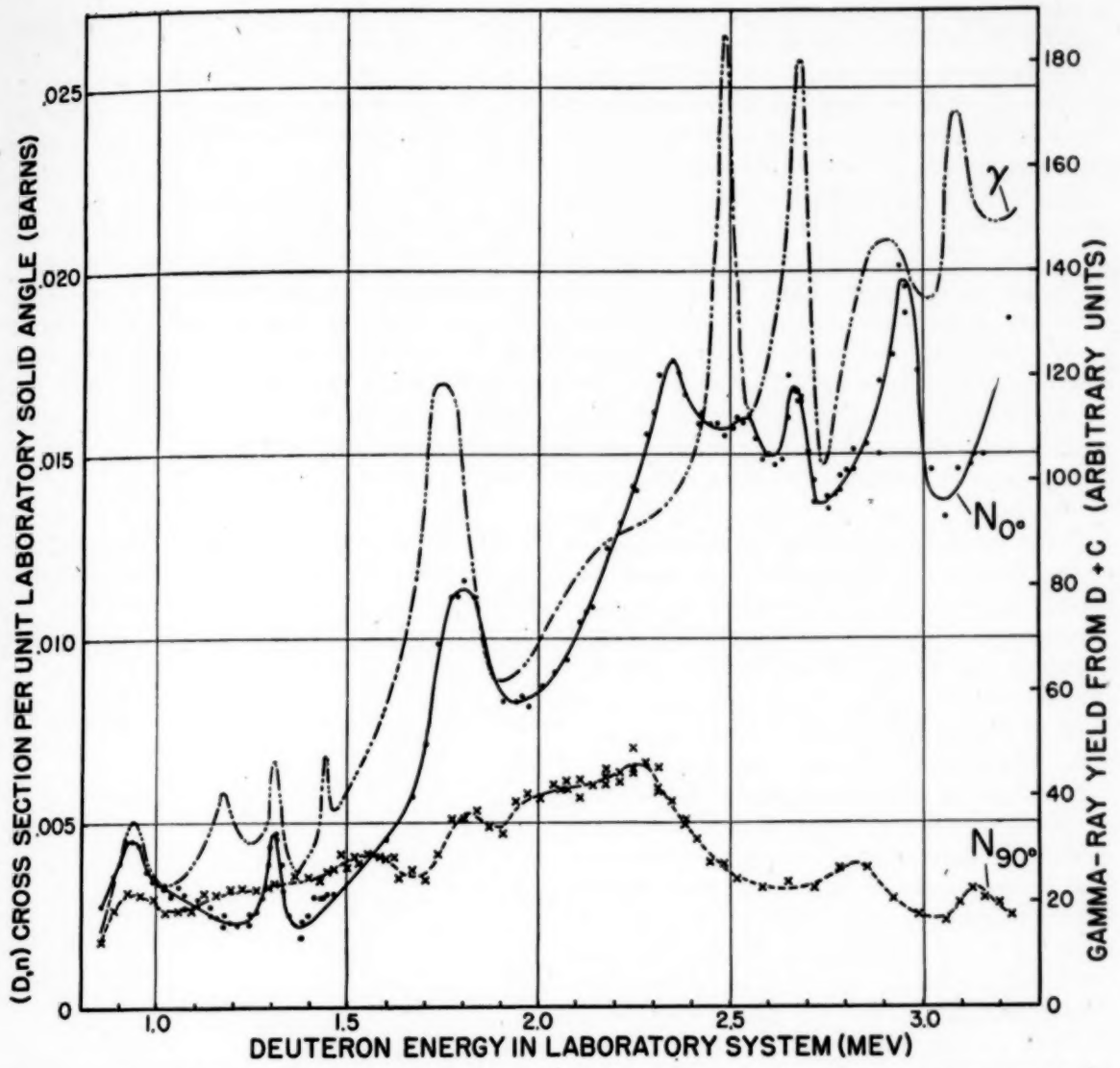

FIG. 2. Absolute yield of neutrons per unit solid angle in laboratory system of coordinates in the forward direct, $N_{0°}$, full curve, and at right angles to the deuteron beam, $N_{90°}$, dashed curve with crosses. The dot-dash curve shows the yield of gamma-rays to an arbitrary scale.

nucleus because these resonances are pronounced and broad for both modes of disintegration. It is not so obvious that the latter pair (2.96 and 2.90 Mev) is a common state of N^{14}. If this assumption is accepted, it is noticed that the gamma-ray resonance occurs for a bombarding energy of the deuteron which is considerably less, 50 kev, than for the neutron resonance. There is no experimental uncertainty as to the reality of this shift in energy since the observations are taken simultaneously.

Any expected effects of the potential barrier would result in a shift in the opposite sense since the gamma-rays are emitted after the emission of a proton. Since the observations of the yield of competitive reactions are, on the basis of theories involving the formation of a compound nucleus, a measure of the product of the probability of the formation of the compound nucleus and the probability of emission of the alternative nuclei, it is not easy to account for the differences in energy observed. For the resonances at 0.92, 1.30, 2.68 Mev, the gamma-rays and 0° neutrons are emitted at the same bombarding energies to

within the accuracy of the experimental observations which can be estimated at ±5 kev.

For deuteron energies of 2.35- and 2.55-Mev, reaction (1) emits neutrons in the forward direction with no corresponding resonance for gamma-rays. Conversely, for deuteron energies of 1.17, 1.43, 2.2, 2.49, and 3.08 Mev the observations show resonances for gamma-ray emission following reaction (2) and no corresponding resonances for neutrons. An explanation of the exclusive nature of these disintegrations from the resonance states of N^{14} must await a detailed description of the quantum states involved.

Considering the angular dependence of reaction (1) it should be noticed that the observations do not serve to measure the number of neutrons at exactly 0° or 90° for at least two reasons. First the angular aperture of the neutron detector is approximately $\pi/16$ steradians, as mentioned earlier. Second, observations of fast neutrons in a laboratory of limited dimensions are always fraught with the practical difficulty of detecting neutrons directly from a target over the atmosphere of neutrons which fills the laboratory.

An estimate of these two effects leads us to suggest that the true ratio of the yield of neutrons at 0° and 90° might be as large as twenty to one when the deuteron energy is of the order of 3 Mev. This marked asymmetry seems to be a common feature of many particle reactions in this range of energy and atomic number. Heitler, May, and Powell[13] have drawn attention to this phenomenon which occurs for the inelastic scattering of 4.2-Mev protons by neon. An analysis of the angular distribution of reactions of this type must await further detailed experimental examination of the distribution.

Only in the case of the lowest resonance energy, 0.92-Mev deuterons, is there a common character to the three curves of Fig. 2. The almost complete dissimilarity between the 0° and 90° neutron curves lacks an explanation at this time. The only common feature is in the neighborhood of 2.3 Mev. Here the decline of the continuum on which the 0° neutron resonances are superimposed and the sharper decline of the 90° neutron yield indicate that a competitive process is becoming important. The endoergic (d,a) process may be expected to play this role at approximately this energy.

[13] H. Heitler, A. N. May, and C. F. Powell, Proc. Roy. Soc. A190, 180 (1947).

6. ACKNOWLEDGMENTS

We are pleased to express our sincere thanks to Dr. J. Morris Blair and Mr. Eugene Lampi for assistance in taking these observations and to Mr. Rudolph Thorness for his continued aid in the mechanical design and construction of the apparatus. We are indebted to Professors C. L. Critchfield and J. W. Weinberg for many stimulating discussions of this problem.

This work was performed while one of the authors, C. L. Bailey, held a National Research Council predoctoral fellowship at the University of Minnesota.

This research was done under the partial support of the Office of Naval Research, Contract N5ori-147. It was also materially assisted by the University of Minnesota Technical Research Fund subscribed to by General Mills, Inc., Minneapolis Honeywell Regulator Company, Minneapolis Star Journal and Tribune Company, Minnesota Mining and Manufacturing Company, and Northern States Power Company.

PHYSICAL REVIEW VOLUME 73, NUMBER 4 FEBRUARY 15, 1948

The Charge Distribution in Nuclei and the Scattering of High Energy Electrons

M. E. Rose
Clinton National Laboratory, Oak Ridge, Tennessee
(Received November 3, 1947)

It is pointed out that the finite size of the nucleus will give rise to large deviations from Mott scattering when the change in wave-length of the electrons is of order of the nuclear dimensions. This deviation from Mott scattering at large scattering angles therefore provides a possibility for determination of the shape of the charge distribution and size of nuclei. In the case of a spherically symmetric charge distribution the nuclear charge density is immediately obtained from the observed angular distribution by a Fourier transform. The effects of competing processes, inelastic collisions with nuclear excitation or disintegration, atomic excitation or ionization and bremstrahlung are considered. It is shown that the first two competing effects may be disregarded if the electron energy is in the neighborhood of 50 Mev, the angle of scattering large (but not near π) and if the scattered electron has an energy equal to or nearly equal to the primary energy. With the latter condition fulfilled the bremstrahlung is reduced by the same factor as the elastic scattering and the two processes are indistinguishable.

I. INTRODUCTION

RECENT developments in the direction of obtaining high energy electron beams, as in the betatron and synchrotron, raise the question of using these high energy electrons in scattering experiments to obtain some information regarding nuclear structure. It will be readily recognized that for large angle scattering of electrons of several Mev (~50 Mev) the intensity of the scattering will depend strongly on the interaction between charges at very small distances. Specifically, the scattering nucleus cannot be regarded as a point charge but must be represented by an extended charge distribution whose shape can be explored by the scattering of electrons which penetrate inside the nucleus. Thus, even if the electrostatic interaction between charged elements is Coulombian down to essentially zero separation, the angular distribution of the scattered electrons will deviate markedly from the so-called Mott scattering.[1]

Actually there are two questions of considerable importance which are involved in the interpretation of scattering experiments of the kind under discussion. These concern (1) the nature of the (electric) interaction between charged particles at very small distances of separation and (2) the charge distribution and size of nuclei. Clearly, at least in principle, one may obtain information as to either question if the answer to the other is known. Unfortunately there is no case in which the nuclear charge distribution is known sufficiently well to allow a determination of possible deviations from the Coulomb interaction. However it should be possible to obtain evidence on this point from the scattering of high energy electrons by protons. It is plausible that deviations from Coulomb interaction, if such exist, are too small to be significant from the point of view of the accuracy obtainable in scattering measurements and we omit consideration of such deviations in the following.

With the assumption of an electrostatic Coulomb interaction between charges[2] it is possible to determine the charge density explicitly in terms of the nuclear form factor or observed scattering intensity. Applications to two important cases are immediately apparent: (1) Scattering in deuterium from which one may hope to obtain, for the first time, detailed information as to the deuteron wave function thereby establishing a criterion for the validity of nuclear force models. Here the effect of the non-central forces are unimportant unless the electron energy is several hundred Mev; i.e., the square of the reduced deBroglie wave-length is about equal to the quadrupole moment of the deuteron. (2) Scattering in heavier nuclei. Here the charge density is uniform, or nearly so, so that the

[1] E.g., see H. A. Bethe, *Handbuch der Physik*, XXIV/1, p. 495f.

[2] Effects of magnetic interaction with the nuclear spin are negligible.

primary information to be obtained is a measurement of nuclear radii.[3]

In the following these considerations are given quantitative formulation. Results for the angular distribution in the cases mentioned above are given as an indication of the magnitude of the effect. Finally, consideration of the feasibility of the measurements from the point of view of competing processes is presented.

II. ELASTIC SCATTERING BY EXTENDED CHARGE DISTRIBUTIONS

In the following the electron energy is sufficiently large to make the effect of nuclear penetration important, which implies extreme relativistic energies, but not so large that magnetic effects from nuclear recoil need be considered. For this reason and because of the considerations presented below our considerations are restricted to electron energies of order 50 Mev. The differential cross section for scattering electrons of total energy W into solid angle $d\Omega$ is

$$\sigma d\Omega=\frac{d\Omega}{4\pi^2}\frac{W^2}{(\hbar c)^4}|V_{if}|^2 \tag{1}$$

where

$$V_{if}=Ze^2\int\int d\tau_e d\tau_p \Psi^*(\mathbf{r}_p)\psi_f^*(\mathbf{r}_e) \times V(|\mathbf{r}_e-\mathbf{r}_p|)\Psi(\mathbf{r}_p)\psi_i(\mathbf{r}_e). \tag{2}$$

Here $\mathbf{r}_e$ and $\mathbf{r}_p$ are vectors defining the position of the electron and a volume element of protonic charge while the interaction energy between the electron and unit charge of the latter is represented by eV. The charge density in the nucleus is

$$\rho(\mathbf{r}_p)=|\Psi(\mathbf{r}_p)|^2$$

which is normalized to unity

$$\int\rho(\mathbf{r}_p)d\tau_p=1. \tag{3}$$

The subscripts i and f on the electron wave functions refer to initial and final states and are taken to be plane waves. Thus

$$\psi_i=a_i(\mathbf{P})\exp(i\mathbf{P}\cdot\mathbf{r}_e/\hbar),$$

$$\psi_f=a_f(\mathbf{P}')\exp(i\mathbf{P}'\cdot\mathbf{r}_e/\hbar),$$

where $\mathbf{P}$ and $\mathbf{P}'$ are the initial and final momenta while a_i and a_f are Dirac amplitudes for the plane wave.

We allow for non-central fields (quadrupole moment!) by writing

$$\int V(|\mathbf{r}-\mathbf{r}_p|)\rho(\mathbf{r}_p)d\tau_p =\sum_0^\infty(2l+1)v_l(r)P_l(\cos\beta) \tag{4}$$

in which the subscript e has been dropped. In (4) the polar axis ($\beta=0$) is the direction of quantization for the nuclear spin. We introduce

$$\psi_f^*\psi_i=a_f^*a_ie^{i\mathbf{q}\cdot\mathbf{r}} =a_f^*a_i\sum_0^\infty(2l+1)j_l(qr)P_l(\cos\Theta), \tag{5}$$

$$j_l=i^l(\pi/2qr)^{\frac{1}{2}}J_{l+\frac{1}{2}}(qr) \tag{5a}$$

where Θ is the angle between $\mathbf{q}$ and $\mathbf{r}$, J is the Bessel function and $\hbar\mathbf{q}$ is the change of momentum. In terms of the scattering angle ϑ we have

$$q=2P/\hbar\sin\vartheta/2.$$

After integration over the angular coordinates, the matrix element becomes

$$V_{if}=4\pi Ze^2(a_f^*a_i)\sum_0^\infty(2l+1)K_l(q)P_l(\cos\theta)$$

where

$$K_l=\int_0^\infty v_l(r)j_l(qr)r^2dr \tag{6}$$

and θ is the angle between $\mathbf{q}$ and the spin axis. Averaging over all directions of the nuclear spin, we get

$$|V_{if}|^2=16\pi^2Z^2e^4|a_f^*a_i|^2\sum_0^\infty(2l+1)K_l^2. \tag{7}$$

Summing over final spin states of the electron and averaging over initial spin states we obtain

$$|a_f^*a_i|^2_{\text{Av}}=c^2/W^2(m^2c^2+P^2\cos^2\vartheta/2). \tag{8}$$

From (1), (7) and (8) the angular distribution is

$$\sigma(\vartheta)=\left(\frac{Ze^2m}{2P^2\sin^2\theta/2}\right)^2 \times(1+(P/mc)^2\cos^2\vartheta/2)\sum_0^\infty(2l+1)f_l^2 \tag{9}$$

[3] Such deviations from the uniform distribution as may arise from the electrostatic repulsion between the protons are sufficiently small to be ignored.

where

$$f_l(q)=q^2K_l(q). \tag{9a}$$

The ratio of expected scattering to Mott scattering[4] is, therefore,

$$\sigma/\sigma_M=\sum_0^\infty(2l+1)f_l^2. \tag{10}$$

It may be noted that the small angle scattering is determined chiefly by the isotropic term in (10) and for $q\approx 0$ the scattering is unchanged. Therefore the total cross section for scattering will be affected very slightly, in agreement with observations of cascade showers in the cosmic radiation, whereas the large angle scattering will be materially reduced by the penetration effect.

a. Scattering by Central Fields

It is clear that deviations from central symmetry make a non-vanishing contribution to the scattering so that in principle one might use such measurements for the determination of nuclear quadrupole moments. However, at energies for which such quadrupole contributions are appreciable the penetration effect arising from the spherically symmetric part of the charge distribution would be important and the two effects would have to be disentangled. For the sake of simplicity we consider only those cases wherein deviations from central symmetry produce negligible or vanishing effects; that is, the quadrupole moment may vanish or be small compared to 10^{-24} cm^2, or the electron energy may have some intermediate value for which the monopole effect is appreciable and the quadrupole effect is very small.[5]

For the monopole term we have from (6) and (5a)

$$K_0=f_0/q^2=\int_0^\infty\frac{\sin qr}{qr}v_0(r)r^2dr$$

so that K_0 is proportional to the Fourier transform of v_0. Inverting we get

$$v_0=\frac{2}{\pi}\int_0^\infty f_0(q)\frac{\sin qr}{qr}dq.$$

For the Coulomb interaction the charge density in the nucleus is given by

$$\rho(r)=-\frac{1}{4\pi r^2}\frac{d}{dr}r^2\frac{dv_0}{dr}$$

$$=\frac{1}{2\pi^2 r}\int_0^\infty f_0(q)q\sin qrdq. \tag{11}$$

Since f_0 is real and for a point charge

$$f_0(q)=1$$

it follows that

$$f_0(q)=(\sigma/\sigma_M)^{\frac{1}{2}}$$

and

$$\rho(r)=\frac{1}{2\pi^2 r}\int_0^\infty(\sigma/\sigma_M)^{\frac{1}{2}}q\sin qrdq. \tag{12}$$

Alternatively the deviation from a point charge distribution is expressed by

$$\rho(r)-\frac{\delta(r)}{4\pi r^2}=\frac{1}{2\pi^2 r}\int_0^\infty[(\sigma/\sigma_M)^{\frac{1}{2}}-1]q\sin qrdq. \tag{13}$$

Either (12) or (13) permit the determination of the shape of nuclear charge distributions directly from experimental data.

b. Scattering by Deuterium Nuclei

For the purpose of illustration we consider the example of electron scattering by a relatively extended nuclear charge distribution, viz: the deuteron for which a reasonable estimate of the nuclear wave function can be made. From (11) we find in general

$$f_0=4\pi\int_0^\infty\rho(r)\frac{\sin qr}{qr}r^2dr. \tag{14}$$

For not too large q this may be written

$$f_0=1-\frac{1}{3!}q^2\langle r^2\rangle_{Av}+\frac{1}{5!}q^4\langle r^4\rangle_{Av}-\cdots. \tag{14a}$$

Appreciable penetration effects may therefore be expected for scattering angles as small as $\hbar/PR$

---

[4] The first two factors in (9) give, of course, the Born approximation to the scattering by a point charge. A first order correction to the Born approximation consists in replacing the second factor by

$$1+(P/mc)^2\cos^2\vartheta/2+(\pi e^2ZPW/\hbar m^2c^4)\sin\vartheta/2,$$

cf. P. Urban, Zeits. f. Physik 119, 67 (1942).

[5] For small q it follows from (6) that

$$f_l\approx\delta_{l0}+\text{const.}(qR)^{l+2}$$

where R is a length of order of nuclear dimensions, δ_{l0} is the Kronecker symbol.

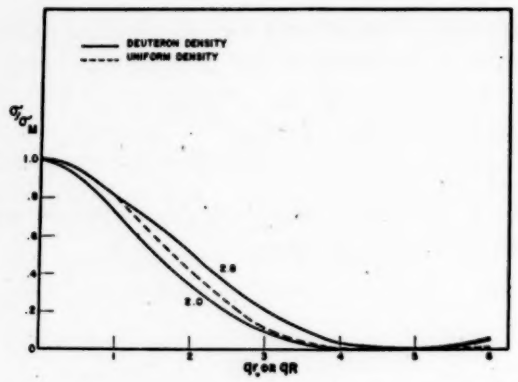

FIG. 1. Full curves give the ratio of expected elastic scattering to Mott scattering in deuterium as a function of qr_0 with $\hbar q$ the change in momentum and r_0 the range for a central square well. Numbers affixed to the curves give r_0 in units 10^{-13} cm. The dashed curve shows the same scattering ratio for a nucleus with constant charge density and radius R as a function of qR.

where again R is of order of nuclear dimensions. For 50 Mev electrons this is an angle of about 10°.

Using the wave function of the deuteron corresponding to a central square well potential of range r_0 and depth V_0 the scattering can be easily calculated from (14). We find

$$f_0=\frac{\cos^2 b}{1+a}\cos\frac{\xi}{2}+\frac{a}{1+a}\left\{4e^{2a}(G/\xi)\sin^2 b+\frac{2}{\xi}Si\left(\frac{\xi}{2}\right)\right.$$
$$+\frac{1}{\xi}[Si(2b-\tfrac{1}{2}\xi)-Si(2b+\tfrac{1}{2}\xi)]$$
$$+\frac{1}{2}\left(1-\frac{\xi}{b}\right)\frac{\sin(2b-\frac{1}{2}\xi)}{2b-\frac{1}{2}\xi}$$
$$\left.+\frac{1}{2}\left(1+\frac{\xi}{b}\right)\frac{\sin(2b+\frac{1}{2}\xi)}{2b+\frac{1}{2}\xi}\right\} \quad (15)$$

where

$$Si(y)=\int_0^y \sin t\,dt/t, \quad \xi=qr_0,$$
$$a=(M\epsilon)^{\frac{1}{2}}r_0/\hbar, \quad b=[M(V_0-\epsilon)]^{\frac{1}{2}}r_0/\hbar \quad (15a)$$

and ϵ is the binding energy = 2.17 Mev. The quantity

$$G=\int_1^\infty e^{-4az}\sin\xi x\,dx/x$$
$$=\arctan\xi/4a-\int_0^1 e^{-4az}\sin\xi x\,dx/x$$

is computed numerically.

The ratio to Mott scattering, that is, f_0^2, is given as the full curves in Fig. 1 for ranges $r_0=2.0$ and 2.8×10^{-13} cm. For the scattering of 50 Mev electrons at $\vartheta=\pi/2$ the scattering is reduced to 23 percent of the Mott scattering in the case of the larger range. At a larger scattering angle, say $\vartheta=\pi$ the deviation from Mott scattering is, of course, even more striking; but of course the cross section becomes smaller and the measurements more difficult (cf. further Section IIIa and b below).

c. Scattering by Heavier Nuclei

As a second example we consider heavier nuclei for which it is reasonable to assume a constant charge density. We find directly from (14)

$$f_0=\frac{3}{\eta^2}\left(\frac{\sin\eta}{\eta}-\cos\eta\right) \quad (16)$$

where $\eta=qR$ and R is the nuclear radius. The scattering ratio f_0^2 is given as the dashed curve in Fig. 1. For typical values of the nuclear radius the large angle scattering is again reduced from the Mott value by a large amount.

III. COMPETING PROCESSES

In order to form some idea as to the feasibility of the proposed scattering experiments we consider what might be expected from concomitant processes. These are (1) excitation and disintegration of the nucleus, (2) inelastic scattering involving atomic excitation and ionization, and (3) bremsstrahlung.

a. Nuclear Excitation and Disintegration

While it is rather difficult to make a quantitative estimate of the angular distribution of scattering with nuclear excitation or disintegration, the total cross section for this process may be evaluated with sufficient accuracy. Since the collision considered takes place mainly through the virtual quanta emitted by the deflected electron and the consequent photo-effect of these quanta, the angular distribution of the scattered electrons will show a strong forward peak very much like that exhibited by the elastic scattering. Therefore, under conditions which make the total cross section for scattering with nuclear excitation small compared to the total elastic scattering cross section, the former may be disregarded.

The total cross section for nuclear disintegration may be calculated by the Williams-Weiszäcker method.[6] For the ejection of a single particle from the nucleus the total cross section is approximately

$$\sigma_{\text{dis}} \sim \frac{\pi e^4}{Mc^2 E_0} \log \frac{MW}{mE_0} \tag{17}$$

where E_0 is the threshold energy and M the mass of the ejected particle. In (17) some numerical factors of order unity have been omitted.[7] For the ejection of a single particle (neutron, or proton) with $E_0 = 6$ Mev and $W = 50$ Mev we have $\sigma_{\text{dis}} \sim 10^{-4}$ barn. The total elastic scattering cross section can be evaluated quite easily. Since the major contribution comes from small angles we have for the differential cross section at high energies (cf. reference 9)

$$\sigma_{\text{el}}(\vartheta) = \left(\frac{Ze^2 \cos\vartheta/2}{2cP \sin^2\vartheta/2} \right)^2 (1-F)^2 \tag{18}$$

where F is the atomic form factor arising from the scattering by orbital electrons.[8] We find for the total elastic scattering cross section

$$\sigma_{\text{el}} \approx 6Z^{4/3}(\hbar/Mc)^2 \tag{19}$$

which is enormously greater than σ_{dis}. While (19) includes essentially unobservable scattering at $\vartheta = 0$ the same is true of the cross section for disintegration, Eq. (17).

In order to be more certain that the disintegration cross section is also negligible at large scattering angles a comparison of the angular distributions for elastic scattering and inelastic scattering with disintegration may be made in the one case where the latter can be readily calculated, *viz*; disintegration of the deuteron.[9] The differential cross section for high energy electrons is approximately

$$\sigma_{\text{dis}}(\vartheta) = \frac{8}{3\pi} \frac{m}{M} \left(\frac{e^2}{Mc^2} \right)^2 \epsilon^{\frac{1}{2}} \int_0^{W-mc^2-\epsilon} \frac{dE E^{\frac{1}{2}}}{(E+\epsilon)^4} \times \left[\frac{W^2+W'^2}{(\hbar cq)^2-(W-W')^2} - \frac{1}{2} \right] \tag{20}$$

where W and W' are the initial and final electron energies and $E = W - W' - \epsilon$ is the kinetic energy of the nucleons. The evaluation of (20) to give the angular distribution leads to the following conclusions: (1) The comparison of total cross sections as given above is somewhat too optimistic insofar as the decrease of $\sigma_{\text{dis}}(\vartheta)$ with the angle of deflection is not nearly so rapid as is the decrease of the elastic differential cross section $\sigma_{\text{el}}(\vartheta)$. (2) Since $\sigma_{\text{dis}}(\vartheta)$ varies only slowly with energy (cf. Eq. (17)), and the differential cross section $\sigma_{\text{el}}(\vartheta)$ varies as W^{-2} (except in the backward direction), the disintegration effect can be neglected only if the electron energy is not greatly in excess of 50 Mev. (3) The scattering angle at which the electrons are observed should not be too near π since in this case elastic scattering is very much reduced (because of factor $P^2 \cos^2\vartheta/2$) and will be considerably larger than $\sigma_{\text{dis}}(\vartheta)$ only for energies so low that the effect of electron penetration into the nucleus is negligible. With $W = 50$ Mev and $\vartheta = \pi/2$, which values represent favorable conditions, $\sigma_{\text{dis}} = 6 \times 10^{-7}$ barn and $\sigma_{\text{el}} = 1.6 \times 10^{-5}$ barn.

b. Ionizing Collisions

The cross section for inelastic collisions with the orbital electrons is not negligible compared to the elastic scattering. However, competition due to such collisions is unimportant if it is arranged to observe electrons which have energies equal or nearly equal to the primary energy and are scattered through angles other than 0 or π. This follows from simple energy and momentum considerations which show that the primary electron scattered through an angle $\mu = \arccos\vartheta$ or a secondary traveling in the same direction has a total energy given by

$$\frac{W'}{mc^2} = \frac{W+mc^2+\mu^2(W-mc^2)}{W+mc^2-\mu^2(W-mc^2)}. \tag{21}$$

Here the binding of the secondary in the initial state is neglected. Therefore, for $W \gg mc^2$ the secondary energy W' cannot be large unless $\mu^2 \approx 1$. Therefore, under the conditions $W \gg mc^2$ and ϑ in the range $\pi/2 \pm \pi/4$ say, there will be no fast electrons which were not elastically scattered. These conditions are the same as those providing a large ratio of elastic scattering to nuclear disintegration.

[6] E. J. Williams, K. Danske Vidensk. Selskab. **13**, no. 17 (1934–36).

[7] For energies such that $\hbar c/W$ is larger than nuclear dimensions the argument of the *log* in (17) is multiplied by W/Mc^2 which reduces the cross section. Cf. further reference 9.

[8] Cf. H. A. Bethe, Ann. d. Physik **5**, 325 (1930).

[9] H. A. Bethe and R. Peierls, Proc. Roy. Soc. **148**, 146 (1935).

c. Bremsstrahlung

The bremsstrahlung competes with the elastic scattering in a way which would make interpretation of measurements ambiguous except when the deflected electrons have energies about equal to the primary energy. In this case, the quanta emitted are soft and, as is well known, the angular distribution of the scattered electrons is precisely the same as the distribution of elastically scattered electrons.[10] Obviously the bremsstrahlung will also be reduced by the same factor f_0^2 due to nuclear penetration and thus, under the conditions cited, one need not distinguish between elastic scattering and bremstrahlung.

[10] F. Bloch and A. Nordsieck, Phys. Rev. **52**, 54 (1937).

IV. ACKNOWLEDGMENT

It is a pleasure to thank Professor H. A. Bethe for interesting discussions. This document is based on work performed under Contract No. W-35-058-eng. 71 for the Manhattan Project at the Clinton Laboratories.

PHYSICAL REVIEW VOLUME 73, NUMBER 4 FEBRUARY 15, 1948

Ionization Currents in Divergent Fields in Hydrogen and in Air

GERALD W. JOHNSON*
Department of Physics, University of California, Berkeley, California
(Received November 3, 1947)

Ionization currents were measured in hydrogen and in dry, mercury-free air between concentric cylinders for pressures from 0.01 mm to 760 mm. Above the pressures corresponding to the minimum sparking potentials, $(1/r)(1/p)\log i/i_0$ was a single-valued, continuous function of $(X/p)_{max}$. Calculated values of apparent α for air agreed with uniform field values at low X/p but were high at higher X/p. In hydrogen apparent α was high over the full range of variables studied. Auxiliary anodes permitted estimates of the location of the ionization which was found to agree with the spatial distribution predicted by Morton. Electrons released in the low and collected in the high field produced the same ionization as for the reverse case except at low pressure in hydrogen where about 10 percent less ionization occurred for electrons released in the low field. The peaks of Morton's i/i_0 *vs.* p curves were identified with the minimum sparking potential. Application of the back diffusion equation of Rice permitted the evaluation of i_0 at higher pressures than hitherto has been possible. Comparison of the present results with those reported by Fisher and Weissler show that the present results can be directly applied if the focal length of the point parabola is substituted for r in the electron multiplication parameter. On the basis of this agreement, it is expected that the present values of the parameter may be applied to any geometry in which the field varies inversely as the distance from a fixed point. A necessary condition for the application of the observed values of the parameter to any system is that the electrons give up all of their ionizing energy to the gas before being collected.

INTRODUCTION

IONIZATION by collision by electrons in a gas has been under experimental and theoretical investigation since about 1900. Since that time, the practical applications of the basic phenomena have assumed great proportions in industry. Yet, at this time, one cannot with assurance predict what the electron multiplication will be, except in plane parallel gaps or in other special geometries which have been given particular study.

The early work of Townsend beginning about 1900 established for plane parallel gaps the well known law,

$$i = i_0 e^{\alpha d}, \tag{1}$$

where i is the total current collected at the anode, i_0 is the primary current, d is the distance between the electrodes, and α, the First Townsend Coefficient, is the number of new electrons produced by an electron in moving one centimeter through the gas in the field direction. In addition to the relationship given in Eq. (1), it was shown that α/p was a single-valued and continuous function of X/p, where X is the field strength in volts/cm and p is the pressure in mm

* Now at the State College of Washington. This work was carried out at the University of California in partial fulfilment of the requirements for the degree of Doctor of Philosophy.

of mercury. Thus once the functional form of the variation of α/p with X/p was determined, α could be calculated for any field and pressure, which by substitution in Eq. (1) would yield the electron multiplication. The relationship cannot be represented by any simple analytic function so that results are usually given in graphical form.

Many of the first determinations of α are of little value today because of the questionable purity of the gases used and particularly because of the fact that all the gases were mercury contaminated. Loeb[1] has given a complete analysis of all of the early measurements as well as the recent ones. Perhaps the best recent determinations were obtained by the following:

Hg-contaminated air	Sanders,[2] Paavola,[3] Masch[4]
Hg-contaminated N_2	Posin[5]
Hg-free A, Ne, and Ne + A	Kruithoff and Penning[6]
Hg-free N_2	Bowls[7]
Hg-free H_2	Hale[8]

Using values of α from these various sources the calculation of i/i_0 is obtained readily by substitution in Eq. (1) for plane parallel gaps. However, in most applications the plane parallel gap is a rarity and, in general, the interest is in non-uniform fields. The practice has been to rewrite Townsend's equation in the form

$$i = i_0 e^{\int \alpha dx} \qquad (2)$$

and to apply it to the non-uniform case. The integral is evaluated usually by some method of numerical or graphical integration using the values of α determined in a uniform field. Since in the uniform field measurement the electrons were always in equilibrium in their gain and loss of energy in the field, one might question whether such functions could be applied where the fields change rapidly. For it is conceivable that with rapidly varying fields the electrons might not adjust to the true field with sufficient rapidity. This doubt in regard to electrons in the Crookes dark space in a glow discharge led P. L. Morton[9] to undertake a careful general study of this ionization in non-uniform fields for a limited pressure range in hydrogen. This study at once revealed that Townsend's uniform field values of α result in serious errors when applied to fields in which the divergence is greater than 2.5 percent over an electron free path. Under such conditions the observed ionization is greater than the calculated values from Eq. (2). As anticipated by Morton, the results obtained are to be attributed to the fact that in a highly divergent field the electrons do not reach their terminal energy distribution. Morton showed further that the ionization does not depend on the field at which the ionizing impact occurs but that the field enters only insofar as it affects the energy distribution. Stimulated by Morton's findings, in an attempt to clarify discrepancies in calculations of breakdown fields in positive corona processes, Fisher and Weissler[10] observed higher multiplication than was to be expected from the Townsend equation for currents between confocal paraboloids at near atmospheric pressure in hydrogen when the field changed by 2 percent over a free path.

Morton's experimental studies were limited to pressures below about 5 mm because back diffusion made it impossible to determine the initial photoelectric current i_0 at the higher pressure. In view of the importance of the deviations observed by Morton, and Fisher and Weissler, it became essential to extend the range of measurements throughout the whole range of pressures and point sizes for hydrogen and air in order that data should be at hand for calculation of currents in fields of industrial application. Thus the present work constitutes an extension of Morton's work to higher pressures. This extension was fortuitously facilitated through the timely derivation by Rice[11] of a back diffusion equation for cylindrical electrode systems.

[1] L. B. Loeb, *Fundamental Processes of Electrical Discharges in Gases* (John Wiley and Sons, Inc., New York, 1939), Chapter VIII.
[2] F. H. Sanders, Phys. Rev. **41**, 667 (1932); **44**, 1020 (1933).
[3] M. Paavola, Archif f. Electrotechnik **26**, 589 (1932).
[4] K. Masch, Archif f. Electrotechnik **26**, 589 (1932).
[5] D. Q. Posin, Phys. Rev. **50**, 650 (1936).
[6] A. A. Kruithoff and F. M. Penning, Physica **3**, 515 (1936); **4**, 430 (1937).
[7] W. E. Bowls, Phys. Rev. **53**, 293 (1938).
[8] D. H. Hale, Phys. Rev. **54**, 241 (1938); **56**, 815 (1939).
[9] P. L. Morton, Phys. Rev. **70**, 358 (1946).
[10] L. H. Fisher and G. L. Weissler, Phys. Rev. **66**, 95 (1944).
[11] C. W. Rice, Phys. Rev. **70**, 228 (1946).

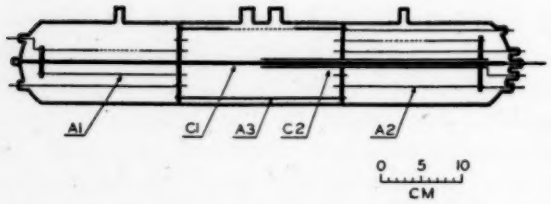

FIG. 1. Tube for measurements below pressures of 10 mm. *C1*—cathode 1; *C2*—cathode 2; *A1*—anode 1; *A2*—anode 2; *A3*—anode 3. The envelope was of Pyrex with quartz windows on graded seals. All metal parts were nickel or monel. The internal insulation was quartz.

APPARATUS

A first consideration in the design of the tube was in regard to the type of divergent field to use. The simple concentric cylindrical electrode system as was used by Morton was chosen because it yields a divergent yet readily calculable field. In addition, the cylindrical geometry offered more flexibility in designing equipment for changing the various parameters concurrently in the same envelope than was possible with other geometries. To get the effect of field strength at the point of release of the electrons, cathodes of different radii were provided. Auxiliary anodes of different diameters were introduced into the design to permit the interception of the electron current at different points in the field and thus to make estimates of the spatial distribution of the ionization. The primary current was produced by photoelectric emission under illumination of the cathode by ultraviolet light.

To cover the desired pressure range it was necessary to use two tubes, one for pressures below about 10 mm and the other for the higher pressure values. The one designed for the low pressures was essentially the same as that used by Morton[9] but with two additional anodes. This tube is shown in Fig. 1 and consists of two cathodes and three anodes, all of different radii. The tube for pressures above 10 mm, shown in Fig. 2, consists of a single cathode and a single anode. All metal parts of both tubes are of nickel or monel, and the insulation is quartz. Pertinent data for the two tubes are listed in Table I. The meaning of symbols used in Figs. 1 and 2 are also listed in Table I.

The primary electron current was produced by photoelectric emission from the cathode under illumination by ultraviolet light. Light from a three-inch section of a mercury arc illuminated a slit whose image was projected upon the cathode by means of a quartz lens. The light entered the tube through quartz windows attached to the tube by graded seals and passed through nickel gauze windows in the anode to the cathode. The nickel gauzes were 80 mesh per inch and were woven from 5-mil wire. The intensity of illumination of the cathode could be varied by means of an opaque slide placed near the lens. The arc was enclosed in a glass chimney and when operated from batteries was very steady after reaching equilibrium.

The voltage supply consisted of a bank of dry cells for voltages up to 1000 volts. Higher voltages were obtained from a voltage doubler circuit (shown in Fig. 3) using two 0.5-mf condensers and kenotrons. The high voltage transformer was operated from a Sola constant voltage transformer (CVT). A Variac placed between the Sola and the high voltage transformer provided the means of varying the voltage. The circuit diagram for rate of charge measurements with anode 3 as collector including the voltage supply is given in Fig. 3.

All voltage measurements were made with a Leeds and Northrup Student potentiometer across a section of a calibrated resistance tower. Each section of the tower was checked by bridge measurements. The standard cell used with the potentiometer was a recently certified standard.

The current measurements were made in part using high resistance J. G. White resistors and a Dolezalek quadrant electrometer with a sensitivity of 1200 mm/volt to measure the potential drop. The current collected by the appropriate anode was passed through a White resistor of resistance 10^9, 10^{10}, or 10^{11} ohms, depending on the magnitude of the current, to ground. The potential drop developed across this resistor was then measured with the electrometer and the current calculated using Ohm's law. The voltage doubler circuit was not sufficiently stable to permit the measurement of current by the steady deflection method, so rate of charge methods were used. For the rate of charge measurements the charge was collected on an amber insulated condenser for a specified interval of time, after which the potential was determined with a

Dolezalek quadrant electrometer with a voltage sensitivity of 44 mm/volt. The procedure followed in getting a measurement was to open sulfur switch *SS*2 with *SS*3 closed (Fig. 3), and to close *SS*1, which applied the high voltage to the tube, for a measured interval of time. At the end of the desired time interval, *SS*1 and *SS*3 were opened, and the electrometer then was switched in to measure the charge collected on the condenser. The switch *SS*3 was found necessary because the ultraviolet illumination of the cathode would otherwise slowly discharge the collecting condenser. The two methods of measurement gave consistent results when checked against each other.

The hydrogen was commercial tank hydrogen which was purified by passing it slowly through a fine capillary over copper shot at 350°C and then through two liquid air traps, one of which was a long spiral, into the ionization chamber. The air was taken from outside the building through an all glass line. The air was filtered through a long glass wool filter and was passed slowly through a calcium chloride drying train and thence through two traps cooled in dry ice and alcohol into the ionization chamber.

Every precaution was taken to prevent the contamination of either of the tubes by mercury. Liquid air or dry ice and alcohol were always on the traps whenever the tubes were exposed to the rest of the system.

When the gas under investigation was hydrogen, on initial evacuation the tube was baked out at 450°C for 12 hours at a pressure of 10^{-6} mm. After several flushings with clean hydrogen the tube was filled to a pressure of about 50 mm and baked at 450°C for 8 hours. This gas was then pumped out and the tube filled to a few millimeters pressure, whereupon it was subjected to a glow discharge for at least an hour. The residual gas was pumped out, and the tube was filled to the desired pressure for an experimental run.

With air, a somewhat different procedure was followed. On the first evacuation the tube was baked at 450°C for 12 hours at a pressure of 10^{-6} mm. The tube was allowed to cool and then was flushed out several times with filtered, mercury-free air. Air could not be admitted to the tube while it was hot because of oxidation of the metal parts. While the oxidation of nickel is slight under such circumstances, the oxidation of monel is excessive. When hydrogen had been used in the tube previously, after the preceding treatment a prolonged glow discharge was run in nitrogen since bake-out alone will not remove all of the hydrogen. After these treatments the tube was pumped out and then filled with clean, dry air to the desired pressure.

The tube was pumped out each time a glow discharge occurred and at the completion of each run.

The ambient temperature during this research was 22°±2°C.

EXPERIMENTAL PROCEDURE

The experimental procedure followed was identical for each gas and is outlined in the following.

The ionization chamber after outgassing was filled to the desired pressure with the gas. When the mercury arc had come to equilibrium, which usually required about an hour, the ultraviolet light was focused on the appropriate cathode. The intensity of illumination was adjusted to give a primary current of the order of 10^{-13} ampere. The current was then measured to one of the anodes as a function of applied voltage for voltages extending from zero up to values at which secondary processes became active.

At the conclusion of each run at a given pressure and intensity of illumination, the voltage was returned to a low value and the current measured again. This procedure gave a measure

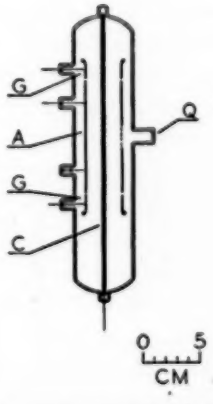

FIG. 2. Tube for measurements above pressures of 10 mm. *C*—cathode; *A*—anode; *G*—guard rings; and *Q*—quartz window. The envelope was Pyrex.

TABLE I. Essential data for the tubes.

Electrode	Symbol	Radius cm	Max. field volts/cm	For 100 volts applied potential volts
	Low pressure tube			
Cathode 1	C1	0.237	145	100
Cathode 2	C2	0.555	62	71
Anode 1	A1	1.51	23	36
Anode 2	A2	2.86	12	15
Anode 3	A3	4.36	8	0
	High pressure tube			
Cathode	C	0.157	277	100
Anode	A	1.58	28	0
Guard rings	G			
Quartz window	Q			

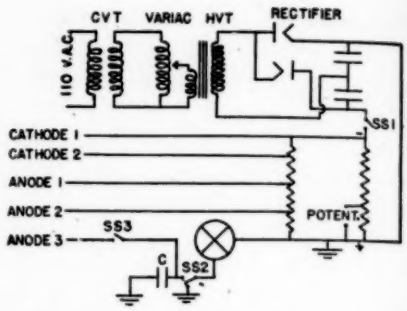

FIG. 3. Circuit diagram. CVT—Sola constant voltage transformer; HVT—10,000 volt high voltage transformer; *SS*1, *SS*2, *SS*3, sulfur insulated switches; *C*—amber insulated cylindrical condenser. Filament transformers not shown.

of the change in emission during the run. In practically all cases the observed change was less than 5 percent. Runs for which the changes were more than 5 percent were repeated. The current through the arc remained steady to one percent for all reported measurements.

The primary currents were kept low to eliminate the effect of space charge. However, as an experimental check, successive runs were made at various times during the course of the research for different intensities of illumination. The agreement of such runs was considered to indicate the lack of space-charge effects. In none of these check runs were there any evidences of space-charge falsification of the data.

The observed currents were plotted as ordinates and the applied potentials as abscissas. The primary current i_0 was determined from such graphs. At pressures below 5 mm, the current-voltage characteristic had a well-defined plateau and i_0 was taken as this plateau value. As the pressure was increased the definition decreased because of back diffusion and, therefore, i_0 could not be evaluated in such a simple fashion. The primary current then becomes a function of the applied potential since, as the potential is increased, fewer and fewer electrons are lost to the cathode by back diffusion.

Recently Rice[11] derived a theoretical expression for the back diffusion limited current for concentric cylindrical electrode systems, which applies precisely to the present geometry. The derived expression was of the following form:

$$i=AV/(V+B), \tag{3}$$

where under given test conditions A and B are constants. A is the value of i at large V or might be considered as the true saturation current. This does not mean that it is the current one uses to compute the electron multiplication since what must be used is the actual electron current escaping the cathode into the gas at any given potential. The parameter B is proportional to the mobility and is, therefore, pressure dependent.

In the determination of A and B it is convenient to rewrite the Rice equation in the following form:

$$V=AV/i-B. \tag{4}$$

To determine A and B a plot is made of V *vs.* V/i. The curve is linear up to the voltage at which cumulative ionization by collision begins to occur. Equation (4) is fitted to the linear part of the curve and A and B therefore determined. These values are then put back in Eq. (3) and the values of i_0 calculated for each potential.

As an illustrative example, in Fig. 4 are shown the experimental values of i and V for air at a pressure of 393 mm. The dotted curve is the i_0 curve calculated as outlined in the foregoing. The character of the fit of the empirical expression for i_0 to the curve is seen for the first four points on the curve. It is also of interest to note that the true saturation current of .75 is not even approximately reached at the highest potentials used.

From the calculated values of i_0, the electron multiplication i/i_0 was then obtained as a function of applied voltage.

EXPERIMENTAL RESULTS

Measurements of electron multiplication were obtained in pure hydrogen and in dry, mercury-free air over a pressure range of 0.01 mm to 760 mm. Cathodes and anodes of three different radii were used. Throughout most of the experiment, the smaller electrodes were used as cathodes and the larger ones as the collector anodes. In some cases, however, the potentials were reversed to get the effect of releasing the electrons in a weak and collecting them in a strong field.

It was found convenient to express the electron multiplication in terms of the parameter $(1/r)(1/p)\log_e i/i_0$, where r is the radius in cm of the electrode in the high field region, and p is the pressure in mm of mercury. When values of this parameter are plotted against the maximum X/p values, that is, for the X/p values at the surface of the electrode in the strong portion of field, a single-valued, continuous curve is obtained over the full range of variables used.

The $1/r$ term is essentially proportional to the maximum field at a given applied potential. The ratio of the surface fields varies inversely as the radii for a specified applied voltage.

The results plotted with $(1/r)(1/p)\log_e i/i_0$ as ordinate and $(X/p)_{max}$ as abscissa for both air and hydrogen are shown for the lower X/p values in Fig. 5 and for the higher X/p values in Fig. 6. It is clearly indicated that the chosen parameter to represent the electron multiplication is indeed a function of $(X/p)_{max}$.

At very low pressures, that is, at pressures corresponding to the minimum sparking potential, at each succeeding lower pressure the curves of $(1/r)(1/p)\log_e i/i_0$ were displaced to lower values so that in this region continuous curves did not result. These departures began to occur in hydrogen at pressures of about 0.5 mm and in air at about 0.2 mm. This downward shift might be attributed to the fact that some of the primary electrons are getting through to the collector without dissipating all of their ionizing energy in the gas (i.e., the electrode spacing is too close or the path in the gas is not long enough). Consequently, the ionization is less than would be expected. However, it is signification to notice that the region at which perceptible departures from the higher pressure equation theory appears is just the region in Figs. 7 and 8 at which the transition for which Morton's step-by-step calculations depending on field divergence changes to the more classical computations which follows Townsend's theory. In other words, the step-by-step analysis applies to a divergent field where this is significant, but begins to fail at higher pressures and merges into a region in which the simpler relations depicted in Figs. 5 and 6 govern. It is below this region in pressure that the departures appear to become appreciable, which is exactly what is to be expected.

From the plots of Figs. 5 and 6, cross-plots were made with i/i_0 as ordinate and p as abscissa. Since i/i_0 is the primary physical quantity in which we are interested, these plots illustrate more clearly than do Figs. 5 and 6, the form of dependence of i/i_0 on p and $(X/p)_{max}$. The curves were plotted for a cathode radius of 0.157 cm, which was the smallest one used in this series of tests. These plots are shown for air in Fig. 7 and for hydrogen in Fig. 8.

At the lower pressure end of the plots of Figs. 7 and 8 are noted a series of peaks for different applied fields similar to those found by Morton.[9] The peaks shift toward lower pressure values as the field is lowered, an effect previously noted by Morton.[9] The highest peaks represent the pressures for each gas at which the minimum sparking potentials are observed. This result is not unexpected since at low X/p, α/p or its equivalent increases more rapidly than linearly with increasing X/p, and thus α, or i/i_0, increases with decreasing pressure for a given applied

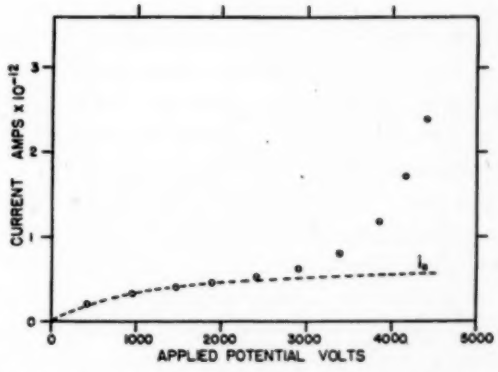

FIG. 4. Typical current voltage characteristic. Dotted line is the empirical fit of the Rice back diffusion equation to the experimental data. Air at 393 mm.

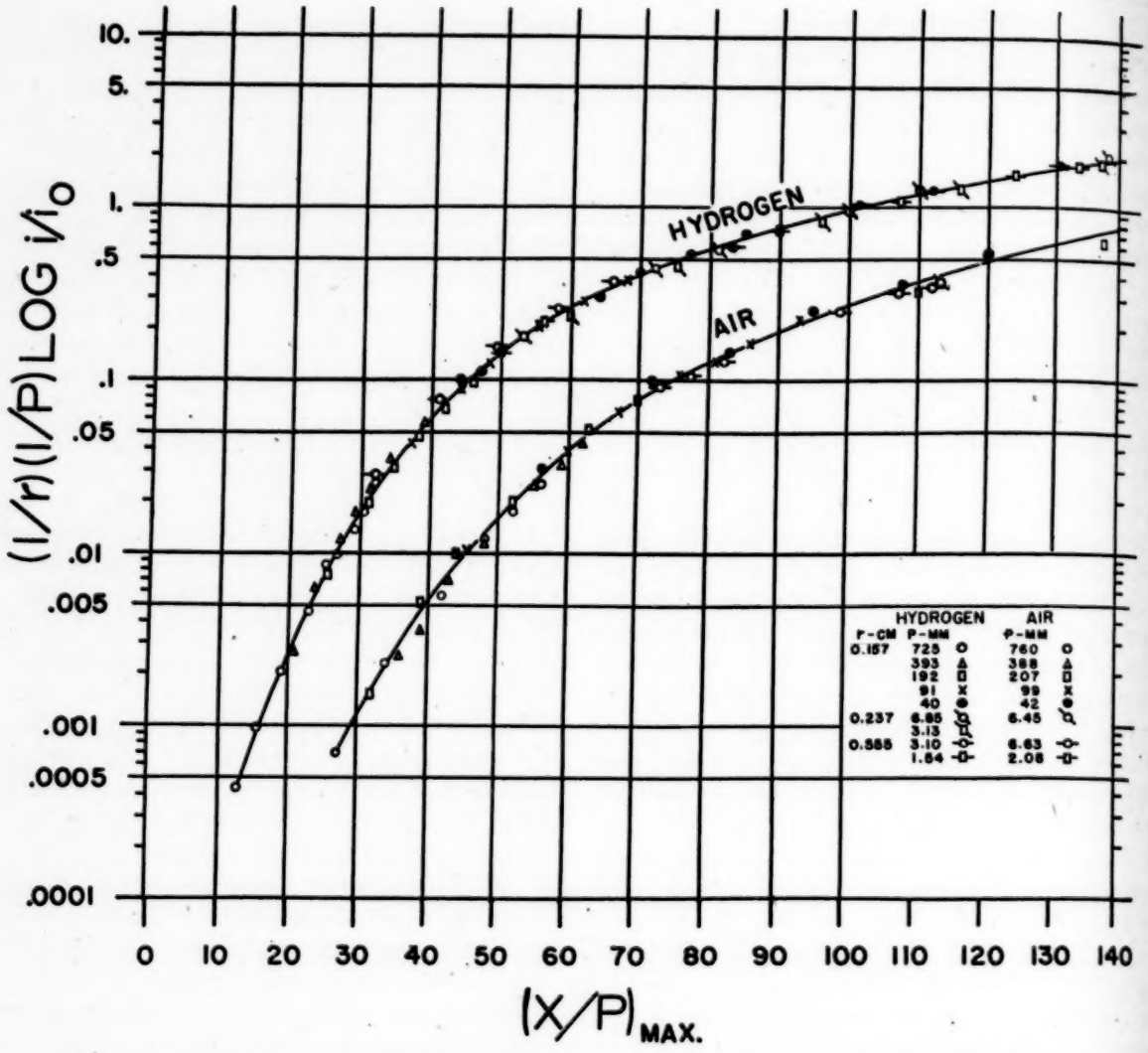

FIG. 5. Variation of electron multiplication parameter with field-to-pressure ratio at the electrode surface. Purified hydrogen and dry, mercury-free air. Low X/p values.

potential. However, the α/p curve passes through a point of inflection and as X/p is increased above this point α decreases. Thus α, and therefore i/i_0, passes through a maximum at a pressure and field corresponding to the point of inflection. Now the minimum sparking potential arises when α ceases to increase with decreasing pressure, which necessitates the increasing of the potential to provide sufficient electrons from α and secondary processes to maintain the discharge. Therefore, the observed coincidence is to be expected.

The reason for the shift of the peaks to lower pressure values as the field is decreased is clear. The peaks are associated with the point of inflection in the α/p *vs.* X/p curve, then since X/p is well defined for this point, lowering the field requires a lowering of the pressure to keep X/p constant. A comparison of the location of the peaks confirms this exactly.

As the pressures are increased above those at which the peaks are observed, at each pressure a rapidly rising, approximately exponential curve is obtained. These curves are all of finite length, since they rise continuously until secondary processes leading to glow set in, at which point a discontinuity appears. The abrupt termination of the curves at lower fields are illustrated in

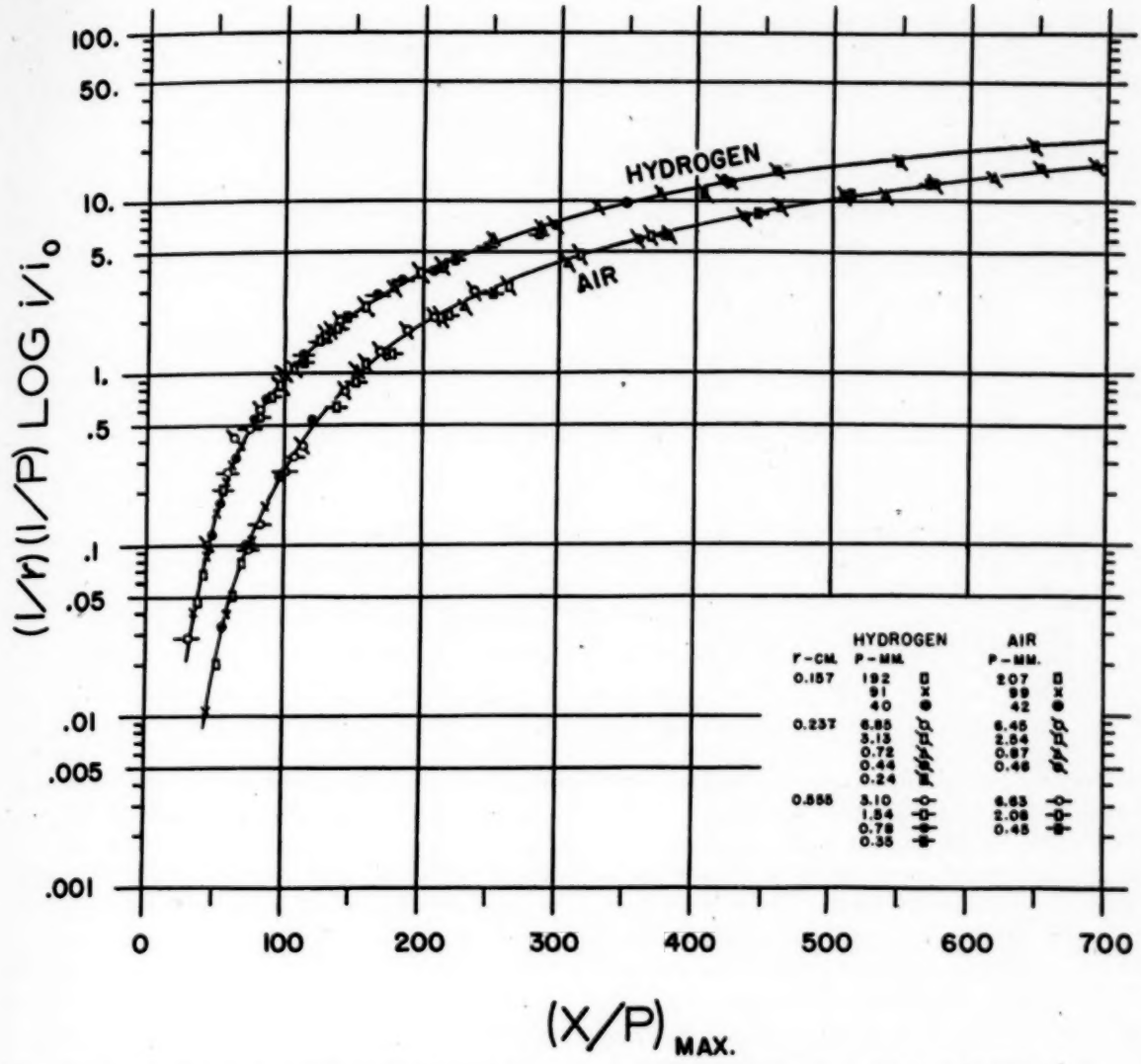

FIG. 6. Variation of electron multiplication parameter with field-to-pressure ratio at electrode surface. Purified hydrogen and dry, mercury-free air. High X/p values.

Fig. 7 at 450, 500, and 600 volts/cm and in Fig. 8 at 400, 500, 600, 750, and 1000 volts/cm. Although the values of X/p at which secondary processes set in were not precisely determined during the experiment, plots of such values as were obtained against pressure for air and hydrogen yield smooth curves. From these curves (Fig. 9) the termination point of each curve given in Figs. 7 and 8 can be obtained. Thus, the field for onset of secondary processes at each pressure can be determined or, conversely, the pressure at which onset would occur for a given field at the electrode surface. The results of Fig. 9 can be used to give orienting magnitudes only. Values of X/p at which breakdown occurs (taken from this graph) agree roughly with sparking potential values in air and hydrogen at atmospheric pressure.

Reversing potentials to release the electrons in the weak and to collect them in the strong field did not result in any change in the electron multiplication over the full pressure range in air. In hydrogen, at the lower pressure region in the vicinity of the peaks of the curves, there were some departures. This departure was to lower values of ionization and amounted to about 10 percent below the values obtained when the electrons were traveling in the reverse direction.

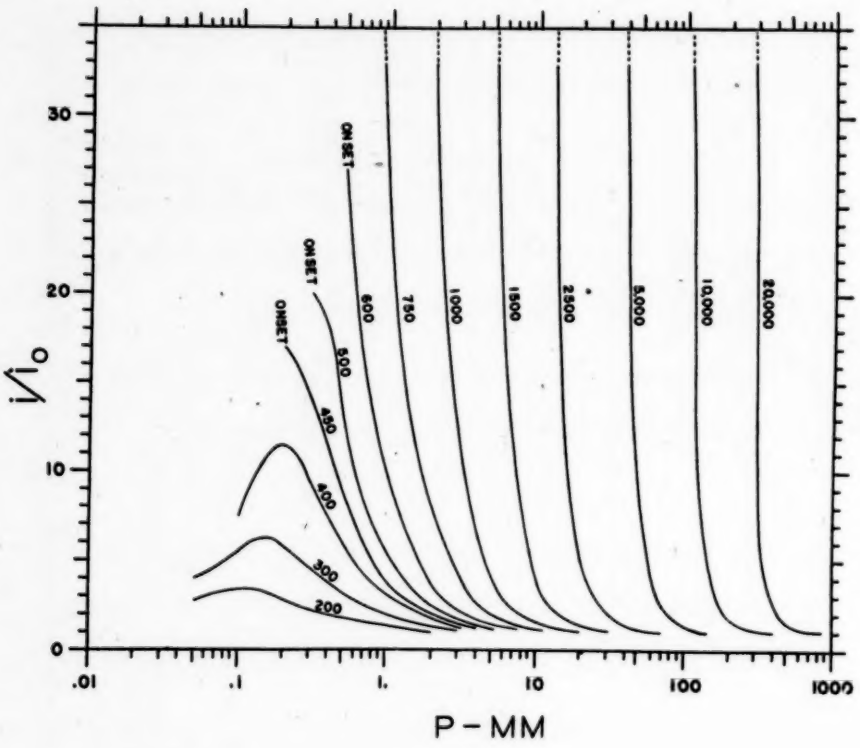

FIG. 7. Measured electron multiplication as a function of pressure at various surface field strengths. Fields in volts/cm. Smaller electrode radius—0.157 cm. Dry, mercury-free air.

The results for reversed potentials are represented by the dashed lines in Fig. 8.

Estimates of the location of ionization using the auxiliary anodes yielded the following results. Above a pressure of about 1 mm all of the ionization occurred within the smallest anode, so that no information on this point was available at the higher pressures. The results for lower pressures are given in Table II. The ionization is given in percent of the ionization observed for an inter-electrode space of 4.2 cm. It is noted that as the pressure is lowered below 1 mm, the ionization moves outward and, at least qualitatively, this confirms the distribution predicted by Morton[9] at these pressures.

The original purpose of the problem undertaken by Morton[9] and extended in the present research was to determine whether or not the physical quantity i/i_0, the electron multiplication, could be calculated from Townsend's integral using the uniform field value of α. In case the Townsend integral did not give the correct results, then the necessary corrections were to be evaluated.

Since the present results can be represented by continuous curves, i/i_0 is readily evaluated for any cylindrical electrode system in hydrogen and air in the indicated pressure ranges. Morton,[9] who was primarily interested in the low pressure region, determined i/i_0 as a function of applied potential and compared these values with the $e^{\int \alpha dx}$. Using a step-by-step approximation, Morton[9] showed that the Townsend integral did not yield proper values of i/i_0 in the low pressure region in which i/i_0 is increasing to a peak with increase of pressure (Figs. 7 and 8). The step-by-step procedure could not be carried out by Morton for the region of pressure beyond the peak since, with many collisions, the approximations used and the data needed were no longer valid. Morton, however, did observe that from the peak up to which his equation apply with increasing pressure the ionization fell until it merged with the predicted ionization obtained by the integration of Townsend's α, as seen in Figs. 5, 6, 7, and 8 of Morton's paper. This transition was to be expected. In order to determine the point of departure between Townsend's method and the observed results guided by his low pressure considerations, Morton logically attempted to find a value of "p" and, therefore, of field gradient over an electron-free path at

which this departure began. In doing so, he failed to note that he had passed out of the region of validity of field gradients, which is not surprising, considering the limited scope of his data. The present work was largely concerned with the higher pressure region and since it has been shown that $(1/r)(1/p)\log i/i_0$ is a function of $(X/p)_{max}$ alone for each gas, then it is apparent that the gradient of the field makes no significant contribution to the ionization in the pressure region above the peak.

Following the procedure used by Morton, an attempt was made to compare the higher pressure results with those of Townsend's by computing the value of $e^{\int \alpha dx}$ and noting the ratio between the Townsend calculations and the current results, attempting to correlate, as did Morton, the point of departure with a field gradient. The peculiar character of the relations obtained led Dr. Joseph Weinberg, by private communication, to call attention to the fact that the results following on the curves of Figs. 5 and 6 precluded any effect of field divergence, and that the procedure and this method of interpretation was inapplicable as indicated above. It was, however, desirable to compare the results of the present investigation with those of Townsend, but the results obtained in the attempt to integrate $\int^{\alpha dx}$ to make such comparison were discouragingly unsatisfactory, as existing data on α were not accurate enough to permit proper integration. Weinberg indicated that the best procedure would be to differentiate the curves of Figs. 5 and 6.

The results of the present investigation give the following functional relationship:

$$(1/r)(1/p)\log_e i/i_0 = f(X/p)_{max},$$

or

$$(1/p)\log_e i/i_0 = rf(X/p)_{max}. \tag{5}$$

Now, the Townsend integral gives

$$(1/p)\log_e i/i_0 = \int (\alpha/p)dx = \int g(X/p)dx. \tag{6}$$

The right-hand members of (5) and (6) are equal for a particular value of r, call it x_0. The limits of the integral then are x_0 and ∞. Let us remember now that $g(X/p) = \alpha'/p$, where α' is the equivalent α. Equating (5) and (6),

$$x_0 f(X/p)_{max} = \int_{x_0}^{\infty} g(X/p)dx. \tag{7}$$

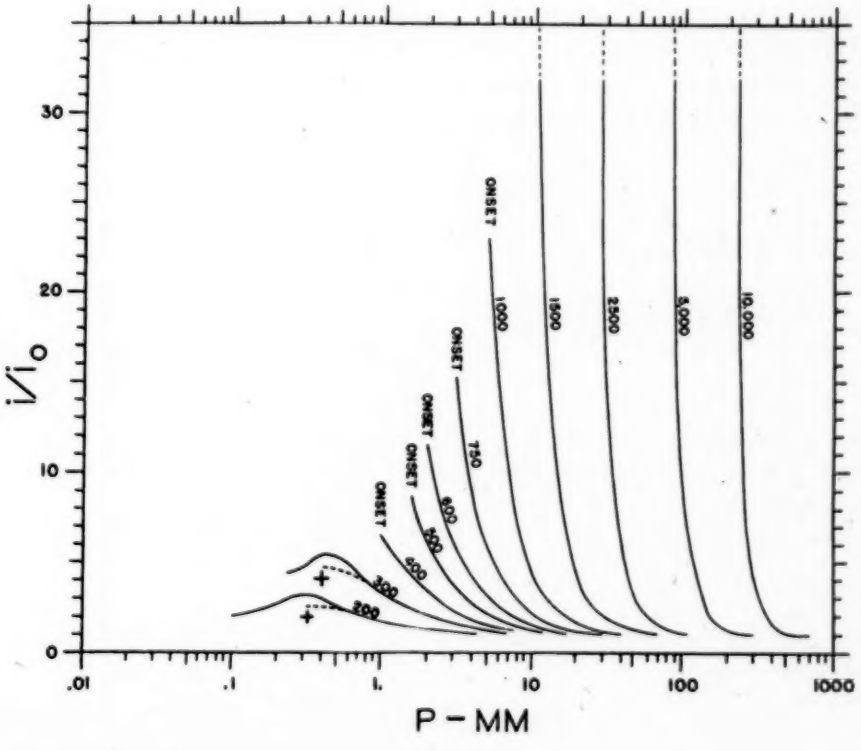

FIG. 8. Measured electron multiplication as a function of pressure at various surface field strengths. Fields in volts/cm. Smaller electrode radius—0.157 cm. Purified hydrogen.

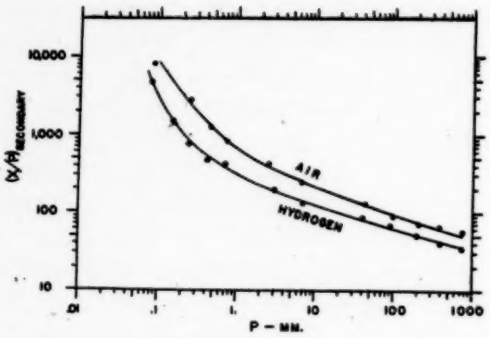

FIG. 9. Dependence of field to pressure ratios at electrode surface for onset of secondary processes on pressure for purified hydrogen and for dry, mercury-free air.

Now let us make the following substitutions:

$$z=X/p=(z_0x_0)/x, \quad dx=-z_0x_0dz/z^2,$$

where $z_0=(X/p)_{max}$. Equation (7) becomes then

$$x_0f(z_0)=\int_0^{z_0}\frac{z_0x_0}{z^2}g(z)dz. \tag{8}$$

Since z_0x_0 is a constant in the integration, we have

$$\frac{f(z_0)}{z_0}=\int_0^{z_0}\frac{g(z)}{z^2}dz. \tag{9}$$

Differentiating with respect to z_0, remembering that the integrand must vanish at the lower limit, since the ionization is zero at that point,

$$-f(z_0)/z_0^2+f'(z_0)/z_0=g(z_0)/z_0^2,$$

or

$$g(z_0)=z_0f'(z_0)-f(z_0). \tag{10}$$

Putting in the substituted values for z_0 we have

$$\frac{\alpha'}{p}=(X/p)_{max}\frac{d[(1/r)(1/p)\log i/i_0)]}{d(X/p)_{max}}-(i/r)(1/p)\log i/i_0. \tag{11}$$

By graphical differentiation of the curves of Figs. 5 and 6 and application of Eq. (11) we get values of α'/p. The results of such calculations together with the results of Hale[8] for hydrogen and Bowls[7] for nitrogen are given in Tables III and IV. The comparison of α'/p for air with Bowls α'/p values for mercury-free nitrogen indicate the results for air are about 20 percent higher than the values for nitrogen up to $(X/p)_{max}$ of 400 which could be within experimental error. Above $(X/p)_{max}$ of 400, there is a rapid increase of α'/p of about 80 percent over the α/p values for nitrogen. The disparity between α'/p and α/p decreases at the highest $(X/p)_{max}$ values, probably indicating that some of the electrons are crossing the gap without loss of all of their ionizing energy, or it may be because the data in this region lie below the peak with decreasing pressure.

The α'/p values for hydrogen are higher than the α/p values of Hale over most of the range of $(X/p)_{max}$ used. At high $(X/p)_{max}$ the difference decreases which, as in the case of air, may have the same explanation. There is observed no sudden increase in α'/p, although it might be expected to appear at about $(X/p)_{max}$ of 100. How much of this discrepancy may be attributed to observational inaccuracy in both Hale's and the calculations from these data, cannot be estimated. The character of the deviations noted in the differentiated curves in comparison to the Townsend theory show the same unsatisfactory condition at the extremities which appeared to falsify the integrated curves. It is, however, clear that in both gases at some value $(X/p)_{max}$ there is a marked deviation from the conventional Townsend values in the direction which might be expected from the considerations laid down at lower pressures by Morton.

Thus, the qualitative explanation of the sudden increase in ionization at $(X/p)_{max}$ of 400 and the high values for hydrogen over the observed range is given in the following for a divergent field. For a given divergence of the field as the field increases, the electrons are accelerated at greater rates and therefore spend less time at low energies. Hence, losses to excitation and inelastic impacts are reduced, and the electrons enter the low field region with more energy. This energy is lost mostly to ionization and the observed ionization is greater than is given by the Townsend equation.

TABLE II. Ionization in air and hydrogen at lower pressures.

Air		Hydrogen	
p mm	% ionization within 1.27 cm	p mm	% ionization within 1.27 cm
0.1	20	0.20	0
0.29	60	0.31	60
0.77	90	0.69	80

TABLE III. Comparison of values of α'/p the apparent α/p, for dry, mercury-free air with the Bowls values of α/p for nitrogen.

Air			
$(X/p)_{max}$	α'/p	$(\alpha/p)_{Bowls}$	$(\alpha'/p)/(\alpha/p)_{Bowls}$
60	0.127	0.17	0.75
80	0.33	0.28	1.17
100	0.60	0.46	1.30
200	2.53	2.00	1.26
300	3.50	3.40	1.03
400	5.15	4.35	1.18
500	7.7	5.15	1.50
600	9.8	5.80	1.69
700	12.0	6.5	1.85
800	12.2	7.2	1.70
900	12.0	7.5	1.60
1000	12.0	7.6	1.58

TABLE IV. Comparison of values of α'/p, the apparent α/p, for hydrogen with Hale's values for hydrogen.

X/p	α'/p	$(\alpha/p)_{Hale}$	$(\alpha'/p)/(\alpha/p)_{Hale}$
30	0.057	0.080	1.40
35	0.106	0.100	1.06
45	0.266	0.170	1.57
60	0.52	0.31	1.68
100	1.06	0.71	1.50
200	3.60	1.95	1.85
300	5.00	3.30	1.52
400	6.00	4.30	1.40
500	5.90	5.05	1.17
600	6.00	5.80	1.03

The fact that the ionization is greater than that given by Townsend's equation when the electrons travel from low to high fields, i.e. in a convergent field, may be explained in the following manner. Electrons released in the low field region traverse a relatively long distance in low fields and, therefore, lose relatively large amounts of energy to excitation and inelastic impacts. However, as the electrons approach the high field region, they assume higher energies and when they get near the anode, instead of being captured immediately, may spend considerable time at high energy in the vicinity of the anode before capture because of their high diffusive velocities. This will result in a large amount of ionization. Thus, despite the dissipation of energy in the low field region, the ionization in this case also turns out to be greater than that given by Townsend. The observed ionization for the convergent field case over most of the pressure range studied was the same as that for divergent fields, but at lower pressures the ionization in the convergent case was about ten percent less as would be expected. The surprising fact is that the high diffusive motion of the electrons in the converging fields makes the ionization observed so nearly the same as for the divergent field.

It might be anticipated with the greater loss of energy in the low field region and the probability of being picked up at the anode, that the convergent electrons, in general, would produce less ionization than the divergent ones. However, in the weaker field regions the amount of ionization for either positive or negative point is small, and the divergence of the results from this source would be inappreciable. In the higher field regions one would expect the loss of electrons to the anode to produce considerable difference. At higher pressures where many molecules are present in the high field region, great diffusion at high energy apparently diminishes the loss to the anode. At lower pressures in the high field regions this would not be true; thus, the further one gets into the Morton regime with high divergence and low pressures, the greater would be the anticipated difference between convergence and divergence. This is in accordance with observation but, because of the complexity of the phenomena involved, is not amenable to quantitative analysis.

Morton[9] showed at low pressures that the electron energies were higher than would be expected from the equilibrium type of ionization characteristic of the Townsend regime. The ionization in the Morton regime at first increases outward from the cathode, while in the Townsend regime the ionization is a maximum at the cathode as shown in Fig. 9 of Morton's[9] paper. In the region of the present experiments, one is between Morton's region and the Townsend region. Thus, the distribution of ionization in space in the region between the peak of the curve of Figs. 7 and 8 and the high pressure limit will lie between that predicted by the two theories with some ionization close to the cathode and an appreciable fraction well beyond the cathode. These factors will lead to changes in interpretation of discharge phenomena in regions which show departures from those characterized by Townsend's integral. In particular, the higher rates of diffusion in the Morton regime and the

type of ionization resulting might have some effect on the streamer mechanism of Loeb and Meek and of Raether. Because of the short time intervals required for propagation, the effect of this increased diffusion may not be too important.

The parametric expression found to express the electron multiplication in the present work involves a term in $(1/r)$, which was shown to be approximately proportional to the field at the electrode surface for a given applied potential. Since it appears to be the maximum field and not the gradient that enters the expression, it might be expected that the results of this investigation might be applied successfully to other geometries. A ready check was found possible through a comparison of the present results with those of Fisher and Weissler.[10]

A direct comparison of the results of Fisher and Weissler[10] with the present results was not possible since they did not evaluate i_0, the determination of which would be complicated by the fact that the back diffusion is not known for a confocal paraboloid system. However, a check is possible through a comparison of their results with the present ones in the following manner. The present work established the following general relationship,

$$(1/r)(1/p)\log i/i_0 = f(X/p)_{\max}, \qquad (12)$$

where the analytic form of the function was not determined but values of it may be taken from the empirical curves of Figs. 5 and 6.

Rearranging Eq. (12) we have

$$\log i - \log i_0 = rpf(X/p)_{\max}. \qquad (13)$$

For a given r and p, then, one can get two equations by substitution of two values of i and the corresponding $f(X/p)_{\max}$ values from the empirical curves in Eq. (13). When these are solved simultaneously we have

$$\log i_1 - \log i_2 = rp[f(X_1/p)_{\max} - f(X_2/p)_{\max}]. \qquad (14)$$

If Eq. (14) is satisfied by the results of Fisher and Weissler[10] for some constant value of r, then it can be assumed that f has the same form for confocal paraboloids as in the present case. If r turns out to be some characteristic parameter of the paraboloid system, then the empirical curves obtained in the present investigation are applicable. It is tacitly assumed in Eq. (14) that i_0 is independent of the applied field, i.e., the back diffusion effects are sensibly constant for the limited ranges of field used.

Using the values of i, p, and $(X/p)_{\max}$ given by Fisher and Weissler[10] and the corresponding values of $f(X/p)_{\max}$ from the present investigation, a series of rp values were calculated at each pressure by means of Eq. (14). At each pressure the rp values were constant to 10 percent, which then indicates that $f(X/p)$ is of the same form for the two systems under consideration. From the mean value of rp at each pressure, a value of r was obtained with the following results:

p mm	r cm
676	0.0037
616	0.0045
548	0.0041
477	0.0045
408	0.0044

The constancy of the values of r is striking. Now the focal length of the point used by Fisher and Weissler[10] was reported as 0.005 cm. The agreement between this value and the values of r given above suggest strongly that the results of the present investigation may be applied to the confocal paraboloid system by substitution of the focal length of the smaller electrode for r of the present investigation. The error which might be introduced by this procedure would not be greater than 10 percent.

The field at the surface of a paraboloid in a confocal system is given by

$$X = V/(x+f)\log(f/F), \qquad (15)$$

where f is the focal length of the point parabola, F is the focal length of the plate parabola, and x is the distance from the point parabola to the point of interest in the field. Thus, for a given system the field falls off in the same manner as in the cylindrical electrode system, that is, inversely as a distance from a fixed point. For cylinders, this point lies in the axis of the system, and for paraboloid systems it is the focal point of the point parabola. The agreement of the results then, perhaps, is not surprising since the variation of the field is of the same form in the two cases, although one is essentially a two-dimensional and the other a three-dimensional

system. A conclusive test of the general applicability of the present functions would be available through an experimental study of the concentric spherical system where the field is an inverse square function of the radius.

The writer is indebted to Professor L. B. Loeb for suggestion of the problem, and, for stimulation and assistance throughout the research, to Professor Loeb and members of his seminar. The writer is also grateful to the Research Corporation of New York whose fellowship grant made this work possible.

PHYSICAL REVIEW VOLUME 73, NUMBER 4 FEBRUARY 15, 1948

Theory of High Frequency Gas Discharges. I. Methods for Calculating Electron Distribution Functions[1, 2]

H. MARGENAU
Yale University, New Haven, Connecticut

(Received August 18, 1947)

After a brief summary of the "free-electron" theory of a.c. currents in gases, which is shown to be inadequate for microwaves, methods for calculating distribution functions for electrons with consideration of all types of collisions are developed and discussed. Conditions are specified under which non-elastic collisions may be introduced as integral and as differential expressions in the Boltzmann transfer equation. In Section VI this equation is solved approximately and the differences between direct current and h.f. current discharges are pointed out. Finally, Section VIII is concerned with an aspect of what is usually called Paschen's law; it indicates that a minimum should exist in the graph of voltage *vs.* pressure, and of voltage *vs.* frequency, both at constant current. This minimum comes when the frequency of the field is of the order of magnitude of the collision frequency of the electrons.

THIS series of papers presents a study of what happens when a gas at low pressure becomes conducting under high frequency electromagnetic waves. While the precise meaning of the term "high frequency" is defined in Article II, it will usually refer to situations in which the frequency of the electromagnetic waves is comparable with the frequency of collisions between free electrons and gas atoms.

Although one's first impression is to the contrary, such microwave discharges are probably less complicated with regard to the physical processes which they involve, and therefore possibly more instructive, than direct current discharges. This is true primarily because conditions can be arranged under which ionization occurs predominantly in the body of the gas, and secondary processes at the electrodes and at the walls of the discharge chamber are of lesser importance. In addition to this simplifying aspect, it is proper to assume that the gas acquires no net volume charge, its condition being similar to a d.c. plasma. Diffusion of electrons, being ambipolar, will be slow; it can, in a certain range of gas pressures, be made the dominant mechanism for the disposal of electrons. In another pressure range it can be made subordinate to volume recombination, permitting this mechanism to be studied.

Unfortunately, theory enjoys in this field at present the large amount of liberty that always goes with a scarcity of experimental data. The subject is new and measurements are difficult. Checks on assumptions are imposed only by comparison with known analogous situations in d.c. discharges, and with the few facts now available. But to show what theory can do is perhaps not wholly useless in advance of experimentation, since the experimenter may be aided

[1] The contents of this paper form part of Radiation Laboratory Report No. 967; they are based on work done for the Office of Scientific Research and Development under Contract OEMsr-262 with the Massachusetts Institute of Technology.

[2] Some of the developments in this paper are parallel to the work of T. Holstein, Phys. Rev. 70, 367 (1946). It is hoped that the difference in approach justifies the inclusion of those portions of the present paper which are already dealt with in Holstein's publication.

by knowing what kind of measurements are, and what are not, theoretically interesting.

The first article contains a development and summary of methods for calculating the energy distribution of electrons in a discharge, as a function of field strength, frequency of the field, and gas pressure. The effect of different physical processes on the shape of the distribution function will be investigated, but the work is based on the assumption that this function departs very little from being isotropic in the velocity space of the electrons and has the periodicity of the impressed electric field.

In Article II these assumptions are scrutinized and the physical conditions are determined under which various possible forms of the distribution function are usable approximations. This is done with neglect of inelastic collisions. The results enable one to set limits depending upon field strength, frequency, and gas pressure, beyond which customary formulas fail.

One of the methods discussed in the present paper is developed in Article III for the purpose of calculating the breakdown potential in a gas filling an infinite region, so that direct recombination is the only process which disposes of electrons, and volume ionization is assumed to be the only mechanism producing them. While it is difficult to define the meaning of a sharp breakdown potential, it does turn out that the number of electrons per unit volume rises quite suddenly at a certain field strength; the value of this more or less critical field strength is smaller than the breakdown fields which have been measured (in finite enclosures). The difference can be ascribed to other disposal mechanisms, such as diffusion of electrons to the walls of the vessel.

In Article IV some general consequences respecting current voltage characteristics of a.c. discharges are discussed, and attention is drawn to the form which the similarity principle, known from d.c. work, takes under conditions of microwave excitation.

I. FREE ELECTRONS IN ALTERNATING FIELDS

For the sake of orientation we first sketch the results of the simple theory[3] of electrons in an alternating field, a theory which neglects collisions. An electron, born with zero velocity at time t' and under the action of the field $Ee^{i\omega t}$ along the x-axis, has a velocity

$$\dot{x}=\frac{ieE}{m\omega}(\exp(i\omega t')-\exp(i\omega t)),$$

and hence a maximum velocity

$$v=\frac{eE}{m\omega}|1\mp\sin\omega t'|.$$

This is reached at $t=\pm\pi/\omega$, when the field reverses its direction. Electrons born at these instants will reach greater speeds than the others since the field has an entire half-period to accelerate them. The maximum speeds of these electrons are

$$v_{\max}=2eE/m\omega=0.94\times10^{7}E/\nu \text{ e-volts}, \quad (1)$$

if E is in volts/cm and ν is the frequency of the field. According to this formula, E must be of the order of 10,000 volts/cm in the microwave region ($\nu\approx10^{10}$/sec.) if an electron is to attain ionizing velocities.

The displacement is

$$x=\frac{eE}{m\omega^2}(1+i\omega t\cdot\exp(i\omega t')-\exp(i\omega t)).$$

It corresponds to an oscillation of amplitude

$$x_0=eE/m\omega^2=0.44\times10^{14}E/\nu^2 \text{ cm}, \quad (2)$$

if E is expressed in volts/cm; this oscillation is superposed on a drift with velocity $(eE/m\omega)\times\sin\omega t'$.

For microwaves at ionizing field strengths as given by Eq. (1)

$$x_0\approx10^{-2} \text{ cm}. \quad (3)$$

The mean current density $ne\langle\dot{x}\rangle_{\text{av}}$, the average being taken over all t', is

$$J=-(ine^2E/m\omega)e^{i\omega t}.$$

It is in quadrature with the field and yields the well-known conductivity

$$J/Ee^{i\omega t}\equiv\sigma=-ine^2/m\omega.$$

The conditions under which this simple theory is applicable are these: (a) the frequency of the

[3] G. Mierdel, Ann. d. Physik **85**, 612 (1928); K. K. Darrow, Bell Sys. Tech. J., XI, 576 (1932); XII, 91 (1933); L. B. Loeb, *Fundamental Processes of Electrical Discharge in Gases* (J. Wiley and Sons, Inc., New York, 1939).

waves, ν, must be much greater than the collision frequency, ν_{coll}; (b) x_0 must be much smaller than the mean free path, λ, of the electrons. Using kinetic-theory expressions for λ and ν_{coll}, these conditions become:

$$x_0 \ll 1/Nq, \tag{a}$$

$$\nu \gg Nq\bar{v}, \tag{b}$$

provided N is the number density of gas molecules, q their collision cross section, and $\bar{v}$ their mean velocity. At a pressure of 1 cm Hg, $(Nq)^{-1}$ is about 10^{-2} cm; hence the value given by Eq. (3) violates condition (a). At electron speeds prevailing in a discharge $Nq\bar{v}$ is about 10^{10} sec.$^{-1}$; hence microwave frequencies violate condition (b).

The simple theory here sketched is therefore inadequate to provide information about microwave discharges.

II. COLLISIONS AND THEIR EFFECT ON THE DISTRIBUTION FUNCTION

To take account of collisions it is necessary to introduce a distribution function, f, whose value is the number of electrons having velocities about $\mathbf{v}$ and enclosed in a volume about $\mathbf{r}$ at time t. It is a function of $\mathbf{r}$, $\mathbf{v}$, t and will be normalized so that

$$\int\int f(\mathbf{v}, \mathbf{r}, t) d\mathbf{v} d\mathbf{r}$$

is the total number of electrons present, and

$$\int f(\mathbf{v}, \mathbf{r}, t) d\mathbf{v} = n(\mathbf{r}, t) \tag{4}$$

the number density of electrons. If n is not a function of t, the state represented by f is said to be steady; if f is not a function of $\mathbf{r}$, the distribution is uniform; if f is a function only of $|\mathbf{v}|$, it is isotropic.

The Boltzmann transfer equation,[4] together with certain physical conditions, determines the distribution function. It reads

$$\partial f/\partial t + \mathbf{v} \cdot \nabla f + \mathbf{a} \cdot \nabla f = \delta f/\delta t. \tag{5}$$

Here $\partial f/\partial t$ is the smooth local rate of change, while $\delta f/\delta t$ represents the rate of change occasioned only by collisions, but by all collisions, elastic and inelastic, including those which result in ionization or capture. The symbols $\mathbf{v}$ and ∇ denote, respectively, the gradients in $\mathbf{r}$-space and in $\mathbf{v}$-space.

The presence of the term $\delta f/\delta t$, which makes the value of f at $\mathbf{v}$ depend on the number of electrons at very different velocities, marks Eq. (5) as a partial differentio-integral equation, for which no general method of solution is known. Even explicit evaluation of $\delta f/\delta t$ is possible only with the use of specific assumptions concerning the collisions as well as the form of the distribution function. As to the latter, we suppose for the present that f does not depart much from being isotropic, and that the small non-isotropic part has the spatial symmetry of the field. Let us also at first assume a uniform density of electrons (thus disregarding diffusion). Then

$$f(\mathbf{v}) = f^{(0)}(v) + v_x \phi(v) \tag{6}$$

and ϕ is presumably small. The term $\delta f/\delta t$ now consists of two parts, $\delta f^{(0)}/\delta t$ and $\delta(v_x\phi(v))/\delta t$, and these require separate treatment in detail.

The general formula for $\delta f/\delta t$, well known from kinetic theory, is obtained as follows. Different types of collision (such as elastic, or causing excitation of molecules between a given pair of levels, or ionizing, and so forth) of which an electron is capable will be labeled by an index μ.[5] Collisions of one electron with another are here disregarded as unlikely. If we denote by $\mathbf{v}_\mu'$ the velocity before encounter of an electron which is about to suffer a collision of type μ, and which after collision will have velocity $\mathbf{v}$, the rate of *increase* of electrons at $\mathbf{v}$ is given by

$$v_\mu' N q_\mu(\mathbf{v}_\mu') f(\mathbf{v}_\mu') d\mathbf{v}_\mu'. \tag{7}$$

To see this, we recall that $v_\mu' \lambda_\mu^{-1}$, λ_μ, representing the mean free path for a collision of type μ, is the number of μ-encounters made by one electron of speed v_μ' per second, and that

$$N q_\mu \lambda_\mu = 1 \tag{8}$$

[4] S. Chapman and T. G. Cowling, *The Mathematical Theory of Non-Uniform Gases* (Cambridge University Press, New York, 1939), Chapter 3; P. M. Morse, W. P. Allis, and E. S. Lamar, Phys. Rev. **48**, 412 (1935).

[5] Collisions of unspecified type will be labeled by the index μ; elastic collisions by e, inelastic (but non-ionizing) by s, ionizing by i. Similar indices will be used on cross sections (q_e etc.) and mean free paths (λ_e etc.).

is the general relation connecting N, the number of gas molecules per cm^3, and q_μ, the cross section for a μ-encounter, with the mean free path. The rate of decrease of electrons at $\mathbf{v}$ is due to collisions which lead from $\mathbf{v}$ to some lower velocity, with cross section q_μ; it is given by an expression similar to (7). Hence

$$(\delta f/\delta t)d\mathbf{v} = N\sum_\mu v_\mu' q_\mu(\mathbf{v}_\mu') f(\mathbf{v}_\mu') d\mathbf{v}_\mu' - N\sum_\mu v q_\mu(\mathbf{v}) f(\mathbf{v}) d\mathbf{v}. \quad (9)$$

If the form of f which was assumed in Eq. (6) is substituted into this formula, the collisional rate of increase of f is obtained. But of the two terms in Eq. (6), the second is much the easier to compute and will be considered first.

We have

$$\frac{\delta}{\delta t}[v_x\phi(v)]d\mathbf{v} = N\sum_\mu v_\mu' q_\mu(\mathbf{v}_\mu') v_{\mu x}'\phi(v_\mu') d\mathbf{v}_\mu' - Nvv_x\phi(v)d\mathbf{v}\sum_\mu q_\mu(\mathbf{v}).$$

The last summation is the total collision cross section q, which by (8) is $(N\lambda)^{-1}$. The remaining summation over μ in the first term on the right includes an integration over all orientations of the vector $\mathbf{v}_\mu'$. This will not be zero if q_μ depends on the orientation of $\mathbf{v}_\mu'$. However, if this is not the case, that is, if the cross section is isotropic, the only term affected by this integration is $v_{\mu x}'$, and it yields zero. Isotropy of collisions will now be assumed, so that we may write

$$\frac{\delta}{\delta t}[v_x\phi(v)] = -\frac{vv_x}{\lambda}\phi(v). \quad (10)$$

We now turn to the calculation of $\delta f^{(0)}/\delta t$, which, in view of Eq. (9), is given by

$$\frac{\delta f^{(0)}}{\delta t}\cdot 4\pi v^2 dv = N\sum_\mu v_\mu' q_\mu f^{(0)}(v_\mu') 4\pi v_\mu'^2 dv_\mu' - N\sum_\mu v q_\mu f^{(0)}(v)\cdot 4\pi v^2 dv. \quad (11)$$

III. ELASTIC COLLISIONS

The relation between v' and v, needed in evaluating (11), is different for elastic and inelastic collisions. The characteristic feature of an elastic one is that the electron loses, on the average over all encounters, a small and constant *fraction* of its original energy or speed, while in an inelastic collision the actual *amount* of energy lost is prescribed. Thus for an elastic encounter,

$$v' = (1+m/M)v \quad (12)$$

provided the molecules, whose mass is M, are effectively at rest, and m is the mass of an electron. The approximation of treating all elastic collisions as belonging to a single type, which involves always the average loss of speed, is made valid by the smallness of each loss.

Equation (11) now reduces to the form

$$v^2\left.\frac{\delta f^{(0)}}{\delta t}\right|_e = \frac{N}{v}[v'^4 q_e(v') f^{(0)}(v') - v^4 q_e(v) f^{(0)}(v)] = \frac{N}{v}\frac{d}{dv}(v^4 q_e f^{(0)})(v'-v).$$

On using (12), we thus obtain

$$\left.\frac{\delta f^{(0)}}{\delta t}\right|_e = \frac{m}{M}\cdot\frac{N}{v^2}\frac{d}{dv}[v^4 q_e f^{(0)}]. \quad (13)$$

If account is taken of the velocity distribution of the molecules, this relation is replaced by

$$\left.\frac{\delta f^{(0)}}{\delta t}\right|_e = \frac{m}{M}\cdot\frac{N}{v^2}\left\{\frac{d}{dv}[v^4 q_e f^{(0)}] + \frac{kT}{m}\frac{d}{dv}\left[v^3 q_e \frac{df^{(0)}}{\mu dv}\right]\right\} \quad (13')$$

as is shown by Chapman and Cowling,[4] pp. 348 ff. The added term, which needs to be introduced in order that the vanishing of $\delta f^{(0)}/\delta t|_e$ shall yield a Boltzmann distribution for $f^{(0)}$, is not exact under discharge conditions. For the most part in this work, it will be regarded as correct in order of magnitude; it may usually be neglected.

IV. NON-ELASTIC COLLISIONS; INTEGRAL REPRESENTATION

This section contains some modifications and a slight extension of the work of Smit[6] and of Chapman and Cowling,[4] Chapter 18. Consideration will be given not only to inelastic collisions, but also to impacts which result in ionization, capture, and so forth. Assume that an ordinary inelastic collision of type s causes the electron

[6] J. A. Smit, Physica **3**, 543 (1937).

to lose an amount of energy equal to $\epsilon_s = \frac{1}{2}mu_s$. In the evaluation of the terms of Eq. (11) which correspond to this collision, we must then put

$$v_s'^2 = v^2 + u_s, \quad v_s' dv_s' = v dv,$$

and the contribution of the collision to that equation is

$$4\pi v dv \left[\frac{f^{(0)}(v_s^0) v_s'^2}{\lambda_s(v_s')} - \frac{f^{(0)}(v) v^2}{\lambda_s(v)} \right]$$

again in view of Eq. (8). But this expression can be written as $(dS_s/dv)dv$ provided the function S_s is defined by

$$S_s(v) = \int_v^{v_s'} \frac{v}{\lambda_s(v)} f^{(0)}(v) \cdot 4\pi v^2 dv. \qquad (14)$$

It represents the rate of increase in the concentration of electrons having speeds below v. In terms of the variable $u = v^2$

$$S_s(u) = 2\pi N \int_u^{u+u_s} f^{(0)}(u) \cdot q_s(u) \cdot u du. \qquad (14')$$

We note that $S_s(\infty) = 0$. If $S = \sum_s S_s$, Eq. (11) can be written

$$\frac{\delta f^{(0)}}{\delta t} = \frac{1}{4\pi v^2} \frac{dS}{dv} + \left. \frac{\delta f^{(0)}}{\delta t} \right|_s.$$

To calculate S, one would have to know the function $f^{(0)}$ in advance; i.e., the use of Eq. (14) would convert the transfer equation into an integro-differential equation. There may be situations, however, in which the physical significance of S leads to a fairly reasonable conjecture as to the form of this function and where this may be used as a starting approximation in the calculation of $f^{(0)}$. A way of doing this is suggested by Chapman and Cowling. An attempt was made in the present investigation to assume a flexible form for $f^{(0)}$ which contained two adjustable parameters, then to compute S, and finally to fix the parameters so as to achieve self-consistency for the solutions of the transfer equation. But the results were not encouraging, even when ionizing collisions were neglected.

A different situation arises when collisions are included in which electrons are produced or captured. To take account of ionization, for example, the first summation on the right of Eq. (11) must be doubled because every ionizing electron of speed v' produces two electrons. Furthermore, to specify v', an assumption regarding the division of energy available to the two electrons after ionization must be made. To say that it is divided equally seems not far from the truth. We may therefore take

$$v_i'^2 = 2v^2 + u_i, \quad v_i' dv_i' = 2v dv,$$

u_i being the ionization "energy" of the atom or molecule. Instead of (11) we then have

$$\left. \frac{\delta f^{(0)}}{\delta t} \right|_i \cdot 4\pi v^2 dv = 2\pi du [4N q_i(u_i') f^{(0)}(u_i') \cdot u_i' - N q_i(u) f^{(0)}(u) \cdot u]$$

provided q_i is the ionization cross section. If this is to be written in the form $dS_i(u)$, S_i must have the form

$$S_i(u) = 2\pi N \left\{ 2 \int_u^{u_i'} f^{(0)} \cdot q_i \cdot u du + \int_0^u f^{(0)} q_i u du \right\}. \qquad (15)$$

The significance of the two integrals occurring here is clear: the first accounts for the two electrons produced at energies below u by ionizations with the energy of the ionizing electron above u; the second for the one additional electron created by ionizations below u. Thus, $S_i(\infty)$ is not zero; it becomes in fact

$$2\pi N \int_0^\infty f^{(0)} q_i u du.$$

The case of capture can be dealt with in a similar way. The total S, defined as the sum of all S_s, S_i, and S_c, must vanish at infinity if the number of electrons in the discharge is to be constant. In Article III, Mr. L. M. Hartman has applied the analysis of this section to the calculation of breakdown potentials in He and Ne under certain conditions.

V. NON-ELASTIC COLLISIONS; DIFFERENTIAL REPRESENTATION

Instead of dealing with each type of non-elastic collision individually, as in the preceding section, we now treat the extreme case in which there

are so many different kinds of inelastic encounters that the index s in Eq. (11) may be regarded as a continuous variable. To simplify matters further, ionization and electron removal will be included among the ordinary inelastic collisions, no account being taken of the effect of "number" production and destruction upon the distribution function.

As before, $v_s'dv_s'=vdv$, and Eq. (11) takes the form

$$\frac{\delta f^{(0)}}{\delta t}=\frac{N}{v}\Big\{\sum_s u_s' q_s(u_s') f^{(0)}(u_s') - uf^{(0)}(u)\sum_s q_s(u)\Big\} \quad (16)$$

so far as *inelastic* collisions are concerned. As will be clear later (see Eq. (28)), if the transfer equation is to reduce to an ordinary second-order differential equation, the right-hand side of (16) must be transformable to

$$\frac{N}{v}\frac{d}{du}\Big\{X(u)\int_u^\infty Y(u,t)f^{(0)}(t)dt\Big\}. \quad (17)$$

Here X and Y are arbitrary functions, at present unknown. But (16) is thus transformable only if certain rather special assumptions are made concerning the cross sections q_s. Two fairly obvious assumptions leading to solutions will here be studied.

The cross section $q_s(u_s')$ is a function of two variables: the initial "energy" u_s' and the final energy u. We therefore put

$$q_s(u_s')=q(u_s', u). \quad (18)$$

But initial and final energy of the electron are not useful variables in terms of which to specify the probabilities of transitions; it seems preferable to use the energy *loss* together with the final (or the initial) energy, because energy loss, i.e., the difference between two molecular energy levels, is more significant in the description of transitions.

Let us therefore characterize a process s by the loss of "speed" $u_s'-u\equiv p$, and let p be a continuous variable. Then

$$q(u_s', u)=A(p, u)\delta(u_s', u+p)du_s'dp, \quad (19)$$

where δ is Dirac's singular function. The summation over s in Eq. (16) then turns into an integration over u_s' and p.

The function $q_s(u)$ is constructed by analogy with (19);

$$q_s(u)=q(u, u_s'') =A(p, u_s'')\delta(u_s'', u-p)du_s''dp. \quad (20)$$

One may then write in place of (16), after integrating over u_s' and u_s'',

$$\frac{\delta f^{(0)}}{\delta t}=\frac{N}{v}\Big\{\int_0^\infty (u+p)A(p, u)f^{(0)}(u+p)dp - uf^{(0)}(u)\int_0^u A(p, u-p)dp\Big\}, \quad (21)$$

if it is remembered that A vanishes when its second argument is negative.

A given value of p characterizes a molecular transition; the probability of its occurrence is a function of u. Hence $A(p, u)$ is factorable,

$$A(p, u)=A_1(p)A_2(u),$$

and

$$\frac{\delta f^{(0)}}{\delta t}=\frac{N}{v}\Big\{A_2(u)\int_u^\infty tA_1(t-u)f^{(0)}(t)dt - uf^{(0)}(u)\int_0^u A_1(t)A_2(u-t)dt\Big\}. \quad (22)$$

To see under what conditions this can be expressed in the form (17) we expand that quantity, taking Y to be $tA_1(t-u)$, and obtaining

$$\frac{N}{v}\Big\{X'(u)\int_u^\infty tA_1(t-u)f^{(0)}(t)dt - X(u)uA_1(0)f^{(0)}(u) - X(u)\int_u^\infty tA_1'(t-u)f^{(0)}(t)dt\Big\}. \quad (23)$$

If this is to be identical with (22), it is seen, first of all, that A_1' must be zero. Therefore, the scheme works only if we take $A_1(p)$ to be a constant, which would imply that every pair of molecular levels has the same intrinsic transition probability. The present method thus limits our consideration to artificial physical situations, which are perhaps approximated in complicated molecules having a great number of excitable levels.

To make Eqs. (22) and (23) agree no further conditions need be imposed, but one must take

$$X'(u)=A_2(u).$$

This causes both the remaining terms in (22) and (23) to become identical. The result is

$$\frac{\delta f^{(0)}}{\delta t}=\frac{N}{v}\frac{d}{du}\left\{\int_0^u A(t)dt\int_u^\infty tf^{(0)}(t)dt\right\},$$

where $A(t)$ is now written for $A_1A_2(t)$. But it is easily shown that $\int_0^u A(t)dt$ is the inelastic collision cross section which will here be written q since we are concerned only with inelastic encounters in this section of the paper. Hence,

$$\frac{\delta f^{(0)}}{\delta t}=\frac{1}{v}\frac{d}{du}\left\{\frac{1}{\lambda_s(u)}\int_u^\infty tf^{(0)}(t)dt\right\}. \quad (24)$$

Another workable method for evaluating the inelastic collision rate has been suggested by Bennett and Thomas.[7] Starting again with Eq. (18) we now put

$$q(u_s', u)=B(u', u)\delta(u_s', u')du_s'du'$$

and use a product function for $B(u', u)$:

$$B(u', u)=B_1(u')B_2(u), \quad u'\gtrless u.$$

Evidently this implies that the collision probability is composed independently of a probability associated with the initial speed and one associated with the final speed. This hypothesis is less reasonable than (19), but it has greater mathematical fertility, for it permits transformation to the form (17) without further restrictions.

Since

$$q_s(u)=q(u, u_s'')=B_1(u)B_2(u'')\delta(u_s'', u'')du_s''du'', \quad u\gtrless u'',$$

Eq. (16) becomes, on combining the two integrals,

$$\frac{\delta f^{(0)}}{\delta t}=\frac{N}{v}\frac{d}{du}\left\{\int_0^u B_2(t)dt\int_u^\infty u'B_1(u')f^{(0)}(u')du'\right\}.$$

In this case

$$q(u)=B_1(u)\int_0^u B_2(t)dt$$

so that, finally,

$$\frac{\delta f^{(0)}}{\delta t}=\frac{1}{v}\frac{d}{du}\left\{\frac{1}{B_1(u)\lambda(u)}\int_u^\infty tB_1(t)f^{(0)}(t)dt\right\}. \quad (25)$$

The result is more general than (24); it is identical with it when B_1 is constant. In the following sections various suppositions will be made regarding $B_1(u)$, and for each of them the distribution function will be computed.

VI. DISTRIBUTION FUNCTION OF ELECTRONS IN AN A.C. FIELD

Having calculated the right-hand side of Eq. (5), we now turn our attention to the terms of the left. Ignoring the diffusion of electrons, we set $\nabla f=0$. We choose the field strength to be of the form $E\cdot\cos\omega t$ along the x-axis, so that $a=(eE/m)\cos\omega t\equiv\gamma\cos\omega t$. The distribution function is given by (6). But ϕ will have one part in phase with the field and another part out of phase. Thus,

$$f(\mathbf{v})=f^{(0)}(v)+(v_x/v)(f^{(1)}\cos\omega t+g^{(1)}\sin\omega t). \quad (26)$$

Substitution of f in Eq. (5) and subsequent reduction in a way similar to that used in a previous publication[8] leads to the following three equations:

$$\frac{\gamma}{6v^2}\frac{\partial}{\partial v}(v^2f^{(1)})=\left.\frac{\delta f^{(0)}}{\delta t}\right|_e+\left.\frac{\delta f^{(0)}}{\delta t}\right|_s \quad (a)$$

$$\gamma\lambda\frac{df^{(0)}}{dv}+\omega\lambda g^{(1)}=-vf^{(1)} \quad (b) \quad (27)$$

$$\omega\lambda f^{(1)}=vg^{(1)}. \quad (c)$$

If we use Eq. (13), they combine to give

$$-\tfrac{2}{3}\gamma^2\frac{1}{v}\frac{d}{du}\left(\frac{\lambda u^2}{u+\omega^2\lambda^2}\frac{df^{(0)}}{du}\right)=\frac{2m}{Mv}\frac{d}{du}\left[\frac{u^2}{\lambda_s}f^{(0)}(u)\right]+\left.\frac{\delta f^{(0)}}{\delta t}\right|_s. \quad (28)$$

Inspection of this equation shows that $\delta f/\delta t$ must be of the form (17) if $f^{(0)}$ is to be the solution of a second-order differential equation. Using the integral representation for the inelastic collision,

[7] W. H. Bennett and L. H. Thomas, Phys. Rev. 62, 41 (1942).

[8] H. Margenau, Phys. Rev. 69, 508 (1946).

Eq. (14) *et. seq.*, we find

$$\delta f^{(0)}/\delta t|_s = (1/2\pi v)(dS/du).$$

Integration of Eq. (28) yields

$$-\frac{4\pi}{3}\gamma^2\frac{\lambda u^2}{u+(\omega\lambda)^2}\frac{df^{(0)}}{du}=2\pi\eta\frac{u^2}{\lambda_e}f^{(0)}+S. \quad (29)$$

Here λ, the gas-kinetic mean free path, is a function of u depending on the gas. It satisfies the relation

$$1/\lambda=1/\lambda_e+1/\lambda_s.$$

If nearly all collisions are elastic, which is the case for small u, λ and λ_e may be identified. This will now be done. Let $F(u)$ be the distribution function calculated without considering inelastic collisions, that is, the solution of Eq. (29) with $S=0$. It was derived and discussed in reference 8. In terms of it, Eq. (29) can be written

$$\frac{d}{du}\left(\frac{f^{(0)}}{F}\right)=-\frac{3\lambda}{\pi}\cdot\frac{u+u_1}{u^2u_2^2}\cdot\frac{S(u)}{F}$$

if we use the abbreviations

$$u_1=(\omega\lambda)^2, \quad u_2=2\gamma\lambda. \quad (30)$$

Since $\lim(f^{(0)}/F)=0$ for $u\to\infty$, this equation has the solution

$$f^{(0)}=\frac{3}{\pi}F\int_u^\infty\lambda\frac{u+u_1}{u_2^2u^2}\frac{S(u)}{F}du. \quad (31)$$

This formula, with refinements, will be used in the work presented in the third paper by Mr. Hartman.

In the remainder of this section we pursue the consequences of the differential representation. If Eq. (28) is integrated with the use of Eq. (25), one obtains

$$-\tfrac{2}{3}\gamma^2\frac{\lambda u^2}{u+u_1}\frac{df^{(0)}}{du}=\frac{2m}{M}\cdot\frac{u^2}{\lambda_e}f^{(0)}+\frac{1}{B_1(u)\lambda_s}\int_u^\infty tB_1(t)f^{(0)}(t)dt, \quad (32)$$

and all three mean-free-paths appear. This equation will be solved for two ranges of u: the "elastic-impact" region where u lies below some critical value and $\lambda_s=\infty$, and the "inelastic-impact" region. The solution for the first region is F and is known. In the second region λ_s is finite and depends on u. We shall assume it to be constant and put

$$\lambda_s=K\lambda$$

so that $\lambda_e=K\lambda/(K-1)$. Moreover, let us put the probability of an inelastic encounter

$$B_1(u)=\text{const.}u^r$$

and see how the distribution function in the inelastic region depends on r. More refined assumptions require numerical integrations of the resulting equations and do not seem worth while at the present time. Equation (32) becomes, after differentiation,

$$\frac{d^2f^{(0)}}{du^2}+\left(\frac{r+2}{u}-\frac{1}{u+u_1}+\frac{12m}{M}\cdot\frac{K-1}{K^\mu}\cdot\frac{u+u_1}{u_2^2}\right)\frac{df^{(0)}}{du}-\frac{6}{u_2^2}\cdot\frac{u+u_1}{Ku}\left[1-2(r+2)\frac{m}{M}(K-1)\right]f^{(0)}=0.$$

Now m/M is of the order 10^{-4}, K and r presumably not far from 1 in the region of inelastic impacts; hence, neglect of the last term in the preceding equation is always legitimate. In the parentheses, u must attain a value of $(12m/M)^{-\frac{1}{2}}u_2$, if its last member is to be considerable. For such high energies the distribution function is usually small and the term in question has no appreciable effect. It is a permissible approximation, therefore, to reduce Eq. (32) to the form

$$\frac{d}{du}\left(\frac{u^{r+2}}{u+u_1}\frac{df^{(0)}}{du}\right)=\frac{6}{K}\cdot\frac{u^{r+1}}{u_2^2}f^{(0)} \quad (33)$$

when dealing with the region of inelastic collisions. In solving this equation we consider two instances: the d.c. case ($u_1=0$) and the high frequency case.

D.C. Case

Equation (33) can be solved exactly. If we put

$$k^2=\frac{6}{Ku_2^2}=\tfrac{3}{2}\frac{m^2}{K(eE\lambda)^2}, \quad f^{(0)}=u^{-\frac{1}{2}r}Z_{-(r/2)}(iku).$$

Since $f^{(0)}$ must vanish at infinity, the Bessel function Z must be identified with the Hankel

function $H^{(1)}$, which has the asymptotic expansion[9]

$$H_{-\frac{1}{3}r}(iku)=\text{const.}u^{-\frac{1}{4}}e^{-ku}S_{\frac{1}{3}r}(2ku)$$

with

$$S_{\frac{1}{3}r}(2ku)=1+\frac{r^2-1}{8ku}+\frac{(r^2-1)(r^2-9)}{128(ku)^2}+\frac{(r^2-1)(r^2-9)(r^2-25)}{3072(ku)^3}+\cdots. \quad (34)$$

Hence

$$f^{(0)}=Au^{-(r+1)/2}e^{-ku}S_{\frac{1}{3}r}(2ku). \quad (35)$$

A.C. Case

It is convenient to write

$$x=\frac{u}{u_1},\quad q^2=\frac{6}{K}\left(\frac{u_1}{u_2}\right)^2.$$

The equation to be solved is

$$\frac{d^2f^{(0)}}{dx^2}+\left(\frac{r+2}{x}-\frac{1}{x+1}\right)\frac{df^{(0)}}{dx}=\left(1+\frac{1}{x}\right)q^2f^{(0)}. \quad (36)$$

Since it is not valid for small x, and our interest is in the region of large x, we endeavor to find a solution valid to terms in x^{-1} and expand the equation with retention of terms in x^{-2}. On writing

$$f^{(0)}=\exp\left[-\int_a^x y(x)dx\right]$$

and employing what is known as the J-W-K-B-method, one finds

$$y=q+\frac{q+r+1}{2x}+\frac{1+(r^2-1)/2q-q/2}{4x^2}+\cdots$$

and therefore

$$f^{(0)}=Ax^{-(q+r+1)/2}\times\exp\left[-qx+\frac{1+(r^2-1)/2q-q/2}{4x}\right]. \quad (37)$$

To facilitate interpretation a summary of the meaning of symbols employed thus far and of the results is given below.

[9] E. Jahnke and F. Ende, *Tables of Functions* (Dover Publications, New York, 1945), p. 137f.

List of Symbols

v = speed of electrons

$u=v^2$

λ, λ_s = total and inelastic electronic mean free path

$K=\lambda_s/\lambda$, treated as constant

ω = radian frequency of field

$u_1=(\omega\lambda)^2$

r defined by: cross section for inelastic collisions $\sim u^r$

E = amplitude of field strength

m = mass of electron

M = mass of molecule

$u_2=2eE\lambda/m$

$k^2=6/Ku_2^2$

$q^2=6/K(u_1/u_2)^2$

$$f_{\text{d.c.}}^{(0)}=Au^{-(r+1)/2}e^{-ku}(1+(r^2-1)/8ku+\cdots)$$

$$f_{\text{a.c.}}^{(0)}=Au^{-(q+r+1)/2}e^{-ku}\times(1+(r^2-1)/8ku+(2-q)u_1/8u+\cdots). \quad (38)$$

It may be noted that the d.c. distribution function (35) is Maxwellian when $r=-1$. It then corresponds to an electron temperature (for electrons capable of inelastic collisions)

$$\theta=(K/6)^{\frac{1}{2}}eE\lambda,$$

where θ is Boltzmann's constant times T. This implies that the mean energy of an electron is about equal to the energy it gains between collisions. The Maxwellian case, however, refers to the rather implausible situation where the collision cross section decreases with growing speed. In all other instances $f^{(0)}$ falls off more rapidly at large u than does e^{-ku}.

For very large frequencies the alternating field has no effect on the distribution function. This is seen from Eq. (28). If $\omega\to\infty$, the left-hand side vanishes, which is equivalent to equating γ to zero.

As an illustrative example we treat the following case. A discharge is excited by the passage of 10-cm waves through argon gas at a pressure of 6 mm of Hg. The resulting distribution function is to be compared with that for a similar d.c. discharge. Assume

$\omega=1.88\times10^{10}$ sec.$^{-1}$; $\lambda=7.2\times10^{-3}$ cm.;

$u_1=1.80\times10^{16}$ cm^2 sec.$^{-2}$;

$u_2=7.65\times10^{15}E$ cm^2 sec.$^{-2}$;

$k=(3.20/E)\times10^{-16}$ cm^{-2} sec.^{2}; $q=5.80/E$;

$m/M=1.36\times10^{-5}$; E is in e.s.u. per cm.

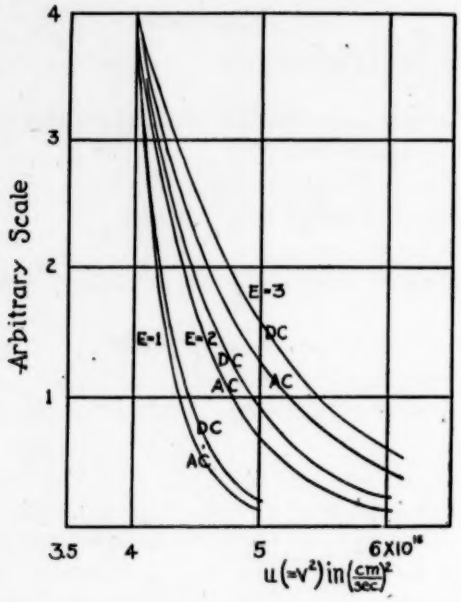

FIG. 1. Plot of $uf^{(0)}(u)$ as a function of u for argon at 6-mm pressure and wave-length 10 cm E is in electrostatic units.

Excitation in argon starts at $u=4.0\times10^{16}$ cm² sec.$^{-2}$.

Below this value of u the distribution function is F and this turns out to be essentially constant for field strengths high enough to cause a discharge. Hence, there arises no distinction between the d.c. and the a.c. distribution in this region. At higher energies, however, there is an important difference which is illustrated in Fig. 1 by plotting $uf^{(0)}$ against u. These curves were drawn for the case $B_1(u)=$constant; they are not normalized, and E for the a.c. curves is the amplitude, not the r.m.s. value of the field strength.

In Table I are collected the results of numerical integrations yielding the relative numbers of electrons capable of inelastic collisions at different field strengths. In the a.c. case these numbers rise faster with the root mean square value of E than the d.c. values rise with E.

VII. DIFFUSION OF ELECTRONS

In this section it is desired to show what modifications are required in the present formalism when diffusion of electrons is to be included. A brief indication will suffice, since the results are not new.

First of all, it is necessary to include the term $v_x\partial f/\partial x$ in the transfer equation (assuming that diffusion occurs in the x-direction). Also, to obtain a steady state, ionization must be included explicitly in the formalism. This is best done by writing

$$\frac{\delta f^{(0)}}{\delta t}=\frac{1}{4\pi v^2}\frac{d}{dv}(S_i+S_h),$$

where S_i refers to ionization, S_h to all other collisions. Finally, Eq. (26) is replaced by

$$f=f^{(0)}(v,x)+\frac{v_x}{v}\times[h^{(1)}(v,x)+f^{(1)}(v)\cos\omega t+g^{(1)}(v)\sin\omega t].$$

On separation one then obtains, instead of Eq. (27), the following set

$$\frac{\gamma}{6v^2}\frac{d}{dv}(v^2f^{(1)})+\frac{v}{3}\frac{\partial h^{(1)}}{\partial x}=\frac{1}{4\pi v^2}\frac{d}{dv}(S_i+S_h)$$

$$\gamma\lambda\partial f^{(0)}/\partial v+\omega\lambda g^{(1)}=-vf^{(1)}$$

$$\omega\lambda f^{(1)}=vg^{(1)}$$

$$\partial f^{(0)}/\partial x=-h^{(1)}/\lambda_d,$$

where λ_d is a mean free path characteristic of the diffusion of electrons. In microwave discharges it corresponds to ambipolar diffusion. When the last of these relations is introduced in the first and the result is multiplied by $4\pi v^2dv$ and integrated over the entire range of v, there results

$$\frac{d^2}{dx^2}\int_0^\infty\frac{v\lambda_d}{3}\cdot f^{(0)}\cdot4\pi v^2dv+S_i(\infty)=0 \qquad (39)$$

since $S_h(\infty)=0$. Now in the kinetic theory of gases the diffusion coefficient, $D(v)$, is defined as $v\lambda_d/3$. The integral in (39) is therefore n times

TABLE I. Values of the relative numbers, ν, of electrons having speeds greater than 2×10^8 cm sec.$^{-1}$.

$$\nu=\int_{4\times10^{16}}^\infty u^{\frac{1}{2}}f^{(0)}du\Big/\int_0^\infty u^{\frac{1}{2}}f^{(0)}du.$$

E (volts cm^{-1})	d.c.	a.c.
300	1.09×10^{-2}	1.08×10^{-2}
600	2.31×10^{-2}	1.99×10^{-2}
900	3.43×10^{-2}	2.90×10^{-2}

the mean of $D(v)$ or nD, and

$$d^2(nD)/dx^2+S_i(\infty)=0.$$

This result implies equality of the rate of removal and the rate of production of electrons.

To proceed from here on, special assumptions have to be made concerning the dependence of $f^{(0)}$ on v and x. The simplest is to say that $f^{(0)}(v,x)=V(v)\cdot X(x)$ so that

$$D=\int_0^\infty \frac{v\lambda_d}{3}\cdot V(v)v^2dv \Big/ \int_0^\infty Vv^2dv,$$

a quantity independent of x but through V a function of E, ω, and λ. Holstein's results are obtained when V is taken to be $f^{(0)}$, computed without taking account of diffusion, as in the previous section.

VIII. MAINTENANCE POTENTIAL IN HIGH FREQUENCY DISCHARGES

The experimental evidence concerning current-voltage characteristics of a.c. discharges is somewhat confused. For a discharge at a given frequency and pressure there is usually observed a "least maintaining potential," a potential below which the discharge is extinguished. To what extent it is a function of the circuit parameters is difficult to say.

When the l.m.p. is plotted against the pressure of the gas, the result is a curve either of type (a) or type (b), Fig. 2. Curve (a) has a minimum and is found in the work of Kirchner.[10] Rohde[11] finds graphs with a horizontal slope like (b). In both of these the current varies from point to point of the curve.

Brasefield's[12] measurements are in one respect more definite, for he determines the potential required to maintain a constant current, as a function of gas pressure and of the frequency. He definitely obtains curves of type (a). His results invite a theoretical interpretation which will be given in the sequel.

Other investigations[13] designed to determine the dependence of voltage on current for a given frequency and pressure, while interesting in themselves, have an indirect bearing upon the l.m.p. They indicate for the graph of V against I a curve like (b), with a horizontal slope. The current is therefore independent of the voltage over a very wide range of values. If this result is accepted and coupled with Brasefield's findings, it would appear that the curves of l.m.p. *vs.* gas pressure should also show a minimum in accordance with (a), since the current corresponding to the l.m.p. must lie on the horizontal part of the characteristic. Deviations from this behavior may well be caused by circuit peculiarities.

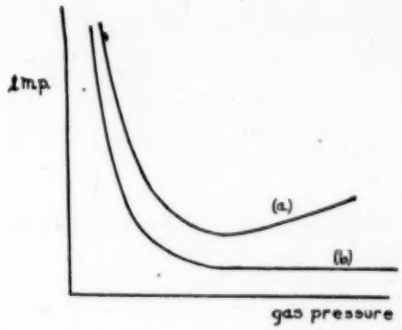

FIG. 2. Least maintaining potential *vs.* gas pressure.

Brasefield has given a qualitative explanation for the occurrence of minima, and the following considerations show how his results are related to the distribution functions computed in this paper.

If, for a given frequency, the pressure is too low, a high field is required to produce ionization, since the electrons are essentially free and have to draw all their energy from the alternating field in a single period, as described in Section I. On the other hand, if the pressure is too high, frequent collisions interfere with the transfer of energy from the field to the electrons.

These facts can be recognized from the following simplified and non-rigorous considerations. The current density across the discharge is given by

$$J=ne\bar{v}_z=e\int_0^\infty v_z^2(f^{(1)}\cos\omega t+g^{(1)}\sin\omega t)\frac{dv}{v}. \quad (40)$$

The first term under the integral represents the dissipative current upon which attention will be

[10] F. Kirchner, Ann. d. Physik (4), 77, 287 (1925).
[11] L. Rohde, Ann. d. Physik (5), 12, 569 (1932).
[12] C. F. Brasefield, Phys. Rev. 35, 1073 (1930).
[13] M. A. Herlin and S. C. Brown, Phys. Rev. 69, 696 (1946); L. D. Smullin and C. G. Montgomery, *Microwave Duplexers*, Radiation Laboratory Series (McGraw-Hill Book Company, Inc., New York (in press)), Vol. 14.

focused here. From Eqs. (27b, c),

$$f^{(1)} = -\frac{u_2}{1+\frac{u_1}{u}}\frac{\partial f^{(0)}}{\partial u}. \tag{41}$$

For $f^{(0)}$ we shall use the approximate formula (37) which may be written

$$f^{(0)} = A' u^{-(q+r+1)/2} \times \exp\left\{-ku + \frac{2-q}{8u}u_1 + 0\left(\frac{1}{ku}\right)\right\} \tag{42}$$

and drop terms of order $1/ku$ and its higher powers. The examples discussed in Section VI show this to be reasonable for microwaves, although it is detrimental to quantitative accuracy. Equation (42) holds above some critical value u'; below u', $f^{(0)}$ is nearly constant and makes a small contribution to $f^{(1)}$. Within this set of simplifications, the integral in (40) is to be extended over an algebraic function of u, u_1, and u_2 times the exponential

$$\phi(u, u_1, u_2) = \exp\left\{-ku + \frac{2-q}{8u}u_1\right\}$$

and between the fixed limits u' and ∞.

The condition that the current be constant under a variation of the independent parameters u_1 and u_2 is that the differential of this integral with respect to these two parameters be zero. The major change in the integral is expected to come from the exponential factor in the integrand, hence we require that

$$\int\left[\frac{\partial\phi}{\partial u_1}du_1 + \frac{\partial\phi}{\partial u_2}du_2\right]h(u, u_1, u_2)du = 0, \tag{43}$$

where h is an algebraic function. But this leads at once to

$$\left.\frac{\partial u_2}{\partial u_1}\right|_{J=\text{const.}} = \left(\frac{u_1}{u_2} - \left(\frac{K}{6}\right)^{\frac{1}{2}}\right)\frac{\int\frac{h\phi}{4u}du}{\int\frac{h\phi}{u_2^2}\left(u+\frac{u_1^2}{8u}\right)du}$$

(cf. Table I, Section VI, for the meaning of q, k). The ratio of the remaining integrals is positive, hence the graph of u_2 *vs.* u_1 has a *minimum* at

$$u_1 = \left(\frac{K}{6}\right)^{\frac{1}{2}}u_2. \tag{44}$$

It will be seen that a similar minimum occurs when E is plotted against λ (or pressure) at constant frequency, or E against ω at constant pressure.

Equation (44) is equivalent to

$$\frac{2eE\lambda}{m} = \left(\frac{6}{K}\right)^{\frac{1}{2}}\omega^2\lambda^2. \tag{45}$$

Now $eE\lambda$ is approximately the energy acquired by an electron between collisions, $\frac{1}{2}mV^2$. Hence the minimum occurs when

$$\omega \approx \frac{V}{\lambda},$$

that is, when the frequency of the field is about equal to the collision frequency.

Equation (45) is in accord with the main results of Brasefield's work, giving correctly both the dependence of E on λ and on ω. As to numerical agreement, we note that in a typical case he finds

$$E \approx 10 \text{ volts cm}^{-1}; \quad \omega = 2\pi \times 1.5 \times 10^7 \text{ sec.}^{-1}; \quad \lambda \approx 5 \text{ cm.}$$

Using formula (45) we find for K the value 10, which is not unreasonable.

Theory of High Frequency Gas Discharges. II. Harmonic Components of the Distribution Function[1]

H. MARGENAU AND L. M. HARTMAN
Yale University, New Haven, Connecticut

(Received August 18, 1947)

The type of distribution function employed in the foregoing paper is not sufficiently general to be applicable to all conditions of frequency and field strength. To examine its limitations, and the limitations of corresponding d.c. treatments, the function is developed as a series in Legendre polynomials of v_x/v, x being the field direction, and Fourier functions of ωt, ω being the field frequency. Attention is limited to steady states and to elastic collisions between electrons and gas molecules. By solving the resulting recurrence equations a number of successive approximations has been obtained, and from each approximation the range of validity of the preceding one is determined. Questions of mathematical convergence are not dealt with, since the physical meaning of the results is usually clear and reasonable. The current through the gas is shown to take on d.c. character when $\omega\lambda \ll (m/M)v$, λ being the mean free path and v the (mean) velocity of the electrons producing the current.

I

IN the first article of this series[2] the distribution function of electrons in a gas under a uniform, sinusoidal electric field was assumed to be approximately isotropic, the current being accounted for by a small additive term. Thus

$$f(\mathbf{v}, t) = f^0(v) + v_x\varphi(v, t),$$

provided the field is taken in the direction of the x-axis with a magnitude given by

$$E\cos\omega t. \tag{1}$$

An expansion of the distribution function in this form, however, cannot be expected to hold for all frequencies of the impressed field. For very low frequencies even the isotropic part must be a function of the time and at high field strengths one cannot expect that non-linear terms in v_x are absent. A more general expansion will be investigated in the present paper, and conditions will be found under which the simple expansion above may be used.

When diffusion is negligible, the distribution function under a field in the direction of the x-axis may be taken to be a function of three variables: time (t), electronic speed (v), and α ($=v_x/v$). The number of electrons contained within an annular element of velocity space is

$$dn = f(\alpha, v, t)2\pi v^2 dv d\alpha. \tag{2}$$

The most general expansion of the distribution function under these conditions and for a field with magnitude given by (1) may be written

$$f(\alpha, v, t) = \sum_{l=0}^{\infty} P_l(\alpha)\left\{f_0{}^l(v) + \sum_{m=1}^{\infty}[f_m{}^l(v)\cos m\omega t + g_m{}^l(v)\sin m\omega t]\right\}, \tag{3}$$

where $P_l(\alpha)$ is the Legendre polynomial of degree l. The electron density becomes:

$$n = 4\pi\int_0^{\infty}\{f_0{}^0 + \sum_m (f_m{}^0\cos m\omega t + g_m{}^0\sin m\omega t\}v^2 dv \tag{4}$$

while the current density is

$$I_x = \frac{4}{3}\pi e\int_0^{\infty}\{f_0{}' + \sum_m (f_m{}'\cos m\omega t + g_m{}'\sin m\omega t)\}v^3 dv, \tag{5}$$

$$I_y = I_z = 0.$$

To determine the functions $f_m{}^l$ and $g_m{}^l$ the Boltzmann equation is employed. In terms of the variables used here this equation may be

[1] Part of a dissertation presented by the second named author to the Faculty of the Graduate School of Yale University in candidacy for the degree of Doctor of Philosophy. This work has been supported by the Office of Naval Research, United States Navy, under Contract N6ori-44.

[2] H. Margenau, Phys. Rev. **73**, 297 (1948).

written:

$$\frac{\partial f}{\partial t}+\gamma\cos\omega t\left[\alpha\frac{\partial f}{\partial v}+\frac{1}{v}(1-\alpha^2)\frac{\partial f}{\partial\alpha}\right]=\frac{\delta f}{\delta t}, \quad (6)$$

where $\gamma=eE/m$ and the operator $\delta/\delta t$ expresses the time rate of increase as the result of collisions of all types between electrons and molecules of the gas. If the distribution function in the form of (3) is substituted in (6) and use is made of the orthogonal properties of both Legendre polynomials and the Fourier terms, a set of recurrence relations is obtained, the general equation for $m>1$ being:

$$\frac{\delta}{\delta t}\begin{pmatrix}f_m{}^l\\ g_m{}^l\end{pmatrix}=\begin{pmatrix}+g_m{}^l\\ -f_m{}^l\end{pmatrix}m\omega$$
$$+\frac{\gamma}{2}\left\{\frac{l+1}{2l+3}\frac{1}{v^{l+2}}\frac{d}{dv}\left[v^{l+2}\begin{pmatrix}f_{m-1}^{l+1}+f_{m+1}^{l+1}\\ g_{m-1}^{l+1}+g_{m+1}^{l+1}\end{pmatrix}\right]\right.$$
$$\left.+\frac{l}{2l-1}v^{l-1}\frac{d}{dv}\left[v^{1-l}\begin{pmatrix}f_{m-1}^{l-1}+f_{m+1}^{l-1}\\ g_{m-1}^{l-1}+f_{m+1}^{l-1}\end{pmatrix}\right]\right\}, \quad (7)$$

where either the upper or the lower expressions are chosen in all parentheses.

For $m=0$:

$$\frac{\delta f_0{}^l}{\delta t}=\frac{\gamma}{2}\left\{\frac{l+1}{2l+3}v^{-l-2}\frac{d}{dv}[v^{l+2}f_1{}^{l+1}]\right.$$
$$\left.+\frac{l}{2l-1}v^{l-1}\frac{d}{dv}[v^{1-l}f_1{}^{l-1}]\right\}. \quad (8)$$

For $m=1$:

$$\frac{\delta}{\delta t}\begin{pmatrix}f_1{}^l\\ g_1{}^l\end{pmatrix}=\begin{pmatrix}+g_1{}^l\\ -f_1{}^l\end{pmatrix}\omega$$
$$+\frac{\gamma}{2}\left\{\frac{l+1}{2l+3}v^{-l-2}\frac{d}{dv}\left[v^{l+2}\begin{pmatrix}2f_0{}^{l+1}+f_2{}^{l+1}\\ g_2{}^{l+1}\end{pmatrix}\right]\right.$$
$$\left.+\frac{l}{2l-1}v^{l-1}\frac{d}{dv}\left[v^{1-l}\begin{pmatrix}2f_0{}^{l-1}+f_2{}^{l-1}\\ g_2{}^{l-1}\end{pmatrix}\right]\right\}. \quad (9)$$

A similar treatment can be carried through for the d.c. distribution. The expansion of the distribution function is then given by:

$$f(\alpha, v)=\sum_l P_l(\alpha)f^l(v), \quad (10)$$

and the recurrence relations become:

$$\frac{\delta f^l}{\delta t}=\gamma_{\text{d.c.}}\left\{\frac{l+1}{2l+3}v^{-l-2}\frac{d}{dv}[v^{l+2}f^{l+1}]\right.$$
$$\left.+\frac{l}{2l-1}v^{l-1}\frac{d}{dv}[v^{1-l}f^{l-1}]\right\}. \quad (11)$$

The notation $\gamma_{\text{d.c.}}$ serves as a reminder that the d.c. field strength corresponds to the a.c. r.m.s. value. As the frequency of the alternating field goes to zero the distribution function in expansion (3) reduces to (10) by means of the identification:

$$f^l=\lim_{\omega\to 0}\sum_m f_m{}^l. \quad (12)$$

If the electron density is constant in the time, as is assumed throughout this paper, an important consequence may be inferred from the recurrence relations (7), for then

$$\int f_0{}^0 4\pi v^2 dv=n; \quad \int f_m{}^0 v^2 dv=\int g_m{}^0 v^2 dv=0, \ m>0.$$

But the recurrence relations connect in the same equation only those functions, $f_m{}^l$ and $g_m{}^l$, for which the sum of the upper and lower indices is either odd or even. Now the electron density is either greater than or equal to zero. If it is equal to zero, all terms of the distribution function vanish; if it is not equal to zero, it is given as above by the integral of $f_0{}^0$, which combines only with functions of even $l+m$. Hence, for a constant electron density one must set equal to zero all terms for which $m+l$ is odd. The distribution function then assumes the form:

$$f(\alpha, v, t)=(f_0{}^0+f_2{}^0\cos 2\omega t+g_2{}^0\sin 2\omega t+\cdots)$$
$$+\alpha(f_1{}'\cos\omega t+g_1{}'\sin\omega t+f_3{}'\cos 3\omega t$$
$$+g_3{}'\sin 3\omega t+\cdots)+\cdots. \quad (13)$$

This form of the distribution function will here be assumed to hold. Physically it means that a sinusoidal electric field can generate only even harmonics in the isotropic part of the distribution function and odd harmonics in the current density, e.g., no d.c. current component.

II

Expressions involving the operator $\delta/\delta t$ may be easily evaluated. Again we shall study here

only the case of elastic collisions. Consider that during an elastic collision at time t the electron leaves the volume element about α' and v' and enters that about α, v; or that it leaves α, v and proceeds to α'', v''. The positions of these three volume elements are mutually related by the nature and the geometry of the collision; the loss in speed was discussed in article I.[2] Consider further that there exists a well defined mean free path $\lambda_e(v)$ and let $A(\alpha, \alpha')d\alpha d\alpha'$ be the probability that during the collision the electron will proceed from $(\alpha', \alpha'+d\alpha')$ to $(\alpha, \alpha+d\alpha)$. Then:

$$\left.\frac{\delta f}{\delta t}\right|_e v^2 dv d\alpha = \int_{\alpha'} \frac{v'}{\lambda_e(v')} f(\alpha', v', t)\cdot v'^2 dv' A d\alpha d\alpha' - \frac{v}{\lambda_e(v)} f(\alpha, v, t)\cdot v^2 dv$$

$$= \sum_l \int P_l(\alpha') A(\alpha, \alpha') d\alpha' \left\{ \frac{v'^3}{\lambda_e(v')} dv' d\alpha [f_0{}^l(v') + \sum_m (f_m{}^l(v') \cos m\omega t + g_m{}^l(v') \sin m\omega t)] \right\}$$

$$- \frac{v}{\lambda_e(v)} \sum_l P_l(\alpha) d\alpha [f_0{}^l(v) + \sum_m (f_m{}^l(v) \cos m\omega t + g_m{}^l(v) \sin m\omega t)] v^2 dv. \quad (14)$$

By Eq. (3), this quantity also equals

$$\sum_l P_l(\alpha) d\alpha \left\{ \left.\frac{\delta f_0{}^l}{\delta t}\right|_e + \sum_m \left(\left.\frac{\delta f_m{}^l}{\delta t}\right|_e \cos m\omega t + \left.\frac{\delta g_m{}^l}{\delta t}\right|_e \sin m\omega t \right) \right\} v^2 dv. \quad (15)$$

We shall assume that scattering is isotropic, so that A becomes a constant and is equal to $\frac{1}{2}$. Then

$$\int P_l(\alpha') d\alpha' A d\alpha' = \delta_{0,l}.$$

Comparison of (14) and (15) yields

$$\text{(a)} \quad \left.\frac{\delta f_m{}^l}{\delta t}\right|_e = -\frac{v}{\lambda_e(v)} f_m{}^l, \quad l>0$$

$$\text{(b)} \quad \left.\frac{\delta f_m{}^0}{\delta t}\right|_e v^2 dv = f_m{}^0(v') \frac{v'^3}{\lambda_e(v')} dv' - f_m{}^0(v) \frac{v^3}{\lambda_e(v)} dv, \quad (16)$$

and expressions of the same form hold for $g_m{}^l$ and $g_m{}^0$. Equation (16a) can be generalized and shown to be true for all, not only elastic collisions, if the meaning of λ is suitably changed. Thus:

$$\frac{\delta f_m{}^l}{\delta t} = -\frac{v}{\lambda(v)} f_m{}^l, \quad l>0 \quad (17)$$

and similarly for $g_m{}^l$, where $\lambda(v)$ is the electron mean free path with respect to all collisions. For the case of elastic collisions (16b) may be written, in the form:

$$\left.\frac{\delta f_m{}^0}{\delta t}\right|_e = \frac{m}{Mv^2} \frac{d}{dv} \left(\frac{v^4}{\lambda_e} f_m{}^0 \right) + \frac{kT}{Mv^2} \frac{d}{dv} \left(\frac{v^3}{\lambda_e} \frac{df_m{}^0}{dv} \right) \quad (18)$$

as discussed in article I[2].

In the remainder of this paper, no attention will be given to inelastic collisions.

III

In order to make use of these results a consistent approximation procedure must be devised, since the recurrence relations, a quadruply infinite set of difference-differential equations, cannot in general be solved. Approximate solutions can be obtained if the distribution function (3), or (10) in the d.c. case, is terminated after several terms. In certain simple cases a solution may be found in closed form. It is then necessary to examine the conditions which must be imposed on the discharge parameters, consistent with the termination adopted. Two requirements must be satisfied if consistency is to be maintained:

(a) For a given pair of indices, m and l, both the sine and cosine terms must be included in the terminated distribution function.

(b) Only these recurrence equations are used for which the term in $\delta/\delta t$ does not vanish. That is, if the left-hand side of any member of (7) is assumed to vanish, the right-hand side must be wholly ignored.

Since a non-vanishing electron density requires the inclusion of $f_0{}^0$, or f^0 in the d.c. case, in the distribution function, and since the recurrence relation in $\delta f_0{}^0/\delta t$, or $\delta f^0/\delta t$, connects $f_0{}^0$,

or f^0, only with f_1', or f', it follows that successive approximations are:

$$\begin{aligned}
&\text{d.c.}\quad (a)\quad f=f^0,\\
&\qquad (b)\quad f=f^0+\alpha f',\\
&\qquad (c)\quad f=f^0+\alpha f'+\tfrac{1}{2}(3\alpha^2-1)f^2;\qquad (19)\\
&\text{a.c.}\quad (a)\quad f=f_0{}^0,\\
&\qquad (b)\quad f=f_0{}^0+\alpha(f_1'\cos\omega t+g_1'\sin\omega t),\\
&\qquad (c)\quad f=(f_0{}^0+f_2{}^0\cos 2\omega t+g_2{}^0\sin 2\omega t)\\
&\qquad\qquad +\alpha(f_1'\cos\omega t+g_1'\sin\omega t)\\
&\qquad\qquad +\tfrac{1}{2}(3\alpha^2-1)(f_0{}^2+f_2{}^2\cos 2\omega t\\
&\qquad\qquad\qquad +g_2{}^2\sin 2\omega t).\qquad (20)
\end{aligned}$$

The equations resulting from the use of (19a) and (20a) are

$$\delta f^0/\delta t=0;\quad \delta f_0{}^0/\delta t=0. \qquad (21)$$

In both the d.c. and a.c. cases the operator $\delta/\delta t$ for $l=0$ has the form given by (18). Hence, on integrating Eqs. (21), the distribution becomes Maxwellian in first approximation, as expected. Similarly, the recurrence equations which correspond to (19b) are obtained immediately from Eqs. (11). They are:

$$\frac{\delta f^0}{\delta t}=\frac{\gamma_{\text{d.c.}}}{3v^2}\frac{d}{dv}(v^2f');\quad -\frac{v}{\lambda}f'=\gamma_{\text{d.c.}}\frac{df^0}{dv}. \qquad (22)$$

These equations may be integrated directly. The solution is the Druyvesteyn distribution[3] ($T=0$) or the Davydov distribution[4] ($T\neq 0$). In the same way, the equations determining (20b) are obtained directly from (7):

$$\begin{gathered}
\frac{\delta f_0{}^0}{\delta t}=\frac{\gamma}{6v^2}\frac{d}{dv}(v^2f_1');\\
-\frac{v}{\lambda}f_1'=\omega g_1'+\gamma\frac{df_0{}^0}{dv};\quad -\frac{v}{\lambda}g_1'=-\omega f_1'.
\end{gathered} \qquad (23)$$

The solution of these equations has been treated by Margenau.[5]

IV

Under a d.c. field the distribution function in the form of (19c) is given by the solution of the following set of recurrence equations:

$$\begin{gathered}
\frac{\delta f^0}{\delta t}=\frac{\gamma_{\text{d.c.}}}{3v^2}\frac{d}{dv}(v^2f');\\
-\frac{v}{\lambda}f'=\gamma_{\text{d.c.}}\left\{\frac{2}{5v^2}\frac{d}{dv}v^2f^2+\frac{df^0}{dv}\right\};\qquad (24)\\
-\frac{v}{\lambda}f^2=\frac{2}{3}\gamma_{\text{d.c.}}v\frac{d}{dv}(v^{-1}f').
\end{gathered}$$

Rather than attempting to handle Eqs. (24), it is of interest to learn when their solution will reduce approximately to that of Eqs. (22). This will be the case when:

$$|f^2|\ll|f'|. \qquad (25)$$

Considering here only the case of low temperatures, let us assume that f^0 and f' satisfy Eqs. (22). Then for $T=0$:

$$f^0=A\exp\left\{-\frac{3mv^4}{4M(\gamma_{\text{d.c.}}\lambda)^2}\right\}. \qquad (26)$$

We evaluate f^1 by the second of Eqs. (22) and f^2 by the third of Eqs. (24). On forming the ratio of f^2 to f' it is seen that condition (25) is satisfied provided

$$\left|\frac{\eta v^2}{\gamma_{\text{d.c.}}\lambda}-\frac{2\gamma_{\text{d.c.}}\lambda}{3v^2}\right|\ll 1,\quad \text{where } \eta=2m/M.$$

Physically, η is the mean energy loss of an electron per collision. It is convenient to introduce a variable χ defined by

$$v^2=\chi\langle v^2\rangle$$

and to express this inequality in terms of χ. The mean value of v^2 is given by

$$\langle v^2\rangle=(8/3)^{\frac{1}{2}}\frac{\Gamma(5/4)}{\Gamma(3/4)}\eta^{-\frac{1}{2}}\gamma_{\text{d.c.}}\lambda.$$

We then have, finally,

$$\eta^{\frac{1}{2}}\left|1.21\chi-\frac{0.55}{\chi}\right|\ll 1. \qquad (27)$$

Since η is of the order of 10^{-4} this is seen to be satisfied over a fairly wide range of energies about the mean energy, e.g., $10^{-1}\lesssim\chi\lesssim\chi$. This

[3] M. J. Druyvesteyn, Physica 10, 61 (1930).
[4] B. Davydov, Physik. Zeits. Sovjetunion, 8, 59 (1935).
[5] H. Margenau, Phys. Rev. 69, 508 (1946).

result is independent of the field strength. Only the very fast and the very slow electrons have a distribution in energy which differs from the Druyvesteyn distribution. These exceptions are not unexpected. The very fast electrons are those whose motion in the field has been largely unimpeded by collisions with molecules, hence those with abnormally long free times. The very slow electrons, on the other hand, are those whose recent history has been relatively unaffected by the field, that is, those which have made a great many collisions with the molecules of the gas and whose distribution, therefore, is not independent of the gas temperature and must approach a Maxwellian form.

V

Under an a.c. field the situation is considerably more complex. The equations which determine the distribution function written in the form (20c) are:

$$\text{(a)}\quad \frac{\chi}{6v^2}\frac{d}{dv}(v^2 f_1') = \frac{\delta f_0^0}{\delta t},$$

$$\text{(b)}\quad 2\omega g_2^0 + \frac{\gamma}{6v^2}\frac{d}{dv}(v^2 f_1') = \frac{\delta f_2^0}{\delta t},$$

$$\text{(c)}\quad -2\omega f_2^0 + \frac{\gamma}{6v^2}\frac{d}{dv}(v^2 g_1') = \frac{\delta g_2^0}{\delta t},$$

$$\text{(d)}\quad \omega g_1' + \frac{\gamma}{5v^3}\frac{d}{dv}[v^3(2f_0^2+f_2^2)] + \frac{\gamma}{2}\frac{d}{dv}(2f_0^0+f_2^0) = -\frac{v}{\lambda}f_1',$$

$$\text{(e)}\quad -\omega f_1' + \frac{\gamma}{5v^3}\frac{d}{dv}(v^3 g_2^2) + \frac{\gamma}{2}\frac{dg_2^0}{dv} = -\frac{v}{\lambda}g_1', \qquad (28)$$

$$\text{(f)}\quad \frac{\gamma v}{3}\frac{d}{dv}(v^{-1}f_1') = -\frac{v}{\lambda}f_0^2,$$

$$\text{(g)}\quad 2\omega g_2^2 + \frac{\gamma v}{3}\frac{d}{dv}(v^{-1}f_1') = -\frac{v}{\lambda}f_2^2,$$

$$\text{(h)}\quad -2\omega f_2^2 + \frac{\gamma v}{3}\frac{d}{dv}(v^{-1}g_1') = -\frac{v}{\lambda}g_2^2,$$

where the form of $\delta/\delta t$ for elastic collisions is again given by (18). These equations do not submit to an exact solution. We shall assume first, as in the d.c. case, that the distribution function may be written approximately in the form (20b) and therefore start with the solution of Eqs. (23). Equation (20c) differs from (20b) by inclusion of (a) isotropic terms f_2^0, and g_2^0, (b) non-isotropic terms f_0^2, f_2^2, and g_2^2. The conditions under which set (a) is negligible are different from those under which set (b) is negligible. Inspection of Eqs. (28) shows that these conditions can be studied separately. In the remainder of this section, we give attention to set b.

According to (28f, g, h), the functions f_0^2, f_2^2, and g_2^2 are expressed in terms of f_1' and g_1'. Now these latter develop peculiarities when v is either very large or very small in comparison with $\omega\lambda$, and are quite regular when $v\sim\omega\lambda$. If, therefore, the roles played by f_0^2, f_2^2, g_2^2 are investigated for these two limiting cases (for which the analysis is easy), predictions for the intermediate range can safely be made.

There are two cases of interest.

(A) $(\omega\lambda)\ll v$ over the important range of the distribution function. Then the first terms on the left of (28g) and (28h) may be neglected. g_2^2 is smaller in absolute value than f_0^2, and f_2^2 is equal to f_0^2. Furthermore

$$f_0^0 \doteq A\exp\left\{-\frac{3\eta v^4}{4(\gamma\lambda)^2}\right\}, \qquad (29)$$

if we restrict ourselves to low temperatures. If f_1' is evaluated by means of (23) and the variable χ is introduced as before, the mean "energy" being given by:

$$\bar{v}^2 = \frac{2}{\sqrt{3}}\frac{\Gamma(5/4)}{\Gamma(3/4)}\eta^{-\frac{1}{2}}\gamma\lambda,$$

we obtain finally the result that the terms in $P_2(\alpha)$ may be neglected provided that

$$\eta^{\frac{1}{2}}\left|0.86\chi - \frac{0.39}{\chi}\right| \ll 1. \qquad (30)$$

The situation is essentially the same as that under a d.c. field and the same remarks apply here.

(B) $(\omega\lambda)\gg v$ over the range of v within which the distribution function is significant. Then f_0^0

is Maxwellian[5] at an effective "temperature" T' given by:

$$T'=T\left[1+\frac{M}{6kT}\left(\frac{\gamma\lambda}{\omega\lambda}\right)^2\right] \tag{31}$$

and

$$f_1'=\frac{mv^2\gamma}{kT'\omega^2\lambda}f_0^0;\quad g_1'=\frac{\omega\lambda}{v}f_1'. \tag{32}$$

Substituting these expressions in (28f, g, h) and solving for f_0^2, f_2^2, and g_2^2, we obtain the following expressions:

$$\begin{aligned}\frac{f_0^2}{f_1'}&=\frac{m\gamma\lambda}{kT'}\left(1-\frac{kT'}{mv^2}\right),\\ \frac{f_2^2}{f_1'}&=\frac{1}{6}\frac{m\gamma\lambda}{kT'},\\ \frac{g_2^2}{f_1'}&=\frac{1}{4}\frac{v}{\omega\lambda}\frac{m\gamma\lambda}{kT'}\left(1-\frac{2kT'}{3mv^2}\right).\end{aligned} \tag{33}$$

Since now $\frac{1}{2}m\langle v^2\rangle=\frac{3}{2}kT'$ it follows that these ratios will all be small if

$$\frac{m\gamma\lambda}{kT'}\ll 1, \tag{34}$$

except for very small values of v. The expression on the left of (34) is usually negligible except in the neighborhood of its maximum with respect to γ which occurs at

$$\gamma=\omega\left(\frac{6kT}{M}\right)^{\frac{1}{2}}. \tag{35}$$

Now γ/ω is roughly the speed acquired by a free electron in one cycle, $(6kT'/M)^{\frac{1}{2}}$ roughly the speed of the molecules. When these are equal, therefore, the necessity for including higher Legendre terms may arise.

As an example we note that for helium at 300°K and at a frequency of 3000 megacycles, Eq. (35) defines a field strength of about 2 volts/cm, and the value of $m\gamma\lambda/kT'$ corresponding to this field strength reaches 1 for pressures of a few millimeters. The present analysis indicates that for pressures as low as this and for field strengths of this critical value, higher Legendre terms may have to be included

Similar conclusions hold when $\omega\lambda\approx v$. Summarizing the results, one may say that the functions of set (b) can usually be ignored. They are of importance only for electron energies differing widely from the mean, and possibly, at small pressures, when condition (35) is true. For these cases they are given by Eqs. (30) and (33).

VI

The situation is somewhat different with respect to the time-dependent isotropic terms in (20c). To neglect them,

$$\left|\frac{f_2^0}{f_0^0}\right|\ll 1;\quad \left|\frac{g_2^0}{f_0^0}\right|\ll 1 \tag{36}$$

must be true. We estimate these expressions from the recurrence Eqs. (28b) and (28c) directly. Assume that the right-hand numbers of these equations are small. We then have at once approximate expressions for f_2^0 and q_2^0 which satisfy automatically the condition of normalization to a constant electron density. These expressions may be used on the right of Eqs. (28b) and (28c) to obtain a second approximation to f_2^0 and g_2^0, etc. This scheme converges well and indicates that the first approximation to g_2^0 is satisfactory. The functions f_0^0 and f_1' are calculated from Eqs. (23). Then, with restriction to zero temperature, one finds

$$g_2^0\doteq-\frac{\eta v}{\omega\lambda}\left\{1-\frac{3\eta v^2(v^2+\omega^2\lambda^2)}{4\gamma^2\lambda^2}\right\}f_0^0.$$

Provided v is not too far from the mean velocity, g_2^0 is appreciable only when $\omega\lambda$ is of the order of ηv or less. Similarly, we obtain from the second approximation for f_2^0 (again neglecting T)

$$f_2^0\doteq\frac{\eta}{4v^2}\frac{d}{dv}\left\{v^3\left(1+\frac{\eta v^2}{(\omega\lambda)^2}\right)f_0^0\right\},$$

in the neighborhood of the mean velocity. If $\eta^{\frac{1}{2}}v<\omega\lambda$ this reduces further and one finds

$$\left|\frac{f_2^0}{f_0^0}\right|=0(\eta)\ll 1.$$

Hence it follows that for $(\omega\lambda)>\eta^{\frac{1}{2}}v$ both f_2^0 and g_2^0 may be neglected. Numerically this means that under discharge conditions $(\omega\lambda)$ must exceed

about 10^7 cm sec.$^{-1}$.[6] The distribution function in the form of (20b) therefore is valid only for frequencies higher than $\eta^{\frac{1}{2}}v/\lambda$.

A similar investigation shows that for very low frequencies, g_2^0 approaches zero while f_2^0 remains finite.

To summarize, therefore, we have three distinct frequency regions in each of which the distribution function assumes a characteristic form:

(a) $\omega\lambda \ll \eta v$

$$f=(f_0^0+f_2^0\cos 2\omega t)+\alpha f_1'\cos\omega t,$$

(b) $\omega\lambda \approx \eta v$

$$f=(f_0^0+f_2^0\cos 2\omega t+g_2^0\sin 2\omega t)+\alpha(f_1'\cos\omega t+g_1'\sin\omega t), \tag{37}$$

(c) $\omega\lambda \gg \eta^{\frac{1}{2}}v$

$$f=f_0^0+\alpha(f_1'\cos\omega t+g_1'\sin\omega t).$$

A d.c. situation is one for which condition (a) is true.

VII

The distribution function in the form of (37a) is amenable to exact solution. The equations to be satisfied are found from (28):

$$\text{(a)}\quad \frac{\gamma}{6v^2}\frac{d}{dv}(v^2f_1')=\frac{\delta f_0^0}{\delta t}=\frac{\delta f_2^0}{\delta t},$$

$$\text{(b)}\quad \frac{\gamma}{2}\frac{d}{dv}(2f_0^0+f_2^0)=-\frac{v}{\lambda}f_1'. \tag{38}$$

We define

$$F=2f_0^0+f_2^0;\quad G=f_0^0-f_2^0. \tag{39}$$

Then from Eqs. (38):

$$\frac{\delta G}{\delta t}=0;\quad G=A\exp\left(-\frac{mv^2}{2kT}\right). \tag{40}$$

Also

$$\frac{\gamma}{2v^2}\frac{d}{dv}(v^2f_1')=\frac{\delta F}{\delta t},\quad \frac{\gamma}{2}\frac{dF}{dv}=-\frac{v}{\lambda}f_1'$$

or

$$F=B\exp\left\{-\int\frac{\frac{m}{2}dv^2}{kT+\frac{M(\gamma\lambda)^2}{4v^2}}\right\}. \tag{41}$$

We write

$$\alpha\equiv\frac{mM\gamma^2\lambda^2}{8k^2T^2},\quad x=\frac{mv^2}{2kT}. \tag{42}$$

Then, integrating (41):

$$2f_0^0+f_2^0=B\left(1+\frac{x}{\alpha}\right)^\alpha$$

or

$$\text{(a)}\quad f_0^0-f_2^0=Ae^{-x},$$

$$\text{(b)}\quad f_0^0+f_2^0=\frac{1}{3}\left\{2B\left(1+\frac{x}{\alpha}\right)^\alpha-A\right\}e^{-x}. \tag{43}$$

But $f_0^0 \mp f_2^0$ is the form taken on by the isotropic part of f when $\omega t=\pi/2$ or 0, respectively, i.e., when the field is zero or a maximum. Hence, once every half-cycle, when the magnitude of the field is zero, the isotropic part of the distribution function is Maxwellian; when the field is a maximum, the isotropic part of the distribution has the form given by (43b). This shows precisely how the theory of a.c. discharges goes over continuously into the d.c. theory. The constants A and B are determined by normalizing f_0^0 to the value n, f_2^0 to zero. On calculation they are found to differ somewhat from the corresponding constant in the d.c. distribution function—as they should because of the neglect of higher harmonics in (37a), but become identical with the latter at small field strengths.

[6] It is interesting to note that in the measurements of L. Rohde (Ann. d. Physik. (5) 12 (1932), especially p. 585) the variation of the critical discharge potential with frequency seemed to cease in the region of $\omega\lambda$ below this value. This is probably an indication of the fact that f_2^0 becomes important, giving the discharge certain direct-current features which will be discussed in the next section.

Theory of High Frequency Gas Discharges. III. High Frequency Breakdown[1]

L. M. HARTMAN[2]
Yale University, New Haven, Connecticut

(Received August 18, 1947)

In search of a definition of "breakdown" of a gas under microwave fields, the density of electrons is investigated as a function of the field strength under the following simplifying assumptions. Ionization occurs as result of single impacts between gas atoms and sufficiently fast electrons. The gas has an infinite volume, and negative ions are not formed, so that the only mechanism for electron removal is recombination with positive ions. The calculations show that, at a certain field strength, the density of electrons rises sharply. The simple model, therefore, leads to a breakdown phenomenon, at field strengths not far from observed values. Gases treated are helium and neon under frequencies of 3000 megacycles.

I

AS was observed in article I[3] of this series, a simple theory of breakdown, concerned with the motion of a free electron in an alternating field such that the electron may reach ionizing velocities after acceleration through a half-period of the field, fails since it predicts values of the field strength which are many times too high. The alternative to this procedure is to construct a theoretical discharge characteristic, that is, a plot of current against field strength for given values of the gas pressure and field frequency. If such a curve exhibits breakdown it will appear as a sharp rise in the current for field strengths above a more or less definite value.

The current density may be written

$$j=ne\langle v_x\rangle_{Av},$$

where n is the electron density and the field is taken to have the direction of the x axis. Since no sudden change in the value of $\langle v_x\rangle_{Av}$ is to be expected as breakdown is reached, it will be assumed that the phenomenon of breakdown may be investigated adequately by studying the dependence of n upon the field strength. In particular n/N, where N is the gas particle density, will be plotted against the field strength E.

We shall make several assumptions which serve to restrict the physical situation being discussed. First, it will be considered that the field is uniform and that the discharge vessel is effectively infinite in extent. Hence the effects of electron diffusion to the boundaries of the discharge vessel and secondary processes occurring at these boundaries will be neglected. Second, it will be assumed that the gas molecules do not form negative ions. Specifically, pure helium and neon will be considered. Hence electrons can be produced by ionizing electron collisions with gas atoms as well as by cosmic radiation and radioactive background and can be removed by volume recombination of electrons and positive ions. Third, we shall assume that the electron distribution function may be written in the form

$$f=f_0{}^0+\frac{v_x}{v}[f_1{}^1\cos\omega t+g_1{}^1\sin\omega t]. \qquad (1)$$

This implies that the gas is in a steady state (constant electron density) and, in view of the conclusions of article II[4], that the field frequency lies in the microwave region.

Actually, the discharge vessel is finite and diffusion plays an important role. Information on the capture cross sections of positive ions seems scant, but these cross sections are often believed to be small. Indeed most investigators in the field of gas discharges would be disposed to ignore recombination in the presence of diffusion. We have deliberately considered here the case of an infinite gas, thus ignoring diffusion,

[1] Part of a dissertation presented to the Faculty of the Graduate School of Yale University in candidacy for the degree of Doctor of Philosophy. This work has been assisted by the Office of Naval Research, United States Navy, under Contract N6ori-44.

[2] Now at General Electric Company, Schenectady, New York.

[3] H. Margenau, Phys. Rev. **73**, 297 (1948).

[4] H. Margenau and L. M. Hartman, Phys. Rev. **73**, 309 (1948).

mainly because this model is easiest to deal with. Initial expectations are that, if anything like breakdown were to emerge at all, it would occur at field strengths quite different from those observed experimentally. Instead of that, however, it was found that the model chosen agreed much better with what is known than could be anticipated. It does produce a sharp rise in electron concentration at a certain field strength, and this field strength, for a great variety of recombination cross sections, is only a few volts per cm below that observed. It seems, therefore, that the present approach does not miss the central issue, although it cannot prove the absence of diffusion. We hope to include this mechanism in subsequent calculations.

Let θ denote the rate at which electrons are being produced per unit volume by external agencies such as cosmic radiation. This is of the order of 10 electrons per cubic centimeter per second at atmospheric pressure. Furthermore, let the electronic mean free paths for ionization and recombination be denoted, respectively, by λ_i and λ_r. Then, normalizing the distribution function to unity, we have the following equation to describe the steady state:

$$\frac{\partial n}{\partial t}=\theta+n\int_0^\infty \frac{v}{\lambda_i}f_0{}^0\cdot 4\pi v^2dv - n\int_0^\infty \frac{v}{\lambda_r}f_0{}^0\cdot 4\pi v^2dv=0. \quad (2)$$

The ionization cross section will be assumed to be a linear function of the excess of the electronic energy over that necessary for ionization:

$$q_i(u)=\begin{cases}K(u-u_i) & u\geqslant u_i\\ 0 & u\leqslant u_i\end{cases} \quad (3)$$

where K is a constant and

$$u\equiv v^2, \quad eV_i\equiv \tfrac{1}{2}mu_i,$$

V_i being the ionization potential of the gas. Multiple ionization will be neglected. Hence, since the electron density and the positive ion density are equal, λ_i is defined by:

$$(N-n)q_i\lambda_i=1. \quad (4)$$

The recombination cross section has been investigated by Wessel and others[5] and has been shown to have the form:

$$q_r(u)=\frac{R}{u}, \quad (5)$$

where R is a constant. The mean free path is defined by:

$$nq_r\lambda_r=1. \quad (6)$$

Finally it is convenient to introduce a new variable δ defined by:

$$u\equiv\delta u_i.$$

Let

$$I_1\equiv\int_1^\infty f_0{}^0\cdot\delta(\delta-1)d\delta, \quad I_2\equiv\int_0^\infty f_0{}^0d\delta.$$

Equation (2) may now be written:

$$\theta+2\pi n(N-n)Ku_i{}^3I_1-2\pi n^2Ru_iI_2=0. \quad (7)$$

This equation may be solved for n/N. We obtain:

$$n/N=\frac{I_1\left\{1+\left[1+\frac{2\theta}{\pi N^2}\left(\frac{Ku_i{}^3I_1+Ru_iI_2}{(Ku_i{}^3I_1)^2}\right)\right]^{\frac{1}{2}}\right\}}{2\left\{I_1+\frac{R}{Ku_i{}^2}I_2\right\}}. \quad (8)$$

For fields that are sufficiently strong θ may be neglected and (8) reduces to:

$$n/N=\frac{1}{1+\left(\frac{R}{Ku_i{}^2}\right)\left(\frac{I_2}{I_1}\right)}. \quad (8a)$$

In this form the electron density does not depend upon the normalization but only upon the shape of the distribution function. For small values of the field strength the integral I_1 may be neglected and (8) reduces to:

$$n/N=\left(\frac{\theta}{2\pi N^2Ru_iI_2}\right)^{\frac{1}{2}}. \quad (8b)$$

By means of these equations the entire discharge characteristic may be plotted. The problem, therefore, is one of determining the function $f_0{}^0$ and the integrals I_1 and I_2 for different values of the discharge parameters.

[5] W. Wessel, Ann. d. Physik **5**, 611 (1930); E. C. G. Stueckelberg and P. M. Morse, Phys. Rev. **36**, 16 (1930).

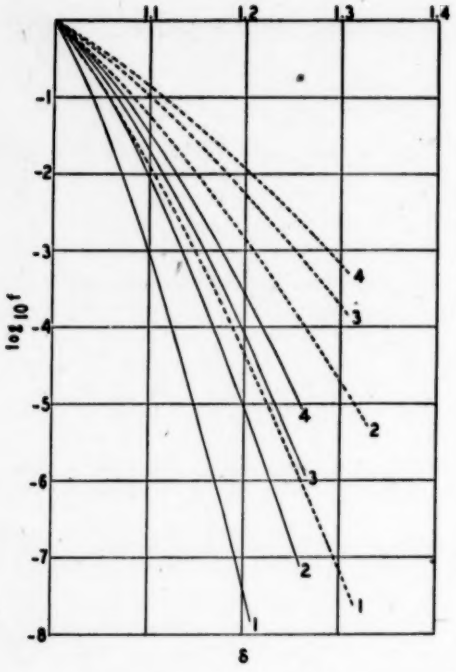

———Ne - - - -He

FIG. 1. Logarithm of distribution function *vs.* energy of electrons.

1. $(10^4)°K$
2. $2(10^4)$
3. $3(10^4)$
4. $4(10^4)$

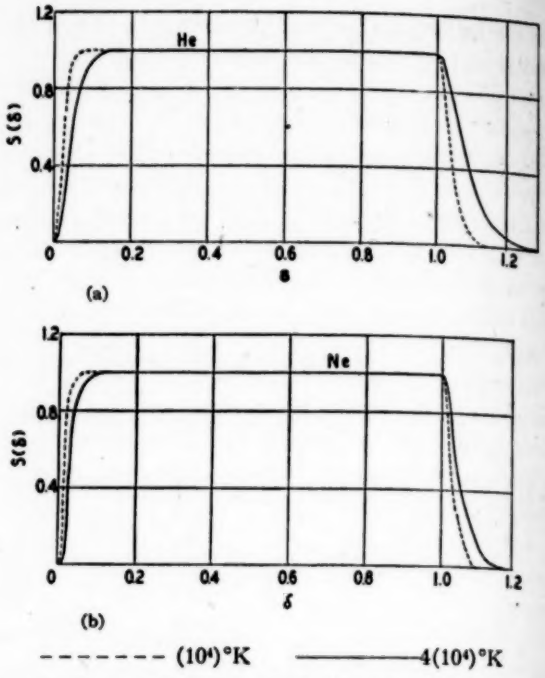

- - - - - - - $(10^4)°K$ ———— $4(10^4)°K$

FIG. 2. Rate of increase of electrons having velocities below δ *vs.* δ.
Normalized to unity at $\delta = 1.0$

II

It has been shown in the first two articles of this series[3,4] that, if the distribution function is written in the form of Eq. (1), f_0^0 must satisfy a differential equation having the form

$$\frac{\gamma}{6v^2}\frac{d}{dv}\left[\frac{(\gamma\lambda)v^3}{v^2+(\omega\lambda)^2}\frac{df}{dv}\right]+\frac{\delta f}{\delta t}=0, \tag{9}$$

where

$$\gamma\equiv\frac{eE}{m};$$

$$\frac{\delta f}{\delta t}=\frac{m}{Mv^2}\frac{d}{dv}\left(\frac{v^4}{\lambda_e}f\right)+\frac{kT}{Mv^2}\frac{d}{dv}\left(\frac{v^3}{\lambda_e}\frac{df}{dv}\right)+\frac{1}{4\pi v^2}\frac{dS}{dv}. \tag{10}$$

(Here and in what follows, we write f in place of f_0^0.) All non-elastic collisions are accounted for by the proper choice of the function S. The large majority of collisions occurring in a discharge at a given electronic energy will be elastic, since the magnitude of the distribution function will fall off rapidly in the energy range immediately above the energy necessary for ionization of the molecules and even in this region the cross sections for ionization and excitation are small as compared with the total collision cross section. We shall assume, therefore, as an approximation in the following that

$$\lambda \doteqdot \lambda_e.$$

Introducing two parameters defined by

$$u_1\equiv(\omega\lambda);\quad u_2\equiv(2\gamma\lambda),$$

we may integrate (9) and obtain

$$f=\left(\frac{3M}{\pi}\right)F\int_u^\infty\frac{(u+u_1)\lambda S du}{u^2F[Mu_2^2+24(u+u_1)kT]}, \tag{11}$$

where

$$F=\exp\left\{-\int\frac{\frac{m}{2}du}{kT+\frac{Mu_2^2}{24(u+u_1)}}\right\}. \tag{12}$$

$F(u)$, therefore, is the form that the isotropic part of the distribution function assumes when only elastic collisions are taken into account.

A number of special cases are of interest.

Since a differential equation of the same form as (9) is obtained for a d.c. field, both the microwave and d.c. distributions may be handled by the present treatment.

(a) $u_1=0$

$$f=\left(\frac{3M}{2\pi}\right)F\int_u^\infty \frac{\lambda S du}{uF[Mu_2^2+12ukT]}, \quad (13)$$

where

$$F=\exp\left\{-\int \frac{\frac{m}{2}du}{kT+\frac{Mu_2^2}{12u}}\right\}.$$

$F(u)$ is the Davydov distribution.[6] Note that u_2 here refers to the r.m.s. field.

(b) $u_1=0$, $T=0$

$$f=\left(\frac{3}{2\pi}\right)F\int_u^\infty \frac{\lambda S du}{uu_2^2F}, \quad (14)$$

where

$$F=\exp\left\{-\frac{3mu^2}{Mu_2^2}\right\}.$$

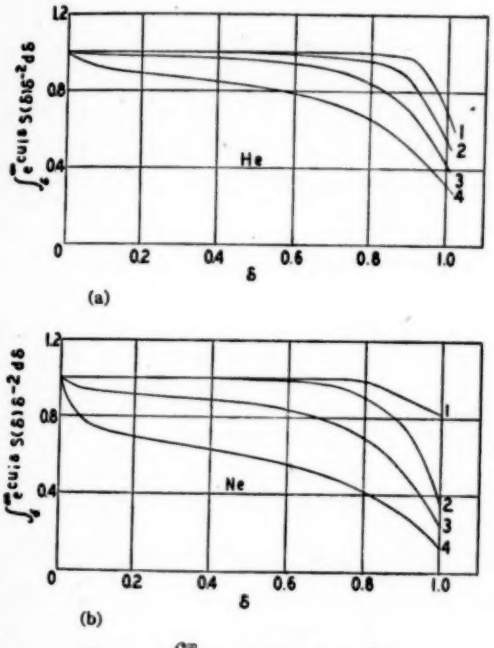

FIG. 3. $\int_u^\infty e^{cu}u^{-2}S(u)du$ vs. $\frac{u}{u_i}$.

Normalized to unity at $\delta=0$

1. $(10^4)°K$
2. $2(10^4)$
3. $3(10^4)$
4. $4(10^4)$

[6] B. Davydov, Physik. Zeits. Sowjetunion **8**, 59 (1935).

$F(u)$ is the Druyvesteyn distribution.[7] Again u_2 refers to the r.m.s. field. This result is given by Chapman and Cowling.[8]

(c) $T=0$

$$f=\left(\frac{3}{\pi}\right)F\int_u^\infty \frac{(u+u_1)\lambda S du}{u^2u_2^2F}, \quad (15)$$

where

$$F=\exp\left\{-\frac{6mu(u+2u_1)}{Mu_2^2}\right\}.$$

This result has already been presented in article I[3] of the present series.

(d) $u_1=0$, $u_2=0$

$$f=\left(\frac{M}{8\pi KT}\right)F\int_u^\infty \frac{\lambda S du}{u^2F}, \quad (16)$$

where

$$F=\exp\left\{-\frac{mu}{2kT}\right\}.$$

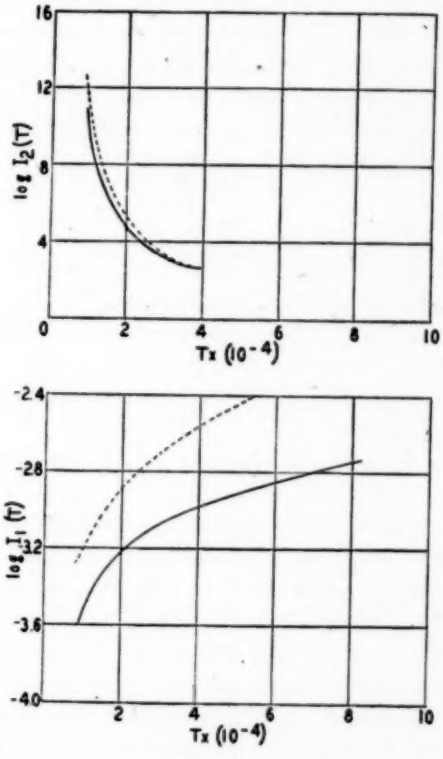

FIG. 4. Plot of log$I$ *vs.* T.

[7] M. J. Druyvesteyn, Physica **10**, 61 (1930).

[8] S. Chapman and T. G. Cowling, *The Mathematical Theory of Non-Uniform Gases* (Cambridge University Press, New York, 1939), p. 354.

$F(u)$ is here a Maxwellian distribution corresponding to a temperature T. This, therefore, represents thermal excitation of the gas.

(e) $u_1 \gg u$. If this inequality holds over the entire range of u within which the magnitude of the distribution function is significant, it has been shown in article II[4,9] that $F(u)$ is Maxwellian at an effective "temperature" T' given by

$$T' = T\left[1+\frac{Mu_2^2}{24u_1kT}\right]. \tag{17}$$

If (17) is used to eliminate T from Eq. (11), the distribution function becomes:

$$f=\left(\frac{M}{8\pi kT'}\right)F\int_u^\infty \frac{\lambda S du}{u^2F}. \tag{18}$$

This is of the same form as (16). Hence, it follows that insofar as the electron distribution function is concerned the effect of an alternating field of sufficiently high frequency is equivalent to that of raising the temperature of the gas and conversely. Thus a thermal "discharge" and a high frequency discharge can be studied simultaneously so long as T' is defined.

III

The results outlined in the preceding section can be given practical meaning only if the form of the function $S(u)$ is specified. From the discussion of this function in article I[3] it is clear that this specification will involve a choice as to the nature and number of inelastic processes which are deemed important for the problem in question. We shall consider two cases. The first, the excitation of a single, discrete state of the molecule, will permit us to develop a method of using the results of the preceding section to compute f. The second case will include ionization of the molecule and volume recombination of electrons and positive ions but will neglect the excitation of quantized states. We shall use the latter to compute the electron density.

Consider then that only a single type of inelastic collision occurs. Denote the cross section for this process by $q_s(u)$ and let the value of u corresponding to the excitation energy be denoted by u_s. Then from article I[3] we have:

$$S(u)=2\pi N\int_u^{u+u_s} f\cdot q_s\cdot u du. \tag{19}$$

If this is used in conjunction with Eq. (16) for thermal excitation or with any of the other integral representations of f, the finite upper limit of the integral in (19) leads to an integro-differential equation in f or a differentio-difference equation and no useful result is obtained. We note, however, that we may rewrite Eq. (19) as follows:

$$\begin{aligned} S(u) &= 2\pi N\int_u^\infty f\cdot q_s\cdot u du \\ &\quad -2\pi N\sum_{j=1}^\infty \int_{u+ju_s}^{u+(j+1)u_s} f\cdot q_s\cdot u du \\ &= 2\pi N\int_u^\infty f\cdot q_s\cdot u du-\sum_{j=1}^\infty S(u+ju_s). \end{aligned} \tag{20}$$

The entire range of u has thus been subdivided into the finite ranges:

$$(0, u_s),\ (u_s, 2u_s),\ (2u_s, 3u_s),\ \cdots.$$

Since f goes to zero strongly as u increases, there will be some range of u within which f is so small that it may be assumed to vanish in the next higher range without causing appreciable error. Hence

$$\begin{aligned} &(1)\ u\geqslant nu_s,\quad f\doteqdot S\doteqdot 0 \\ &(2)\ (n-1)u_s\leqslant u\leqslant nu_s, \\ &\qquad S=2\pi N\int_u^\infty f\cdot q_s\cdot u du \\ &(3)\ (n-2)u_s\leqslant u\leqslant (n-1)u_s, \\ &\qquad S=2\pi N\int_u^\infty f\cdot q_s\cdot u du-S(u+u_s) \\ &\cdots \\ &(n+1)\ 0\leqslant u\leqslant u_s, \\ &\qquad S=2\pi N\int_{u_s}^\infty f\cdot q_s\cdot u du-\sum_{j=1}^{n-1} S(u+ju_s). \end{aligned} \tag{21}$$

Expression (21.2) may now be combined with (11) or one of its reduced forms; $S(u)$ may be eliminated and the result is a second-order

[9] See also H. Margenau, Phys. Rev. 69, 508 (1946).

differential equation in f. The solution of this equation is the distribution function in the corresponding range of energy. Similarly (21.3) may then be combined with (11) to yield a differential equation in f in the next lower energy range since now $S(u+u_s)$ is known as a function of u. The solution is then fitted to the preceding solution, and so on. In this way the distribution function may be found over the entire range of u. A cumulative error can be avoided by using the solution corresponding to (21.2) to compute f in the energy range corresponding to (21.1) and then repeating the process until consistency has been achieved. This method of procedure would appear to be impractical were it not for the fortunate circumstance that under certain conditions only two steps are required. Thus, for example, in the case of the rare gases the distribution function may be considered to be negligibly small for energies greater than that corresponding to twice the excitation potential. When this is the case (21) may be reduced to:

$$\begin{aligned} &\text{(a)}\ u \geqslant u_s \qquad S = 2\pi N \int_u^\infty f \cdot q_s \cdot u\,du \\ &\text{(b)}\ 0 \leqslant u \leqslant u_s \quad S = S(u_s) - S(u+u_s). \end{aligned} \tag{22}$$

A similar procedure is possible when only ionization and volume recombination are assumed to occur. Again following article I[3] and making use of the neutral molecule and positive ion particle densities in (4) and (6) we have:

$$\begin{aligned} S(u) = 2 \cdot 2\pi(N-n) &\int_u^{2u+u_i} f \cdot q_i \cdot u\,du \\ &+ 2\pi(N-n) \int_0^u f \cdot q_i \cdot u\,du \\ &- 2\pi n \int_0^u f \cdot q_r \cdot u\,du. \end{aligned} \tag{23}$$

Furthermore, from the definition of a steady state we must also have:

$$\begin{aligned} S(\infty) = 2\pi(N-n) &\int_0^\infty f \cdot q_i \cdot u\,du \\ &- 2\pi n \int_0^\infty f \cdot q_r \cdot u\,du = 0. \end{aligned} \tag{24}$$

The cross section for recombination becomes negligibly small for energies of the order of that corresponding to the ionization potential or larger; the ionization cross section is zero for energies less than this value. In addition and in line with the foregoing procedure we shall assume that the distribution function may be neglected for energies greater than that corresponding to *three* times the ionization potential. Hence, making use of these approximations and the condition (24), we may easily show that:

(a) $u \geqslant u_i$

$$\begin{aligned} S(u) \doteq 2 \cdot 2\pi(N-n) &\int_u^\infty f \cdot q_i \cdot u\,du \\ &+ 2\pi(N-n) \int_{u_i}^u f \cdot q_i \cdot u\,du \\ &- 2\pi n \int_0^\infty f \cdot q_r \cdot u\,du \\ &= 2\pi(N-n) \int_u^\infty f \cdot q_i \cdot u\,du. \end{aligned} \tag{25}$$

(b) $0 \leqslant u \leqslant u_i$

$$\begin{aligned} S(u) = 2 \cdot 2\pi(N-n) &\int_{u_i}^{2u+u_i} f \cdot q_i \cdot u\,du \\ &- 2\pi n \int_0^u f \cdot q_r \cdot u\,du \\ = \{S(u_i) &- S(2u+u_i)\} \\ &+ \left\{ 2\pi n \int_u^\infty f \cdot q_r \cdot u\,du - S(2u+u_i) \right\}. \end{aligned}$$

The second expression in braces in (25b) vanishes at both ends of the interval: accurately at zero, approximately at u_i since both terms become negligibly small. Within the interval, as u increases, both terms decrease monotonically in magnitude. In a first approximation, therefore, this term will be neglected. To anticipate the results of the calculation, it will be found that when $n \ll N$, which is still true in the region of breakdown, this approximation is a good one.

IV

We are now in a position to find an expression for the distribution function. In the remainder

of this paper only thermal or quasi-thermal (high frequency) excitation will be discussed. Consider first the case of excitation of a single discrete level. The function $S(u)$ is given by (22). We shall assume a linear cross section of the form:

$$q_s(u)=\begin{cases}K(u-u_s) & u\geqslant u_s\\ 0 & u\leqslant u_s\end{cases} \tag{26}$$

$S(u)$ may be eliminated between (22a) and (16):

$$(f)''+\left[\frac{2}{u}+c\right](f)'+\left[\frac{\alpha}{u}-\beta\right](f)=0, \tag{27}$$

where

$$c\equiv\frac{m}{2kT};\quad \alpha\equiv 2c+\beta u_s;\quad \beta\equiv\frac{cKM}{2mq};\quad Nq\lambda=1$$

and the mean free path, λ, has been assumed for convenience to be a constant in the energy. The second term of (27) is removed by the substitution:

$$f=u^{-1}e^{-\frac{1}{2}cu}g. \tag{28}$$

We have finally:

$$g''+\left\{-\frac{1}{4}+\frac{k}{z}\right\}g=0,$$

where

$$z\equiv(c^2+4\beta)^{\frac{1}{2}}u;\quad k\equiv\frac{\alpha-c}{(c^2+4\beta)^{\frac{1}{2}}}. \tag{29}$$

This is a special form of the differential equation of the confluent hypergeometric function. Since $z>cu$ and $W_{-k,\frac{1}{2}}(-z)$ increases as $\exp(\frac{1}{2}z)$ for large values of z, we must choose as the solution consistent with the boundary condition that f must vanish at infinity:

$$g=AW_{k,\frac{1}{2}}(z). \tag{30}$$

Hence, by means of (16) and (22) the distribution function may be found over the entire range of u. There are four steps:

$$\begin{aligned}&\text{(a)}\quad u\geqslant u_s\quad f=Au^{-1}e^{-\frac{1}{2}cu}W_{k,\frac{1}{2}}(z),\\ &\text{(b)}\quad u\geqslant u_s\quad S=2\pi N\int_u^\infty f\cdot K_s(u-u_s)u\,du,\\ &\text{(c)}\quad u\leqslant u_s\quad S=S(u_s)-S(u+u_s),\\ &\text{(d)}\quad u\leqslant u_s\quad f=\left(\frac{M\lambda}{8\pi kT}\right)e^{-cu}\int_u^\infty\frac{e^{cu}S\,du}{u^2}.\end{aligned} \tag{31}$$

For the case of ionization and volume recombination (no excitation of discrete levels) we note that since the form of (25a) is identical with that of (22a) the same solution may be used as before, if a linear cross section in the form of (3) is adopted. Hence, the distribution function may again be computed over the entire range of u by means of four steps. We shall assume henceforth that $n\ll N$. Then Eqs. (31) remain valid for ionization provided we make the following simple changes:

u_s must be replaced by u_i; the constant K_s by the appropriate K_i, and Eq. (31c) reads

$$S=S(u_i)-S(2u+u_i). \tag{32}$$

The parameters of the Whittaker function are defined as in the first case. It is interesting to note that in first approximation the form of the distribution function does not depend upon any specific assumptions concerning the recombination cross section but only upon its existence in the equation of the steady state.

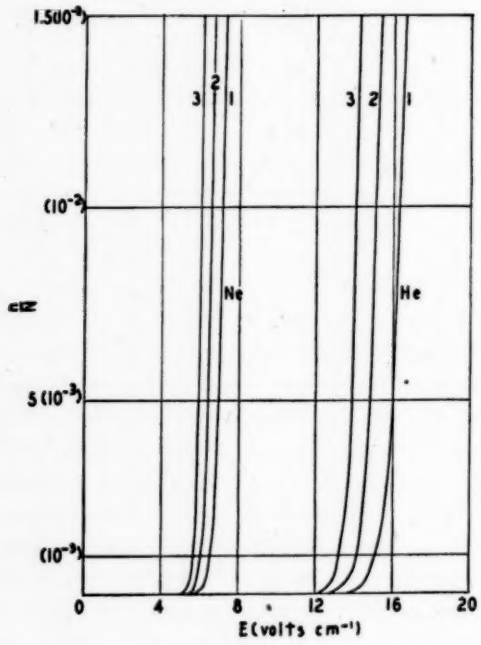

FIG. 5. Plot of n/N vs. field strength.

$p<1$-mm Hg
$\nu=3(10^9)$ sec.$^{-1}$

1. $R=10^{-6}$ cm^4 sec.$^{-2}$
2. $R=10^{-7}$
3. $R=10^{-8}$

V

The distribution function has been calculated by means of (31) and (32) for helium and neon, since only for these two, among the rare gases, can the assumption of a constant mean free path

be justified even in approximation. The calculation was made for four temperatures: (10^4), $2(10^4)$, $3(10^4)$, $4(10^4)$°K. The results could then be interpreted in terms of the high frequency field by means of the relation, obtained from (17):

$$E=7.98(10^{-11})\nu\left[\frac{T'-T}{A}\right]^{\frac{1}{2}}. \tag{33}$$

Here E is measured in volts per centimeter, ν is the field frequency, A is the molecular weight of the gas molecule, and T is taken to be room temperature. The frequency of the field was assumed to be $3(10^9)$ sec.$^{-1}$ since measurements exist at this frequency. The treatment as one of "thermal" ionization is then valid for pressures below about 1-mm Hg, in accordance with the conditions attending the use of (17).

The slopes, K_i, of the ionization cross sections for helium and neon were measured from the published curves of Druyvesteyn and Penning.[10] The total collision cross sections were obtained by averaging over the collision probabilities as published by Brode.[11]

Direct evaluation of the Whittaker function in (31a) was found to be possible only for helium and at the temperature $4(10^4)$°K. This was due, first, to the fact that the large values of the parameter k required by the problem necessitated the evaluation of a very large number of terms of either the power series or asymptotic series expansions of the Whittaker function, and, second, to the circumstance that over the range of z in question we are near the zero of the coefficient of g in Eq. (29) and hence were forced to use an impracticably large number of significant figures. The matter was resolved by obtaining approximate, numerical solutions of Eq. (29) directly. Let z_0 denote the value of z corresponding to u_i. Then for $z\geqslant z_1>z_0$ the J.W.K.B. solution was found to be satisfactory. A suitable value of z_1 was that corresponding to $\delta=1.05$, where the variable δ may be defined, as in article I of this paper, by either of the relations:

$$u=\delta u_i, \quad z=\delta z_0. \tag{34}$$

[10] M. J. Druyvesteyn and F. M. Penning, Rev. Mod. Phys. 12, 92 (1940).
[11] R. B. Brode, Rev. Mod. Phys. 5, 263 (1933).

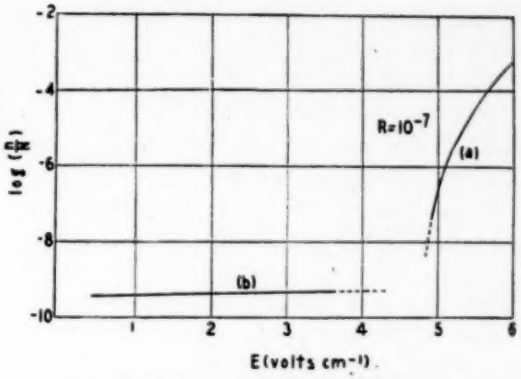

FIG. 6. Plot of $\log n/N$ *vs.* field strength.
Neon
$\nu=3(10^9)$ sec.$^{-1}$ $\quad p=1$-mm Hg

Thus:

$$W_{k,\frac{1}{2}}(z)\doteq\left[\frac{\rho(z_1)}{\rho(z)}\right]^{\frac{1}{2}}\exp\left\{-\int_{z_1}^{z}\rho(z)dz\right\} \qquad z\geqslant z_1>z_0 \tag{35}$$

where

$$\rho^2(z)\equiv\left(\frac{1}{4}-\frac{k}{z}\right). \tag{36}$$

For $z_0\leqslant z\leqslant z_1$ we may rewrite Eq. (29):

$$g''-\frac{1}{16k}(z-4k)g=0.$$

This has the solution:

$$W_{k,\frac{1}{2}}(z)=(z-4k)^{\frac{1}{2}}\left\{AJ_{1/3}\left[\frac{i(z-4k)^{\frac{1}{2}}}{6k^{\frac{1}{2}}}\right]+BJ_{-1/3}\left[\frac{i(z-4k)^{\frac{1}{2}}}{6k^{\frac{1}{2}}}\right]\right\} \qquad z_0\leqslant z\leqslant z_1. \tag{37}$$

The solutions (35) and (37) may be equated at z_1. An additional relation in A and B is obtained by equating the derivatives at this point. Thus:

(a) $$W_{k,\frac{1}{2}}'(z)=-\left\{\rho+\frac{k}{4\rho^2z^2}\right\}W_{k,\frac{1}{2}}(z) \qquad z\geqslant z_1,$$

(b) $$W_{k,\frac{1}{2}}'(z)=\frac{i}{4k^{\frac{1}{2}}}(z-4k)\times\left\{AJ_{-2/3}\left[\frac{i(z-4k)^{\frac{1}{2}}}{6k^{\frac{1}{2}}}\right]-BJ_{2/3}\left[\frac{i(z-4k)^{\frac{1}{2}}}{6k^{\frac{1}{2}}}\right]\right\} \qquad z_1\geqslant z\geqslant z_0, \tag{38}$$

and

$$A=\frac{aJ_{2/3}+bJ_{-1/3}}{J_{1/3}J_{2/3}+J_{-1/3}J_{-2/3}} \qquad z=z_1, \qquad (39)$$

$$B=\frac{aJ_{-2/3}-bJ_{1/3}}{J_{1/3}J_{2/3}+J_{-1/3}J_{-2/3}},$$

where

$$a\equiv\frac{W_{k,\frac{1}{2}}(z)}{(z-4k)^{\frac{1}{4}}}, \quad b\equiv-\frac{i4k^{\frac{1}{2}}W_{k,\frac{1}{2}}'(z)}{(z-4k)}.$$

The Bessel functions were evaluated at z_1 by interpolation from the tables of Jahnke-Emde,[12] at z_0 by using the series expansion for the Bessel functions,[13] the first three terms being sufficient.

It was found convenient to let $f(u_i)=1$ throughout the calculation. A check of the approximation outlined above was possible for helium at the temperature $4(10^4)$°K since at this temperature the asymptotic expansion of the Whittaker function could be used. Agreement to within five percent was found over the range of energies considered. In Fig. 1 the common logarithm of f is plotted as a function of δ for the four temperatures considered and for both helium and neon.

$S(\delta)$ is plotted in Fig. 2 for both helium and neon and for the two extreme temperatures considered. The function has a maximum at $\delta=1$. The curve becomes progressively flatter for $\delta<1$ as the temperature is reduced and may be approximated by a horizontal, straight line over most of this range for the temperatures in question.

In Fig. 3 is plotted the integral of (31d) for both gases. These curves illustrate the way in which the distribution function approaches a Maxwellian distribution for $\delta<1$ as the temperature is reduced. At a temperature of (10^4)°K the integral is effectively constant over the whole range of δ less than about 0.8 and, as seen by inspection of (31d), the distribution function is accordingly Maxwellian in this range. The integrand of (31d) actually possesses two maxima: one, quite sharp, near the origin, and a second, considerably broader, near 1.0. As the temperature decreases the latter maximum increases rapidly in height relative to the former.

In Fig. 4 the common logarithm of the integrals I_1 and I_2 as defined in article I is plotted as a function of the temperature. In Fig. 5 the quantity n/N is plotted as a function of the field strength; it was calculated by means of Eq. (8a), the relation between the field strength and the temperature being given by (33). The range of n/N is an arbitrary one satisfying the relation $n\ll N$. The proper values of R (cf. Eq. (5)) remain uncertain, and the values indicated on the graphs are taken as being probably representative, on the basis of Wessel's calculations for doubly charged helium ions, for the singly charged ions here involved. Several facts should be noted. First, the characteristics for neon are steeper than for helium. Second, the characteristic becomes steeper as the value chosen for R is reduced. Third, the characteristic becomes steeper as the field strength is reduced and hence as n/N becomes smaller. This last is better illustrated in Fig. 6 where the common logarithm of n/N is plotted as a function of the field strength for neon and where, in addition, the weak field characteristic is plotted with the use of (8b). The latter calculation was carried out by assuming that the distribution is Maxwellian, that ionization by electron-molecule collision could be neglected for the small field strengths involved, and that 10 ion pairs per cubic centimeter per second are produced by external agencies at atmospheric pressure. The calculation was made for a pressure of 1-mm Hg and for $R=(10^{-7})$. Similar results are obtained for other values of R and for other pressures. In order to connect the two curves it would be necessary to use (8) in its full form.

It is clear from Figs. 5 and 6 that the phenomenon of breakdown into a Townsend type discharge may be studied by this method and that the essential mechanisms cooperating to produce breakdown may well be ionizing electron-molecule encounters and volume recombination of electrons and positive ions. Rough values of the field strengths at breakdown may be estimated from Fig. 5, e.g., 5 volts/cm for neon and 13 volts/cm for helium. These may be

[12] E. Jahnke and F. Emde, *Funktionentafeln* (Dover Publishers, New York, 1943), p. 235.
[13] E. T. Whittaker and G. N. Watson, *A Course of Modern Analysis* (Cambridge University Press, New York, 1935), p. 358.

compared with the observed values obtained at M.I.T.[14] The experiments indicate that at about 1-cm Hg the r.m.s. fields at breakdown are about 9 volts/cm for neon and 19 volts/cm for helium. The fact that the calculated values are too low is encouraging, for it leaves room for disposal of electrons by other mechanisms. The calculated results here are independent of the pressure, but the approximation upon which they are based breaks down for pressures above about 1-mm Hg. On the other hand, because of the small volume of the discharge vessel used for the measurements at M.I.T. the results below about 1-cm Hg are diffusion dependent. Additional calculations must be carried out at higher pressures, therefore, before a detailed comparison between experiment and theory will be in order. Taking these considerations into account and also the facts that inelastic collisions have been neglected, that additional mechanisms such as radiation trapping, diffusion, etc., will have a significant effect upon the shape of the characteristic, agreement between experimental results and the predictions of the present treatment appear to be satisfactory.

It should be noted finally that specific assumptions concerning the detailed shape of the cross sections involved have little effect upon the results of these calculations. Additional calculations made for helium with the slope of the ionization cross section multiplied by 2 shift the positions of the curves of n/N towards higher fields by less than 2 volts/cm. Similarly, an even smaller effect is introduced by varying the exponent of u in the recombination cross section (5) about the value unity.

[14] S. C. Brown, report at M.I.T. Conference on Physical Electronics, March, 1947; material unpublished.

Theory of High Frequency Gas Discharges. IV. Note on the Similarity Principle[1]

H. MARGENAU
Yale University, New Haven, Connecticut
(Received August 18, 1947)

The similarity principle of Steenbeck is derived from the differential equation for the electron distribution function and is extended to cover h.f. discharges. Possible applications and its limitations are discussed.

THE similarity principle is a statement of the conditions under which "similar" discharges may take place in vessels having different dimensions and containing the same gas at different pressures. First introduced by Steenbeck, the application of the principle to d.c. discharges is discussed fully in *vs.* Engel and Steenbeck's book.[2]

The term "similar" discharges is somewhat ambiguous, and it is usually specified to mean equal currents at equal potential differences. In h.f. work potentials are not of primary interest, and it will appear that consideration of currents is not very useful. Hence we shall here define similar discharges to mean discharges in which *the distribution in energy of the electrons at corresponding points of space is the same.* Whether and how the current changes under these circumstances can then be considered afterwards.

The principal differences between the d.c. and h.f. cases lie in the minor roles played by space charge and by the electrodes in the latter. Most of the electrons are produced within the gas, and their diffusion to the walls or the electrodes is presumably ambipolar, producing no separation of positive ions and electrons. These simplifying features make the similarity principle perhaps even more attractive for consideration with h.f. than with d.c. discharges. The following treatment deduces it from the transfer equation and is in a sense complementary to the analysis given by Steenbeck.

Study of the similarity principle may be based on Eqs. (39) of Article I in this series. From them one obtains by elimination an equation for $f^{(0)}$, which will now be normalized to unity and denoted by $n\varphi(v, x)$; n is the number density of electrons. This equation is

$$-\frac{n\gamma^2}{6}\frac{\partial}{\partial v}\left[\frac{\lambda v^3}{v^2+(\omega\lambda)^2}\frac{\partial\varphi}{\partial v}\right]-\frac{nv^3}{3}\lambda_d\frac{\partial^2\varphi}{\partial x^2}=\frac{1}{4\pi}\frac{\partial s}{\partial v}. \quad (1)$$

As to symbols,

$\gamma = e/m$ times amplitude of the electric field, E
λ = mean free path
λ_d = mean free path characteristic for diffusion of electrons
ω = radian frequency of microwaves
$S(v)$ = rate of increase in the concentration of electrons having speeds below v, due to all non-elastic collisions.

S includes the effects of ionization, as well as all mechanisms removing electrons from the discharge with the exception of diffusion, which is represented by the second term on the left of Eq. (1). For each process, S has the form

$$n\int_{v_1}^{v_2}\frac{v}{\lambda_s}\varphi 4\pi v^2 dv.$$

The limits of the integral differ for different processes, as is apparent from the discussion in Articles I and III, but they do not depend on such extraneous parameters as field strength, frequency, density, and gas pressure. Usually they are zero, infinity, the variable v, or some v characteristic of the molecular nature of the gas. The mean free path λ_S for the process in question always satisfies

$$N_s q_s \lambda_s = 1,$$

where N_s is the number of obstacles of collision permitting the process s, and of q_s its cross section. Again, q_s is independent of extraneous parameters though it will depend on v.

[1] This work has been supported by the office of Naval Research, United States Navy, under Contract N6ori-44.
[2] M. Steenbeck, Wiss. Veröff. a.d. Siemens Konzern, 11, 36 (1932); A. v. Engel and M. Steenbeck, Elektrische Gasentladungen II (1934), p. 95.

The number of ways in which electrons can be generated or destroyed is very large indeed, and it is not the purpose of this note to survey them all. We single out three which seem to be of importance.

1. Primary ionization by electron impact. Here $N_s=N$, the concentration of gas molecules. Accurately, $N_s=N_0-n$, the initial number of gas molecules less the number of positive ions (or electrons). But n may here be neglected and N will henceforth be identified with N_0.

2. Capture of electrons by neutral molecules. The rate at which this happens depends upon the manner of neutralization of the negative ions thus formed. But in many instances the rate will be proportional to N. Hence again, $N_s=N$.

3. Recombination with positive ions; $N_s=n$, the electron concentration which is equal to the concentration of negative ions.[3]

The quantity S, therefore, consists of 3 parts, the first two being proportional to nN, the third to n^2. The mean free paths λ and λ_d appearing in Eq. (1) are proportional to N^{-1}. After division by nN Eq. (1) takes this form:

$$C\left(\frac{\gamma}{N},\frac{\omega}{N}\right)\varphi+DN^{-2}\frac{\partial^2\varphi}{\partial x^2}=I\varphi+nN^{-1}R\varphi. \quad (2)$$

The notation is meant to indicate that C, D, I, R are operators applied to φ and affecting only its v-dependence. Of the four, C depends parametrically on γ/N and ω/N, while the others retain their form for all field strengths and frequencies. C represents all "normal" effects entering into the transfer equation, such as the acceleration of electrons by the field and their deceleration by elastic collisions; its form in Eq. (1) is an approximation which holds for the case of low gas temperature. The operators D, I, and R represent diffusion, ionization, and direct recombination. Capture is included in I, since the term in S which describes capture has the same dependence on n and N as does ionization.

From Eq. (2) one can derive the similarity principle at once; *The dependence of φ on v is unchanged if the following four quantities retain their values:*

$$\frac{E}{N}\left(\text{i.e.,}\frac{\gamma}{N}\right);\quad \frac{\omega}{N};\quad Nx;\quad \frac{n}{N}. \quad (3)$$

The first two remain unchanged provided the field strength, the frequency, and the pressure are altered by the same factor. Invariance of the third requires that all linear dimensions of the discharge must be changed in inverse proportion to the pressure. Constancy of n/N means that *the electron concentration changes in the same way as the gas pressure.*

Theoretically, the essentially new feature in the similarity principle for high frequency discharges is the requirement that not only E/N be kept constant (Paschen's law), but also ω/N (in addition to the other restrictions which come from the production and destruction processes chosen for consideration). Practically, however, the situation may be rather different in the two cases. In d.c. work, where the field is produced between electrodes, the requirement that E and x, and hence the distance between electrodes, be changed in contragredient fashion forces one to use the same potential difference. In h.f. work there is probably greater freedom.

When ionization does not occur, and the electron concentration is maintained by agencies external to the gas, Eq. (2) implies the more special result that the distribution function can depend on E/N and on ω/N only. This is apparent in previous work,[4] where f was found to be determined by two quantities having the dimensions of energy: $\epsilon_1=\frac{1}{2}m(\omega\lambda)^2$ and $\epsilon_2=eE\lambda$.

Conditions (3) do not imply equality of currents or equal power in two discharges satisfying these conditions; they merely assure equal energy distributions of the electrons. Probe measurements and spectroscopic determinations of the relative intensities of spectral lines emitted by the gas could be used to verify the similarity principle in the present form.

Current density and power density are proportional to n for discharges in which the electrons have equal energy distributions φ. Hence, the similarity principle predicts that, under conditions 3, current and power density should be proportional to the gas pressure. The following

[3] If the gas molecules have an electron affinity, recombination via the formation of negative ions is more probable than direct recombination between electrons and positive ions. For this effect, N_s is proportional to the concentration of negative ions and this, in turn, is usually proportional to N. Hence the effect can be combined with (1) and (2) and merely gives rise to a modified I in Eq. (2). Recombination with positive ions is included specifically here because it has an important effect on the similarity principle.

[4] H. Margenau, Phys. Rev. 60, 508 (1946).

comments will show why this is true and to what extent it may be experimentally observed.

If recombination is disregarded, the term in Eq. (2) containing R is absent. Similarity of φ then requires only E/N, ω/N, and Nx to remain unchanged. The electron density n is quite unaffected by the changes in E, N, ω, and x. Hence one might conclude that n remains the same. But this would be fallacious, for Eq. (2) in this case does not determine n at all and is satisfied for any n. Variation of n in discharges is therefore a very critical matter; diffusion alone leaves it indeterminate, the presence of recombination causes it to vary with N, other mechanisms impose a more peculiar variation. All this is true, of course, for d.c. as well as for h.f. discharges. It shows that similarity applies strictly only to the energy dependence of φ, not necessarily to the observable properties of discharges.

If diffusion is disregarded in Eq. (2), D is zero and the constancy of Nx is no longer required for similarity of φ. The role of diffusion is thus rather distinctive, and its importance should be settled by experimentation. The obvious procedure would be to study discharges with the same E, ω, and N but with different dispositions of electrodes and sizes or shapes of discharge vessels. A difficulty encountered in this attempt is that, in practice, one rarely gets the same E in a cavity if its dimensions or its shape are altered. Here the similarity principle would help, for it says that a change in E can be compensated by changes in ω and in N. In performing such experiments it would be desirable primarily to measure quantities depending on φ, such as breakdown and maintenance potentials. Though these are ill defined theoretically, it would seem that equality of these potentials indicates equality of energy distributions.[5]

The importance of the principle arises from the fact that failure of a given type of discharge to conform to it exposes the presence of processes whose cross sections have a peculiar dependence on n and N.

[5] Cf. L. M. Hartman, Phys. Rev. **73**, 316 (1948).

PHYSICAL REVIEW VOLUME 73, NUMBER 4 FEBRUARY 15, 1948

Electronic Component of Cosmic Rays in the Low Atmosphere. I. Theoretical

G. BERNARDINI, B. N. CACCIAPUOTI, AND R. QUERZOLI
Physics Department, University of Rome, Rome, Italy

(Received June 5, 1947)

The authors discuss the problem of the equilibrium conditions between meson and secondary electronic component. Following William's concept of *electron track*, some formulas are deduced for the number of electrons with energy $\geqslant \eta$ generated in coulombian collisions and in equilibrium with the meson component, in a substance having a critical energy ϵ_c. Similarly a general formula is given for the number of disintegration electrons in equilibrium with the meson component in atmosphere. Such formulas present a remarkable generality because they include the fundamental parameters explicitly, and the meson spectrum appears in them in integral form; this makes them particularly suitable for comparison with experiments.

With the aid of these formulas the following calculations have been performed: (1) Number of secondary electrons generated in Pb and in equilibrium with the meson component for $\eta=2$, 3, 4, 5 Mev and for different values of the lower limit of meson energy. (2) Number of secondary collision electrons arising from the atmosphere for different values of η at sea level and at 3500 m. above sea level. (3) Number of secondary disintegration electrons for different values of the cut-off energy, etc.

I. INTRODUCTION

MEASUREMENTS concerned with the electronic component of cosmic rays near the earth's surface are not well understood in terms of the usual theories of their origin. According to the theoretical work of Heitler,[1] Euler and

[1] W. Heitler, Proc. Roy. Soc. **161**, 261 (1937).

Heisenberg,[2] Ferretti,[3] Bhabha,[4] Lyons,[5] etc., only electrons in equilibrium with the hard component should be expected between sea level and an altitude of 4–5 km.

On the other hand, experiments performed by Cacciapuoti[6] and Bernardini, Cacciapuoti, Ferretti, Piccioni and Wick[7] seem to indicate that the soft component is not in equilibrium with the hard one; in fact, the increase in intensity of the soft component with height is somewhat faster than is theoretically predicted. These results were confirmed by further experiments performed by Cocconi and Tongiorgi[8] and by Rossi and Greisen.[9]

Many theoretical and experimental investigations have since been performed to establish the equilibrium conditions between electronic and meson components but the conclusions are not as yet in satisfactory agreement. In most of these works,[10–19] the excess in the intensity of the soft component is ascribed mainly to the presence of slow mesons (energy between 0 and 200 Mev). According to Greisen,[14] the number of these slow mesons would be, even at sea level, so high as to rule out the normal process of disintegration of a meson into an electron and a neutrino.[20]

Since several experiments performed by the Rome Center of Nuclear Physics during the war seem to suggest a rather different conclusion, we thought it would be useful to discuss the whole problem over again, taking also into account the recent results published by Hazen,[21] Nassar and Hazen,[22] and by Powell.[23]

II. GENERAL REMARKS ON THE EQUILIBRIUM CONDITIONS BETWEEN MESON AND SECONDARY ELECTRONIC COMPONENTS

Following the well-known Williams' argument, Ferretti[24] and Rossi and Klapman[25] have pointed out that in treating the equilibrium conditions between meson and electronic components, it is useful to introduce the concept of *electron track*. If $N(\epsilon, \eta, x)$ is the number of electrons with energy $\geqq\eta$ in a shower originated by an "ancestor electron" having the initial energy ϵ and present at a distance x from the origin of the shower, the electron track is defined by the integral:

$$z(\epsilon, \eta) = \int_0^\infty N(\epsilon, \eta, x)dx.$$

This expression denotes the total length of the paths described by the electrons of the shower while their energy is larger than η. According to Ferretti,[24] if β denotes the ionization loss per unit length and ϵ_c the critical energy of the substance in which the shower has originated, a sufficiently approximated value of $z(\epsilon, \eta)$ is given by:

$$z(\epsilon, \eta, \epsilon_c) = \frac{\epsilon}{\beta}\left\{1 - \frac{\eta}{\epsilon}\exp\left[-\frac{2(\epsilon-\eta)}{\epsilon_c}\right] - \frac{2\eta}{\epsilon_c}\exp\left[\frac{2\eta}{\epsilon_c}\right]\left[E_i\left(-\frac{2\epsilon}{\epsilon_c}\right) - E_i\left(-\frac{2\eta}{\epsilon_c}\right)\right]\right\}. \quad (1)$$

Ferretti's relation is particularly convenient because of its simplicity and its explicit dependence upon the fundamental parameters ϵ, η, ϵ_c.

Now, according to the already mentioned intuitive considerations of Williams,[26] when the genetic equilibrium between electronic and meson

[2] H. Euler and W. Heisenberg, Ergeb. d. exakt Naturwiss. **17**, 1 (1938).
[3] B. Ferretti, Ricerca Scient. **7–8**, 736 (1939).
[4] H. J. Bhabha, Proc. Roy. Soc. **164**, 25 (1938).
[5] Lyons, Phys. Zeits. **42**, 166 (1941).
[6] B. N. Cacciapuoti, Ricerca Scient. **12**, 1082 (1939).
[7] G. Bernardini, B. N. Cacciapuoti, B. Ferretti, O. Piccioni, and G. C. Wick, Phys. Rev. **58**, 1017 (1940).
[8] G. Cocconi and V. Tongiorgi, Zeits. f. Physik **118**, 88 (1941).
[9] B. Rossi and K. Greisen, Phys. Rev. **61**, 121 (1942).
[10] Tamm and Belenky, Z. Phys. Ac. Sc. USRR **1**, 177 (1939).
[11] J. A. Richards and L. W. Nordheim, Phys. Rev. **61**, 735 (1942).
[12] P. V. Auger, Phys. Rev. **61**, 684 (1942).
[13] W. E. Hazen, Phys. Rev. **65**, 67 (1944).
[14] K. Greisen, Phys. Rev. **63**, 323 (1943).
[15] H. E. Stanton, Phys. Rev. **66**, 48 (1944).
[16] D. B. Hall, Phys. Rev. **66**, 321 (1944).
[17] S. V. Chandrashekhar Aiya and R. C. Saxena, Phys. Rev. **66**, 183 (1944).
[18] A. Alichanow and A. Alichanian, J. Phys. U.S.S.R. **9**, 73 (1945).
[19] S. Nassar and W. E. Hazen, Phys. Rev. **69**, 298 (1946).
[20] The different behavior of positive and negative mesons predicted by Tomonaga and Araky (Phys. Rev. **58**, 90 (1940)) and confirmed experimentally by Conversi, Pancini and Piccioni (Phys. Rev. **68**, 232 (1945)) does not affect the mesons in the atmosphere because it concerns only mesons at the end of their range and practically at rest.
[21] W. E. Hazen, Phys. Rev. **64**, 7 (1943) and **65**, 67 (1944).
[22] S. Nassar and W. E. Hazen, Phys. Rev. **69**, 298 (1946).
[23] W. M. Powell, Phys. Rev. **69**, 385 (1946).
[24] B. Ferretti, Ricerca Scient. **13**, 532 (1942).
[25] B. Rossi and S. J. Klapman, Phys. Rev. **61**, 414 (1942).
[26] E. J. Williams, Proc. Camb. Phys. Soc. **36**, 183 (1940).

components is reached, the number of electrons with energy $\geqq\eta$ generated by coulombian collision processes which accompany the mesons of energy E to $E+dE$, is given by

$$J(E)dE\int_{\eta}^{\epsilon_m(E)}\sigma(\epsilon, E)z(\epsilon, \eta)d\epsilon,$$

where $\sigma(\epsilon, E)$ denotes the total effective cross section for coulombian collisions, $\epsilon_m(E)$ the maximum energy that can be transferred from a meson to an electron in the collision and $J(E)$ the meson differential spectrum. The total number of electrons with energy $\geqq\eta$ generated in coulombian collisions and in equilibrium with the meson component, in a substance having a critical energy ϵ_c, is therefore

$$n_c(\eta)=\int_{E^*}^{\infty}J(E)dE\int_{\eta}^{\epsilon_m}\sigma(\epsilon, E)z(\epsilon, \eta)d\epsilon, \quad (2)$$

where E^* denotes the minimum energy a meson must have in order to generate, through a collision, an electron having at least an energy equal to η.

For the study of the equilibrium conditions near sea level, it may be assumed that the spin of the meson is zero.[27] In this case, if k indicates a well-known coefficient which depends on the substance (see below), we can write with good approximation

$$\sigma(\epsilon, E)=\sigma(\epsilon, \epsilon_m)=[k/\epsilon^2][1-(\epsilon/\epsilon_m(E))], \quad (3)$$

where $\epsilon_m(E)$ is the maximum energy that a meson with energy E can transfer to an electron in a coulombian collision, and is given by

$$\epsilon_m=[E^2-(\mu c^2)^2]/[\mu c^2(\mu/2m)-(E/\mu c^2)], \quad (4)$$

where μ is the mass of the meson, m the mass of the electron. The value of E^* to be taken as a lower limit for the first integral in (2) is therefore

$$E^*(\eta)=(\eta/2)+\{(\eta^2/4)+(\mu c^2)^2[(\eta/2mc^2)+1]\}^{\frac{1}{2}}. \quad (5)$$

Moreover, for an electron generating a shower and having an energy much greater than the cut-off energy, Ferretti's relation assumes the following simple form*

$$z_\infty(\epsilon, \eta)=S_\infty\epsilon/\beta,$$

with

$$S_\infty=1+\frac{2\eta}{\epsilon_c}\exp\left[\frac{2\eta}{\epsilon_c}\right]E_i\left(-\frac{2\eta}{\epsilon_c}\right). \quad (6)$$

In order to calculate the integral (2) we have split it in the following way:

$$n_c(\eta)=\int_{E^*}^{E_c}J(E)dE\int_{\eta}^{\epsilon_m}\sigma z d\epsilon + \int_{E_c}^{\infty}J(E)dE\int_{\eta}^{\epsilon_c}\sigma z d\epsilon+\int_{E_c}^{\infty}J(E)dE\int_{\epsilon_c}^{\epsilon_m}\sigma z d\epsilon$$

where E_c is the energy of a meson which can transfer to an electron only an energy $\leqq\epsilon_c$.

Since the differential spectrum of mesons deduced from Wilson chamber measurements is not known with great precision, neither at high nor at low energies, we have proceeded with an integration by parts so as to express the results in terms of the integral spectrum.

Indicating with

$$I(E)=\int_{E}^{\infty}J(E)dE, \quad (7)$$

the integral spectrum, it can easily be seen that the number of collision electrons is given by the following general formula:

$$\frac{n_c}{k}=I(E^*)\phi(E^*)+I(E_c)\{\psi(E_c)+\theta(E_c)-\phi(E_c)\}+\int_{E^*}^{E_c}I(E)\frac{\partial\phi}{\partial E}dE + \int_{E_c}^{\infty}I(E)\frac{\partial\psi}{\partial E}dE+\int_{E_c}^{\infty}I(E)\frac{\partial\theta}{\partial E}dE, \quad (8)$$

[27] R. E. Lapp, Phys. Rev. 69, 321 (1946). The value of the spin of the mesons is not important for this purpose on account of the low mean energy of the mesons.

* The critical energy ϵ_c is very often much larger than the cut-off energy and, in these cases, the asymptotic formula can be used when $\epsilon>\epsilon_c$.

where

$$\phi(E)=\frac{1}{k}\int_{\eta}^{\epsilon_m}\sigma z d\epsilon=\frac{1}{\beta}\left\{S_\infty\left(\log\frac{\epsilon_m}{\eta}+\frac{\eta}{\epsilon_m}-1\right)-\eta\left(\frac{2}{\epsilon_c}+\frac{1}{\epsilon_m}\right)\left[E_i\left(-\frac{2\eta}{\epsilon_c}\right)-E_i\left(-\frac{2\epsilon_m}{\epsilon_c}\right)\right]\exp\left[\frac{2\eta}{\epsilon_c}\right]\right.$$

$$\left.+\frac{\eta}{\epsilon_m}\exp\left[\frac{2(\eta-\epsilon_m)}{\epsilon_c}\right]-1+\frac{\eta}{\epsilon_m}\exp\left[\frac{2\eta}{\epsilon_c}\right]\int_{2\mu/\epsilon_c}^{2\epsilon_m/\epsilon_c}E_i(-x)dx-\frac{2\eta}{\epsilon_c}\exp\left[\frac{2\eta}{\epsilon_c}\right]\int_{2\mu/\epsilon_c}^{2\epsilon_m/\epsilon_c}E_i(-x)\frac{dx}{x}\right\}, \quad (9)$$

$$\theta(E)=\frac{1}{k}\int_{\epsilon_c}^{\epsilon_m}\sigma S_\infty\epsilon\frac{d\epsilon}{\beta}=S_\infty\left[\log\frac{E_m}{\epsilon_c}+\frac{\epsilon_c}{\epsilon_m}-1\right]\frac{1}{\beta}, \quad (9')$$

and the functions ψ_1 and ψ_2 are respectively:

$$\psi_1=S_\infty\log\frac{\epsilon_c}{\eta}+\frac{\eta}{\epsilon_c}\exp\left[\frac{2(\eta-\epsilon_c)}{\epsilon_c}\right]-1-\frac{2\eta}{\epsilon_c}\exp\left[\frac{2\eta}{\epsilon_c}\right]\left\{E_i\left(-\frac{2\eta}{\epsilon_c}\right)-E_i(-2)+\int_{2\eta/\epsilon_c}^{2}E_i(-x)\frac{dx}{x}\right., \quad (10)$$

$$\psi_2=(\epsilon_c-\eta)S_\infty+\eta\exp\left[\frac{2\eta}{\epsilon_c}\right]\left\{E_i\left(-\frac{2\eta}{\epsilon_c}\right)-E_i(-2)-\int_{2\eta/\epsilon_c}^{2}E_i(-x)dx\right\}, \quad (10')$$

$$\psi(E)=\frac{1}{k}\int_{\eta}^{\epsilon_c}\sigma z d\epsilon=\frac{1}{\beta}\left\{\psi_1(\eta,\epsilon_c)-\frac{1}{\epsilon_m}\psi_2(\eta,\epsilon_c)\right\}. \quad (9'')$$

Remembering (4) we can write (8) in the following form

$$\frac{n_c}{k}=I(E^*)\phi(E^*)+I(E_c)\{\psi(E_c)+\theta(E_c)-\phi(E_c)\}-\int_{E^*}^{E_c}I(E)\frac{\partial}{\partial E}\left(\frac{1}{\epsilon_m}\right)dE\int_{\eta}^{\epsilon_m}\frac{z}{\epsilon}d\epsilon$$

$$-\frac{\psi_2-S_\infty\epsilon_c}{\beta}\int_{E_c}^{\infty}I(E)\frac{\partial}{\partial E}\left(\frac{1}{\epsilon_m}\right)dE-\frac{S_\infty}{\beta}\int_{E_c}^{\infty}I(E)\frac{\partial}{\partial E}\left(\frac{1}{\epsilon_m}\right)\epsilon_m dE. \quad (11)$$

We can now consider three cases:

(1) $E^*>E_c$. In this case, if $\Theta=\vartheta/\beta$ and $\Psi=\psi/\beta$, we can write (11) as follows:

$$\frac{\beta}{k}n_c=I(E^*)[\Psi(E^*)-\Theta(E^*)]-S_\infty\int_{E^*}^{\infty}I(E)\frac{\partial}{\partial E}\left(\frac{1}{\epsilon_m}\right)\epsilon_m dE-\{\psi_2-S_\infty\epsilon_c\}\int_{E^*}^{\infty}I(E)\frac{\partial}{\partial E}\left(\frac{1}{\epsilon_m}\right)dE, \quad (11')$$

where the last two integrals are independent of the substance, that is of β and ϵ_c.

(2) $-E^*=E_c$. In this case (11′) becomes

$$\frac{\beta}{k}n_c=I(E_c)\Psi(E_c)-S_\infty\int_{E_c}^{\infty}I(E)\frac{\partial}{\partial E}\left(\frac{1}{\epsilon_m}\right)(\epsilon_m-\epsilon_c)dE \quad (11'')$$

(3) $E^*<E_c$. This case is the most complicated one because it is not possible to isolate completely the dependence of $I(E)$ in the first integral of (11).

It is easily seen that in this case we obtain

$$\frac{\beta}{k}n_c=I(E^*)\phi(E^*)-S_\infty\int_{E^*}^{\infty}I(E)\frac{\partial}{\partial E}\left(\frac{1}{\epsilon_m}\right)\epsilon_m dE-\eta\exp\left[\frac{2\eta}{\epsilon_c}\right]E_i\left(-\frac{2\eta}{\epsilon_c}\right)\int_{E^*}^{\infty}I(E)\frac{\partial}{\partial E}\left(\frac{1}{\epsilon_m}\right)dE$$

$$-0.014\eta\exp\left[\frac{2\eta}{\epsilon_c}\right]\int_{E_c}^{\infty}I(E)\frac{\partial}{\partial E}\left(\frac{1}{\epsilon_m}\right)dE+\eta\exp\left[\frac{2\eta}{\epsilon_c}\right]\int_{E^*}^{E_c}I(E)\frac{\partial}{\partial E}\left(\frac{1}{\epsilon_m}\right)$$

$$\times\left\{\left(1+\frac{2\epsilon_m}{\epsilon_c}\right)E_i\left(-\frac{2\epsilon_m}{\epsilon_c}\right)+\exp\left[\frac{-2\epsilon_m}{\epsilon_c}\right]\right\}dE, \quad (11''')$$

that obviously reduces to (11″) when $E^*=E_c$. The relations (11) present the following advantages over those generally used by other authors:

(1) a remarkable generality, because they include the fundamental parameters, explicitly, for comparison with experiments;

(2) the meson spectrum appears in integral form and can therefore be obtained directly with great accuracy from the ordinary absorption curves.

The validity of (11), however, fails for $\eta\to 0$, which is an interesting case, for instance, when the interpretation of Wilson chamber experiments is required. Yet it is obvious that we can find some relations similar to (11) in the way we followed for the preceding calculations. In this case, the calculations are even easier because Ferretti's "track" reduces to the electron track of Williams, that is $z=\epsilon/\beta$. For the electrons arising from coulombian collision (spin $=0$) in any kind of material, we have, therefore, this limit value of

$$\frac{\beta}{k}n_c=\int_{E^*}^{\infty}I(E)\log\frac{\epsilon_m}{\eta}dE+\eta\int_{E^*}^{\infty}I(E)\frac{dE}{\epsilon_m}-\int_{E^*}^{\infty}I(E)dE, \tag{12}$$

from which we easily obtain

$$\frac{\beta}{k}n_c=\int_{E^*}^{\infty}I(E)\frac{\partial}{\partial E}(\epsilon_m)\frac{dE}{\epsilon_m}+\eta\int_{E^*}^{\infty}I(E)\frac{\partial}{\partial E}\left(\frac{1}{\epsilon_m}\right)dE, \tag{13}$$

where the lower limits of the integrals do not now correspond to the cut-off of the apparatus, but to the maximum value we can give to the energy of the electrons so as to maintain the validity of the formula used for the collision cross section. If we take $\epsilon=3\ mc^2$, where m is the electron mass, we surely reach a sufficient approximation. We shall emphasize that William's concept of "electron track" must be understood likewise.

At sea level, we deduced from (13) a limiting value for collision electrons which amounts to ~12 percent of the meson components.

With a procedure similar to those just described, we have found a formula giving the number n_d of disintegration electrons in equilibrium with the meson component in atmosphere, which contains the parameters, and the integral meson spectrum. Starting from the following relation, the meaning of which is obvious,

$$n_d=\frac{\mu}{\tau c\rho}\left[\int_0^{p(\epsilon_c)}\frac{I(p)}{p^2}dp\int_{\eta}^{\epsilon(p)}z(\epsilon,\eta)d\epsilon+\int_{p(\epsilon_c)}^{\infty}\frac{I(p)}{p^2}dp\int_{\eta}^{\epsilon_c}z(\epsilon,\eta)d\epsilon+\int_{p(\epsilon_c)}^{\infty}\frac{I(p)}{p^2}dp\int_{\epsilon_c}^{\epsilon_p}z(\epsilon,\eta)d\epsilon\right], \tag{14}$$

where p indicates the momentum of the mesons, $\epsilon(p)=\frac{1}{2}[c\{p^2+(\mu c)^2\}^{\frac{1}{2}}+p]$, the maximum energy of a disintegration electron, and ρ and $I(p)$ indicate the density of the atmosphere and the differential spectrum at a height of about 130 g/cm² above the observation station (9), it is readily seen that the first integral gives a vanishing contribution and, therefore,

$$n_d=\frac{1}{\tau c\rho\mu c^2}\left\{\int_{\eta}^{\epsilon_c}z(\epsilon,\eta)d\epsilon+\frac{S_\infty}{2\beta}\left[\frac{(\mu c^2)^2}{4}-\epsilon_c^2\right]\right\}\int_{\lambda_c}^{\infty}\frac{I(\lambda)}{\lambda^2}d\lambda+\frac{\mu c^2 S_\infty}{4\tau c\beta\rho}\left\{\int_{\lambda_c}^{\infty}\frac{I(\lambda)}{\lambda}(\lambda^2+1)^{\frac{1}{2}}d\lambda+I(\lambda_c)\right\}, \tag{15}$$

where we have introduced the numerical variable $\lambda=p/\mu c$. We can substitute in (15) the differential spectrum with the integral spectrum $I(\lambda)$ by means of an integration by parts. We see then explicitly that n_d does not depend much upon the particular form of the spectrum, especially when high energies are concerned. For low energies instead there is an appreciable dependence and, for this reason, it may be convenient to substitute the differential spectrum with the integral one also for the disintegration electrons. In the calculations of the following paragraph, we proceeded in this way.

We also calculated the number of disintegration electrons in the case $\eta\to 0$, that is, substituting

Ferretti's track with the simplified one of Williams. However, we proceeded with a greater accuracy than in the case of collision electrons, finding the limit value of the integral,

$$n_d=\frac{\mu}{c\rho\tau}\int_0^\infty \frac{I(p)}{p^2}dp\int_\eta^{\epsilon_p}\frac{\epsilon}{\beta}d\epsilon,$$

for $\eta\to 0$.

We found, for this extrapolated value, $n_d=30.7$ for 100 mesons.

III. NUMERICAL VALUES

Using the preceding formulae, we performed the following calculations:

(1) Number of secondary electrons generated in lead and in equilibrium with the meson component, for $\eta=2$, 3, 4, 5 Mev and for different values of the lower limit of meson energy. In Fig. 1 the results relative to the cut-off energy $\eta=2$ Mev are plotted in a graph.

Table I gives the number of knock-on electrons generated in lead from the total meson spectrum. These values agree rather well with those of Tamm and Belenky.

(2) Number of secondary collision electrons arising from the atmosphere for different values of η at sea level and at 3.500 meters above sea level.

(3) Number of secondary disintegration electrons for different values of the cut-off energy, etc. In these calculations the paths are measured in g/cm², the energies in Mev and we have used the following notations

$k=2\pi NZr_0^2mc^2/A$, where Z is the atomic number, A the atomic weight, N Avogadro's number.

$\mu c^2=90$ Mev,

$\tau=2.3\times10^{-6}$ sec.,

$\beta_{Pb}=1.18$ Mev/(g/cm²); $\epsilon_c=7$ Mev,

$\beta_{air}=2.27$ Mev/(g/cm²); $\epsilon_c=98$ Mev.

For the integral spectra we took the absorption curves at sea level and at 3500 meters obtained from many experiments performed by different authors and by us. These curves were reduced in an energy scale (expressed in μc^2) by means of Wick's nomogram.[28] For energies higher than 25 μc^2 we used the spectra obtained by the law $E^{-2.87}$, taking into account the disintegration processes, after having verified their agreement with the spectra of Blackett and Jones.[29]

In Table II we report the calculated values, in percent, of the number of secondary electrons present in air at sea level and at 3500 meters.

4. Comparison of theoretical results with Wilson-Camber observations.

(*a*) Knock-on electrons in lead. In this case a direct comparison of our calculation with the experimental results does not give too significative results because, on account of the low energies of knock-on electrons, the scattering becomes quite important. Nevertheless, considering Wilson chamber experiments, the comparison is roughly possible, because, in this case, we observe also electrons with very large scattering angles.

Stuhlinger,[30] with $\eta\sim 0$ found about 10 percent of secondary electrons. Hazen, for an η estimated about 2 Mev, finds, at 3000 meters altitude,

TABLE I. Number of knock-on electrons generated in lead from the total meson spectrum.

η (in Mev)	2	3	4	5
η_e (percent)	9	7	5.5	4.5

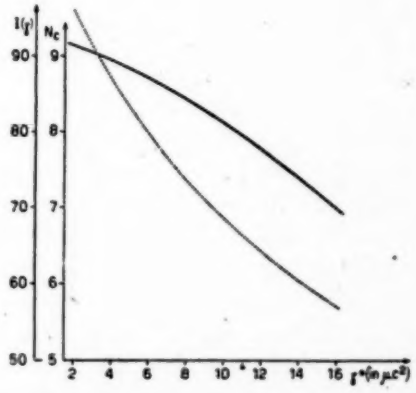

FIG. 1. Number of knock-on electrons generated in lead by mesons having an energy $\geqslant\gamma^*$ ($\eta=2$ Mev). The dotted line gives the corresponding integral meson's spectrum $I(\gamma^*)$; $(I(0)=100)$.

[28] G. C. Wick, Nuovo Cimento X, 1, 302 (1943).

[29] It is well known that the greatest uncertainty is at low energies.

[30] E. Stuhlinger, Zeits. f. Physik 116, 281 (1940).

TABLE II. Calculated value in percent of the number of secondary electrons in air at sea level.

Sea level			3500 meters		
η	n_e	n_d	η	n_e	n_d
5	7.0	23.5	10	3.8	33.5
10	5.2	20.0	20	2.7	25.9
20	3.8	15.1	50	1.0	12.7
50	1.7	6.5			
~ 0	12.4	30.7			

about 7.4 knock-on electrons for 100 mesons. Considering the error due to the scattering, both the results agree with our calculations.

(*b*) Secondary electrons in the atmosphere. Hazen also measured very carefully, still at 3000 meters above sea level, the ratio between the number of electrons and mesons in the atmosphere. He discriminated between the two types of particles through their behavior in lead screens. For electrons, the energy was measured by counting the number of shower electrons at the maximum of the shower's development. As the energy of the descendant's at the maximum is ϵ_c (i.e., 7.0 Mev in lead), it is clear that the scattering effect will reduce the number of secondary electrons actually observed. Therefore, the energy values estimated in this way are surely too low.

Hazen discovered over 8678 particles, which were presumably mesons, 1090 showers having at their maximum four or more electrons and 605 showers with five or more electrons. According to the shower theory, this means that at 3000 meters, for every 100 mesons there are about 10 electrons with an energy of at least about 150 Mev.

But as it was pointed out by Belenky,[31] the simplifying assumptions usually used in the shower theory are inapplicable to heavy elements, like lead, in which the shower production is extremely intensive. Using a more accurate expression for pair production, but still disregarding the scattering,** one finds, for electrons which generate in lead, a shower with four or more electrons of the maximum, an energy of about 350 Mev. Now, according to Stanton,[18] whose calculations complete ours for high energies, the number of the secondary electrons of 350 Mev, generated by the mesons of 2.3^{-6} sec. lifetime, does not exceed the 5 percent.

The comparison shows that at 3000 m. above sea level *the electronic component is largely constituted by electrons which cannot be secondary to ordinary mesons.* This is especially true for high energies. This conclusion will be amphasized in the second part of this paper.

[31] S. Belenky, J. Phys. U.S.S.R. **8**, 305 (1944).
** Unfortunately we are not acquainted with a successive work published by Belenky.

Electronic Component of Cosmic Rays in the Low Atmosphere. II. Experimental

G. BERNARDINI, B. N. CACCIAPUOTI, AND R. QUERZOLI
Physics Department, University of Rome, Rome, Italy
(Received June 5, 1947)

A comparison is made between the results of some cosmic ray counter experiments and the numerical values obtained in a preceding paper (Part I—Theoretical) for the number of secondary electrons in the low atmosphere. This comparison seems to give the following conclusions: (1) Even at 3000–4000 meters above sea level the electron component is not in equilibrium with the meson component, regardless of what may be the background of slow mesons. (2) At 3500 meters above sea level the electronic component contains some electrons of high energy which are not secondaries of mesons with 2.3×10^{-6} sec. lifetime. (3) The slow mesons are negligible at sea level and their intensity increases rapidly with height, roughly as the electron component.

I. ELECTRONIC COMPONENT

IN the preceding paper[1] we have deduced theoretically some simple formulae by means of which it is possible to evaluate the number of secondary cosmic ray electrons in the low atmosphere.

In the present paper we shall compare the numerical values obtained from these formulae with some results of counter experiments. For such a comparison we shall refer first of all to experiments in which an attempt has been made to separate distinctly the electron and meson components by means of the shower generating property of electrons. Experiments of this kind have been performed by Bernardini and Cacciapuoti,[2] Aiya and Saxena,[3] and by Hall,[4] but the experimental device used by Aiya and Saxena for the detection of showers was probably not sufficient for the purpose. Hall's apparatus is very similar to the one used by Bernardini and Cacciapuoti although the evaluation of the shower intensity is more indirect on account of the lower efficiency of the shower detecting counter system.

The apparatus used by Bernardini and Cacciapuoti is indicated in Fig. 1. Counters 1, 2, and 3 form a normal vertical telescope, while the counter sets (a,b) and (c,d) under the lead layer S (1.5 cm thick) work as detectors for the showers (or for mesons accompanied by secondaries) arising from S. Counters 1, 2, and 3 are connected to a threefold coincidence apparatus and each group (a,b) or (c,d) to a twofold coincidence device. We also counted the fivefold coincidences arising from twofold and threefold ones. According to a rough geometrical estimate, the probability for a group of at least two particles to be detected by the twofold coincidence set was rather high (about 75 percent), while a single particle crossing the telescope 1, 2, 3 could generate no twofold and, therefore, no fivefold coincidence. The measurements were performed with different lead absorbers, A. In this way, the threefold coincidences gave a normal absorption curve, while the fivefold coincidences detected the following events: (a) mesons crossing 1, 2, 3 and therefore A, but emerging from S accompanied by a secondary particle; (b) electrons crossing counter 1 and generating in S a shower at least one electron of which traverses A.

We must point out that the solid angle for mesons which cause the fivefold coincidences was possibly different from the solid angle for electrons. This cause of error is not peculiar to our device, e.g., it appears also in Hall's device, yet possibly with less consequence. The particles emerging from S with large deflection angles are, however, likely to be removed by A so that the difference between the two solid angles may be rather small when $A \neq 0$. In any case, in the following we shall deal essentially with direct comparisons between different values of the electron component only.

With the apparatus just described some

[1] G. Bernardini, B. N. Cacciapuoti, and R. Querzoli, Phys. Rev. **73**, 328 (1947).
[2] G. Bernardini and B. N. Cacciapuoti, Ricerca Scient. **10**, 981 (1941).
[3] S. V. C. Aiya and R. C. Saxena, Phys. Rev. **66**, 183 (1944).
[4] D. B. Hall, Phys. Rev. **66**, 321 (1944).

measurements have been performed at two different heights, at sea level, and at 3500 meters.

Unfortunately, our device was particularly sensitive to side showers. This cause of error is certainly the most important one and for this reason, generally, counter experiments may seem objectionable. In order to estimate the effect of side showers, we have counted the threefold and fivefold coincidences with counter 1 situated in the position 1′ of Fig. 1; a second run was made by shifting the whole upper set of counters to one side (those on the Al support).

In both cases we found that for $A=0$ and at 3500 meters the side showers gave over one-third of the pulses obtained with counters 1, 2, 3 on a vertical line. However, the measurements taken with counter 1 shifted to position 1′ show the same variation with height as the fivefold and threefold coincidences, within the experimental errors. Moreover, the intensity ratio of these showers (about 1 to 9) between sea level and 3500 meters agrees fairly well with the average ratio observed by many authors for not very wide showers in air. These two circumstances lead us to believe that a satisfactory correction for side showers may be obtained by subtraction of the

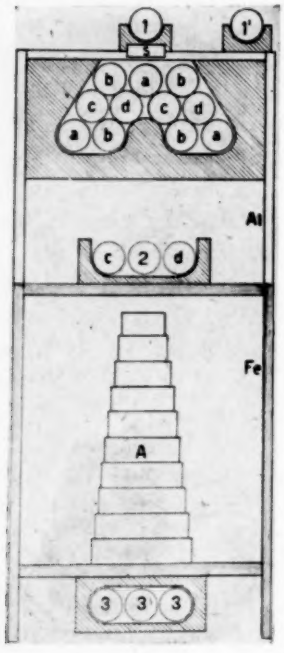

FIG. 1. Experimental arrangement of Bernardini and Cacciapuoti.

three and fivefold coincidences with counter 1 in position 1′, from the three and fivefold coincidences with counters 1, 2 3 in the normal position.

The results of the fivefold coincidence measurements, corrected as mentioned above, are depicted in Fig. 2. In the two curves we can distinguish clearly a background of collision electrons and a part due to atmospheric electrons.

The secondaries in lead have been calculated by means of formula (11) of the foregoing paper[1] and the full curves indicate the theoretical results for a cut-off, $\eta=4$ Mev, and a geometrical efficiency of 75 percent. We wish to point out that, on account of the large angle covered by the twofold counter system, the scattering is not so dangerous, as in other devices.

The curves are in very good agreement with the experimental points; yet the multiplication factor for the curve at 3500 meters, in order to make it agree with the experimental data, is a little higher than the corresponding factor at sea level (0.85 instead of 0.75). Therefore, we believe that our correction for side showers is too small at 3500 meters and that the whole curve at this height must be reduced by a factor about 1.15. In the following, we shall take account of this correction, although the comparison between Hazen's measurements and those of Nassar and Hazen shows an intensity variation for the secondaries arising from lead which agrees with ours and although the threefold coincidences seem to indicate that these ultimate corrections are excessive.

With this correction, if we subtract from the two curves the background due to collision secondaries (and this can now easily be done), we find that the two "difference" curves are similar and that the intensity ratio is 1:5.4.

Hall's experiment allows us to make a further determination of the increase with height of the electron component. Hall's measurements refer to only one level (4500 meters) but his results show that the electrons which can generate a shower arising from 1.5 cm Pb (as those considered in our experiment for $A=0$) have an intensity which is 18 percent of the meson intensity. According to the meson intensity increase with height, we find that the intensity increase of the electron component between sea

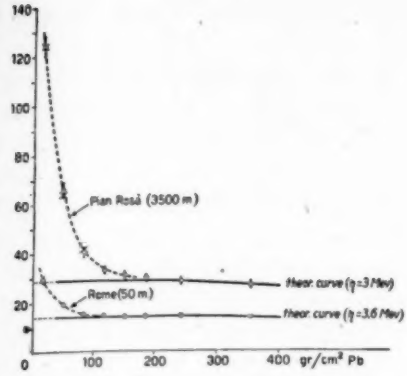

FIG. 2. Fivefold coincidences corrected for the side showers. The full lines give the evaluated knock-on electrons in Pb. The x points in Pian Rosà curve are obtained from the Rome curve by multiplying by a factor 6. The evaluated factor, if the electrons in atmosphere would be generated only by mesons of $2.3\cdot10^{-6}$ sec. lifetime, would be 3.5.

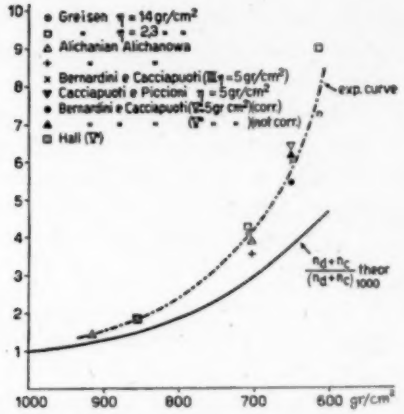

FIG. 3. Theoretical and experimental curves for the electron component.

level and 4500 meters is in the ratio of 1 to 9. This ratio may be overestimated on account of the different solid angles for the mesons and for the electrons, but in Hall's device the error is certainly small.

The full curve in Fig. 3 represents the electron component obtained from the tables in Section III of our foregoing paper[1] and from similar calculations for 4500 meters and 2000 meters for $\eta=10$ Mev (the cut-off value does not affect the ratio much); the points are the experimental data obtained by Hall and other authors, including the rough values obtained from normal absorption curves (corrected for side showers).

If the correction for side showers does not affect the measurements with a great error (and the Wilson chamber experiments seem to indicate that it does not), we believe it is possible to conclude that, even at 3000–4000 meters *the electron component is certainly not in equilibrium with the meson component, regardless of what may be the background of slow mesons* ($E<200$ Mev).

This statement can be checked, furthermore, by the following considerations. Bhabha,[5] in a recent paper, gives a very useful formula which establishes the maximum penetration t (given in radiation units) of a shower as a function of the ancestor electron energy. For $t\geqq4$ Bhabha's formula seems to be correct to within 2 percent.

With reference to Fig. 2 and to the calculated behavior of the background due to the knock-on electrons in lead, it is possible to deduce the electron spectrum at 3500 meters above sea level. The results of these calculations are reported in Fig. 4. As abscissa, we have plotted the log of energy values (measured in 100 Mev) and as ordinate, the intensity of the electronic component (setting the intensity corresponding to 100 Mev equal to 100). The experimental points are deduced from the experiments performed by Hall and by us. The full line curve indicates the spectrum we should expect according to the calculations of Stanton if only electrons generated by $2.3\cdot10^{-6}$ sec. lifetime mesons were present. The electronic component, therefore, seems to consist of electrons of high energy in amount greater than what would be predicted on the base of Stanton's calculations. We have checked these calculations and we found that Stanton's results are substantially correct. We must then conclude that, at 3500 meters altitude, *the electronic component contains some electrons of high energy which are certainly not secondaries of mesons with* $2.3\cdot10^{-6}$ *sec. lifetime.* We may formulate several hypotheses in the origin of these electrons; the simplest one is to assume that the generation of $2.3\cdot10^{-6}$ lifetime mesons in the high atmosphere is accompanied by a generation of other mesons with a shorter lifetime. We will come back to this point in a later paper.

II. THE SLOW MESONS

We shall now discuss the problem of the slow mesons and establish at the same time a more

[5] H. J. Bhabha, Proc. Ind. Acad. Sci. **XIX**, 23 (1944).

careful comparison with the tabulated data in section 3 of our preceding paper,[1] and some other results on the electron component.

Let us consider, therefore, the absorption curve at sea level represented in Fig. 5; this curve is obtained with the consistent measurements of many authors and especially with the data of Cacciapuoti and Piccioni[6] and of Greisen.[7]

In order to separate the meson from the electron component in this curve, let us disregard momentarily the existence of slow mesons, generated locally. Then, since intensity variation of the meson component in the low atmosphere agrees very well with the disintegration hypothesis, for $\tau/\mu c^2 = 2.9 \cdot 10^{-8}$ sec./Mev[8] we can start from the meson absorption curve at 2000 meters[8] and calculate the low energy end of the integral spectrum of mesons at sea level. The dotted curve in Fig. 5 represents the result of such calculation. This curve has been adjusted so as to fit the experimental value corresponding to 170 g/cm² Pb.

Now, if we subtract the fivefold from the threefold coincidences obtained in the measurements of Bernardini and Cacciapuoti, we have directly the points indicated with a cross. When corrected for geometrical efficiency, these points lie practically on the calculated meson curve.

Notwithstanding the possible criticism mentioned above, we believe that this agreement is not purely accidental and that, *at sea level, the local generation of slow mesons must be considered as negligible when compared with the total meson intensity.**

We can then establish a quantitative comparison between the calculated values in our preceding paper[1] and the difference of the two curves in Fig. 5; we attribute this difference mainly to the presence of electrons. For this, we must find an energy-range relation. It can be given directly by some measurements of Bernardini and Franchetti[9] and by the data kindly supplied to us by Professor E. Amaldi, on the penetration in Al and Pb of Compton electrons generated by gamma-rays of 17 Mev from D+Li. With this energy-range relation we obtained, for the soft part of the electron spectrum at sea level, the curve indicated in Fig. 6, where the experimental points can also be seen. The agreement is very good and we conclude that, at sea level, the electronic component is mainly composed of the secondary electrons of the $2.3 \cdot 10^{-6}$ lifetime mesons.

Considering that the above mentioned energy-range relation is referred only to the maximum penetration (in counterwall and screens) of low energy electrons, we have tried to correct the theoretical curve of Fig. 5. Using a rough approximation for the behavior of our experimental absorption curves of mono-energetic electrons, we found that the theoretical curve in Fig. 5 must be modified as is indicated by the dotted line in Fig. 7. The full line gives the experimental curve. It can be seen that the two curves are quite similar and the electrons surely do not seem to be less than the calculated ones.

A similar analysis can be done on the absorp-

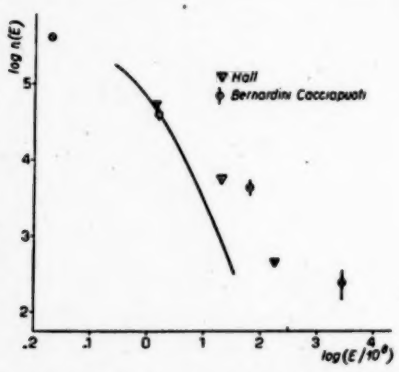

FIG. 4. Electron spectrum at 3500 meters.

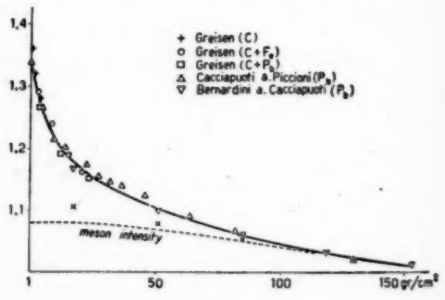

FIG. 5. Absorption curve at sea level.

[6] B. N. Cacciapuoti and O. Piccioni, Nuovo Cimento I, 3 (1943).
[7] K. I. Greisen, Phys. Rev. 61, 212 (1942).
[8] See, for example, G. Bernardini, Zeits. f. Physik 120, 413 (1943).

* This conclusion is checked by the results of J. G. Wilson, Nature 158, 414 (1946).
[9] G. Bernardini and S. Franchetti, Ricerca Scient. 8, 406 (1937).

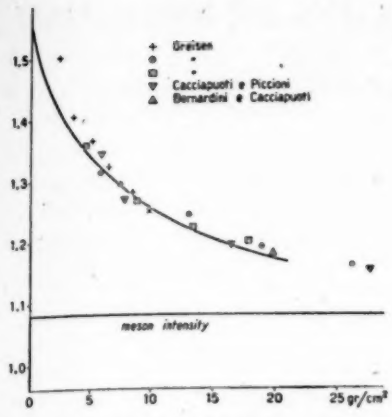

FIG. 6. Soft part of electron spectrum at sea level.

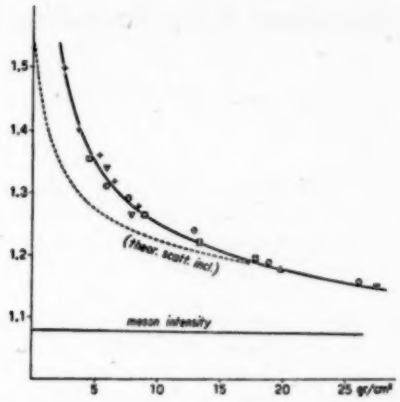

FIG. 7. Correction to the theoretical curve of Fig. 5.

tion curve at 3500 meters. For this we took the results of Bernardini and Cacciapuoti[9] and those of the experiment performed by Cacciapuoti and Piccioni[8] in which a very accurate absorption curve for the first 200 g/cm² has been obtained for Pb and Al. The two curves have then been treated in the manner followed by Auger[10] in his discussion on the nature of the soft component.

Our analysis leads to the conclusion that some slow mesons probably exist at 3500 meters, but their number is not higher than 10 percent of the total meson component, and they certainly do not constitute the whole part of the soft component in excess of the electron component generated by mesons with an energy beyond 200 Mev; this is in disagreement with what seems to be the opinion of Alichanow and Alichanian.[11] Hall has found, however, at 4500 meters, a number of slow mesons that is twice as large, and Schein, Wollan and Groetzinger[12] report that they have detected 30 percent of the meson component, at 6700 meters, in the energy band between 2.9 and 5.2×10^8 ev. We must then conclude that the number of slow mesons increases very rapidly with height; i.e., about at the same rate as the soft component. Therefore, we should argue once more that an intimate bond exists between this band of slow mesons and the electron-photon component. We believe, however, that the excess in the electron component must not be considered as a product of the disintegration of these slow mesons, in disagreement with the opinion of several authors.[13] A simple calculation shows indeed that the disintegration products of such mesons are quite insufficient, in number and in energy, in order to account for so large a contribution to the electron component. On the contrary, it can be thought that the slow mesons may be partially due to the electron-photon component (pairs, etc.).

III. CONCLUSIONS

As a conclusion of this discussion we may argue:

(1) At sea level no objection can be raised against the hypothesis that the penetrating part (beyond 10 cm. Pb) of cosmic radiation consists mainly of mesons with a $\tau/\mu c^2=10^{-8}$ sec./Mev, which disintegrate into an electron and a neutrino, because the electron component accompanying these mesons does not seem to be in default, but rather in excess of what should be expected for the equilibrium condition between the two components.

(2) The electronic component at 3000 to 4000 meters above sea level is, in large part, composed of electrons which do not arise from the disinregration of the above mentioned mesons.

(3) The slow mesons are negligible, at sea level and their intensity increases rapidly with height, roughly, as the electron component.

(4) It is likely that the slow mesons are secondaries of the electron-photon component because the electron-photon component is composed also of high energy electrons.

[10] P. V. Auger, Phys. Rev. **61**, 684 (1942).
[11] A. Alichanow and A. Alichanian, J. of Phys. USSR **9**, 73 (1945).
[12] M. Schein, E. C. Wollan and G. Groetzinger, Phys. Rev. **58**, 1027 (1940).
[13] See, for instance, M. Schein, W. P. Jesse, and E. O. Wollan, Phys. Rev. **57**, 847 (1940).

Radiations From Tantalum (182), Antimony (122), and Indium (116)*

C. E. MANDEVILLE AND MORRIS V. SCHERB
Bartol Research Foundation of the Franklin Institute, Swarthmore, Pennsylvania

(Received October 31, 1947)

The 100-day activity was induced in tantalum irradiated by slow neutrons in the Clinton pile. The beta-rays of this isotope were found to have a range in aluminum of 0.112 g/cm², and the gamma-rays a maximum energy of 1.16±0.1 Mev as determined by coincidence absorption. The beta-gamma coincidence rate was 0.93×10^{-3} coincidence per beta-ray, independent of the beta-ray energy, and a gamma-gamma coincidence rate of $(0.27\pm0.03)\times10^{-3}$ coincidence per gamma-ray was obtained. These data indicate that beta-emission by Ta^{182} leads to an exited state of W^{182} and that de-excitation occurs with the emission of two or more gamma-rays in cascade.

The 2.8-day activity of antimony (122) was also prepared in the pile. The beta-gamma coincidence rate was found to drop to zero at 0.487 g/cm² in aluminum, corresponding to 1.19 Mev. The maximum energy of the beta-rays was measured to be 1.77 Mev.

The beta-gamma coincidence rate of the 54-minute isomer of indium (116) was found to be 1.3×10^{-3} coincidence per beta-ray independent of the beta-ray energy, and a gamma-gamma coincidence rate of $(0.9\pm0.1)\times10^{-3}$ coincidence per gamma-ray was also observed.

A disintegration scheme is given for Sb^{122}.

1. INTRODUCTION

THE radiations of tantalum (182), antimony (122), and indium (116) have been investigated by absorption and coincidence methods. An attempt has been made to correlate the coincidence rates with spectrometric results when such data are available.

The procedure for measuring beta-ray energies was the standard one of placing aluminum foils before a single counter and observing the counting rate as a function of absorber thickness. The maximum energy of the gamma-rays emitted by Ta^{182} was measured by coincidence absorption. The radioactive source was placed behind an aluminum block which served as a radiator of Compton recoils. The recoils passed through two thin-walled counters in coincidence. Aluminum absorbers were placed between the two counters, and the coincidence rate was plotted as a function of the absorber thickness. The quantum energy was taken from the end-point.

For measurement of coincidences between the beta-rays and gamma-rays emitted by each isotope, a radioactive source of low surface density was placed between two counters. Aluminum

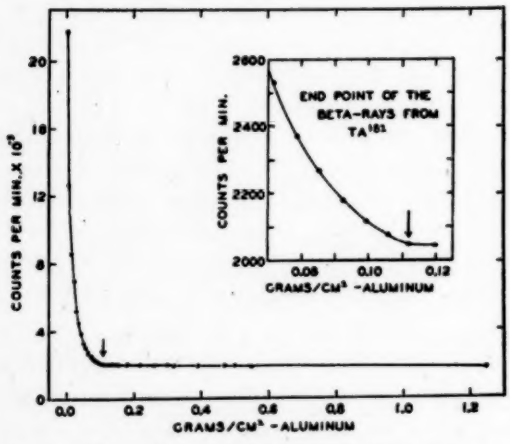

FIG. 1. Absorption in aluminum of the beta-rays of tantalum (182).

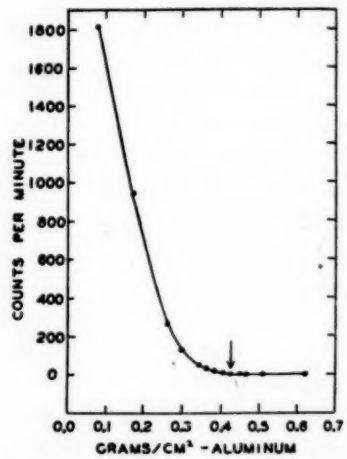

FIG. 2. Coincidence absorption of the secondary electrons of the gamma-rays from tantalum (182).

* Supported by the Office of Naval Research.

blocks of sufficient thickness to stop the primary beta-rays were placed before each counter when the gamma-gamma coincidence rate was measured. For the measurement of beta-gamma coincidences, thin aluminum foils were placed before the beta-ray counter, and the coincidence rate was determined as a function of the aluminum thickness. The accidental coincidence rate was determined by the equation

$$A = N_1 N_2 (K\tau),$$

where $K\tau$ was two microseconds. Other details of the coincidence arrangement have been previously described.[1]

2. TANTALUM (182)

When tantalum is irradiated by slow neutrons, radioactive tantalum (182), having a half-period of about 100 days,[2] is formed. The radiations of this isotope have been investigated by a number of workers.[2-5] TaO_2 was irradiated by slow neutrons in the pile, and a chemical separation was performed. The absorption curve for the beta-rays of this isotope is given in Fig. 1. The absorption limit is seen to be 0.112 g/cm² in aluminum, corresponding to an energy of about 0.36 Mev calculated from the range-energy relation for homogeneous beta-rays. No beta-rays of higher energy were observed.[3]

The data for coincidence absorption of the gamma-rays from Ta^{182} are given in Fig. 2. The end point, 0.425 g/cm², corresponds to a quantum energy of 1.16±0.1 Mev. The coincidence absorption method measures accurately only the maximum energy of the gamma-rays. Quantum energies of 0.15, 0.22, 1.13, and 1.22 Mev have been reported as measured by a thin magnetic lens spectrometer.[4] More recently, the gamma-rays of low energy have been resolved into about sixteen lines by Cork.[5]

The beta-gamma coincidence rate of Ta^{182} is given in Fig. 3 where it is seen to be 0.93×10^{-3} coincidence per beta-ray recorded in the beta-ray counter, independent of the beta-ray energy.

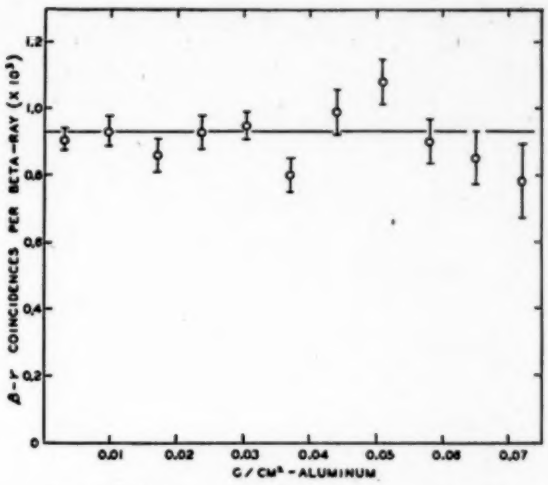

FIG. 3. The genuine beta-gamma coincidence rate of tantalum (182).

This would suggest that only one beta-ray spectrum is present. A gamma-gamma coincidence rate of $(0.27\pm0.03)\times10^{-3}$ coincidence per gamma-ray recorded in the gamma-ray counter was also observed. From these coincidence rates, it may be concluded that the beta-transition in Ta^{182} leads to an excited state of the W^{182} residual nucleus. The gamma-rays of energy 1.13 and 1.22 Mev have been reported to be of comparable intensity.[4] However, using the same counters and geometry, the coincidence rates for Sc^{46} were found to be 1.4×10^{-3} beta-gamma coincidence per beta-ray and 0.62×10^{-3} gamma-gamma coincidence per gamma-ray.[1] Since scandium (46) is known to disintegrate with the emission of a beta-ray of energy 0.36 Mev followed by gamma-rays of energy 0.90 and 1.12 Mev in cascade,[6] it seems improbable that the two gamma-rays of high energy from Ta^{182} are in cascade.

The beta-ray energy of 0.53 Mev obtained by the thin lens[4] should be regarded as more reliable than the value reported in this paper which was calculated from the absorption limit.

3. ANTIMONY (122)

Sb^{122} was prepared when metallic antimony was irradiated by neutrons in the pile. The exposure time was only 2 hours, so that the 60-day period was present with only a small intensity.

[1] C. E. Mandeville and M. V. Scherb, Phys. Rev. **73**, 141 (1948).
[2] O. Oldenburg, Phys. Rev. **53**, 35 (1938).
[3] R. V. Zumstein, J. D. Kurbatov, and M. L. Pool, Phys. Rev. **63**, 59 (1943).
[4] W. Rall and R. G. Wilkinson, Phys. Rev. **71**, 321 (1947).
[5] J. M. Cork, Phys. Rev. **72**, 581 (1947).
[6] A. E. Miller and M. Deutsch, Phys. Rev. **72**, 527 (1947).

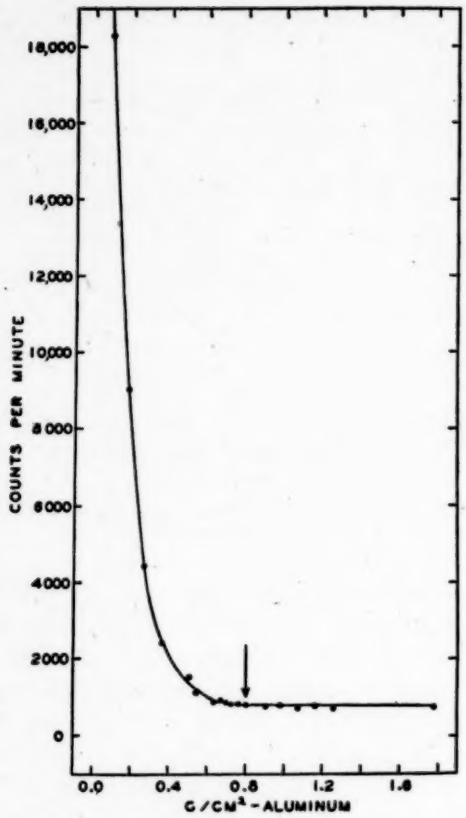

FIG. 4. Absorption in aluminum of the beta-rays of antimony (122).

Measurements were begun about 20 hours after removal of the isotope from the pile. The beta-rays of Sb^{122} have been measured previously by the absorption method by Amaki and Sugimoto,[7] who found a maximum energy of 1.64 Mev and by Mitchell, Langer, and McDaniel,[8] who report an absorption limit corresponding to 1.76±0.10 Mev.

The data obtained for absorption in aluminum of the beta-rays of Sb^{122} in the present experiment, are given in Fig. 4, where the absorption limit occurs at 0.806 g/cm² corresponding to an energy of 1.77±0.10 Mev as calculated by Feather's equation.[9] A source of radioactive material was placed in the standard position between two thin-walled Geiger counters. The beta-gamma coincidence rate plotted in Fig. 5, was observed to decrease from 0.19×10^{-3} coincidence per beta-ray recorded in the beta-ray counter at zero absorber thickness to zero at 0.487 g/cm² in aluminum, corresponding to an energy of 1.19±0.05 Mev. These data indicate that two beta-ray spectra are present having end points which differ by 0.58±0.11 Mev. Since a gamma-ray energy of 0.57 Mev has been previously reported,[4] the disintegration scheme of Fig. 6 may now be drawn for Sb^{122}. These results disagree somewhat with earlier coincidence experiments[8] which indicated an end point at 0.81 Mev for the beta-spectrum of lower energy.

Miller and Curtiss[10] have reported beta-ray energies of 1.36 and 1.94 Mev as determined by a thin magnetic lens spectrometer. These values differ in absolute value from those reported by the writers, but the energy difference is the same.

4. INDIUM (116)

The 54-minute activity was induced in a strip of indium metal (thickness 0.018 cm), irradiated by slow neutrons from a radium-beryllium source of strength 600 Mc. The genuine beta-gamma

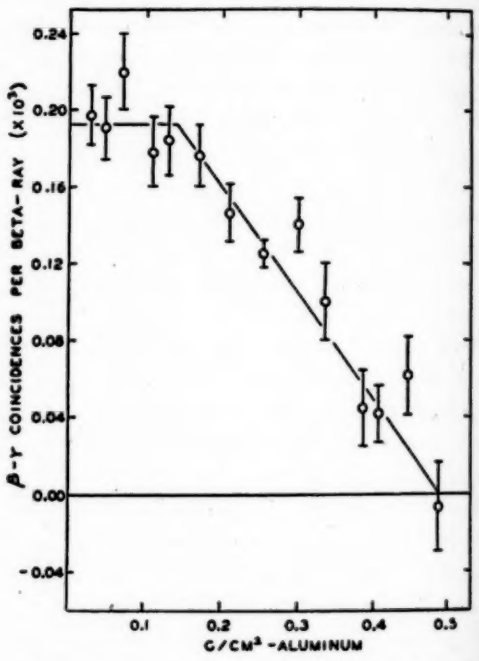

FIG. 5. Beta-gamma coincidence rate of antimony (122) as a function of the surface density of aluminum placed before the beta-ray counter.

[7] T. Amaki and A. Sugimoto, Inst. Phys. and Chem. Research, Tokyo, paper No. 853, 1650 (1938).
[8] A. C. G. Mitchell, L. M. Langer, and P. W. McDaniel, Phys. Rev. 57, 1107 (1940).
[9] N. Feather, Proc. Camb. Phil. Soc. 34, 599 (1938).
[10] L. C. Miller and L. F. Curtiss, Phys. Rev. 70, 982 (1946).

coincidence rate for indium (116) is plotted in Fig. 7, where it is seen to be independent of the beta-ray energy. From the figure it is clear that no genuine coincidences exist beyond about 0.22 g/cm² of aluminum, 0.7 Mev by Feather's equation. These data are in agreement with the findings of Langer, Mitchell, and McDaniel,[11] who found genuine coincidence as far out as 1.2 Mev but seem to have correctly dismissed those above 0.8 Mev as arising from a Compton-recoil gamma-effect growing out of their geometry.

The coincidence measurements of this investigation agree reasonably well with the spectrometric findings of Lawson and Cork[12] who report an upper limit of 0.85±0.1 Mev for the beta-rays of indium (116).

The effect of the decay of the short-lived indium upon all other corrections was taken into account.[13]

5. ACKNOWLEDGMENTS

The writers wish to express their appreciation to Professor W. B. Keighton of Swarthmore College, for having carried out the chemical separation. They also wish to acknowledge the kindly interest and advice of Dr. W. F. G. Swann, Director of the Bartol Research Foundation.

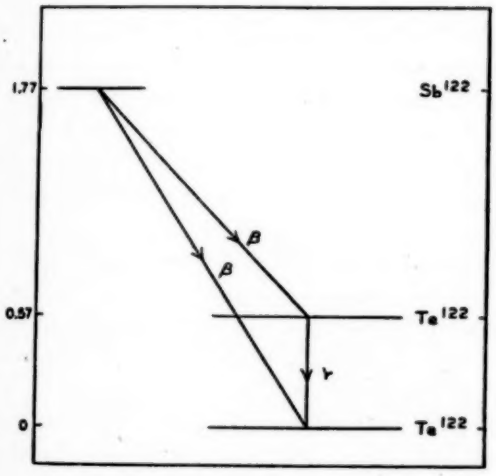

FIG. 6. Disintegration scheme of Sb^{122}.

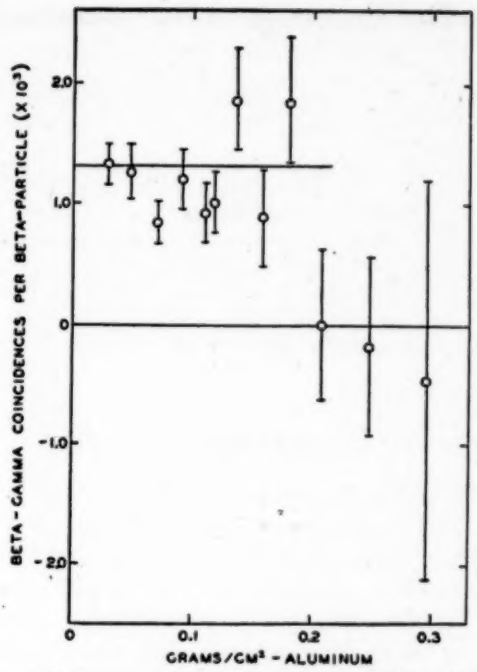

FIG. 7. Beta-gamma coincidence rate for indium (116).

6. APPENDIX: CHEMICAL PROCEDURE FOR TANTALUM

A 27-mg sample of active tantalum oxide was mixed with 150 mg of inactive Ta_2O_5 and 140 mg of inactive ZrO_2, the latter to serve as a carrier for hafnium. The mixture was fused with potassium bisulfate until clear. The fused mass dissolved completely in hot saturated ammonium oxalate solution, and from this solution the yellow tantalum-tannin complex was precipitated by tannic acid. The precautions usually taken in analysis of tantalum compounds were observed (Hillebrand and Lundell, *Applied Inorganic Analysis*, pp. 474–5). The fusion and precipitation were repeated, and the precipitate ignited to Ta_2O_5.

This partly purified Ta_2O_5 was now fused with potassium carbonate, and the melt was dissolved in aqueous potassium hydroxide. Sodium tantalate was precipitated by the addition of solid sodium chloride and the precipitate collected and washed. The sodium tantalate was converted to Ta_2O_5 by acidifying its aqueous suspension with HCl and boiling. After washing the precipitate with diluted ammonium nitrate it was collected by filtration and ignited.

The purification process was intended to separate hafnium, zirconium, tungsten, iron, calcium, potassium, and phosphorus from Ta_2O_5.

[11] L. M. Langer, A. C. G. Mitchell, and P. W. McDaniel, Phys. Rev. **56**, 380 (1939).
[12] J. L. Lawson and J. M. Cork, Phys. Rev. **57**, 982 (1940).
[13] L. M. Langer, A. C. G. Mitchell, and P. W. McDaniel, Phys. Rev. **56**, 422 (1939).

The Absorption of Na^{24} Gamma-Radiation in Lead, Copper, and Aluminum

DAVID E. ALBURGER
Sloane Physics Laboratory, Yale University, New Haven, Connecticut*
(Received November 12, 1947)

The absorption of sodium (24) gamma-radiation has been measured with a Geiger-Müller counter out to 16 cm of lead, 22 cm of copper, and 61.5 cm of aluminum. Each of the curves obtained can be analyzed into two components. These give absorption coefficients 0.454 ± 0.004 cm^{-1} and 0.62 ± 0.01 cm^{-1} for lead, 0.311 ± 0.005 cm^{-1} and 0.46 ± 0.01 cm^{-1} for copper, and 0.088 ± 0.001 cm^{-1} and 0.144 ± 0.005 cm^{-1} for aluminum. All of these are in agreement with theoretical values as obtained from Heitler's curves for the sodium gamma-rays of energies 2.76 Mev and 1.38 Mev, respectively.

1. INTRODUCTION

THE absorption of gamma-rays in various materials provides an experimental check on theoretical predictions of absorption coefficients. Such calculations have been performed by Heitler who gives[1] absorption coefficient curves for lead, tin, copper, and aluminum over a wide range of gamma-ray energies. McMillan, using the 5.4 Mev gamma-ray from the proton bombardment of fluorine, obtained[2] absorption coefficients for all four of these elements in agreement with Heitler's curves at this energy. His results furnished a check on pair-production absorption at 5.4 Mev, assuming the validity of the theory of Compton scattering as formulated[3] by Klein and Nishina and applied by Heitler.

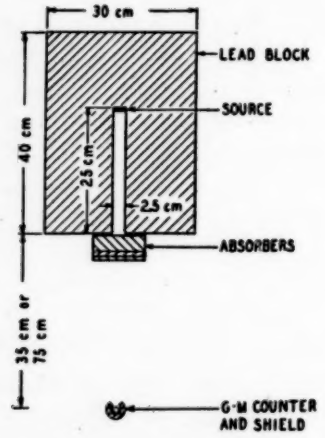

FIG. 1. Experimental arrangement for gamma-ray absorption measurements.

More recently, sodium (24) has been used for absorption studies. Accurate measurements[4] by Siegbahn, employing a magnetic electron lens spectrometer, have shown the sodium (24) gamma-ray energies to have the values 1.380 Mev and 2.758 Mev and to be present in equal numbers indicating a cascade transition process. A study of the absorption of this radiation in lead and copper was made[5] by Cork and Pidd who also used zinc (65) and cobalt (60) sources. They obtained absorption coefficients in agreement with Heitler's curves in all cases except the 2.8-Mev component of sodium. For this energy they obtained coefficients 0.285 cm^{-1} and 0.405 cm^{-1} for copper and lead, respectively, both ten percent lower than theoretical values. The discrepancy was attributed to a deficiency in the Klein-Nishina formula for Compton scattering. As a detector they employed an ionization chamber having a 50 percent greater efficiency for the lower energy gamma-ray.

Later, Groetzinger and Smith measured[6] the absorption of the 2.8-Mev component of sodium at four thicknesses of lead from 9.5 cm to 19 cm, and obtained a coefficient of 0.467 ± 0.009 cm^{-1} in agreement with Heitler's theoretical curve.

The high sensitivity of a Geiger-Müller counter makes it desirable for measurements at large absorber thicknesses. In the present ap-

* Assisted by the Office of Naval Research under Contract N6ori-44.

[1] W. Heitler, *The Quantum Theory of Radiation* (Clarendon Press, Oxford, 1936).
[2] Edwin McMillan, Phys. Rev. 46, 863 (1934).
[3] O. Klein and Y. Nishina, Zeits. f. Physik 52, 853 (1929).
[4] Kai Siegbahn, Phys. Rev. 70, 129 (1946).
[5] J. M. Cork and R. W. Pidd, Phys. Rev. 66, 227 (1944).
[6] Gerhardt Groetzinger and Lloyd Smith, Phys. Rev. 67, 53 (1945).

plication the further inherent advantage is gained that a counter discriminates against the lower energy gamma-ray. Bradt *et al* have shown[7] that for a brass cathode the efficiency of a Geiger-Müller counter for gamma-radiation of energy 2.76 Mev is 1.55 percent, while at 1.38 Mev it is 0.76 percent. A logarithmic plot of the composite absorption curve will, for this reason, display higher curvature in the low absorption region and at high absorption will more quickly approach a straight line corresponding to the harder component.

2. EXPERIMENTAL

The experimental arrangement is shown in Fig. 1. The gamma-ray source is placed in a lead block approximately 30 cm square and 40 cm long, having a centrally located hole 2.5 cm square and 25 cm deep. Absorbers are placed in front of the hole so as to intercept the collimated beam. A Geiger-Müller counter with a copper cathode, 3 cm long and 1 cm in diameter, is located on a line with the hole at a distance of 60 cm from the source for lead absorbers and 100 cm for copper and aluminum absorbers. The counter is shielded except on the side exposed to the radiation. A Higinbotham circuit is used for high voltage, scaling, and recording.

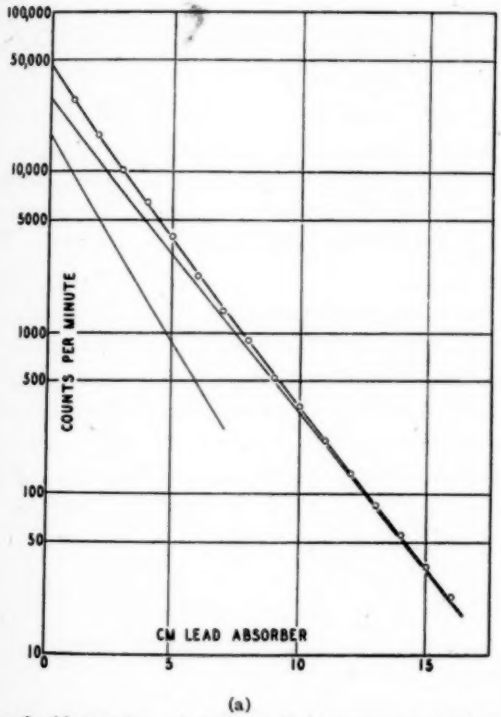

(a)

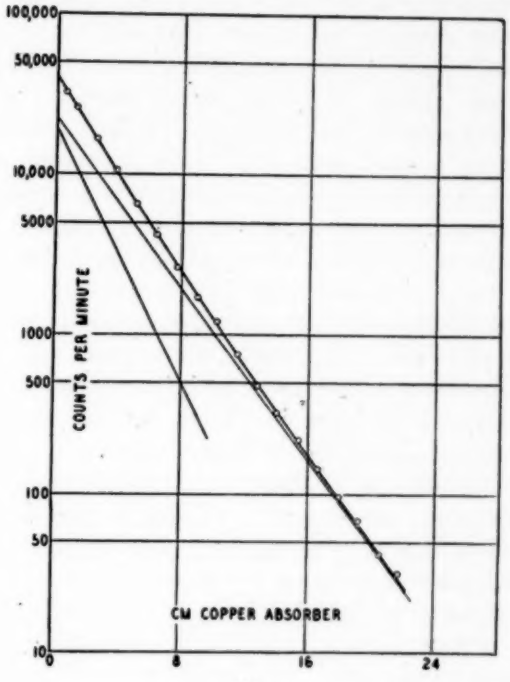

(b)

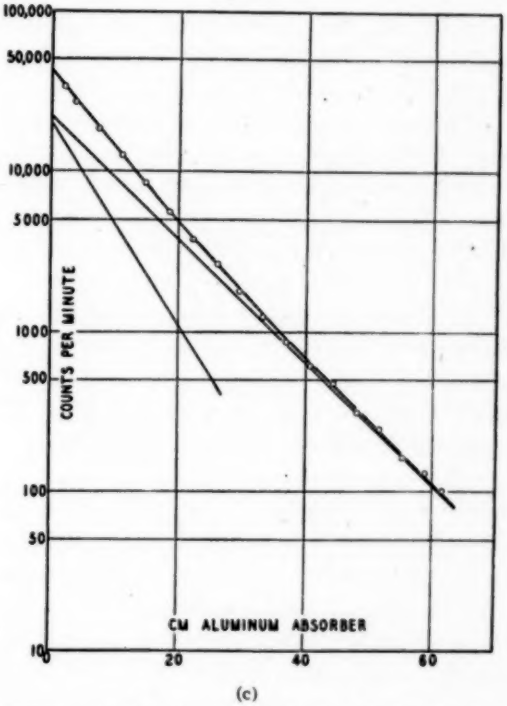

(c)

FIG. 2. Absorption of sodium (24) gamma-radiation in lead, copper, and aluminum showing resolution into two components.

[7] Bradt, Gugelot, Huber, Medicus, Preiswerk, and Scherrer, Helv. Phys. Acta. 19, 77 (1946).

Lead absorbers were made from castings by machining to 10 cm square and various integral thicknesses. The average density of the absorbers was found to be 11.24 g per cm^3 which is 0.9 percent below the published value of 11.347 g per cm^3 for compressed lead. Four-inch square pieces of $\frac{1}{4}$-inch copper bus-bar were bolted together to form a conveniently handled set of copper absorbers. The aluminum absorbers were similarly constructed from pieces of 2s aluminum plate approximately $\frac{3}{8}$ inch thick.

Sources were made by cyclotron bombardment of metallic sodium with deuterons. For both lead and copper data were taken out to an absorption where the counting rate was approximately three times background, these points having thicknesses of 16 cm and 22 cm, respectively. In the case of aluminum a practical limit of 61.5 cm of absorption was used, at which point the counting rate was eleven times background. To test the shielding effectiveness of the lead block containing the source 27 cm of lead absorber was placed in front of the hole in order to reduce direct radiation to a fraction of a count per minute. The counting rate then observed was equal to the background counting rate with no source present (9.3 counts per minute) within the expected deviation, indicating that the amount of radiation filtered through the lead block and scattered from the walls of the room into the counter was negligible. A number of readings were taken at each value from medium to high absorption over a ten-hour period following preparation of the source. Low absorption and overlap check points were obtained several days later when sufficient decay had occurred that the counting rate was not excessive. Using 14.8 hours as the half-life of sodium (24), readings were corrected for decay and referred to a standard source strength.

3. RESULTS

Two runs were made with lead absorbers and one with copper and aluminum absorbers. The results are shown in Fig. 2. Points at zero absorption were high because of the presence of beta-rays and have, therefore, been omitted. At high absorption all three curves clearly become tangent to a straight line. Making a 0.9 percent correction for the density of the lead absorbers, the average of two runs gives an absorption coefficient for the lead tangent line of 0.454 ± 0.004 cm^{-1}. By subtracting this from the experimental curve a second straight line is obtained corresponding to an absorption coefficient of 0.62 ± 0.01 cm^{-1}. It may be noted that flaws or low density impurities in the lead absorbers would make the observed absorption coefficients appear too low.

The curves obtained using copper and aluminum absorbers may similarly be resolved, as shown in Fig. 2, into components having absorption coefficients 0.311 ± 0.005 cm^{-1} and 0.46 ± 0.01 cm^{-1} for copper, and 0.088 ± 0.001 cm^{-1} and 0.144 ± 0.005 cm^{-1} for aluminum. All of the absorption coefficients obtained appear to be in agreement with Heitler's theoretical curves at the sodium gamma-ray energies of 2.76 Mev and 1.38 Mev, respectively. It is seen from the curves that in all cases the 2.76-Mev gamma-ray gives a greater yield at zero absorption, but that the ratio of hard to soft component yields is somewhat lower than would be expected from the efficiency curves previously mentioned. This may be caused in part by a difference in counter cathode material and gas filling. Also the observed efficiency ratio is quite sensitive to the slope of the tangent line, a one percent variation in slope making a change of approximately twenty-five percent in the yield ratio.

X-Ray Spectrum of Element 43

L. E. BURKHART, W. F. PEED, AND B. G. SAUNDERS[1]
Clinton Engineer Works, Carbide and Carbon Chemicals Corporation, Oak Ridge, Tennessee
(Received October 10, 1947)

The x-ray spectrum of a sample containing Element 43 supplied by the Clinton Laboratories has been studied. Lines ascribable to $K\alpha_1$, $K\alpha_2$, $K\beta_1$, $K\beta_2$ of Element 43 were identified. Their wave-lengths followed closely the values calculated by interpolation between elements 41, 42, 44, and 45.

1. INTRODUCTION

SINCE the systematic study of the x-ray spectra of the elements by Moseley, the x-ray spectrograph has been used extensively as a research tool and especially by workers endeavoring to establish proof of new or missing elements. The striking thing about x-ray spectra is its regularity and simplicity. It will be noted in the spectra of the three elements presented in this paper that as one goes from lighter to the heavier elements, the wave-lengths of the corresponding lines decrease in a regular manner. It has long been known, therefore, that the large gap existing in the x-ray spectral region between the two elements molybdenum 42 and ruthenium 44 indicates that the K lines of missing Element 43 should fall between the K lines of molybdenum and ruthenium.

2. DISCUSSION

In the past, investigators seeking the x-ray spectra of Element 43 have been saddled with the problem of taking long exposures and finding weak lines which were assumed to arise from the presence of very small amounts of the element in unseparated compounds.

Segrè[2] states he obtained 10^{-10} g of Element 43 by cyclotron bombardment of molybdenum. He mentions that P. Abelson photographed a characteristic K line of Element 43 which was emitted through the mechanism of internal conversion.

There has been considerable work done in the search for Element 43 in minerals of the earth's crust by Noddack and Tacke,[3] Berg,[4] and others.

Despite the considerable efforts of these prior workers, it is felt that the x-ray photographs obtained by direct excitation of the sample separated by G. W. Parker of Clinton Laboratories presents the most convincing evidence of the existence and isolation of Element 43.

3. EXPERIMENTAL

Approximately 1.5 mg of sample was submitted as an ammonium salt made by dissolving the sulfide in concentrated NH_4OH and H_2O_2 and evaporating to dryness. The sample was known to contain approximately 10 percent rhenium with the chief constituent being 0.7 mg of Element 43. The problem resolved itself into determining whether or not the purified sample was 43 or some other element.

The sample was applied to the target by evaporating very small drops of the solution from a micro-pipette under an infra-red lamp. The target has been previously scored to facilitate holding the sample on the target. After the loaded target had been heated until dry, it was placed in the x-ray tube for the exposure.

From an examination of the x-ray spectrogram, Fig. 1, it is obvious that the K lines of 43 appear between the K lines of molybdenum 42 and ruthenium 44. The separation of the densitometer peaks makes evident the resolution of the various lines. Smoother tracing was not attained because of the large grain size of the film. The calculated and observed wave-lengths of Element 43 are shown in Table I. The observed wave-length values of 43 were obtained by interpolating with a calibrated eyepiece between the wave-lengths of molybdenum, ruthenium, and the silver absorption edge listed in Siegbahn.[5]

[1] Now with the Atomic Energy Commission, Oak Ridge, Tennessee.
[2] E. Segrè, Nature **143**, 460 (1939).
[3] W. Noddack and I. Tacke, Sitz. Preuss. Akad. Wiss. **19**, 400 (1925).
[4] O. Berg, I. Tacke, Naturwiss. **13**, 571 (1925).
[5] M. Siegbahn, *The Spectroscopy of X-Rays* (Oxford, 1925).

In this region the dispersion of the spectrograph is 10.84X units/mm. The calculated values for the wave-lengths of Element 43 were obtained by plotting the screening constants of elements 41, 42, 44, 45 and interpolating for the constants for Element 43. Wave-lengths were then calculated using Moseley's formula.

In checking for the possible interference of lines from elements other than 43, Table II shows the second-order wave-lengths of lines of the elements involved in this region. The threshold excitation voltages for these elements are also listed.

The difference in voltage applied, 35 kv, and the threshold voltages for the rare earths and rhenium, as shown in Table II, exclude the possibility of any interference from these elements, had they been present in the sample. The threshold voltage given for cesium is near the applied voltage; however, this is of no concern since its interference is with the molybdenum $K_{\alpha 1}$ line and in no way affects the lines of Element 43. The voltage used in the present experiment is sufficiently high to excite the L series of rhenium, but since the L_I absorption edge of rhenium lies at 987 XU, no interfering rhenium L lines of lower wave-lengths are possible.

The experimental conditions of the exposures are listed in Table III.

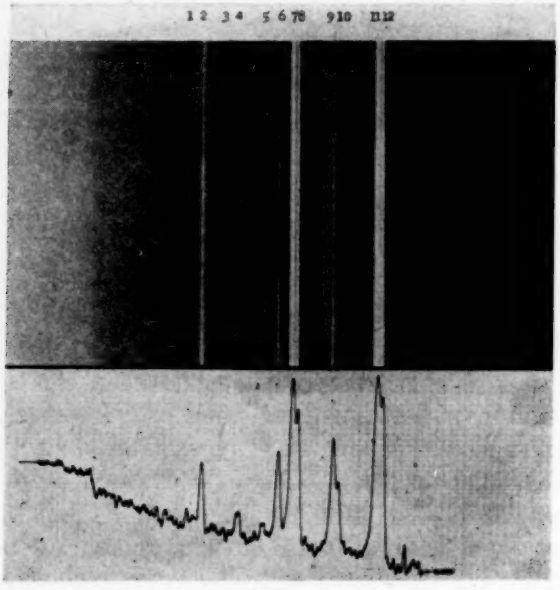

Line identification

	Element	Line		Element	Line
1	Ru	$K_{\beta 2}$	7	Ru	$K_{\alpha 1}$
2	Ru	$K_{\beta 1}$	8	Ru	$K_{\alpha 2}$
3	43	$K_{\beta 2}$	9	43	$K_{\alpha 1}$
4	43	$K_{\beta 1}$	10	43	$K_{\alpha 2}$
5	Mo	$K_{\beta 2}$	11	Mo	$K_{\alpha 1}$
6	Mo	$K_{\beta 1}$	12	Mo	$K_{\alpha 2}$

FIG. 1. X-ray spectrograms. Molybdenum element 42, Element 43, ruthenium element 44.

TABLE I. Observed and calculated values for x-ray lines of Element 43.

Element	Line	Calculated XU	Observed XU
43	$K_{\alpha 2}$	677.77	677.8
43	$K_{\alpha 1}$	673.37	673.5
43	$K_{\beta 1}$	600.14	601.4
43	$K_{\beta 2}$	589.18	589.9

4. APPARATUS

The x-ray spectrograph of a 25-cm radius was the conventional Bragg-focusing type, employing the internal standard method of wave-length calibration. The spectrograph chamber was pumped down to 100μ. A Be window 0.010 inch thick between the chamber and the slit permitted the x-ray tube to be evacuated to 0.02μ, the operating pressure. Eastman No-Screen safety film was exposed in the camera and developed seven minutes in DK 50.

The tube was operated with the anode at ground potential and the cathode at high negative potential. The separation of the cathode-target was set at $1\frac{1}{4}$ inches, and the distance of the anode spot to slit was fixed at $1\frac{1}{2}$ inches, the radius of the tube body. The filament assembly was insulated from the tube body by a 2×6-inch Pyrex flanged pipe and was cooled by a blast of air directed towards the flange. The regulated high voltage supply was rated at 60 kv and 100 ma.

The targets were flanged at one end to make them interchangeable and permit water cooling. They were fabricated from aluminum in order to minimize continuous background. The $\frac{3}{4}$ inch face of the target was cut with its normal at 70° to the slit-crystal-film axis.

The diffracting crystal[6] was of rocksalt and measured 70 mm across the face. It was rocked by a cam mechanism through an angle of 5°.

[6] Grown by Harshaw Chemical Company, Cleveland, Ohio.

TABLE II. Second-order interference lines.

Element	Line	Wave-length	Element	Line	Thresh-old V
Mo	$K_{\alpha 1}$ 708	704	Cs	$K_{\beta 1}$	35.9 kv
		710	Ce	$K_{\alpha 1}$	40.3
Mo	$K_{\alpha 2}$ 712	710	Ce	$K_{\alpha 1}$	40.3
No. 43	$K_{\alpha 1}$ 673	670	Nd	$K_{\alpha 2}$	43.6
No. 43	$K_{\alpha 2}$ 677	—	—	—	—
Ru	$K_{\alpha 1}$ 642	—	—	—	—
Ru	$K_{\alpha 2}$ 646	—	—	—	—
Mo	$K_{\beta 1}$ 631	628	Ce	$K_{\beta 1}$	40.3
Mo	$K_{\beta 2}$ 619	628	Ce	$K_{\beta 1}$	40.3
No. 43	$K_{\beta 1}$ 601	602	Pr	$K_{\beta 1}$	41.9
No. 43	$K_{\beta 2}$ 590	584	Nd	$K_{\beta 1}$	43.6
Ru	$K_{\beta 1}$ 574	584	Nd	$K_{\beta 1}$	43.6
Ru	$K_{\beta 2}$ 564	—	—	—	—
			Re	K series	71.5

The crystal was set at a median grazing angle of 6° 30′ by means of a bevel protractor.

The slit was composed of two $\frac{1}{16}$ inch stainless steel jaws. The slit was set under a measuring microscope to a width of 0.001 ± 0.0001 inch.

5. SUMMARY

The sample shown by the x-ray spectra is chiefly Element 43. The lines of Element 43 measured were $K_{\alpha 1}$, $K_{\alpha 2}$, $K_{\beta 1}$, and $K_{\beta 2}$. The agreement of the observed wave-length assignment and calculated values are apparent in Table I.

The chemical and physical history of the material together with the controlled conditions in obtaining the x-ray spectra is conclusive evidence that this material is Element 43.

This document is based on work performed under Contract No. W-7401-eng-23 for the Atomic Energy Commission at the Tennessee Eastman Corporation, Oak Ridge, Tennessee and under Contract No. W-7405-eng-26 for the Atomic Energy Commission at the Carbide and Carbon Chemicals Corporation, Oak Ridge, Tennessee.

TABLE III. Experimental conditions for the exposures.

Print No.	Element	Po-tential kv[a]	Emis-sion cur-rent ma[a]	Cam	Expo-sure per de-gree	Total expo-sure min-utes	Tube pres-sure[a]	Cam-era pres-sure
1	No. 43	35	7.0	5°	20	100	0.02μ	100μ
2	43 and Mo	35	8.0	5°	24	120	0.02μ	100μ
3	Mo, 43, Ru	35	8.0	5°	24	120	0.02μ	100μ
4	Mo and Ru	40	8.0	5°	8	40	0.02μ	100μ

[a] The values in columns 3, 4, and 8 are average values.

The Half-Life of Carbon 14*

L. D. NORRIS, *Clinton National Laboratories, Oak Ridge, Tennessee*

AND

M. G. INGHRAM, *Argonne National Laboratories, Chicago, Illinois*

(Received November 3, 1947)

By determining the specific activities of two mass-spectroscopically analyzed samples of barium carbonate containing C^{14}, the half-life of the C^{14} was found to be 5100 ± 200 years. In order to determine the relative abundance of C^{12}, C^{13}, and C^{14}, the CO_2 was roasted from the barium carbonate and introduced into the mass spectrometer. Weighed portions of the barium carbonate were subsequently counted in a low absorption beta-counter. Details of the analysis, weighing, and counting are given.

1. INTRODUCTION

WHEN C^{14} was discovered,[1] its half-life was found to be too long to lend itself to measurement by direct decay. It was necessary, therefore, to resort to measurement through the relation $dN/dt=0.693N/T_{\frac{1}{2}}$, necessitating an estimate of the total number N of C^{14} atoms present in a given sample, and a determination of the absolute rate of beta-disintegration. Early estimates of the amount of C^{14} produced in an irradiation were based upon rather rough guesses as to the cross sections for the reactions $C^{13}(d,p)C^{14}$ and $N^{14}(n,p)C^{14}$. Later, more careful work was performed by Kamen,[2] and by Langsdorf and Purbrick,[3] using the $N^{14}(n,p)C^{14}$ reaction, in which the advancing knowledge of the cross section and better methods of neutron irradiation measurement permitted closer approach to a reliable value for the half-life. When the first production unit at Clinton Laboratories started yielding samples with an isotopic abundance of several percent of C^{14},[4] it became practicable to measure the half-life more directly by means of a mass-spectrometer analysis, a careful weighing of a small sample, and an absolute beta-count. The present paper describes such a determination.

During the course of our work, the problem was taken up independently at Columbia University.[5] The Columbia figure of 4700 ± 5–10 percent is in essential agreement with the value resulting from our measurements. The importance of independent determinations is obvious, particularly since a rather difficult beta-count is involved.

The C^{14} originated in the ammonium nitrate solution "factory" described by L. D. Norris and A. H. Snell.[4] The product appeared as $BaCO_3$ precipitate in a saturated solution of $Ba(OH)_2$. It was routinely separated from the $Ba(OH)_2$ by filtration, washed carefully with warm water and ethyl alcohol, dried, and stored in a desiccator. Two separate samples from the factory were chosen for the half-life determination. Each was divided into two portions, of which one was subjected to mass-spectrometric analysis by M. G. Inghram, and the other used for the absolute beta-count by L. D. Norris. In view of the method by which the samples were made and washed, there could be no doubt that the activity was distributed homogeneously throughout the solid.

2. DETERMINATION OF THE ISOTOPIC ABUNDANCE

The abundances of the carbon isotopes in the two samples were determined by measurement with a mass spectrometer as follows.

The $BaCO_3$ samples were made to evolve CO_2 for mass-spectrometric analysis by heating them in a quartz tube to about 1100°C. This technique proved to be convenient because the $BaCO_3$ could be well prepumped to remove most gaseous

* This document is based on work performed under Contract No. W-35-058-eng-71 for the Atomic Energy Project at the Clinton Laboratories.

[1] S. Ruben and M. D. Kamen, Phys. Rev. **59**, 349 (1941).

[2] M. D. Kamen, Manhattan Project Literature A-316.

[3] A. S. Langsdorf, Jr. and R. L. Purbrick, Manhattan Project Literature CP-G-3272.

[4] L. D. Norris and A. H. Snell, Science **105** (March 7, 1947).

[5] A. F. Reid, J. R. Dunning, S. Weinhouse, and A. V. Grosse, Phys. Rev. **70**, 431 (1946).

impurities. The usual technique of liberating the CO_2 by addition of acid was not satisfactory for the following reasons: (1) Mass spectrometric-measurements of different fractions of the CO_2 obtained by baking showed that the first one-hundredth of the sample evolved by this method had a C^{14} content appreciably below that in the rest of the sample. Probably this was because of the fact that some CO_2 from the air was adsorbed on the surface of the $BaCO_3$ which could not be removed by prolonged outgassing at low temperatures. The importance of this effect is that if acid had been used to liberate the CO_2 the resulting gas would not have been characteristic of the carbon isotopic content of the sample.

(2) In handling these very small quantities of CO_2, any acid used on the $BaCO_3$ for liberating the CO_2 might carry detectable amounts of foreign carbon into the reaction vessel.

(3) The baking method removes the problem of trapping out unwanted vapors from the gas-handling system.

It is of interest to note that all of the above errors lead to a value of the C^{14} half-life which is too low.

After about 10-millimeter cubic centimeters of carbon dioxide had been obtained from the samples they were transferred to the sample system of a 60° six-inch radius of curvature, Nier-type mass spectrometer for analysis. The spectrometer was operated without the usual source magnet, and thus the usual source discriminations were eliminated.[6] The ion beams were swept across the collector by an automatic continuous variation of the analyzer magnetic field. Other systematic discriminations were less than one percent.[7] The carbon isotopic composition in the samples was determined by studying the mass spectrum of the ions of form CO_2^+.

TABLE I. Relative ion intensities with 3.2 percent C^{14}; mass 44, $C^{12}O^{16}O^{16}=100$.

Mass 45	Mass 46	Mass 47	Mass 48
$C^{13}O^{16}O^{16}=1.10$ $C^{12}O^{16}O^{17}=0.08$	$C^{14}O^{16}O^{16}=3.34$ $C^{13}O^{16}O^{17}=0.40$ $C^{13}O^{16}O^{17}=0.00$ $C^{12}O^{17}O^{17}=0.00$	$C^{13}O^{16}O^{18}=0.0045$ $C^{14}O^{16}O^{17}=0.0027$ $C^{12}O^{17}O^{18}=0.0002$ $C^{13}O^{17}O^{17}=0.0000$	$C^{14}O^{16}O^{18}=0.0132$ $C^{13}O^{16}O^{18}=0.0004$ $C^{13}O^{17}O^{18}=0.0000$ $C^{14}O^{17}O^{17}=0.0000$
1.18	3.74	0.0074	0.0136

[6] N. D. Coggeshall and E. B. Jordan, J. App. Phys. **13**, 539 (1942).

[7] M. G. Inghram, Phys. Rev. **70**, 653 (1946).

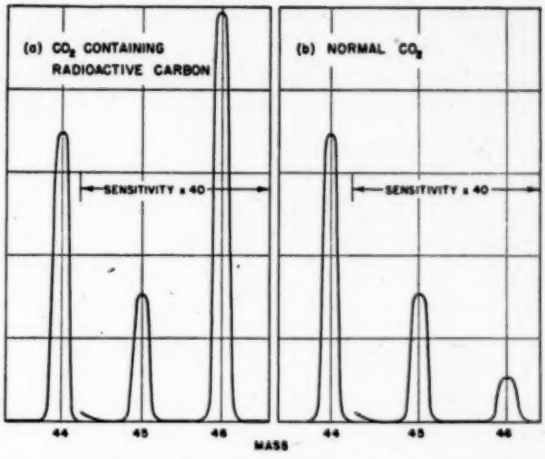

FIG. 1. Recorder tracing of the isotopes in normal carbon dioxide and in carbon dioxide containing C^{14}. The regions about mass 45 and 46 are recorded at 40 times the sensitivity used in recording the mass 44 peaks.

Assuming that the CO_2 has normal isotopic composition except for the addition of 3.20 percent C^{14}, the contribution of each combination of isotopes has been computed and tabulated according to mass in Table I. This was done to show which ions are of importance in computing the isotopic abundances. The C^{14} content was chosen to approximate that in the C^{14} sample, so that the important combinations of oxygens and carbon which were computed in Table I apply only for C^{14} abundances approximating 3.2 percent. It is important to note in computing the contribution of the molecules containing two oxygen atoms, that there are two permutations which will give rise to ions of one mass when the two oxygen atoms have different mass.

Figure 1 shows tracings of two typical recorder curves. Curve *b* is a trace of the mass 44, 45, and 46 ion currents in the mass spectrometer when normal CO_2 was introduced. Curve *a* is a trace of the same masses with one of the CO_2 samples obtained from the radioactive $BaCO_3$. In both curves the regions about mass 45 and 46 were recorded at 40 times the sensitivity used for recording the 44. The presence of the abnormal peak at mass 46 in the radioactive carbon is immediately apparent. Assuming pure CO_2 in the machine, this increase in the peak height must be due to $C^{14}O^{16}O^{16}$ or possibly to

an increased amount of O^{18}, giving an abnormal $C^{12}O^{16}O^{18}$. An appreciable increase in the amount of O^{18} would not be expected from the neutron bombardment used to produce the radioactive carbon, and the chemical preparation of the $BaCO_3$ was such that the oxygen in the sample should have reached equilibrium with the normal oxygen almost immediately. Thus normal oxygen isotopic composition would be expected in the CO_2, and hence the abnormal peak at mass 46 must be due to C^{14}.

Direct evidence that the oxygen of mass 18 was not increased above the normal values is given by combining the observation of the intensity ratio of the 46 to 44 peak with that of the 48 to 46. If we designate the ratio of the C^{14} to C^{12} atoms by x, and the ratio of the O^{18} to O^{16} by y, the 46/44 and the 46/48 ratios are

$$\frac{\text{Intensity at mass 46}}{\text{Intensity at mass 44}} = \frac{C^{14}O^{16}O^{16}+C^{12}O^{16}O^{18}}{C^{12}O^{16}O^{16}} = x+2y, \quad (1)$$

$$\frac{\text{Intensity at mass 46}}{\text{Intensity at mass 48}} = \frac{C^{14}O^{16}O^{16}+C^{12}O^{16}O^{18}}{C^{14}O^{16}O^{18}+C^{12}O^{18}O^{18}} = \frac{x+2y}{2xy+y^2}. \quad (2)$$

The multipliers 2 appear in these formulae for the reason that there are two permutations of $C^{12}O^{16}O^{18}$ which give rise to the same peak.

Experimentally, the average value of the ion

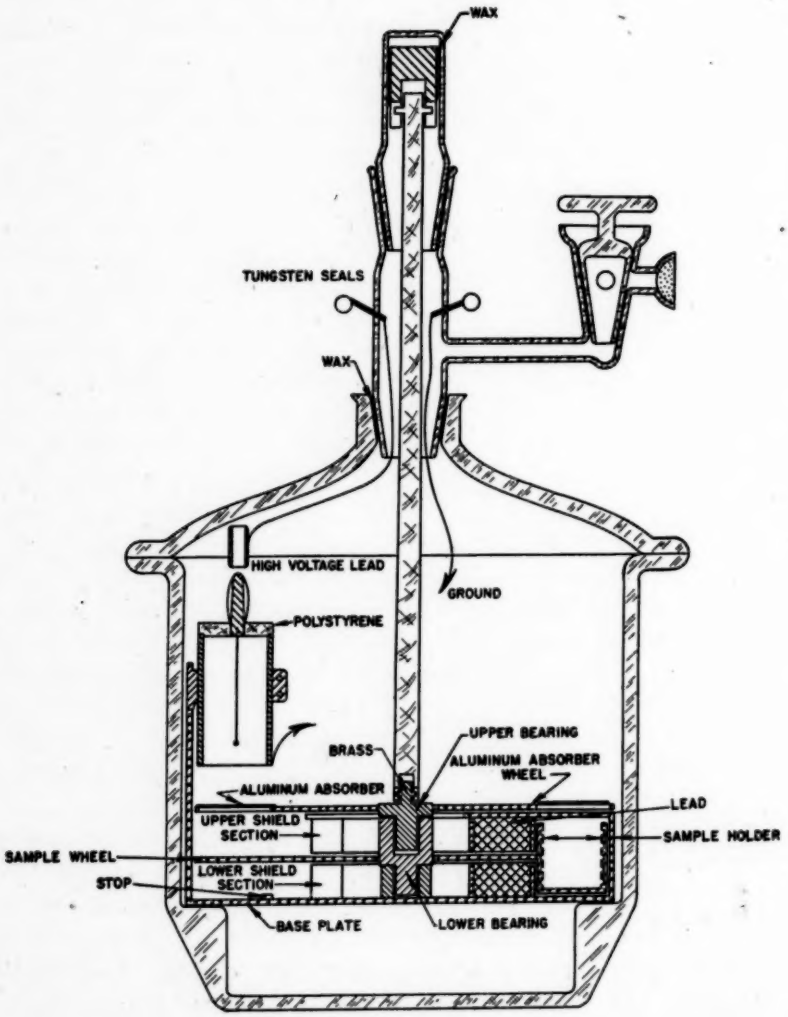

FIG. 2. Cross section—low absorption counter.

ratio 46/44 for sample 1 was 0.0390. The average background corrected value of the ion ratio 46/48 was 272. Hence, Eqs. (1) and (2) can be solved for the O^{18} isotopic composition:

$$y_1 = O^{18}/O^{16} = 0.00199. \quad (3)$$

A cross check is obtainable by utilizing the 30/28 ratio in place of the 46/44, thus

$$\frac{\text{Intensity at mass 30}}{\text{Intensity at mass 28}} = \frac{C^{14}O^{16}+C^{12}O^{18}}{C^{12}O^{16}} = x+y. \quad (4)$$

Experimentally, the average value of (4) was found to be 0.0370. Solving between (2) and (4)

$$y_2 = O^{18}/O^{16} = 0.00199, \quad (5)$$

in excellent agreement with the value obtained in (3). Determination of y by solving between Eqs. (1) and (4) should be avoided in this range of isotopic compositions, since in both (1) and (4) y is only a correction term.

It may, therefore, be concluded from the results of (3) and (5) that the O^{18} content is normal at 0.199 percent.

The determination of the C^{14} content can now be made by substitution of the determined value for y in Eq. (1),

$$x = C^{14}/C^{12} = 0.0350. \quad (6)$$

Finally, the measured value of the 45 peak was corrected for the normal amount of $C^{12}O^{16}O^{17}$ to give the intensity of the $C^{13}O^{16}O^{16}$ ion and thus the ratio of the C^{12} to C^{13} in this sample.

Carrying through the same analysis on the second sample gives the carbon isotopic composition of the two samples as

	% C^{12}	% C^{13}	% C^{14}
Sample 1	95.61±0.03	1.04±0.01	3.35±0.03
Sample 2	95.72±0.03	1.05±0.01	3.23±0.03

The errors quoted on these abundances are the limit set to include any possible systematic errors in the mass spectrometer. The internal consistency of the data was about three times better than this quoted value.

3. THE ABSOLUTE BETA-COUNT

The radioactive strengths of the samples were measured in a low absorption counter, the

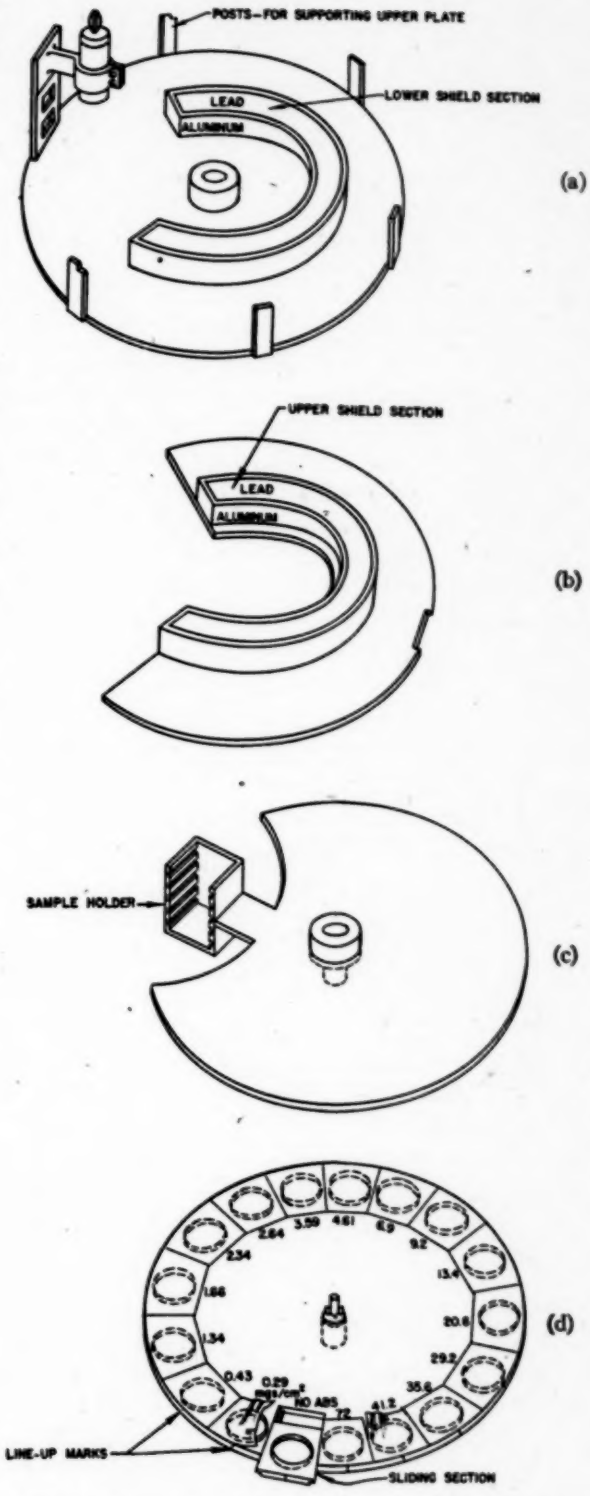

FIG. 3(a) Low absorption counter—base plate. (b) Low absorption counter—upper plate (as seen from bottom side). (c) Low absorption counter—sample wheel. (d) Low absorption counter—absorber wheel.

effective solid angle of which was determined by means of a "weightless" sample of UX_1 and UX_2.

4. THE LOW ABSORPTION COUNTER

This instrument is similar in principle to the one first designed by N. Elliot,[8] and is somewhat more like the one built at Ames by W. H. Sullivan, N. R. Sleight, and E. M. Gladrow,[9] with several important modifications and improvements.

In Fig. 2 is shown a cross-sectional view of the apparatus. A 250-mm diameter Pyrex vacuum desiccator is used to house the counter. Figure 3 shows isometric projections of the four major components within the desiccator: (a) the base plate; (b) the upper plate, which holds the upper shield section; (c) the sample wheel, to which is attached the shelved sample holder; and (d) the absorber wheel. The whole assembly is made of aluminum with the exception of the shafts, bearings, shields, and counter tube. The counter tube is 1-in. I.D. brass, with a 0.005-in. tungsten wire as the center electrode. A standard, made of $BaC^{14}O_3$,** weighing approximately the same as the samples we wished to count, and mounted in exactly the same fashion, was permanently placed on the sample wheel at 120° to the sample holder. The weights of the sixteen aluminum absorbers cemented to the absorber wheel are noted on the drawing in Fig. 3.

To operate the counter, one mounts a sample on a light aluminum frame, which is then inserted in the sample holder. The components are assembled within the desiccator, the desiccator is lubricated with a high quality vacuum grease, pumped out, and filled with the counting mixture. The sample and absorber wheels can be rotated by turning the taper joint on the top of the desiccator. A polystyrene center shaft, which is coupled to the taper joint and the absorber wheel by very simple key and slot arrangements, turns with the taper joint, and drives the absorber wheel directly. The absorber wheel in turn drives the sample wheel by virtue of the friction between the upper bearing and shaft surfaces, the degree of rotation of the sample wheel being confined by two stops fastened to the base plate. The design of the counter allows one to bring the sample directly beneath the tube, in which position the various absorbers may be rotated into place between sample and counter, and an absorption curve obtained. Alternatively, one can bring the standard into position under the tube and take a standard count. When the

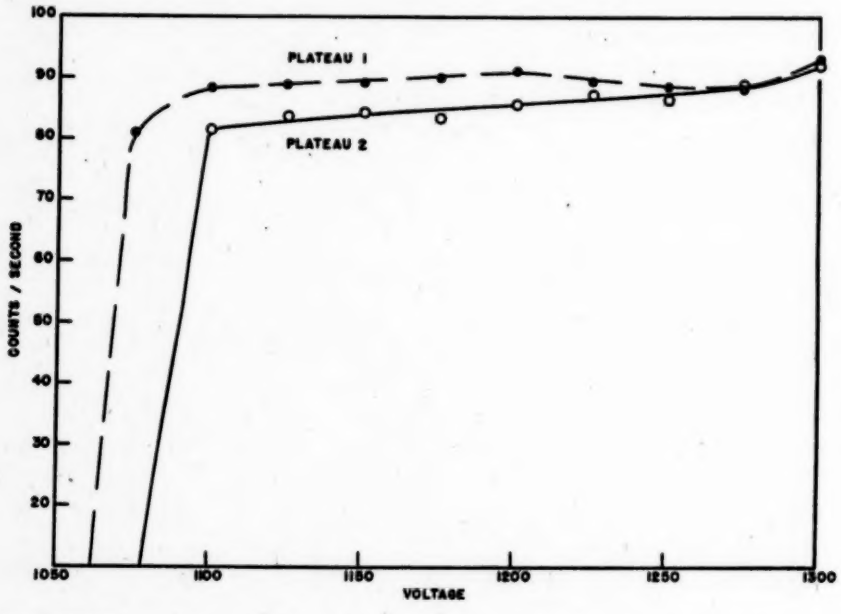

FIG. 4. Low absorption counter plateaus. Plateau 1, taken 30 minutes after filling. Plateau 2, taken immediately after plateau 1.

[8] N. Elliot, Manhattan Project Literature CC-763.
[9] W. H. Sullivan, N. R. Sleight, and E. M. Gladrow, Manhattan Project Literature CC-1380.
** The symbol $BaC^{14}O_3$ may be taken to mean any $BaCO_3$ containing some percentage of C^{14}. It does not imply that the material referred to contains no other carbon isotopes.

sample is being counted the standard is behind the lead shield sections, and when the standard is being counted the sample is behind the lead shield sections. One may also place both standard and sample behind the shields in order to take backgrounds.

The background over practically all the foils in the counter was approximately 25 counts per minute, but it was some 600 counts per minute over the two lightest ones. Since we were certain that these foils were not contaminated, it was suspected that such high backgrounds might be a corona phenomenon associated with the nature of the surfaces of these thin foils. Evidence that this might be true lies in the fact that the two absorbers giving high backgrounds were both beaten foils, not rolled as were the others, and they exhibited rough, jagged surfaces when examined under a low power microscope. Evidently these very thin absorbers would have been better made of some non-conducting material.

In using the counter, we followed a standard procedure, beginning with the filling process and ending with the last count. This was desirable for several reasons: (1) It was obvious that the counting mixture should be identical from filling to filling. The counting mixture used was 1.0-cm Hg pressure of absolute ethyl alcohol and 9.0-cm Hg pressure of argon; (2) these low absorption counters take thirty minutes or more to degas; and (3) when the counter is first filled its sensitivity is greater than it is after an appreciable amount of counting has been done. This is illustrated in Fig. 4, where the dotted line is a plateau taken after the counter has been filled and allowed to degas, and the solid line is a second plateau taken immediately after the first, using the same C^{14} sample. This we consider the true plateau, and the slope can be seen to be approximately 3.7 percent per 100 volts.

When the standard procedure was adhered to, the counter was found to perform in a very consistent fashion. The threshold was always 1070 ± 10 volts, and the counter was operated at 1200 volts for all our work. The standard, over an interval of thirty fillings, gave an average counting rate of 24.8 counts per second, the maximum recorded being 25.3 counts per second, the minimum 24.5 counts per second, the average deviation in parts per hundred being 0.65. The samples were placed at a distance of 3.7 cm from the counter tube, and the intervening gas had an absorbing effect of 0.81 mg per cm^2.

5. DETERMINATION OF THE EFFECTIVE SOLID ANGLE OF THE COUNTER

For this determination, the beta-particles of $UX_1(Th^{234})$ and $UX_2(Pa^{234})$ were used. The specific activity of natural uranium has been given as 1501 alpha-disintegrations per minute per milligram by Kovarik and Adams;[10] Novey and Levy have made corrections for the U^{235} and U^{234} activities, arriving at a figure of 724 disintegrations per minute per mg for the specific activity of pure U^{238}.[11] Since the UX_1 and UX_2 are in equilibrium with the U^{238}, this is also the UX_1 and UX_2 beta-activity per milligram of natural uranium. By separating the UX_1 out of the uranium, one eliminates the bulk contributed by the uranium and avoids undesirable absorption and scattering effects. The separation is performed[11, 12] by taking a dried, weighed portion of old U_3O_8 or U, and dissolving it in HNO_3. Lanthanum carrier is added, and the lanthanum fluoride precipitated, using HF and KF. The precipitation is again carried out in the supernatant, and the fluoride precipitates combined. The fluoride is then dissolved, by use of H_3BO_3 and HNO_3, and the lanthanum reprecipitated as the hydroxide. The hydroxide may be dissolved in dilute HCl, and the solution transferred to a volumetric flask and diluted to volume. Since the UX_2 is again in equilibrium with the UX_1 shortly after separation, it is sometimes convenient to use it, rather than the UX_1, because of its high energy beta-particles. For our purposes, both were utilized, the UX_1 being especially useful since its beta-rays are of approximately the same energy as those from C^{14}.

Consideration of our sample mounting technique, i.e., confining the activity to a $\frac{7}{16}$-in. diameter circle in the center of a film or foil, made it necessary to have a solution of $UX_{1,2}$ of

[10] A. F. Kovarik and N. I. Adams, Jr., J. App. Phys. 12, 296 (1941).
[11] T. B. Novey and P. W. Levy, Manhattan Project Literature Memo.
[12] C. D. Coryell and co-workers, Manhattan Project Literature CN-2815.

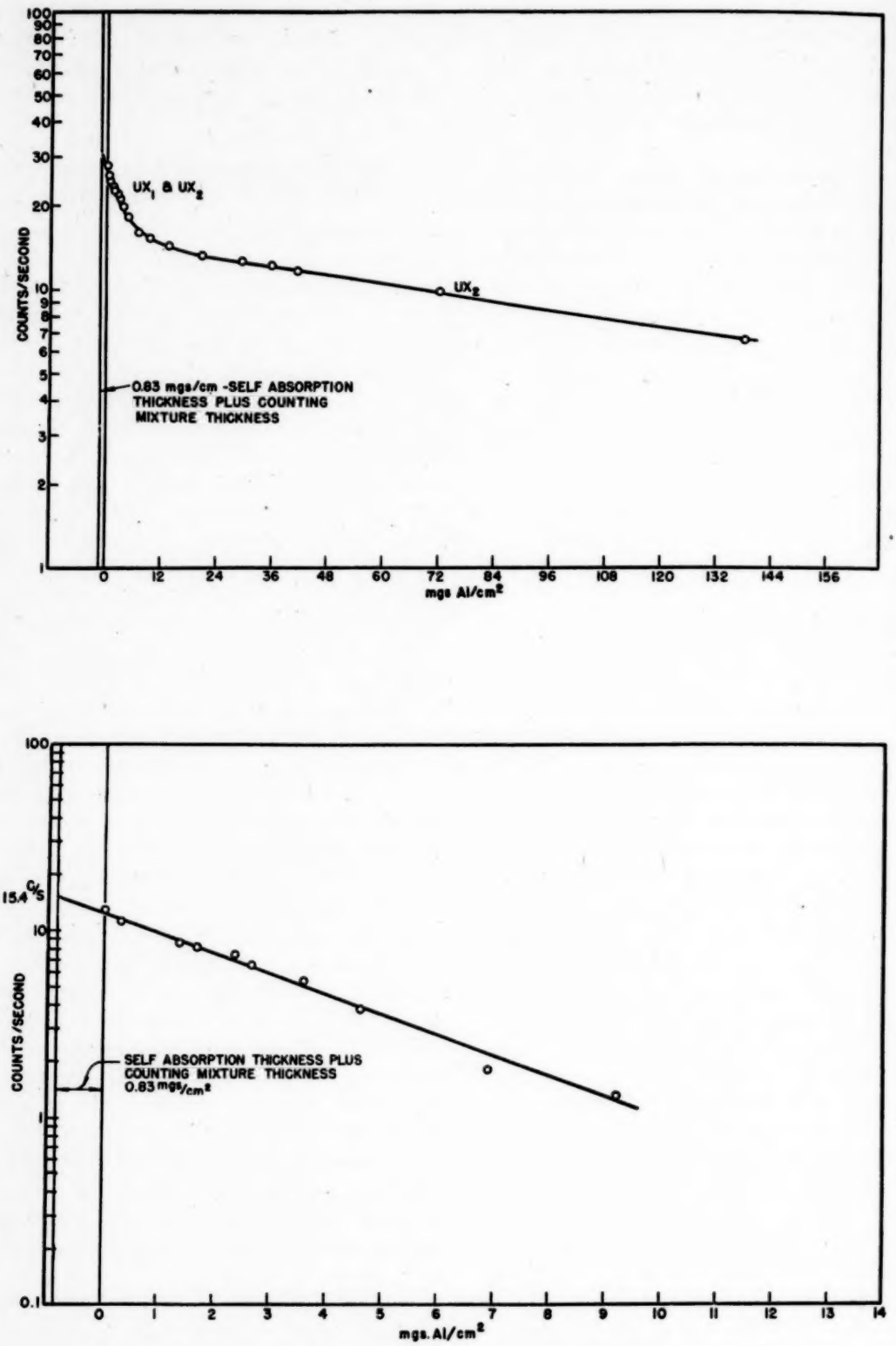

FIG. 5(a) $UX_{1,2}$ absorption curve with low absorption counter. (b) UX_1 absorption curve—obtained from curve in Fig. 5(a) by subtraction of UX_2 component.

high specific activity, since 0.1–0.2 ml of solution will cover such a circle. This introduced a problem because the quantitative separation of UX_1 from uranium is best carried out in dilute solutions of uranium.[12] As a consequence, reference solutions of $UX_{1,2}$ of low specific activity were made from dilute uranium solutions. Large aliquots (approximately 5 ml) of these solutions were evaporated in Coors porcelain capsules, and the UX_2 betas counted with a mica window counter. Then a very strong solution of $UX_{1,2}$ was made by roughing through the separation, and aliquots of this solution were also evaporated in Coors porcelain capsules. By counting the UX_2 betas from these aliquots with the mica window counter, an accurate comparison could be made with the reference solutions, and the specific activity of the strong solution determined.

A zapon film, weighing less than 0.02 mg/cm², was then cemented over a $\frac{7}{8}$-in. diameter hole in a light aluminum frame, and 0.100 ml of the strong $UX_{1,2}$ solution delivered quantitatively on the center of the film so as to cover a circular area $\frac{7}{16}$ in. in diameter. The solution was evaporated with a radiant lamp, leaving the activity deposited uniformly on the film. Three samples so prepared were counted in the low absorption counter, and an absorption curve was obtained for each. Figure 5 is a reproduction of one of these absorption curves. The counts were corrected for coincidence losses, and the absorption curves were extrapolated back to absolute zero absorber thickness to correct for self-absorption and absorption in the counting mixture, giving for the UX_1 beta-particles a factor of 1.22 as the ratio of the counting rate at absolute zero absorber to the counting rate at zero aluminum absorber. Back-scatter and self-scatter were assumed negligible. After appropriate decay corrections, comparison of the extrapolated counts with the known beta-disintegration rate of the samples (1360 ± 30 per second) gave, respectively, 0.0230, 0.0223, and 0.0231 for the effective solid angle of the counter when used under these geometrical conditions. The mean value is 0.0228 ± 0.0006. This value was checked three months later with an independently calibrated Y^{91} source, agreement being obtained within one percent.

6. THE CARBON 14 COUNT

Weighing the Samples

The portions were weighed by difference with an Ainsworth Type FDJ microbalance, the $BaC^{14}O_3$ being contained in Pregl weighing bottles. The sensitivity and precision of the balance were determined before each set of weighings, the average sensitivity of the loaded balance being 1.18 deflection units per microgram, and the average precision ± 1 deflection unit.[13] The transfer of $BaC^{14}O_3$ from weighing bottle to mounting foil was accomplished by means of a small aluminum spoon within each bottle. The weights of the samples lay within the range 141 to 252 micrograms.

Mounting

The $BaC^{14}O_3$ was spread in shallow depressions $\frac{7}{16}$ in. in diameter pressed into disks of 0.001-in. aluminum foil. The depressions were centered and the disks cemented over the $\frac{7}{8}$-in. holes in aluminum frames identical with those used for the $UX_{1,2}$ samples in the solid angle determination. It was necessary to be extremely careful about the uniformity of the $BaC^{14}O_3$ deposits; any lumping or aggregation reduced the apparent specific activity appreciably.

After considerable trial and error, a mounting technique was devised which gave reasonably good results. The $BaC^{14}O_3$ was slurried with methanol containing a small amount of aerosol, and then spread with a fine platinum wire, after which the methanol was evaporated. This slurrying, spreading, and drying was repeated until the deposit was uniform. Then the wire was rinsed with a drop of methanol, and the plate redried. Any plates with non-uniform deposits were discarded. Eleven mounts were prepared from the sample of 3.35 percent C^{14} concentration, and six were made from the 3.23 percent sample. In addition, four other mounts were prepared from the 3.35 percent sample, using a technique devised by Hendricks and

[13] For a discussion of microbalances and their uses, see such texts on microchemical procedures as J. B. Niederl and V. Niederl, *Micromethods of Quantitative Organic Analysis* (John Wiley and Sons, Inc., New York, 1942), second edition.

co-workers for $BaS^{35}O_4$,[14] and later by others for $BaC^{14}O_3$.[15,16]

7. CORRECTIONS TO THE COUNTS

Coincidence Loss

This correction, arising from the loss of counts at high counting rates because of the "dead" time of the counter tube, was assumed to be 0.5 percent per 1000 counts per minute for the "self-quenched" low absorption counter.[17] The highest counting rates we employed were of the order of 6000 counts per minute, and thus the maximum coincidence loss correction factor was 1.03.

Self-Scattering

The non-isotropic scattering of beta-particles in the $BaC^{14}O_3$ itself we considered to be negligible because of the thinness of the samples.

Back-scattering

As noted previously, 0.001-in. aluminum foil was used as backing for the $BaC^{14}O_3$ mounts. This foil was used because: (1) it lends itself to the slurrying and spreading of solid materials, and (2) experiments showed that 0.001-in. aluminum would provide "saturation" back-scatter.

To determine the amount of back-scatter at saturation, a solution containing $Na_2C^{14}O_3$ was employed, since liquid aliquots are easily delivered and evaporated on the zapon films we wished to employ. Three zapon films were cemented to the same aluminum frames used for counting the analyzed $BaC^{14}O_3$. Aliquots of the $Na_2C^{14}O_3$ solution were delivered on the centers of the films so as to cover the standard circular area of $\frac{7}{16}$-in. diameter, and then evaporated to dryness with a radiant lamp. After evaporation each film contained approximately 170 micrograms of solid. Each of the frames was inserted in the low absorption counter and an absorption curve obtained. The frames were removed and beneath each zapon film, less than 0.5 mm from it, was cemented a piece of 0.001-in. aluminum. The samples were then recounted. The absorption curves were extrapolated to correct for self-absorption and absorption in the

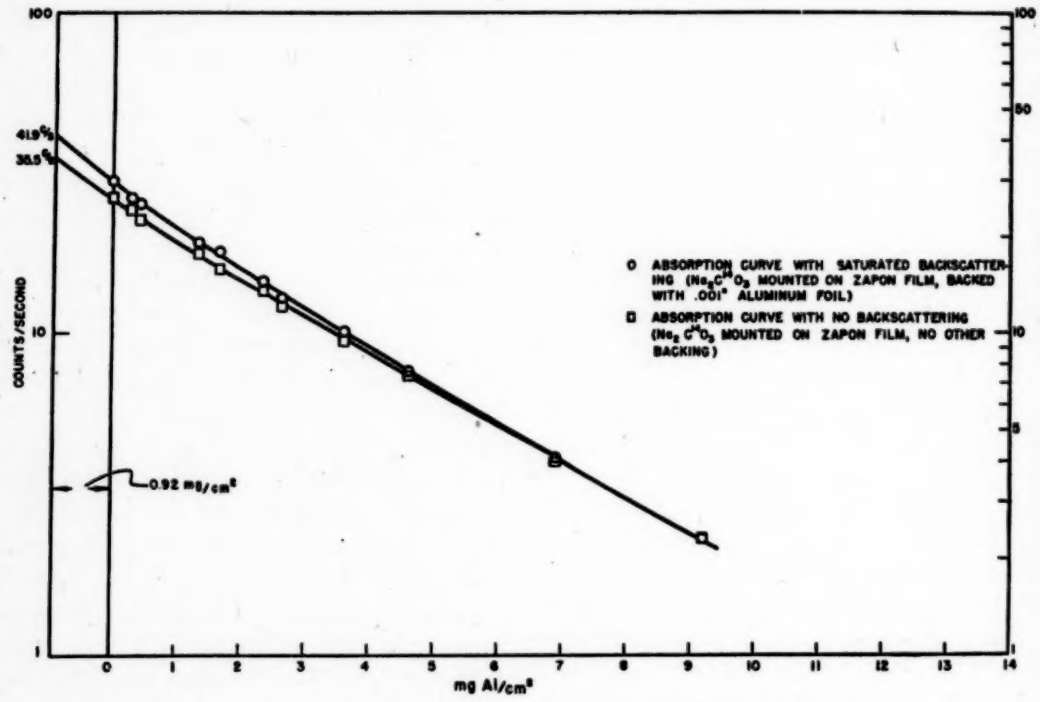
100
50
10
5
1
41.9%
38.9%
COUNTS/SECOND
0.92 mg/cm²
O ABSORPTION CURVE WITH SATURATED BACKSCATTERING (Na₂C¹⁴O₃ MOUNTED ON ZAPON FILM, BACKED WITH .001" ALUMINUM FOIL)
□ ABSORPTION CURVE WITH NO BACKSCATTERING (Na₂C¹⁴O₃ MOUNTED ON ZAPON FILM, NO OTHER BACKING)
0 1 2 3 4 5 6 7 8 9 10 11 12 13 14
mg Al/cm²

FIG. 6. C^{14} absorption curves with no back-scattering and saturated back-scattering.

[14] Hendricks, Bryner, Thomas, and Ivie, J. Phys. Chem. **47**, 469 (1943).
[15] P. E. Yankwich, G. K. Rollefson, and T. H. Norris, J. Chem. Phys. **14**, 131 (1946).
[16] P. E. Yankwich, Manhattan Project Literature CC-3567.
[17] A. Jaffey, T. Kohman, and J. Crawford, Manhattan Project Literature, M-CC-1602.

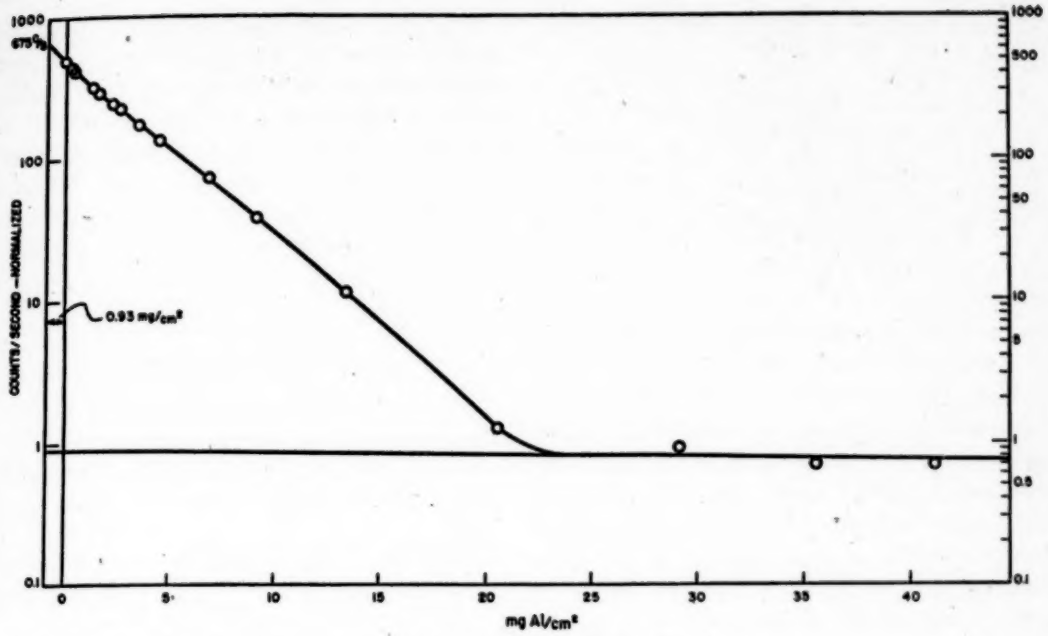

FIG. 7. Standard absorption curve—$C^{14}As\ BaC^{14}O_3$, 0.001-in. aluminum backing.

counting mixture, and it was found that the samples, when backed by the aluminum foil, counted, respectively, 1.18, 1.20, and 1.20 times as rapidly as they did with the zapon alone, i.e., with "weightless" backing. Accordingly, the figure 1.19 was adopted as the back-scatter correction. In Fig. 6 is reproduced a pair of these absorption curves, the one with and the other without the 0.001-in. aluminum backing.

Absorption in the Counting Mixture

Figure 7 shows a standard absorption curve obtained in the low absorption counter with a $BaC^{14}O_3$ sample mounted on 0.001-in. aluminum. When the curve is extrapolated back to compensate for the absorption by the counting mixture (0.81 mg/cm²), one gets a factor of 1.32 for the ratio of the counting rate at absolute zero absorber to the counting rate at 0.81 mg/cm² of absorber.

It should be noted that the absorption curve in Fig. 7 turns unexpectedly upward at low absorber thicknesses. Since those absorption curves taken during the course of the back-scatter determination with samples of $Na_2C^{14}O_3$ mounted on zapon film band upward in a similar fashion (see Fig. 6), and since the UX_1 absorption curves obtained with the low absorption counter appear to be straight lines on the standard semilog plot (see Fig. 5), it is difficult to explain the change of slope as resulting from a peculiarity of the counter or from scattering. However, if such bending actually represents an uncorrected scattering phenomenon, or perhaps the presence of a conversion line in the C^{14} beta-spectrum, the absorption corrections may be incorrectly evaluated, in which case our value for $T_{\frac{1}{2}}$ would be somewhat low.

Self-Absorption

The absorption taking place within the $BaC^{14}O_3$ itself was corrected for by assuming it to be equivalent to half the thickness of the deposit in mg/cm². This correction varied from 1.02 for the lightest mounts to 1.04 for the heaviest.

8. RESULTS

The mounts made from the 3.23 percent C^{14} sample were at first found to exhibit a consistently lower specific activity than those made from the 3.35 percent sample. This suggested the presence of impurities, probably siliceous in nature, and consequently portions of both samples were repurified. This was accomplished by acidifying the $BaC^{14}O_3$ in a small glass system which had previously been freed of natural

TABLE II. Mean values of $T_{\frac{1}{2}}$ for C^{14} as derived from four groups of mounts.

Group	Sample	Description	$T_{\frac{1}{2}}$
I	3.35% C^{14}	not repurified (mean result from 5 mounts)	5000 yrs.
II	3.35% C^{14}	repurified (mean result from 6 mounts)	5100 yrs.
III	3.23% C^{14}	repurified (mean result from 6 mounts)	5200 yrs.
IV	3.35% C^{14}	repurified, mounted by technique Hendricks (mean result from 4 mounts)	5100 yrs

carbon by flaming and flushing with CO_2-free oxygen. The $C^{14}O_2$ was eluted with 1 N HCl, reprecipitated as the $BaC^{14}O_3$, and washed, dried, mounted, and counted in the standard fashion. The specific activity of the 3.35 percent sample remained unchanged, while that of the 3.23 percent sample increased into essential agreement. The results of the groups of samples, variously treated, are given in Table II in terms of the deduced half-life of C^{14}.

For the twenty-one individual mounts, the highest value for $T_{\frac{1}{2}}$ was 5500 years, and the lowest 4700 years. We conclude that the half-life of C^{14} is 5100 ± 200 years; the indicated error is the probable error of the mean as obtained from the two analyzed samples, and includes the uncertainties in the solid angle and back-scatter determinations. This value is lower by 200 years than a preliminary value reported previously by the authors.[18]

9. ACKNOWLEDGMENTS

The authors are indebted to Dr. A. H. Snell and Professor A. J. Dempster. Their interest has made these measurements possible, and they have offered many valuable suggestions and criticisms during the course of the work.

[18] L. D. Norris and M. G. Inghram, Phys. Rev. **70**, 772 (1946).

PHYSICAL REVIEW VOLUME 73, NUMBER 4 FEBRUARY 15, 1948

The Influence of Retardation on the London-van der Waals Forces

H. B. G. CASIMIR AND D. POLDER
Natuurkundig Laboratorium der N. V. Philips' Gloeilampenfabrieken, Eindhoven, Netherlands

(Received May 16, 1947)

The influence of retardation on the energy of interaction between two neutral atoms is investigated by means of quantum electrodynamics. As a preliminary step, Part I contains a discussion of the interaction between a neutral atom and a perfectly conducting plane, and it is found that the influence of retardation leads to a reduction of the interaction energy by a correction factor which decreases monotonically with increasing distance R. This factor is equal to unity for R small compared with the wave-lengths corresponding to the atomic frequencies, and is proportional to R^{-1} for distances large compared with these wave-lengths. In the latter case the total interaction energy is given by $-3\hbar c\alpha/8\pi R^4$, where α is the static polarizability of the atom. Although the problem of the interaction of two atoms discussed in Part II is much more difficult to handle mathematically, the results are very similar. Again the influence of retardation can be described by a monotonically decreasing correction factor which is equal to unity for small distances and proportional to R^{-1} for large distances. In the latter case the energy of interaction is found to be $-23\hbar c\alpha_1\alpha_2/4\pi R^7$.

PART I. GENERAL FEATURES OF THE PROBLEM

1. Introduction

THE problem treated in this paper, though apparently a somewhat academic exercise in quantum electrodynamics, arose directly from the work of Verwey and Overbeek[1] on the stability of colloidal systems. Starting from work of Hamaker, Verwey and Overbeek have in recent years developed a theory in which the attraction between colloidal particles is exclusively ascribed to London-van der Waals forces, the repulsion being accounted for by the interaction of electric double layers. In applying this

[1] E. J. W. Verwey, J. T. G. Overbeek, and K. van Nes, *Theory of the Stability of Lyophobic Colloids* (Elsevier Publishing Company, Inc., Amsterdam, in press); E. J. W. Verwey and J. T. G. Overbeek, Trans. Faraday Soc. (In press); E. J. W. Verwey, J. Phys. and Colloid Chem. **51**, 631 (1947).

theory to suspensions of comparatively large particles, they found a discrepancy between their theory and the experimental results which could be removed only by assuming that at large distances the attractive force between two atoms decreases more rapidly than R^{-7}. Overbeek then pointed out that on the basis of the picture customarily used for visualizing London forces, an influence of retardation on the interaction is to be expected as soon as the distance between the particles becomes comparable to the wavelength corresponding to the atomic frequencies. Although this argument is suggestive, we have not succeeded in deriving an expression for the influence of retardation based on such a simple model, and we doubt very much whether a result can be obtained in that way. In this paper hardly any reference will be made to Overbeek's original considerations. Also, the application to the problems of colloid chemistry will not be touched upon but will be left for a future publication. We want, however, to emphasize our indebtedness to Overbeek's suggestion.

So far, problems of retardation have only occasionally been treated by means of quantum electrodynamics. There is, of course, the work of Møller[2] and its justification by Bethe and Fermi.[3] Also in the work of Breit[4] on the interaction of the electrons in the He atom, retardation is taken into account. In these cases, however, we have to deal with the influence of retardation on expressions containing the square of the electronic charge, which means that we can restrict ourselves to studying the interaction between electrons and the radiation field to a second approximation. In our case, which concerns the interaction between two neutral atoms, the approximation has to be pushed to the fourth order, as the usual expression for the London energy contains the fourth power of the electronic charge. We found, however, that what seemed to us the most essential features of the final result are already clearly revealed by a problem which can be treated by means of quite simple mathematics, involving only second-order perturbation theory, i.e., the interaction of a neutral atom with a perfectly conducting wall. According to classical ideas the energy should always be given by the interaction of the atomic dipole with its image, and retardation effects are to be expected when its distance from the wall becomes large. The result of a direct calculation by means of quantum electrodynamics, which will be given in Section 12, is not in disagreement with this notion. Yet the final result is rather unexpected. For short distances we find the usual value for the London energy between a neutral atom and a conducting wall, which is proportional to R^{-3}. With increasing R, however, the usual value must be multiplied by a monotonically decreasing factor, and for large values of R the London energy is found to be proportional to R^{-4} rather than to R^{-3}. It is remarkable that the asymptotic expression for large R contains Planck's constant and, in addition, the static polarizability of the atom as the only quantity characterizing the specific properties of the atom.

The calculations in Part II, dealing with the interaction of two neutral atoms, are much more complicated, but it is of interest to remark that here also the present-day formulation of quantum electrodynamics, if properly handled, is able to give an unambiguous result. For short distances the usual expression for the London energy, in this case being proportional to R^{-6}, is valid again, whereas for large distances the energy of interaction is proportional to R^{-7}. The asymptotic expression contains Planck's constant and the product of the polarizabilities of the two atoms.

2. Interaction of a Neutral Atom with a Perfectly Conducting Plane

Consider a region of space, defined by $0<x<L$, $0<y<L$, $0<z<L$, enclosed in a box with perfectly conducting walls. The eigenstates of the electromagnetic field in this box are described by solutions of Maxwell's equations satisfying the boundary condition that the tangential components of $\mathbf{E}$, the electric field, vanish at the walls. These solutions are easily found to be

$$\begin{aligned} E_x(\mathbf{k},\lambda) &= e_x(\mathbf{k},\lambda)\cos k_1 x \sin k_2 y \sin k_3 z \cdot C_e, \\ E_y(\mathbf{k},\lambda) &= e_y(\mathbf{k},\lambda)\sin k_1 x \cos k_2 y \sin k_3 z \cdot C_e, \\ E_z(\mathbf{k},\lambda) &= e_z(\mathbf{k},\lambda)\sin k_1 x \sin k_2 y \cos k_3 z \cdot C_e, \end{aligned} \tag{1}$$

[2] C. Møller, Zeits. f. Physik **70**, 786 (1931).
[3] H. Bethe und E. Fermi, Zeits. f. Physik **77**, 296 (1932).
[4] G. Breit, Phys. Rev. **34**, 353 (1929); Phys. Rev. **36**, 383 (1930); Phys. Rev. **39**, 616 (1932).

where $\mathbf{k}$ is a wave vector with components $k_i=n_i\pi/L$, with $n_i=0, 1, 2, 3\cdots$, and $\mathbf{e}$ is a unit vector perpendicular to $\mathbf{k}$. To each vector $\mathbf{k}$ belong two vectors $\mathbf{e}$, corresponding to the two directions of polarization; they are indicated by the symbol λ ($\lambda=1, 2$). The normalization factor C_e is given by

$$C_e^2=16\pi\hbar c/kL^3. \tag{2}$$

In order to verify that this is the correct normalization we write for the vector potential of the electromagnetic field in the box:

$$\mathbf{A}=\sum_{k,\lambda}(A_{k\lambda}e^{-i\omega t}+A_{k\lambda}^{\dagger}e^{i\omega t})\mathbf{E}(\mathbf{k},\lambda), \tag{3}$$

and determine the energy ϵ of the field:

$$\epsilon=\frac{1}{8\pi}\int(E^2+H^2)dv=\frac{1}{4\pi}\int E^2dv$$

$$=\frac{1}{4\pi}\frac{L^3}{8}\sum_{k,\lambda}\frac{16\pi\hbar c}{kL^3}k^2(A_{k\lambda}^{\dagger}A_{k\lambda}+A_{k\lambda}A_{k\lambda}^{\dagger})$$

$$=\sum_{k,\lambda}\tfrac{1}{2}\hbar\omega(A_{k\lambda}^{\dagger}A_{k\lambda}+A_{k\lambda}A_{k\lambda}^{\dagger}). \tag{4}$$

In quantum electrodynamics A and $A^{\dagger}$ are operators satisfying:

$$A_{k\lambda}A_{l\mu}^{\dagger}-A_{l\mu}^{\dagger}A_{k\lambda}=\delta_{kl}\delta_{\mu\lambda}, \tag{5}$$

and the eigenvalues of $A_{k\lambda}^{\dagger}A_{k\lambda}$ are $0, 1, 2\cdots$. In this way we have obtained the usual formulation of the quantization of the radiation field in an empty box.

We now consider the operator G of the interaction between a neutral atom and the radiation field:

$$G=\sum_j\left\{-\frac{e}{mc}(\mathbf{p}_j\mathbf{A})+\frac{e^2}{2mc^2}A^2\right\}, \tag{6}$$

where the summation is over all electrons in the atom and $\mathbf{p}_j$ is the operator of the momentum of an electron. We determine the energy perturbation of the lowest level of the system consisting of the atom and the radiation field. Since A has no diagonal elements, there is no first-order perturbation proportional to e. Therefore we use second-order perturbation theory for the terms with e in G and first-order perturbation theory for the terms with e^2. In the course of the following calculation we shall determine the perturbation energies for the case in which the atom is situated at a very large distance from the walls of the box and for the case in which it is at a short distance from one of the walls. In both cases the result is given by a divergent series over the excited states of the atom, each term of which is a convergent sum over the excited states of the radiation field. The difference between the perturbation energies in both cases can be found without ambiguity and is finite; this difference will be interpreted as the energy of interaction between the atom and the wall so far as it is due to the interaction of the atom with the radiation field.

The second-order perturbation energy of the lowest level due to an operator H is given by

$$\Delta_2E=-\sum_g\frac{|H_{0g}|^2}{E_g-E_0}. \tag{7}$$

In our system the excited states g are labeled by the index n for the states of the atom and by the indices k, λ for the states of the radiation field in which one light quantum is present. The energy difference between the level n, k, λ of our system and the lowest level is given by $\hbar c(k_n+k)$ and, therefore, the perturbation energy is

$$\Delta_2E=-\frac{e^2}{m^2c^2}\sum_{n,k,\lambda}\frac{|(\mathbf{A}_{0;\,k\lambda}\mathbf{p}_{0;\,n})|^2}{\hbar c(k_n+k)} \tag{8}$$

(where $\mathbf{p}=\sum_j\mathbf{p}_j$), to which must be added the first-order perturbation due to terms with e^2, which according to the laws of matrix multiplication can be written as:

$$\Delta_1E=\sum_j\frac{e^2}{2mc^2}\sum_{k,\lambda}\sum_{x,y,z}|A_{0;\,k\lambda}{}^{x}|^2. \tag{9}$$

In writing these formulae we have made one approximation: we have neglected the variation of the electromagnetic field inside the atom. It is well known that due to this approximation the contribution to the second-order perturbation energy from one excited level of the atom already becomes infinite since the integral over $\mathbf{k}$ does not converge for $|k|\to\infty$. Instead of taking these effects into account rigorously we shall introduce a factor $e^{-\gamma k}$, which makes the integral convergent, and put $\gamma=0$ in the final result. In reality it should be of the order of the radius of

the atom, but this does not appreciably affect the results.

In order to obtain a simple expression for $\Delta_r E=\Delta_2 E+\Delta_1 E$, we make use of the sum rule

$$\delta_{rs}\sum_i \frac{e^2}{2mc^2} = \frac{e^2}{m^2c^2}\sum_n \frac{\frac{1}{2}(p_{0;\,n}{}^x p_{n;\,0}{}^y+p_{0;\,n}{}^y p_{n;\,0}{}^x)}{\hbar c k_n}, \quad (10)$$

and the relation $ep_{0;n}=-imck_n q_{0;n}$, where q is the operator of the total dipole moment. We find for the total perturbation energy

$$\Delta_r E=\frac{1}{\hbar c}\sum_{n,k,\lambda}\frac{kk_n}{k+k_n}|(\mathbf{A}_{0;\,k\lambda}\mathbf{q}_{0;\,n})|^2. \quad (11)$$

In order to simplify the problem we assume the zero state of the atom to be a state with angular momentum $J=0$, which means that matrix elements of $\mathbf{p}$ exist only between this state and the threefold degenerate states with $J=1$. The three wave functions belonging to a state with $J=1$ may be chosen without loss of generality in such a way that they have the same transformation properties under a rotation as x, y, and z. Then all cross products of the type $q_{0;\,n}{}^x q_{0;\,n}{}^y$ vanish and (11) can be written as:

$$\Delta_r E=\frac{1}{\hbar c}\sum_{n,k,\lambda}\frac{kk_n}{k+k_n}\sum_{x,y,z}|A_{0;\,k\lambda}{}^x|^2|q_{0;\,n}{}^x|^2, \quad (12)$$

where n denotes the states with $J=1$. Substituting (3) and (1) in (12) we have

$$\Delta_r E=\frac{16\pi}{L^3}\sum_{n,k,\lambda}\frac{k_n}{k+k_n}\{|q_{0;\,n}{}^x|^2 e_x{}^2(\mathbf{k},\lambda)\cos^2 k_1 x\sin^2 k_2 y\sin^2 k_3 z + |q_{0;\,n}{}^y|^2 e_y{}^2(\mathbf{k},\lambda)\sin^2 k_1 x\cos^2 k_2 y\sin^2 k_3 z + |q_{0;\,n}{}^z|^2 e_z{}^2(\mathbf{k},\lambda)\sin^2 k_1 x\sin^2 k_2 y\cos^2 k_3 z\}. \quad (13)$$

In order to carry out the summation over λ we use the relation

$$\textstyle\sum_\lambda e_i{}^2(\mathbf{k},\lambda)=1-k_i{}^2/k^2. \quad (14)$$

We assume that the box is very large and therefore the summation over all values of $\mathbf{k}$ can be replaced by an integral. Since the integrand is an even function of k_i, the summation is equal to $L^3/8\pi^3$ times a threefold integral from $-\infty$ to $+\infty$ over k_1, k_2 and k_3. At the same time we introduce the convergence factor $e^{-\gamma k}$. We obtain

$$\Delta_s E=\frac{2}{\pi^2}\int_{-\infty}^{+\infty}\!\!\int\!\!\int dk_1 dk_2 dk_3 \sum_n \frac{k_n e^{-\gamma k}}{k+k_n}\Big\{|q_{0;\,n}{}^x|^2\Big(1-\frac{k_1{}^2}{k^2}\Big)\cos^2 k_1 x\sin^2 k_2 y\sin^2 k_3 z + |q_{0;\,n}{}^y|^2\Big(1-\frac{k_2{}^2}{k^2}\Big)\sin^2 k_1 x\cos^2 k_2 y\sin^2 k_3 z + |q_{0;\,n}{}^z|^2\Big(1-\frac{k_3{}^2}{k^2}\Big)\sin^2 k_1 x\sin^2 k_2 y\cos^2 k_3 z\Big\}. \quad (15)$$

We assume that the distance of the atom from the walls $y=0$ and $z=0$ is very large so that the value of the integral does not change if we put $\sin^2 k_2 y$, $\cos^2 k_2 y$, $\sin^2 k_3 z$, and $\cos^2 k_3 z$ equal to $\frac{1}{2}$. When the distance from the wall $x=0$ is also very large, the same may be done with $\sin^2 k_1 x$ and $\cos^2 k_1 x$. For the difference between the perturbation energies in the case in which the atom is situated at a distance R from the wall $x=0$ and in the case in which the atom is at a large distance, we find, therefore:

$$\Delta_s E=\frac{1}{4\pi^2}\sum_n\int_{-\infty}^{+\infty}\!\!\int\!\!\int dk_1 dk_2 dk_3 \frac{k_n e^{-\gamma k}}{k+k_n}\Big\{|q_{0;\,n}{}^x|^2\Big(1-\frac{k_1{}^2}{k^2}\Big)(2\cos^2 k_1 R-1) + |q_{0;\,n}{}^y|^2\Big(1-\frac{k_2{}^2}{k^2}\Big)(2\sin^2 k_1 R-1)+|q_{0;\,n}{}^z|^2\Big(1-\frac{k_3{}^2}{k^2}\Big)(2\sin^2 k_1 R-1)\Big\}. \quad (16)$$

Introducing polar coordinates in the **k** space we obtain:

$$\Delta_d E=\sum_n \int_0^\infty -dk\left[\frac{e^{-\gamma k}}{2\pi i}\frac{k^2 k_n}{(k+k_n)}\left\{|q_{0;\,n}{}^x|^2\frac{e^{2ikR}}{2kR}\left(\frac{2i}{2kR}-\frac{2}{4k^2R^2}\right)\right.\right.$$
$$\left.\left.+(|q_{0;\,n}{}^y|^2+|q_{0;\,n}{}^z|^2)\frac{e^{2ikR}}{2kR}\left(1+\frac{i}{2kR}-\frac{1}{4k^2R^2}\right)\right\}+\text{complex conjugate}\right]. \quad (17)$$

It is interesting to remark that the expression in { } suggests the existence of an interpretation of formula (17) on the basis of the correspondence principle. If multiplied by a factor k^3, the first term in the expression equals the energy of a complex dipole $q^x e^{-ikct}$ in the retarded electric field of a dipole $q^x e^{ikct}$ at a distance $2R$, and this second dipole might be interpreted as the "electrical image" of the complex conjugate of the first dipole, with regard to a perfectly conducting plane at a distance R from the first dipole. A similar interpretation can be given to the second term in { }, but we have not been able to find a general consideration, based on the correspondence idea, by means of which at least the form of Eq. (17) could be foretold. In this connection we should like to point out that in dealing with the behavior of an atom in an excited state we usually meet with a factor $1/(k-k_n)$ instead of the factor $1/(k+k_n)$ occurring here, and the result is mainly determined by the residue at $k=k_n$ so that one definite frequency is singled out and an interpretation in terms of oscillators with well-determined frequencies becomes possible.

We now proceed with the calculation of the energy of interaction between an atom and a conducting wall by taking into consideration the electrostatic interaction. The electrostatic energy between a dipole q^x at $x=R$ and a conducting wall at $x=0$ is

$$\epsilon_x{}^e=-(q^x)^2/8R^3. \quad (18)$$

For a dipole q^y or q^z the energy is:

$$\epsilon_{y,z}{}^e=-(q^{y,z})^2/16R^3. \quad (19)$$

The first-order perturbation energy of the lowest level of our system due to the electrostatic terms is:

$$\Delta_e E=-\left[\frac{2((q^x)^2)_{00}+((q^y)^2+(q^z)^2)_{00}}{16R^3}\right]$$
$$=-\frac{\sum_n(2|q_{0;\,n}{}^x|^2+|q_{0;\,n}{}^y|^2+|q_{0;\,n}{}^z|^2)}{16R^3}. \quad (20)$$

The total interaction energy between the atom and the wall is

$$\Delta_t E=\Delta_d E+\Delta_e E. \quad (21)$$

A closer examination of $\Delta_d E$ shows that the integrand in (17) remains finite at $k=0$, but that both the term within [ ] that is completely written out and its complex conjugate have a simple pole. We shall integrate each of these terms separately from ϵ to ∞ and let ϵ tend to zero afterwards. We now want to replace the integration along the real axis by the integration along path 1 in Fig. 1 for the first integral and along path 2 for the second. In the limit $\epsilon\to 0$, we easily find for the integration on the semicircle:

$$\frac{1}{16R^3}\sum_n(2|q_{0.\,n}{}^x|^2+|q_{0;\,n}{}^y|^2+|q_{0;\,n}{}^z|^2),$$

which exactly cancels the term $\Delta_e E$ in $\Delta_t E$. Introducing the variable $u=-ik$ for the integration from $i\epsilon$ to $i\infty$ and $u=ik$ for the integration from $-i\epsilon$ to $-i\infty$, we find

$$\Delta_t E=-\frac{1}{\pi}\sum_n\int_0^\infty \frac{k_n u^2 du}{u^2+k_n{}^2}\frac{e^{-2uR}}{2R}$$
$$\times\left\{2|q_{0;\,n}{}^x|^2\left(\frac{1}{2uR}+\frac{1}{4u^2R^2}\right)\right.$$
$$\left.+(|q_{0;\,n}{}^y|^2+|q_{0;\,n}{}^x|^2)\left(1+\frac{1}{2uR}+\frac{1}{4u^2R^2}\right)\right\}. \quad (22)$$

In the limit of very small distances R, it is

easily found that the formula reduces to

$$\Delta_t E(R\to 0) = -\frac{1}{16R^3}\sum_n (2|q_{0;n}{}^x|^2+|q_{0;n}{}^y|^2+|q_{0;n}{}^z|^2), \quad (23)$$

being equal to the value of the London energy, derived by the elementary theory which takes into account the electrostatic interaction only. For very large R (R larger than all $\lambda_n=2\pi/k_n$) it is immediately seen that (22) reduces to

$$\Delta_t E(R\to\infty) = -\sum_n \frac{(|q_{0;n}{}^x|^2+|q_{0;n}{}^y|^2+|q_{0;n}{}^z|^2)}{4\pi k_n R^4}, \quad (24)$$

which can be written in terms of the static polarizability α of the atom:

$$\Delta_t E(R\to\infty) = -\frac{\hbar c}{8\pi R^4}(\alpha_x+\alpha_y+\alpha_z). \quad (25)$$

Because we wanted to see more clearly the role of the x, y, and z dipoles individually, we have not yet used the relation

$$\sum|q_{0;n}{}^x|^2=\sum|q_{0;n}{}^y|^2=\sum|q_{0;n}{}^z|^2=|q_{0;n}|^2, \quad (26)$$

where the summation extends over the three states with $J=1$, belonging to one degenerate level, which will be indicated from now by one symbol n. With the aid of this relation, Eq. (22) may be written as

$$\Delta_t E = -\frac{2}{\pi}\sum_n \int_0^\infty \frac{k_n u^2 du}{u^2+k_n{}^2}\frac{e^{-2uR}}{2R} \times |q_{0;n}|^2\left(1+\frac{2}{2uR}+\frac{2}{4u^2R^2}\right), \quad (27)$$

where each term of the sum over n represents the contribution of all three states with $J=1$ belonging to one degenerate level. In Fig. 2 we have given the result of a numerical calculation of the factor $\Delta_t E/\Delta_e E$ for the case in which only one excited level n (with $E_n=hc/\lambda_n$) gives a contribution to the London energy. It is seen that the value of the factor decreases monotonically with increasing R. It starts with the value 1 (for $R\to 0$), while for large R it is approximately equal to $3\lambda_n/2\pi^2 R$.

PART II. THE INTERACTION BETWEEN TWO ATOMS

1. Outline of Method

The energy of interaction between two neutral atoms will be determined by solving the following perturbation problem. The unperturbed states of the system, consisting of two atoms and the radiation field, will be assumed to be the states which are completely defined by the indication of the states of the two atoms and the state of the radiation field in empty space.

The perturbation operator, which is responsible for the interaction of the two atoms, contains the electrostatic interaction Q between the charged particles of the first atom with those of the second atom, the interaction G_A between the first atom and the radiation field, and the interaction G_B between the second atom and the radiation field.

With the aid of the perturbation operator G_A+G_B+Q we shall determine the energy perturbation; we have already remarked in Part I that the approximation has to be pushed to the fourth power of the electronic charge e. For this purpose we shall apply first-, second-, third-, and fourth-order perturbation theory. By the order of the perturbation theory we mean the degree in which the perturbation operator occurs in the expression for the energy perturbation. It does not indicate the power of the electronic charge occurring in this expression, as the perturbation operator contains terms with e as well as with e^2. The total result of the calculation will be divergent, but, as in Part I, we shall find a finite value for those terms that depend on the distance R between the two atoms; this value will be interpreted again as the total energy of interaction between the atoms.

In order to carry out the perturbation procedure we shall have to examine carefully the matrix elements occurring in the expression for the first-, second-, third-, and fourth-order perturbation in the energy. The examination does not give rise to special difficulties and, therefore, we shall only mention the results. Restricting outselves to those terms in the energy perturbation which depend on R and which are proportional to e^m, with $m\leqslant 4$, we find that in our problem there is no first-order perturbation in

the energy. Further, matrix elements of Q occur only in the expression for the second-order perturbation in the energy, namely, as the products of two matrix elements of Q, and in the third-order perturbation in the energy, namely, as the products of one matrix element of Q, one matrix element of G_A, and one matrix element of G_B. All the other terms in the energy perturbations do not involve Q.

We have thus to deal with the following terms:

(a) Terms obtained by applying second-order perturbation theory with the electrostatic interaction, which itself is proportional to e^2. The result is proportional to e^4 and is equal to the usual expression for the London energy.

(b) Terms obtained by applying third-order perturbation theory, restricting ourselves to the terms involving Q. We shall carry out the perturbation procedure in a somewhat unconventional way by successively applying first-order perturbation theory for the electrostatic interaction and second-order perturbation theory for the interaction with the radiation field: We calculate to the first order of the perturbation (which is an approximation proportional to e^2) the wave functions of the two atoms coupled by electrostatic interaction, and we then proceed to calculate, in exactly the same way as in the first part of this paper, the second-order interaction energy of this compound system with the radiation field. Again the result is proportional to e^4.

(c) Terms obtained by determining the energy perturbation with the aid of the operator G_A+G_B, the electrostatic interaction now being omitted. Again we shall solve this perturbation problem in a somewhat unconventional way: We first calculate in the usual way the second-order interaction energy of the atom A with a radiation field. In this way we obtain also the interaction between the two atoms if for the vector-potential we do not use the matrix representations corresponding to the electromagnetic field in empty space, but the matrices corresponding to a regular solution for the system, consisting of atom B and the radiation field. It is obviously sufficient to know these matrix elements of the vector potential correctly to the order of approximation e^2. The vector potential satisfies Maxwell's equations also in quantum electrodynamics and the terms with e^2 in the vector potential can be derived, therefore, by means of classical formulae from the expression for the current involving first powers of e. This method is often referred to as Heisenberg's method.[5] The resulting energy perturbation is again proportional to e^4.

It may be remarked that the terms (b) and (c) can also be calculated by systematically writing down all the products of matrix elements occurring in the expressions for the second-, third-, and fourth-order perturbation in the energy. We have carried out this systematic calculation and found the result to be in agreement with the results derived in this paper.

In the following sections we shall first restate briefly the field theory and verify Heisenberg's method for the case of a single atom. This will also teach us in which way the singularities in the solution of the perturbation equations are to be avoided. In a subsequent section (Section 4) we calculate the terms mentioned under (a) and (b). The terms under (c) will be determined in Section 5, and the final result is discussed in Section 6.

Since the perturbation procedure involves a number of rather lengthy calculations, we do not want to go into the details but shall only mention the most important steps and give the results.

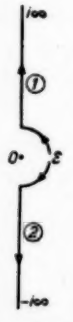

FIG. 1. Path of integration for the integral in (17).

2. The Radiation Field

We want to carry out the quantization of the radiation field by means of traveling waves, from which we demand periodicity in the x, y, and z directions with a period L. Using the

[5] W. Heisenberg, Ann. d. Physik (5) 9, 338 (1931).

notation of Section I2, we write for the vector potential

$$\mathbf{A}=\sum_{k,\lambda} cC_k\mathbf{e}(\mathbf{k},\lambda) \times\{A_{k,\lambda}e^{-i(\omega t-\mathbf{kr})}+A_{k,\lambda}^{\dagger}e^{i(\omega t-\mathbf{kr})}\}, \quad (28)$$

where the values of the components of the wave vector $\mathbf{k}$ are restricted to $k_i=2\pi n_i/L$; with $n_i=0, \pm1, \pm2, \cdots$. For some details of the calculations of the following sections it is suitable to assume $\mathbf{e}(\mathbf{k},\lambda)=\mathbf{e}(-\mathbf{k},\lambda)$. The value of the normalization factor C_k,

$$C_k=(2\pi\hbar/\omega L^3)^{\frac{1}{2}}, \quad (29)$$

can easily be verified by determining the energy of the field. In the following work we only need the matrix element of A or $A\dagger$ between the zero state of the field, $\psi(0, 0\cdots)$, and the state in which one light quantum is present, $\psi(0, 0\cdots 1_{k\lambda}\cdots)$:

$$\int\psi^*(0, 0\cdots)A_{k\lambda}\psi(0, 0\cdot 1_{k\lambda}\cdot)=1. \quad (30)$$

We shall always assume that L is very large so that a summation over all values of $\mathbf{k}$ can be replaced by $L^3/8\pi^3$ times an integration over all values of $\mathbf{k}$.

We want to remark that the vector potential $\mathbf{A}$ satisfies $\mathrm{div}\mathbf{A}=0$. For the interest of the next section we now write down the classical expression for the retarded vector potential satisfying the same condition and belonging to a periodic current $I=I_0\exp(ikct)$ inside an atom. Neglecting the dimensions of the atom as being small in comparison with R, it is easy to derive from Maxwell's equations that

$$A_x^{(\mathrm{ret})}=\frac{I_x}{c}\left[\frac{e^{-ikR}}{R}\left(-\frac{2}{ikR}+\frac{2}{k^2R^2}\right)-\frac{2}{k^2R^3}\right],$$

$$A_{z,y}^{(\mathrm{ret})}=\frac{I_{z,y}}{c}\left[\frac{e^{-ikR}}{R}\left(1+\frac{1}{ikR}-\frac{1}{k^2R^2}\right)+\frac{1}{k^2R^3}\right], \quad (31)$$

where for the sake of simplicity, we assumed $\mathbf{R}$ to point in the direction of the positive z axis. We shall use this formula also in Section 5.

3. Heisenberg's Method

The fundamental idea of Heisenberg's method is that even when the quantities of the electromagnetic field are considered as matrices, they satisfy Maxwell's equations. When we regard the elementary charge, e, as the perturbation parameter in the perturbation problem arising from the interaction, G, of the charged particles with the radiation field, it follows that, in order to determine the matrix elements of a field quantity to the order of approximation e^a, it is sufficient to know the matrix elements of the electric current to the order e^{a-1}.* In this section we shall give an illustration of Heisenberg's method by discussing the matrix element of the vector potential $(m;00\cdots|A|0;000\cdots)$ when one neutral atom is present in the radiation field. In the notation of the two states the first number indicates the level of the atom and the following numbers denote the number of quanta with different $(\mathbf{k}\lambda)$ in the radiation field. We shall first give a direct calculation of the matrix element in first approximation, and afterwards we shall verify that the result can be obtained with the aid of Maxwell's equations from the matrix element of the current in the zero approximation.

In the following calculation we assume that the atom is situated at $x=y=z=0$. The dimensions of the atom are assumed to be very small in comparison with the distance R at which we want to know the vector potential. We also neglect the variation of the electromagnetic field within the atom. The last approximation gives rise to divergencies of the type discussed in Section I2, but they can always be removed by introducing a factor $\exp(-\gamma|k|)$.

With the use of G as perturbation operator, we find for the first approximation of the zero state $\psi(0;00\cdots)$ of our system, consisting of the atom and the radiation field:

$$\psi'(0;0\cdots)=\psi(0;0\cdots) +\sum_{n,k,\lambda}\frac{eC_k}{mhc}\frac{(\mathbf{e}(\mathbf{k},\lambda)\mathbf{p}_{n;0})}{k_n+k}\psi(n;0\cdots 1_{k\lambda}\cdots), \quad (32)$$

* *Note added in proof.* This statement may be misleading. What is meant is, that since the current operator always contains one factor e explicitly, the matrix element multiplying this factor has only to be known to the order e^{a-1}.

and for the excited states we are interested in:

$$\psi'(n;00\cdots)=\psi(n;00\cdots)$$

$$+\sum_{k,\lambda}\frac{eC_k}{m\hbar c}\frac{(\mathbf{e}(k,\lambda)\mathbf{p}_{0;n})}{k-k_n}\psi(0;0\cdots 1_{k\lambda})+\cdots, \quad (33)$$

$$\psi'(0;0\cdots 1_{k\lambda}\cdots)=\psi(0;0\cdots 1_{k\lambda}\cdots)$$

$$+\sum_{n}\frac{eC_k}{m\hbar c}\frac{(\mathbf{e}(\mathbf{k},\lambda)\mathbf{p}_{n;0})}{k_n-k}\psi(n;00\cdots)+\cdots. \quad (34)$$

In the last two formulae we have omitted a number of terms which we shall not need in the following calculations. The matrix element of the vector potential **A** in first approximation is now easily found with the aid of (32) and (33).

$$(m;0\cdots|\mathbf{A}|0;0\cdots)=\sum_{k,\lambda}\frac{eC_k^2}{m\hbar}\mathbf{e}(\mathbf{k},\lambda)(\mathbf{e}(\mathbf{k},\lambda)\mathbf{p}_{m;0})$$

$$\times\left\{\frac{e^{i\mathbf{kr}}}{k_m+k}-\frac{e^{-i\mathbf{kr}}}{k_m-k}\right\}. \quad (35)$$

After a small calculation we find for the z component of **A** at the point **r**, given by $x=y=0$, $z=R$:

$$(m;0\cdots|A_z|0;0\cdots)=-\frac{ep_{m;0}{}^{(z)}}{2\pi mc}$$

$$\times\int_{-\infty}^{+\infty}\frac{dk}{k_m-k}\left\{\frac{e^{ikR}}{iR}\left(-\frac{2i}{kR}+\frac{2}{k^2R^2}\right)\right.$$

$$\left.+\text{complex conjugate}\right\}\exp(-\gamma|k|), \quad (36)$$

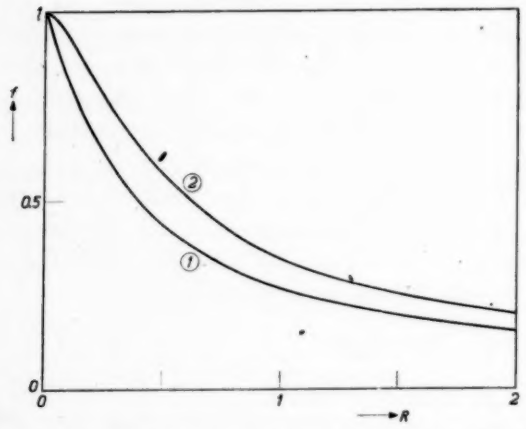

FIG. 2. Correction factor due to retardation for the contribution of one excited state to the usual London energy. (1) For the interaction between a neutral atom and a metallic wall. R is measured in units $\frac{1}{2}\lambda_n$. (2) For the interaction between two neutral atoms. R is measured in units λ_1.

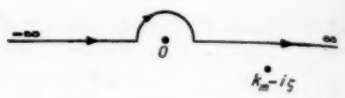

FIG. 3. Path of integration for the integral in (36).

in which formula we have introduced again the factor $\exp(-\gamma|k|)$.

The integrand is regular at $k=0$, but has a simple pole at $k=k_m$. In order to see in which way this singularity must be avoided, we remark that finally we want to obtain a retarded expression for the vector potential, i.e., an expression in which the terms with $\exp(ikR)$ do not occur. (The time factor of our matrix element is $\exp(ik_mct)$, thus retarded expressions will contain a factor $\exp(-ik_mR)$.) For this purpose we write $k_m-i\zeta-k$ instead of k_m-k in the denominator, by means of which the singularity is now fixed at a small distance ζ below the real axis of the complex k plane. It will turn out that this procedure gives the desired retarded expression in the final result. For the integration from $-\infty$ to $+\infty$ we take the path illustrated in Fig. 3. We carry out the integration of the terms with $\exp(ikR)$ and $\exp(-ikR)$ separately. The integral of the terms first mentioned can be replaced by an integral over a closed contour with the aid of a large semicircle above the real axis, and since there are no singularities within this contour, the value of the integral is zero. The integral with the other terms can be replaced by an integral over a closed contour with the aid of a large semicircle below the real axis. Within this contour there are two singularities for the terms with $\exp(-ikR)$, one at $k=k_m-i\zeta$ and one at $k=0$. The residues at these points determine the value of the integral, which is now easily found to be

$$(m;0\cdots|A_z|0;0\cdots)=$$

$$\frac{ep_{m;0}{}^{z}}{mc}\left[\frac{e^{-ik_mR}}{R}\left(-\frac{2}{ik_mR}+\frac{2}{k_m{}^2R^2}\right)-\frac{2}{k_m{}^2R^3}\right]. \quad (37)$$

With the foregoing calculation we have obtained the matrix elements of the vector potential in first approximation. The operation of the current is given by

$$I=\sum_j\frac{e}{m}\left(\mathbf{p}_j-\frac{e}{c}\mathbf{A}\right),$$

and, therefore, $ep_{m;0}{}^{i}/m$ are the corresponding matrix elements of the current in the zero approximation. It is seen, by comparing (37) with (31), that the matrix elements of the vector potential in first approximation could have been obtained immediately from the matrix elements of the current in the zero approximation.

In Section I12 we have explicitly restricted ourselves to retarded solutions of Maxwell's equations. The restriction to retarded solutions is also implied in the calculation of this section, namely, by the way in which the singularity at $k=k_m$ is avoided. It was found to be adequate to write $k_m-i\zeta$ instead of k_m in the denominator of (36), and as the complex conjugate of the function $\psi(m;00\cdots)$ occurred in the matrix element of the vector potential, we have to write $k_n+i\zeta$ instead of k_n in the denominator of (33) in order to stay in the domain of retarded expressions.

In the course of the following sections we shall also use Eq. (34), and we shall have to determine in which way singularities arising form the denominator in (34) must be avoided. Remarking that the perturbed eigenfunctions can be obtained from the unperturbed functions by means of a unitary transformation, we conclude that in (34) k_n must be replaced by $k_n-i\zeta$.

4. Perturbation Terms Involving Electrostatic Interaction

The electrostatic interaction between two neutral atoms A and B is given by

$$Q=\frac{\mathbf{q}_A\mathbf{q}_B}{R^3}-\frac{3(\mathbf{q}_A\mathbf{R})(\mathbf{q}_B\mathbf{R})}{R^5}, \tag{38}$$

when we neglect higher powers of the ratio between the atomic dimensions and $\mathbf{R}$. We shall assume at once that the vector $\mathbf{R}$, pointing from atom B to atom A, is in the direction of the positive z axis and that atom B is situated at $x=y=z=0$. Further, we shall assume, as in Section I2, that each of the two atoms has a state with $J=0$ as zero state. The second-order perturbation energy is now easily found to be

$$\Delta_2 E=-\frac{1}{R^6}\sum_{l,m}\frac{(q_l{}^x q_m{}^x)^2+(q_l{}^y q_m{}^y)^2+4(q_l{}^z q_m{}^z)^2}{\hbar c(k_l+k_m)}. \tag{39}$$

In this notation the indices l and m denote the states with $J=1$ of the atoms A and B, respectively; $q_l{}^i$ is the matrix element of the total dipole moment between the zero state of atom A and the state l of this atom. The matrix elements are assumed to be real, which can be done without loss of generality. It is obvious that the symbols A and B can be omitted in this notation without giving rise to confusion. As in Section I2, we do not yet use relation (26). The expression (39), being the usual London energy between two neutral atoms, gives the terms mentioned under (a) in Section I11.

The calculation of the terms mentioned under (b) proceeds along the lines indicated in the outline of method. In the calculation we restrict ourselves to the terms which give a contribution proportional to the fourth power, or to a smaller power, of the electronic charge to the final result. The result will be divergent, but we determine the difference between the energy perturbation in the case of a distance R between the two atoms and the case of a very large distance; this difference will be finite.

The calculations are rather elaborate but do not give rise to special difficulties. Taking into consideration that for the zero states of the atoms $I=0$, we find finally:

$$\Delta_3 E=+\frac{2}{R^6}\frac{(q_l{}^x q_m{}^x)^2+(q_l{}^y q_m{}^y)^2+4(q_l{}^z q_m{}^z)^2}{\hbar c(k_l+k_m)}-\frac{4}{\pi\hbar c R^4}\sum_{l,m}\int_0^\infty\frac{k_l k_m u^2\,du}{(k_l{}^2+u^2)(k_m{}^2+u^2)}$$
$$\times\left\{((q_l{}^x q_m{}^x)^2+(q_l{}^y q_m{}^y)^2)e^{-uR}\left(1+\frac{1}{uR}+\frac{1}{u^2R^2}\right)+4(q_l{}^z q_m{}^z)^2 e^{-uR}\left(\frac{1}{uR}+\frac{1}{u^2R^2}\right)\right\}. \tag{40}$$

In the course of the calculations the two terms in (40) were obtained by means of the same procedure of complex integration as was applied to Eq. (17) in Section I2.

5. The Terms Not Involving the Electrostatic Interaction

So far we have carried out our perturbation procedures in an entirely symmetrical way with respect to the atoms A and B. In this section it is our aim to determine the terms mentioned under (c) in the outline of method. We have to solve a perturbation problem in which $G_A+G_B=G$ is the perturbation operator:

$$G=\sum_{i_A}\left\{-\frac{e}{mc}(\mathbf{p}_{iA}\mathbf{A}_A)+\frac{e^2}{2mc^2}A_A{}^2\right\}+\sum_{i_B}\left\{-\frac{e}{mc}(\mathbf{p}_{iB}\mathbf{A}_B)+\frac{e^2}{2mc^2}A_B{}^2\right\}. \quad (41)$$

Now we have to take recourse to an unsymmetrical attack on the situation. The reason is the following. We have already remarked several times that, in consequence of the form of the operator of the interaction between the charged particles and the radiation field, there is no first-order perturbation between an atom and the electromagnetic field that is proportional to e. The terms in G that are proportional to e only give rise to a second-order perturbation, while the terms with e^2 are responsible for the first-order perturbation. As we are interested only in terms with e^4 in the final expression for the energy perturbation, we now have the opportunity to solve our perturbation problem in two steps. First, we calculate the vector potential to the order of approximation e^2 in the system consisting of atom B+radiation field, and then proceed to determine the first- and second-order perturbation energy of the atom A in this perturbed electromagnetic field. This procedure is necessarily unsymmetric in the atoms A and B, but in the final stage of the calculation the asymmetry vanishes, as must be the case for any consistent treatment of our problem.

We label the states of the system (B+radiation field) with the index N. The energy perturbation of the atom A in the electromagnetic field of this system is now given by

$$\Delta_4E=\frac{1}{\hbar c}\sum_{l,N}\frac{k_Nk_l}{k_N+k_l}\sum_{x,y,z}|A_{0;N}{}^x(A)|^2|q_{0;l}{}^x|^2. \quad (42)$$

Here we have at once combined the first-order and the second-order perturbation in the same way as was done in Section 12. The index l denotes the states with $J=1$ of the atom A.

We want to know $|A_{0;N}{}^x|^2$ to the order of approximation e^2. There are two possibilities: either the matrix element $A_{N;0}{}^i$ vanishes in zeroth approximation, i.e., terms not containing the factor e do not occur in the matrix element, or the matrix element does not vanish in zeroth approximation. In the first case, we only need to know the matrix element to the order of approximation e. Matrix elements of this type that do not vanish in this approximation, are found only if the state N is one of the states with wave functions $\psi'(m;0,0\cdots)$. This statement immediately follows from Heisenberg's method, discussed in Section 3. In that section the matrix element $(m;00|A_i|0;00\cdots)$ has already been calculated, so that we can at once write down the contribution to (42) from this special series of states N:

$$\Delta_2E=\frac{1}{\hbar cR^2}\sum_{l,m}\frac{k_m{}^3k_l}{k_m+k_l}(q_l{}^xq_m{}^x)^2\times\left\{\left(1-\frac{1}{k_m{}^2R^2}+\frac{2}{k_m{}^4R^4}\right)+\left[\frac{e^{ik_mR}}{k_m{}^2R^2}\left(1+\frac{i}{k_mR}-\frac{1}{k_m{}^2R^2}\right)+\text{complex conjugate}\right]\right\}. \quad (43)$$

In order to simplify the formula we have not written down terms proportional to $(q_l{}^yq_m{}^y)^2$ and $(q_l{}^zq_m{}^z)^2$. We shall omit these terms in all formulas of this section. In the second case, where the matrix element of the vector potential contains terms independent of e, we must know the vector potential to the order of approximation e^3. This case is realized only if the state N is of the type $\psi'(0;00\cdots1_{k\lambda}\cdots)$. By Heisenberg's method it is easily seen that the corresponding matrix element of the vector potential contains no terms proportional to e, so that we can write

$$(0;0\cdots1_{k\lambda}\cdots|A_i|0;0\cdots0\cdots)=A_{k\lambda;0}{}^{(0)i}+A_{k\lambda;0}{}^{(2)i}. \quad (44)$$

When we insert these matrix elements in (42), we shall have to deal only with the cross products:

$$A_{0;\,k\lambda}{}^{(0)i}A_{k\lambda;\,0}{}^{(2)i}+A_{0;\,k\lambda}{}^{(2)i}A_{k\lambda;\,0}{}^{(0)i},$$

the other products being either independent of R or proportional to a too high power of e.

The vector potential in second approximation is calculated by means of Heisenberg's method with the aid of the current in first approximation:

$$I_{k\lambda;\,0}{}^{i}=\int\psi'^{*}(0;0\cdots 1_{k\lambda}\cdots)\times\left\{\sum_{jB}\frac{e}{m}\left(p_{jB}{}^{i}-\frac{e}{c}A_{B}{}^{i}\right)\right\}\psi'(0;0\cdots). \quad (45)$$

Here we use the wave functions given by (32) and (34), introducing at once the term $i\zeta$ in the denominator of (34). Collecting the terms with e^2 in (45) we find

$$I_{k\lambda;\,0}{}^{i}=\sum_{m}\frac{e^2C_k}{m^2\hbar c}|p_{m;\,0}{}^{i}|^2e_i(\mathbf{k}\lambda)\times\left(\frac{1}{k_m-k+i\zeta}+\frac{1}{k_m+k}\right)-\sum_{jB}\frac{e^2C_k}{m}e_i(\mathbf{k}\lambda), \quad (46)$$

and with the aid of (31) we find the matrix element $A_{k\lambda;0}{}^{(2)i}(A)$. The matrix element $A_{k\lambda;0}{}^{0i}$ is simply

$$A_{k\lambda;\,0}{}^{0i}(A)=cC_ke_i(\mathbf{k}\lambda)e^{-ik_zR}. \quad (47)$$

Applying the sum rule (10) to the last term in (46), we can now calculate the contribution to (42) arising from the states $\psi'(0;0\cdots 1_{k\lambda}\cdots)$.

The calculation leads to a rather complicated integral over k, and the integrand requires a careful examination at the points $k=0$ and $k=k_m$ before the integral can be evaluated by means of complex integration. The way in which the singularity at $k=k_m$ must be avoided is prescribed unambiguously, however, by a term $i\zeta$ occurring in a denominator which originates from the corresponding denominator with the term $i\zeta$ in Eq. (46). Therefore, a straightforward evaluation of the integral is possible. We find finally:

$$\Delta_BE=\sum(q_l{}^{x}q_m{}^{x})^2(B_1+B_2+B_3), \quad (48)$$

where

$$B_1=-\frac{1}{\hbar cR^2}\left[\frac{1}{k_mR^4}+\frac{k_m{}^3k_l}{k_m+k_l}\left(1-\frac{1}{k_m{}^2R^2}+\frac{1}{k_m{}^4R^4}\right)\right],$$

$$B_2=-\frac{1}{\hbar cR^4}e^{ik_mR}\left(1+\frac{i}{k_mR}-\frac{1}{k_m{}^2R^2}\right)\frac{k_mk_l}{k_m+k_l}+\text{complex conjugate},$$

$$B_3=\frac{4}{\pi\hbar c}\int_0^\infty\frac{k_lk_mu^2du}{(k_l{}^2+u^2)(k_m{}^2+u^2)}\times\frac{e^{-uR}}{R^4}\left(1+\frac{1}{uR}+\frac{1}{u^2R^2}\right)-\frac{2}{\pi\hbar c}\int_0^\infty\frac{k_lk_mu^4du}{(k_l{}^2+u^2)(k_m{}^2+u^2)}\times\frac{e^{-2uR}}{R^2}\left(1+\frac{1}{uR}+\frac{1}{u^2R^2}\right)^2.$$

6. Result and Discussion

We have now calculated all the terms that contribute to the energy of interaction Δ_LE of two neutral atoms in S states:

$$\Delta_LE=\Delta_qE+\Delta_3E+\Delta_\alpha E+\Delta_\beta E. \quad (49)$$

Fortunately a number of terms cancel, and the final result is comparatively simple. It may be remarked that this result has regained symmetry with respect to the atoms A and B. Adding at once the terms proportional to $(q_l{}^{y}q_m{}^{y})^2$ and $(q_l{}^{z}q_m{}^{z})^2$ we find:

$$\Delta_LE=-\frac{2}{\pi\hbar c}\sum_{l,m}\int_0^\infty\frac{k_lk_mu^4du}{(k_l{}^2+u^2)(k_m{}^2+u^2)}\frac{e^{-2uR}}{R^2}\times\left\{((q_l{}^{x}q_m{}^{x})^2+(q_l{}^{y}q_m{}^{y})^2)\left(1+\frac{1}{uR}+\frac{1}{u^2R^2}\right)^2+4(q_l{}^{z}q_m{}^{z})^2\left(\frac{1}{uR}+\frac{1}{u^2R^2}\right)^2\right\}. \quad (50)$$

In the limit of a very small distance R, $R\ll\lambda_l=2\pi/k_l$, $R\ll\lambda_m$ it is easily found that the formula reduces to:

$$\Delta_LE(R\to 0)=-\frac{1}{R^6}\sum_{l,m}\frac{(q_l{}^{x}q_m{}^{x})^2+(q_l{}^{y}q_m{}^{y})^2+4(q_l{}^{z}q_m{}^{z})^2}{\hbar c(k_l+k_m)}, \quad (51)$$

being equal to the value of the London energy as derived by the elementary theory, which takes into account the electrostatic interaction only. For very large R (R larger than all λ_l and λ_m) it is found, after a short calculation, that (50) reduces to:

$$\Delta_L E(R\to\infty) = -\frac{1}{2\pi\hbar c R^7} \times \sum_{l,m} \frac{13[(q_l^x q_m^x)^2+(q_l^y q_m^y)^2]+20(q_l^z q_m^z)^2}{k_l k_m}, \quad (52)$$

which can be written in terms of the static polarizability of the atoms:

$$\Delta_L E(R\to\infty) = -\frac{\hbar c}{8\pi R^7}\{13(\alpha_x(A)\alpha_x(B) + \alpha_y(A)\alpha_y(B)) + 20\alpha_z(A)\alpha_z(B)\}. \quad (53)$$

So far we have not yet used the relations

$$\sum|q_l^x|^2 = \sum|q_l^y|^2 = \sum|q_l^z|^2 = q_l^2, \quad \sum|q_m^x|^2 = \sum|q_m^y|^2 = \sum|q_m^z|^2 = q_m^2, \quad (54)$$

where the summation extends over the three states with $J=1$ belonging to one degenerate level, which will be indicated hereafter by one symbol l or m, respectively. With the aid of (54), Eq. (50) can now be written as:

$$\Delta_L E = -\frac{4}{\pi\hbar c}\sum_{l,m}\int_0^\infty \frac{k_l k_m u^4 du}{(k_l^2+u^2)(k_m^2+u^2)}(q_l q_m)^2 \times \frac{e^{-2uR}}{R^2}\left(1+\frac{2}{uR}+\frac{5}{u^2R^2}+\frac{6}{u^3R^3}+\frac{3}{u^4R^4}\right), \quad (55)$$

where each term of the sum over l, m represents the contribution from all three states with $J=1$ belonging to one degenerate level l together with all three states belonging to the level m.

Equation (53) may now be written

$$\Delta_L E(R\to\infty) = -\frac{23\hbar c}{4\pi R^7}\alpha(A)\alpha(B), \quad (56)$$

which is equal to

$$\Delta_L E(R\to\infty) = -\frac{23}{4\pi}\frac{\hbar c}{e^2}\cdot\frac{e^2}{R^7}\alpha(A)\alpha(B) \approx 251\frac{e^2}{R}\frac{\alpha(A)\alpha(B)}{R^6}. \quad (57)$$

In Fig. 2 we have given the result of a numerical calculation of the factor $\Delta_L E/\Delta_q E$ for the case in which the two atoms are identical and in which for both atoms only one excited state l (with $E_l=hc/\lambda_l$) gives a contribution to the London energy. The factor decreases monotonically with increasing R. It starts with the value 1 (for $R\to 0$) while for large R it is approximately equal to $23\lambda_l/6\pi^2 R$.

The very simple form of Eq. (56) and the analogous formula (25) suggest that it might be possible to derive these expressions, perhaps apart from the numerical factors, by more elementary considerations. This would be desirable since it would also give a more physical background to our result, a result which in our opinion is rather remarkable. So far we have not been able to find such a simple argument.

PHYSICAL REVIEW VOLUME 73, NUMBER 4 FEBRUARY 15, 1948

The Thermodynamics of Irreversible Processes. IV. The Theory of Elasticity and Anelasticity*

CARL ECKART
University of California, Marine Physical Laboratory, San Diego, California
(Received November 4, 1947)

The traditional theory of the solid state rests on two false assumptions. One is the principle of a constant relaxed (or standard) state. The other is the principle of relaxability-in-the-large, first formulated mathematically by de Saint-Venant. His equations are essentially identical with Riemann's equations expressing the condition that a geometry be Euclidean-in-the-large. It is shown that a principle of relaxability-in-the-small is sufficient for the geometry of strain—which then becomes a three-dimensional Riemannian geometry. The kinematics of strain is next developed without introducing the principle of a constant relaxed state.

The ground is thus cleared for the construction of a classical theory of anelasticity. It is first shown that the variability of the relaxed state makes the density of the substance independent of the strains. Consequently, the internal energy can depend on the specific volume as well as on the strains and the entropy. The expression for the rate of increase of entropy is then derived. As usual, this suggests, but does not uniquely determine the form of the dissipative laws. In addition to the usual equations for the viscous stresses, one is led to another set of equations involving parameters that quantitatively describe the anelastic properties of the substance.

These results are used to derive the equations for the waves of distortion and dilation in an ideal isotropic anelastic medium. When the two coefficients of viscosity and two coefficients of anelasticity all vanish, these reduce to the usual equations for such waves. In addition to the four dissipative coefficients, the isotropic anelastic substance is characterized by four elastic moduli, rather than by the two that characterize an isotropic elastic substance. Thus, there are eight parameters whose values can be adjusted to describe the particular substance. When the four dissipative parameters do not vanish, the propagation of the waves can be described by five relaxation times. The ideal isotropic anelastic substance thus has a relaxation spectrum of about the same complexity as those of actual substances.

The kinematic independence of the density and the strains causes a hydrostatic pressure to have different dynamic effects than a uniaxial pressure. This is in accord with experiment—the latter being much more effective in producing anelastic deformation than the former.

1. INTRODUCTION

THE phenomena of anelasticity have been known for centuries. They are the basis of the metallurgical and other plastic arts. Possibly this has caused them to be too familiar to be easily analyzed from a theoretical point of view. In any case, there is a marked disparity between the amount of thought that has been expended on the theory of elasticity and that expended on the theory of anelasticity. There is a tendency among theoretical physicists to excuse this by claiming that there have, as yet, been no critical experiments in the field of anelasticity. This is scarcely a valid claim, for the experimental literature of this subject is more extensive than that of atomic spectra, and some of the greatest experimenters have contributed to it.

It is the purpose of this paper to indicate that the classical theory of elasticity can be extended to include anelastic phenomena. To accomplish this, it must first be noted that the traditional theory rests on two false assumptions. It must then be shown that they can be eliminated without serious alteration of the concepts of the theory, and finally, the untenable assumptions must be replaced by definite laws of anelasticity whose consequences can be compared with experiment.

The first of the false assumptions may be called the principle of a constant relaxed state. It asserts that, if the strains of a solid object were to be completely relaxed at time t, the resulting state would be the same as if the strains had been relaxed at any other time t_0. While some substances, such as spring steel, conform to this principle within wide limits, it is in direct conflict with all that we know about ductility, malleability, etc. There is little doubt that it should be replaced by some law of a quantitative nature, such substances as spring steel being characterized by extreme values of

* This work represents one of the results of research carried out under contract with the Bureau of Ships, Navy Department.

the parameters, and such substances as copper, by moderate values.

The second false assumption may be called the principle of relaxability-in-the-large. It asserts that the strains in a solid object can be completely relaxed by removing all external forces. It is trite to remark that the strains in an optical blank cannot be relaxed in this way: it must be carefully annealed and aged. Such counter-examples could be multiplied indefinitely, but one suffices to show that this principle, also, is an unsuitable basis for a theory of the solid state.

The principle of relaxability-in-the-large has an interesting history. It apparently entered the theory as a tacit assumption and remained unrecognized, until in 1864, de Saint-Venant criticized Maxwell for ignoring it in the development of a general method for the solution of elastic problems.[1] The former gave a precise and general mathematical formulation of the principle, and it has been accepted as basic ever since. His work is very closely related to that of his contemporary, Riemann. In 1861, the latter published his work on differential geometries, i.e., geometries that are Euclidean-in-the-small. He also formulated the necessary and sufficient conditions which such a geometry must satisfy in order to be Euclidean-in-the-large. It is a remarkable fact that de Saint-Venant's conditions for relaxability-in-the-large are essentially identical with Riemann's geometrical conditions. This relationship has become fairly well known, and physicists have become accustomed to dealing with geometries that are only Euclidean-in-the-small. It does not appear to have occurred to anyone that, by postulating only relaxability-in-the-small, the ground is cleared for the construction of a theory of anelasticity.

In the following pages, a general theory of strain will be developed. It will first be shown that relaxability-in-the-small is sufficient for the discussion of its geometrical aspects. Next, the kinematics of strain will be developed without using the principle of a constant relaxed state. After these negative tasks have been completed, an attempt will be made to find positive laws of anelasticity. The only source of guidance in this phase of the work will be the second law of thermodynamics; since this is an inequality rather than an equality, the equations will not be uniquely determined. This is, in a sense, fortunate. For, if it should prove that the equations do not correspond with the facts, there is always the possibility of replacing them by other, more complicated, equations. Finally, equations for the propagation of waves of distortion and dilatation in an isotropic anelastic medium are derived. These reduce to the usual equations when four coefficients of dissipation vanish. When these do not vanish, the propagation of the waves can be described by means of five relaxation times. Thus, even the simplest ideal anelastic substance has a relaxation spectrum comparable in its complexity to those of actual substances.

[1] A. E. H. Love, *Mathematical Theory of Elasticity* (Dover Publications, New York, 1944), 4th edition, pp. 17, 49, 101.

2. THE RIEMANNIAN GEOMETRY OF STRAIN

Let P and Q be two neighboring points of a material object that is under strain. Two lengths are associated to these points: one is dl, the actual distance between them, and the other is $d\lambda$, the distance that would separate them if all strains in the small region surrounding PQ were relaxed. If dx_i are the cartesian components of the vector $P \rightarrow Q$, then[2]

$$(dl)^2 = \delta_{ij} dx_i dx_j, \tag{1}$$

$$(d\lambda)^2 = g_{ij} dx_i dx_j, \tag{2}$$

where

$$\delta_{ij} = 0 \quad \text{if} \quad i \neq j \quad \text{and} \quad \delta_{11} = \delta_{22} = \delta_{33} = 1, \tag{3}$$

is the Euclidean metric tensor, and g_{ij} is a tensor that specifies the state of strain at the point P. Since a real value of $d\lambda$ (greater than zero), must be associated to every distinct pair of

[2] The indices $i, j, \cdots$, have the values 1, 2, 3, and the summation convertion for pairs of identical indices will be followed. Since the coordinates are cartesian throughout, there will be no need to distinguish between covariant and contravariant components; consequently inferior indices will be used by preference although not exclusively. The use of superior indices is convenient for the designation of the reciprocal g-matrix: i.e., the matrix g^{ij} is defined by the equation

$$g^{ij} g_{jk} = \delta_{ik}.$$

More generally, if $a_i \cdots$ is any quantity, then

$$a^i \cdots = g^{ij} a_j \cdots.$$

This convention makes it possible to use all of the ordinary formulae for the Riemann-Christoffel symbols, etc., while preserving the convenience of writing $a^i b^i$ instead of $\delta_{ij} a^i b^j$.

points P, Q it follows that the symmetric tensor g_{ij} is positive definite.[3]

The question of a physical procedure for relaxing the strains in a given neighborhood immediately arises. For this purpose, it is not sufficient to relieve the object of all external forces: the various parts of the object may also be exerting forces on neighboring parts and thus causing "internal" strains to exist. Geometrically, there is no difference between internal strains and those produced by external forces. However, if a small bit of the matter surrounding P is cut out of the larger object, then all strains in this bit will be relaxed, since it will have no forces acting on it. There is no other general way of relaxing the strains at a point, although in special cases there may be simpler ways. Saint-Venant's problem was to characterize those cases in which the removal of the external forces is sufficient to relax all strains at every point of an extended object.

Let P, Q, Q', etc., be points in a dissected bit of matter; it will be necessary to compare their configuration before and after the strains have been relaxed. Unmodified words, such as "length," "angle," will always refer to the former state, and the adjective "relaxed" will be prefixed to corresponding words referring to the latter state. The coordinate differentials will always, however, be in the cartesian system associated to the state before the strains have been relaxed, unless explicitely stated otherwise.

With these understandings, let dx_i be the vector $P\rightarrow Q$ and $d'x_i$ the vector $P\rightarrow Q'$; their lengths and relaxed lengths will be given by Eqs. (1) and (2). Let a be the angle QPQ' and α the relaxed angle QPQ'; then it is clear that,

$$\cos a=(dx_i/dl)(d'x_i/d'l); \tag{4}$$

and it can be proven[4] that

$$\cos\alpha=g_{ij}(dx_i/d\lambda)(d'x_i/d'\lambda). \tag{5}$$

For this purpose note that the relaxed length, $d''\lambda$, of $Q\rightarrow Q'$ is given by

$$(d''\lambda)^2=g_{ij}(d'x_i-dx_i)(d'x_j-dx_j)$$
$$+\text{terms of third order.}$$

To second order, therefore, the Euclidean definition

$$\cos\alpha=\frac{(d''\lambda)^2-(d'\lambda)^2-(d\lambda)^2}{2d\lambda d'\lambda}$$

will be identical with Eq. (6). The neglect of the terms of third order is justified, since the formula is to be applied only "in the small."

Let $x_i=x_i(h)$ be any curve, Γ (not closing on itself), in the strained object. Then it is reasonable to suppose that, if a filament having Γ as axis could be cut out of the object, the strains in this filament would be completely relaxed. Let P and Q be points on Γ; then the length of this curve in the strained state will be

$$l=\int_P^Q\left(\frac{dx_i}{dh}\frac{dx_i}{dh}\right)^{\frac{1}{2}}dh, \tag{6}$$

and the relaxed length of the filament axis will be

$$\lambda=\int_P^Q\left(g_{ij}\frac{dx_i}{dh}\frac{dx_j}{dh}\right)^{\frac{1}{2}}dh. \tag{7}$$

One problem of the geometry of strains will be to determine the shape of the relaxed filament; the determination of its length is only one part of this problem.

Conversely, it may be required to determine the curve Γ so that the axis of the relaxed filament will have a given shape. If this is to be a straight line, the solution is simple: Γ must be a geodesic of the strain metric g_{ij}; such a filament will therefore be called a geodesic filament. The proof follows: let P and Q be two points on the axis of a geodesic filament, and P', Q' two points in the neighborhood of P and Q such that $Q\rightarrow Q'=d''x_i$ and $P\rightarrow P'=d'x_i$, while the relaxed angles α' and α'' (see Fig. 1) are both $\pi/2$. The relaxed length of the axis between P and Q will be given by Eq. (8). Let Γ be any curve joining P' to Q', provided only that it is everywhere close to the axis; its length will be[5] $\lambda+\delta\lambda$, where

[3] L. P. Eisenhart, *Riemannian Geometry* (Princeton University Press, Princeton, New Jersey, 1926), p. 23.

[4] Reference 3, p. 38.

[5] The proof follows readily from a slight modification of that given in *RG*, pp. 48–49. It is only necessary to replace Eq. (17.1) by $\epsilon\omega^i=d'x_i$ for $h=h_P$, and $\epsilon\omega^i=d''x_i$ for $h=h_Q$. On integrating Eq. (17.4) by parts and using Eq. (17.5), the equation in the text is obtained in a slightly different notation.

$$\delta\lambda=\left(g_{ij}\frac{dx_i}{d\lambda}\right)_Q d''x_j-\left(g_{ij}\frac{dx_i}{d\lambda}\right)_P d'x_i$$
$$+\text{terms of second order},$$
$$=d''\lambda\cos\alpha''-d'\lambda\cos\alpha'+\cdots,$$
$$=0+\cdots. \tag{8}$$

Hence the relaxed distance between any pair of points in the two cross sections perpendicular to the relaxed axis at P and Q is the same, to first order. This, however, is the condition that the planes of the two sections be parallel after relaxation. Since P and Q are arbitrary points on the axis, it follows that the latter must be a straight line.

The more general problem of determining the relaxed shape of an arbitrary filament will not be discussed, although the assumptions underlying the preceding discussion are presumably adequate for its treatment. Of greater interest is the remark that, if Γ is a closed (rather than an open) curve, and a closed filament be cut from the object with Γ as axis, the strains in the filament will not always be completely released. To prove this, consider a curvilinear triangle PQR in the object, whose sides are geodesics. Let this be the closed curve Γ, and cut a filament from the object with this as axis (see Fig. 2). If the strains in the filament were completely relaxed, its axis would become a plane triangle, and hence the sum of the angles at P, Q and R would be π. However, Eq. (5) affords the means of calculating these angles, and their sum will usually not be π, so that the triangle must be curvilinear, and the strains only partially relaxed. If one side of the filamentary triangle be cut, further relaxation will occur, and it will assume some such form as Fig. 3.

In general, the relaxation of the strains in thin sheets cut from the object will therefore also be incomplete. For, we may consider the above

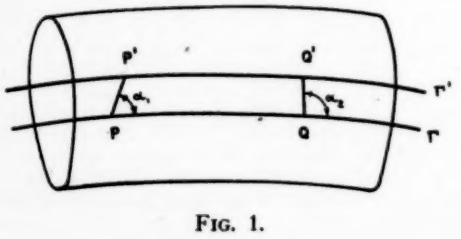

FIG. 1.

triangular filament to have been prepared by first cutting a thin sheet from the object, and then cutting out the triangle. Since each new cut will cause some further relaxation, the conclusion follows.

Finally, we may return to de Saint-Venant's problem, and consider the condition that the strains in an object may be completely relaxed by merely removing the external forces, without making any cuts. Let x_i be the cartesian coordinates of a point, P, in the object before relaxation and y_i those of P after relaxation. They will be related by equations of the form $y_i=f_i(x_1x_2x_3)$ and since points that were distinct but neighboring before relaxation will be so afterwards, the Jacobian of this transformation will not vanish. Moreover, the functions will be single-valued throughout the interior of the object. In terms of the dy_i, the relaxed distance between two neighboring points will be given by the Euclidean metric:

$$(d\lambda)^2=\delta_{ij}dy_idy_j, \tag{9}$$

while Eq. (2) will still hold for $d\lambda$ in terms of the dx_i. The conditions that must be satisfied by the g_{ij}, in order that the functions f_i shall exist, were investigated by Riemann[6] as has been remarked above. The necessary and sufficient condition is the vanishing of the Riemann tensor formed from the g_{ij} and their derivatives with respect to the x_i. If the interior of the object is a simply-connected region, this condition is also sufficient for the complete relaxation of the strains. If the interior is multiply connected, it will, in addition, usually be necessary to cut the object along a sufficient number of surfaces to make it simply connected, before the strains can relax completely. The theory of such cuts has also been developed by Riemann. The filamentary triangles discussed above are a primitive example of the difference between simply and multiply connected regions.

Riemann's condition is thus the vanishing of complicated functions of the g_{ij}. If the strains are small, one may write

$$g_{ij}=\delta_{ij}-2\sigma_{ij}, \tag{10}$$

and neglect the squares and products of σ_{ij} and its derivatives. Riemann's fourth-order tensor

[6] Reference 3, pp. 23–25.

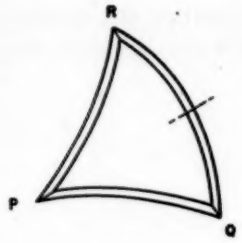

FIG. 2.

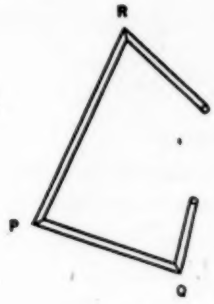

FIG. 3.

then simplifies to the approximate form

$$-R_{lijk}=\frac{\partial^2\sigma_{kl}}{\partial x_i\partial x_j}+\frac{\partial^2\sigma_{ij}}{\partial x_k\partial x_l}-\frac{\partial^2\sigma_{ik}}{\partial x_l\partial x_j}-\frac{\partial^2\sigma_{lj}}{\partial x_i\partial x_k}. \quad (11)$$

Since each of the four indices can take on any of three values, there are 81 components R_{lijk}. However, many of them are equal, especially because $\sigma_{ij}=\sigma_{ji}$, and others vanish identically. The distinct non-vanishing components are six in number and can be obtained from

$$-R_{1231}=\frac{\partial^2\sigma_{11}}{\partial x_2\partial x_3}-\frac{\partial}{\partial x_1}\left\{\frac{\partial\sigma_{21}}{\partial x_3}+\frac{\partial\sigma_{31}}{\partial x_2}-\frac{\partial\sigma_{23}}{\partial x_1}\right\}, \quad (12.1)$$

$$-R_{1221}=\frac{\partial}{\partial x_1}\left(\frac{\partial\sigma_{22}}{\partial x_1}-\frac{\partial\sigma_{12}}{\partial x_2}\right)+\frac{\partial}{\partial x_2}\left(\frac{\partial\sigma_{11}}{\partial x_2}-\frac{\partial\sigma_{12}}{\partial x_1}\right), \quad (12.2)$$

by the cyclic permutation of 1, 2, 3. Except for a difference in notation, de Saint-Venant's equations are $R_{lijk}=0$.[1]

The rejection of the principle of relaxability-in-the-large permits the above six components of R_{lijk} to have any values whatever. However, this negative action is not sufficient for the construction of a complete theory of anelasticity. The six equations must be replaced by others, otherwise most problems will not have a unique solution. This is the valid portion of de Saint-Venant's criticism of Maxwell's work in this field.

3. THE KINEMATICS OF STRAIN

Thus far, only the momentary state of an object has been considered, and the relaxation of its strains has been supposed to be accomplished by an idealized destructive process. Actually, the changes in the state of strain of an object are very often accompanied by motions that leave its integrity unimpaired; obviously, exceptions to this rule do occur (rupture, fracture) but they will not be considered here.

Let $u_i(x_1x_2x_3t)$ be the velocity of the matter that at time t occupies the point $P=x_i$; the velocity, at time t and at $Q=x_i+dx_i$ will be

$$u_i+\frac{\partial u_i}{\partial x_j}dx_j.$$

The relative velocity of the points P and Q will thus cause the vector $P\rightarrow Q$ to change; the rate of its change will be (to first order)

$$\frac{Ddx_i}{Dt}=\frac{\partial u_i}{\partial x_j}dx_j \quad (13)$$

and its length will change according to the formula

$$\frac{D(dl)^2}{Dt}=\left(\frac{\partial u_i}{\partial x_j}+\frac{\partial u_j}{\partial x_i}\right)dx_idx_j$$

$$=2u_{(ij)}dx_idx_j, \quad (14)$$

where

$$u_{(ij)}=\tfrac{1}{2}\left(\frac{\partial u_i}{\partial x_j}+\frac{\partial u_j}{\partial x_i}\right). \quad (15)$$

Such changes in the distance separating neighboring points are called deformations: hence $u_{(ij)}$ may be called the deformation tensor. The corresponding anti-symmetric tensor is the vorticity:

$$u_{[ij]}=\tfrac{1}{2}\left(\frac{\partial u_i}{\partial x_j}-\frac{\partial u_j}{\partial x_i}\right); \quad (16)$$

the identities

$$\frac{\partial u_i}{\partial x_j}=u_{(ij)}+u_{[ij]} \quad (17)$$

and

$$\frac{\partial u_i}{\partial x_i}=u_{(ii)} \tag{18}$$

will be needed below.

The rate at which the relaxed length of dx_i is changing may also be calculated, and is

$$\frac{D(d\lambda)^2}{Dt}=\left\{\frac{\partial g_{ij}}{\partial t}+u_k\frac{\partial g_{ij}}{\partial x_k}+g_{ik}\frac{\partial u_k}{\partial x_j}+g_{kj}\frac{\partial u_k}{\partial x_i}\right\} \times dx_i dx_j=2a_{ij}dx_i dx_j, \tag{19}$$

where a_{ij} is an obvious abbreviation, and may be called the anelasticity tensor. The principle of a constant relaxed state would require that the relaxed length of dx_i be independent of t, and hence that $a_{ij}=0$ at all times and places. The rejection of this principle again has the negative effect of leaving a_{ij} physically indeterminate.

Before attempting to find positive laws governing the anelasticity tensor, certain purely kinematic equations connecting it to other quantities will be derived. The Eq. (19) may be written

$$a_{ij}=\tfrac{1}{2}\frac{Dg_{ij}}{Dt}+U_{(ij)} \tag{20}$$

where

$$U_{(ij)}=\tfrac{1}{2}\left(g_{ik}\frac{\partial u_k}{\partial x_j}+g_{kj}\frac{\partial u_k}{\partial x_i}\right). \tag{21}$$

It should be noted that because of Eq. (17), $U_{(ij)}$ depends on the vorticity as well as on the deformation of the motion:

$$U_{(ij)}=\tfrac{1}{2}(g_{ik}u_{(kj)}+g_{kj}u_{(ki)}) +\tfrac{1}{2}(g_{ik}u_{[kj]}+g_{kj}u_{[ki]}). \tag{22}$$

The matrix reciprocal to g_{ij} is denoted by g^{ij} where (see reference 2)

$$g^{ij}g_{jk}=\delta_{ik}; \tag{23}$$

hence Eq. (21) results in

$$g^{ij}U_{(ij)}=u_{(ii)}=\frac{\partial u_i}{\partial x_i}, \tag{24}$$

which is analogous to Eq. (18). Consequently Eq. (20) leads to

$$\frac{\partial u_i}{\partial x_i}=g^{ij}\left(a_{ij}-\tfrac{1}{2}\frac{Dg_{ij}}{Dt}\right). \tag{25}$$

The determinant of the matrix g_{ij} is denoted by g; the rule for the differentiation of a determinant results in

$$\frac{D}{Dt}(\log g)=g^{ij}\frac{Dg_{ij}}{Dt} \tag{26}$$

and hence Eq. (25) becomes

$$\frac{\partial u_i}{\partial x_i}=g^{ij}a_{ij}-\tfrac{1}{2}\frac{D}{Dt}(\log g), \tag{27}$$

an equation that will prove important below.

4. THE THERMODYNAMICS OF STRAIN

The general equations of thermodynamics will be briefly summarized in the present notation, and their implications for anelastic phenomena discussed. The conservation of matter is expressed by

$$\frac{\partial \rho}{\partial t}+\frac{\partial}{\partial x_i}(\rho u_i)=0,$$

where ρ is the density of the substance. This may also be written

$$\frac{D\rho}{Dt}=-\rho\frac{\partial u_i}{\partial x_i}. \tag{28}$$

Introducing the specific volume, $v=1/\rho$, this becomes, on referring to the previous equations,

$$\frac{D}{Dt}(\log v)=\frac{\partial u_i}{\partial x_i}. \tag{29}$$

Combining this with Eq. (27), the important equation

$$\frac{D}{Dt}(\log v g^{\frac{1}{2}})=g^{ij}a_{ij} \tag{30}$$

is obtained. One consequence of the principle of a constant relaxed state would thus be that the product $vg^{\frac{1}{2}}$ is constant for each bit of the substance. It is the most commonly used consequence of this principle. In the present theory, the quantities v and g become independent, and must both be specified before the state of the substance is known.

The conservation of momentum is expressed by

$$\rho\frac{Du_i}{Dt}=\frac{\partial S_{ij}}{\partial x_j} \tag{31}$$

where $S_{ij}=S_{ji}$ is the stress tensor; and the conservation of energy is expressed by

$$\rho\frac{D}{Dt}(\tfrac{1}{2}u_iu_i+\epsilon)+\frac{\partial q_i}{\partial x_i}=\frac{\partial}{\partial x_j}(u_iS_{ij}) \qquad (32)$$

where ϵ is the internal energy in ergs per gram of the substance and q_i is the heat flow, in ergs per cm^2 sec.$^{-1}$ Equation (31) combines with Eq. (32) to give the first law of thermodynamics:

$$\rho\frac{D\epsilon}{Dt}+\frac{\partial q_i}{\partial x_i}=S_{ij}u_{(ij)}. \qquad (33)$$

It is worth noting that only the deformation tensor enters into the expression, $S_{ij}u_{(ij)}$, for the rate of thermodynamic work.

From the previous discussion, it follows that the internal energy must be a function of, at least, the entropy, η; the specific volume, v; and of the strain metric, g_{ij}. In the traditional discussions, v is assumed to be expressible as a function of g, and thus does not appear explicitly in ϵ. The rejection of the principle of a constant relaxed state thus finds a first positive expression in the equation

$$\frac{D\epsilon}{Dt}=\frac{\partial\epsilon}{\partial v}\frac{Dv}{Dt}+\frac{\partial\epsilon}{\partial g_{ij}}\frac{Dg_{ij}}{Dt}+\frac{\partial\epsilon}{\partial\eta}\frac{D\eta}{Dt}. \qquad (34)$$

The various terms on the right can be transformed into more interesting expressions. Using the usual thermodynamic definition of the hydrostatic pressure:

$$p=\frac{\partial\epsilon}{\partial v}, \qquad (35)$$

and referring to Eq. (29),

$$\rho\frac{\partial\epsilon}{\partial v}\frac{Dv}{Dt}=-pu_{(ii)}. \qquad (36)$$

The usual definition of the absolute temperature, θ, is equivalent to

$$\rho\frac{\partial\epsilon}{\partial\eta}\frac{D\eta}{Dt}=\rho\theta\frac{D\eta}{Dt}. \qquad (37)$$

The remaining term results in a more complicated expression; since g_{ij} is a symmetric tensor, it depends only on the symmetric tensor

$$E_{ij}=-\rho\left(\frac{\partial\epsilon}{\partial g_{ij}}+\frac{\partial\epsilon}{\partial g_{ji}}\right) \qquad (38)$$

which may be called the elastic stress. (It will appear below that the total stress is the resultant of three components: the hydrostatic pressure, the elastic stress, and the viscous stress.) Equation (38) results in

$$\rho\frac{\partial\epsilon}{\partial g_{ij}}\frac{Dg_{ij}}{Dt}=-\tfrac{1}{2}E_{ij}\frac{Dg_{ij}}{Dt},$$

$$=-E_{ij}(a_{ij}-U_{(ij)})$$

by Eq. (20). Using Eq. (22), it becomes

$$\rho\frac{\partial\epsilon}{\partial g_{ij}}\frac{Dg_{ij}}{Dt}=\tfrac{1}{2}[g_{ik}E_{kj}+g_{jk}E_{ki}]u_{(ij)}$$

$$-E_{ij}[a_{ij}-\tfrac{1}{2}g_{ik}u_{[kj]}-\tfrac{1}{2}g_{jk}u_{[ki]}]. \qquad (39)$$

Using these results, the first law may be transformed into

$$\rho\frac{D\eta}{Dt}+\frac{\partial}{\partial x_i}\left(\frac{q_i}{\theta}\right)=-\left(\frac{1}{\theta}\right)^2q_i\frac{\partial\theta}{\partial x_i}$$

$$+\left(\frac{1}{\theta}\right)u_{(ij)}[S_{ij}+p\delta_{ij}-\tfrac{1}{2}g_{ik}E_{kj}-\tfrac{1}{2}g_{jk}E_{ki}]$$

$$+\left(\frac{1}{\theta}\right)E_{ij}[a_{ij}-\tfrac{1}{2}g_{ik}u_{[kj]}-\tfrac{1}{2}g_{jk}u_{[ki]}]. \qquad (40)$$

The second law of thermodynamics asserts that, for all motions compatible with the laws of physics, the right side of this equation is greater than zero. If the physical laws are unknown, this imposes restrictions on their possible forms.[7]

One particular set of laws that satisfies these restrictions is

$$q_i=-k\frac{\partial\theta}{\partial x_i}, \qquad (41)$$

$$S_{ij}=-p\delta_{ij}+\tfrac{1}{2}g_{ik}E_{kj}+\tfrac{1}{2}g_{jk}E_{ki}$$

$$+N_{((ij)(kl))}u_{(kl)}, \qquad (42)$$

$$a_{ij}=\tfrac{1}{2}g_{ik}u_{[kj]}+\tfrac{1}{2}g_{jk}u_{[ki]}+M_{((ij)(kl))}E_{kl}, \qquad (43)$$

[7] Carl Eckart, Thermodynamics of irreversible processes, Phys. Rev. **58**, 267, 269, 919 (1940).

provided that $k>0$ and the two quadratic forms

$$N_{((ij)(kl))}u_{(ij)}u_{(kl)} \quad \text{and} \quad M_{((ij)(kl))}E_{ij}E_{kl}$$

are positive definite.

The Eq. (41) will be recognized as Fourier's law of heat conduction, k being the thermal conductivity. Equation (42) is a generalization of the usual formulae for the total stress, the first term being the hydrostatic pressure, the second two the elastic stress, and the last, the viscous stress. This last depends only on the deformation tensor $u_{(ij)}$, and, since the fourth-order tensor $N_{((ij)(kl))}$ has 21 independent components, it is clearly that generalization of the Stokes-Navier formulae which is appropriate to an aeolotropic substance.

Since Eq. (43) involves the anelasticity tensor, it has no counterpart in the traditional theory, unless one wishes to consider the principle of a constant relaxed state ($a_{ij}=0$) as such. It can be given a more useful form by using Eq. (20) and (22):

$$\tfrac{1}{2}\frac{Dg_{ij}}{Dt}=-\tfrac{1}{2}(g_{ik}u_{(kj)}+g_{jk}u_{(ki)})+M_{((ij)(kl))}E_{kl}. \quad (44)$$

In this form, it asserts that changes in the strain metric at a given bit of matter are caused, not only by the deformation of the matter, but also by the elastic stresses. It is very interesting to note that the hydrostatic pressure, p, does not contribute to these irreversible changes in the strain metric.

Perhaps this is the strongest argument for supposing that Eq. (44) will be found consistent with the experimental facts. There are indications that the permanent deformations produced by a purely hydrostatic pressure are second-order effects compared to those produced by uniaxial pressures. Thus, a cube of lead may be subject to great hydrostatic pressure without apparent anelastic deformation; a much smaller pressure exerted by the jaws of a vise will deform it noticeably and permanently.

5. THE PROPAGATION OF WAVES IN AN ISOTROPIC ANELASTIC MEDIUM

One method of obtaining information concerning a substance is to study the propagation of waves through it. In such experiments, the strains are usually small, so that Eq. (10) is useful, and the equations can be simplified by neglecting second-order terms in the σ_{ij}. The specific volume, v, also departs only slightly from its normal value $v_0=1/\rho_0$. The abbreviations

$$s=1-\rho_0 v, \quad \sigma=\sigma_{ii}, \quad (45)$$

will be used; if the waves are purely elastic, $s+\sigma=0$ to the present approximation. It will be supposed, for simplicity, that all thermal effects can be neglected, so that the internal energy can be treated as a function only of s and σ_{ij}. Since it must be a minimum for $s=0$, $\sigma_{ij}=0$, a quadratic function will suffice for the present purposes. It will also be supposed that the medium is intropic, so that all of its 28 coefficients except four will vanish:

$$\epsilon=(1/2\rho_0)(\lambda_3 s^2+2\lambda_2 s\sigma+\lambda_1\sigma^2+2\mu\sigma_{ij}\sigma_{ij}). \quad (46)$$

The condition that this be a positive definite form is

$$\lambda_3>0, \quad \mu>0, \quad \lambda_3(3\lambda_1+2\mu)>3\lambda_2^2. \quad (47)$$

It should be noted that, although the preceding discussion has been couched in terms of a theory of the solid state, it ought to be possible to apply it with little modification to fluids. For a completely fluid substance, the coefficient $\mu=0$. It is likely that substances for which μ is small will have properties that differ only slightly from those of a completely fluid substance. The distinction between hydrodynamics and the theory of elasticity is merely quantitative and not qualitative.

Substituting Eq. (46) into the general equations, it is easily seen that

$$p=\lambda_3 s+\lambda_2\sigma, \quad (48)$$

$$E_{kl}=(\lambda_2 s+\lambda_1\sigma)\delta_{kl}+2\mu\sigma_{kl}. \quad (49)$$

The total stress is

$$S_{kl}=[(\lambda_2-\lambda_3)s+(\lambda_1-\lambda_2)\sigma]\delta_{kl} +2\mu\sigma_{kl}+2Nu_{(kl)}+N'u_{(ii)}\delta_{kl}, \quad (50)$$

where N and N' are the two coefficients of viscosity of an isotropic substance, and $N>0$, $3N'+2N>0$. For an ideal gas, $3N'+2N=0$.

The conservation of matter reduces to the equation

$$\frac{\partial s}{\partial t}=-u_{(ii)}. \quad (51)$$

The conservation of momentum becomes

$$\rho_0\frac{\partial u_k}{\partial t}=(\lambda_2-\lambda_3)\frac{\partial s}{\partial x_k}+(\lambda_1-\lambda_2)\frac{\partial \sigma}{\partial x_k}+2\mu\frac{\partial \sigma_{kl}}{\partial x_l}$$
$$+N\nabla^2 u_k+(N+N')\frac{\partial}{\partial x_k}u_{(ii)}. \quad (52)$$

The isotropic nature of the substance reduces Eq. (44) to

$$-\frac{\partial \sigma_{kl}}{\partial t}=-u_{(kl)}+2ME_{kl}+M'E_{ii}\delta_{kl} \quad (53)$$

where M and $3M'+2M$ are both positive. The M's may be called the coefficients of anelasticity. As yet, there is no kinetic theory of these constants, but it is possible that they do not vanish for an ideal gas. In that case, a kinetic theory would be possible. Because of Eq. (50), Eq. (53) reduces to

$$\left[\frac{\partial}{\partial t}+4M\mu\right]\sigma_{kl}=u_{(kl)}-\{(3M'+2M)\lambda_2 s$$
$$+[(3M'+2M)\lambda_1+2M'\mu]\sigma\}\delta_{kl}. \quad (54)$$

Setting $k=l$ in Eq. (54) and summing, one obtains the simple equation

$$\frac{\partial}{\partial t}(s+\sigma)=-(3M'+2M)$$
$$\times[3\lambda_2 s+(3\lambda_1+2\mu)\sigma], \quad (55)$$

which shows that when the coefficients of anelasticity vanish, $s+\sigma$ is constant.

The terms in σ_{kl} can be eliminated between Eqs. (52) and (54), resulting in

$$\left[\frac{\partial}{\partial t}+4M\mu\right]\left[\rho_0\frac{\partial u_k}{\partial t}+(\lambda_3-\lambda_2)\frac{\partial s}{\partial x_k}\right.$$
$$\left.+(\lambda_2-\lambda_1)\frac{\partial \sigma}{\partial x_k}+(N+N')\frac{\partial^2 s}{\partial t\partial x_k}-N\nabla^2 u_k\right]$$
$$=\mu\left[\nabla^2 u_k-\frac{\partial^2 s}{\partial t\partial x_k}\right]-2\mu\left\{(3M'+2M)\lambda_2\frac{\partial s}{\partial x_k}\right.$$
$$\left.+[(3M'+2M)\lambda_1+2M'\mu]\frac{\partial \sigma}{\partial x_k}\right\}. \quad (56)$$

As in the traditional theory, the equation for the vorticity is comparatively simple, since most of the terms in Eq. (56) are gradients. Taking the curl of this equation eliminates the gradients and results in

$$\left[\frac{\partial}{\partial t}+4M\mu\right]\left[\rho_0\frac{\partial u_{[kl]}}{\partial t}-N\nabla^2 u_{[kl]}\right]=\mu\nabla^2 u_{[kl]}. \quad (57)$$

If M and N vanish, this reduces to the well-known equation for the waves of distortion.

On taking the divergence of Eq. (56), one obtains the generalization of the dilatational wave equation:

$$\left[\frac{\partial}{\partial t}+4M\mu\right]\left[-\rho_0\frac{\partial^2 s}{\partial t^2}+(\lambda_3-\lambda_2)\nabla^2 s\right.$$
$$\left.+(\lambda_2-\lambda_1)\nabla^2\sigma+(N'+2N)\nabla^2\frac{\partial s}{\partial t}\right]$$
$$=-2\mu\nabla^2\frac{\partial s}{\partial t}-2\mu\{(3M'+2M)\lambda_2\nabla^2 s$$
$$+[(3M'+2M)\lambda_1+2M'\mu]\nabla^2\sigma\}. \quad (58)$$

When the coefficients of viscosity and anelasticity vanish, and $s+\sigma=0$, this reduces to

$$\frac{\partial}{\partial t}\left[-\rho_0\frac{\partial^2 s}{\partial t^2}+(\lambda_1-2\lambda_2+\lambda_3+2\mu)\nabla^2 s\right]=0.$$

For simple harmonic waves, this is equivalent to the usual equation for the dilatational waves except that the coefficient of elasticity usually denoted by λ is replaced by $\lambda_1-2\lambda_2+\lambda_3$.

These equations have plane wave solutions of the form $\exp i(kx-nt)$ where k is in every case, expressible as a function of n. These functions are such that k and n cannot both be real numbers. The ratio

$$c(n)=(n/k)^{\frac{1}{2}}$$

is also a complex number in general, but may still be called the velocity of the waves: for real values of n, its real part is the phase velocity and its imaginary part is related to the absorption coefficient of the waves. For certain real values of $in=1/\tau$, $c(n)=0$. These values of τ are called the relaxation times of the medium. It is an empirical fact that anelastic media have many widely different relaxation times: collectively they form the relaxation "spectrum." The num-

ber of lines in this spectrum depend on the crystalline structure and on the degree of chemical purity of the substance. It is therefore important to discuss the relaxation spectrum of the idealized medium considered above, in order to see whether it conforms to these general empirical facts about anelasticity.

The case of the distortional waves is quite simple; Eq. (57) yields the formula

$$\rho_0 c^2 = \mu(1+4NM)\frac{in[1-in\tau_r]}{in-4M\mu}, \tag{59}$$

where

$$\tau_r = N/\mu(1+4NM). \tag{60}$$

Therefore these waves contribute two lines to the relaxation spectrum: $\tau=\tau_r$ and $\tau=\infty$. The line at infinity would presumably move to a finite position if the thermal conductivity were not set equal to zero, and it might split up into several.

The case of the dilational waves results in a more complicated formula, since Eq. (55) and (58) must be treated simultaneously. The general result is that c is determined by the condition that the determinant of two linear equations vanish. These equations have the form

$$\begin{aligned}(in-a)s+(in-b)\sigma&=0,\\ s\{(-in+4M\mu)(-\rho_0c^2+A+Bin)-2\mu in+C\}&\\ +\sigma\{(-in+4M\mu)(\lambda_2-\lambda_1)+D\}&=0,\end{aligned}$$

where $abA\cdots D$ are functions of the coefficients of elasticity, anelasticity, and viscosity. It is readily seen that ρ_0c^2 will be a rational function of in, the numerator being a cubic and the denominator a quadratic. It is not easily proven that the roots of the numerator occur for real values of $1/in$, but this is probably a consequence of Eq. (47) and the restrictions on the coefficients of viscosity and anelasticity. Assuming this, the dilational waves contribute three lines to the relaxation spectrum. Again, a finite value of the thermal conductivity will undoubtedly introduce at least one additional line.

The present theory, therefore, predicts that a pure isotropic substance will have a minimum of five lines in its relaxation spectrum. If the substance is not chemically pure, but contains impurities that are capable of diffusing, their concentrations will enter into the expression for ϵ and their concentration gradients and chemical potentials will enter into the expression for the rate of increase of entropy. The equations for small departures from equilibrium will therefore contain additional variables, and increase in number. This will increase the number of relaxation times. In the same way, departures from isotropy will increase the number of types of waves and the number of kinds of dissipation, with a corresponding complication of the relaxation spectrum.

It would thus seem that the present theory is capable of explaining any given relaxation spectrum without resorting to the device of integro-differential equations. The crucial empirical test of the theory must therefore depend on its ability to explain changes in the relaxation spectrum caused by adding impurities, and similar phenomena.

On the Radiation of Sound from an Unflanged Circular Pipe

HAROLD LEVINE AND JULIAN SCHWINGER
Harvard University, Cambridge, Massachusetts

(Received November 3, 1947)

A rigorous and explicit solution is obtained for the problem of sound radiation from an unflanged circular pipe, assuming axially symmetric excitation. The solution is valid throughout the wave-length range of dominant mode (plane wave) propagation in the pipe. The reflection coefficient for the velocity potential within the pipe and the power-gain function, embodying the characteristics of the radiation pattern, are evaluated numerically. The absorption cross section of the pipe for a plane wave incident from external space, and the gain function for this direction, are found to satisfy a reciprocity relation. In particular, the absorption cross section for normal incidence is just the area of the mouth. At low frequencies of vibration, the velocity potential within the pipe is the same as if the pipe were lengthened by a certain fraction of the radius and the open end behaved as a loop. The exact value of the end correction turns out to be 0.6133.

I. INTRODUCTION

IT is known that nearly complete reflection of a dominant mode sound wave occurs at the open end of a pipe of circular cross section, if the diameter is small compared to the wave-length. Within the pipe, the velocity potential is the same as if the pipe were lengthened by a certain fraction of its radius and the open end behaved as a loop.

An approximate calculation of the end correction was performed by Lord Rayleigh,[1] who assumed the open end of the pipe fitted with an infinite flange. In the absence of theoretical information, the influence of the flange was investigated experimentally. From his own work, and that of Bosanquet,[2] Rayleigh obtained the probable value of the unflanged end correction as 0.6 the radius of the pipe. This value was substantially confirmed by the subsequent experiments of Blaikley[3] (0.576), Boehm[4] (0.656), and Bate[5] (0.66). Bosanquet, Blaikley, and Anderson and Ostensen[6] found small changes in the magnitude of the end correction, as the wave-length was varied.

[1] Lord Rayleigh, *Theory of Sound* (*Macmillan and Company, London, 1940*), Vol. II, Chapter 16 and Appendix A; Phil. Mag. **3**, 456 (1877). L. V. King, Phil. Mag. **21**, 128 (1936).
[2] R. H. M. Bosanquet, Phil. Mag. **4**, 216 (1877).
[3] D. J. Blaikley, Phil. Mag. **7**, 339 (1879).
[4] W. M. Boehm, Phys. Rev. **31**, 341 (1910).
[5] A. E. Bate, Phil. Mag. **10**, 617 (1930); **24**, 453 (1937).
[6] S. H. Anderson and F. C. Ostensen, Phys. Rev. **31**, 267 (1928).

II. STATEMENT OF THE PROBLEM AND RESULTS

We consider a steady-state situation, in which air vibrations are communicated to free space from the interior of an open-ended, rigid circular pipe of negligible wall thickness. If the incident wave-length lies in the proper range, only dominant mode (plane) waves can propagate in the pipe. When the dominant mode waves fall on the open end, part of the incident energy is returned in reflected waves of the same type and the remainder is carried away by waves propagating into the external space.

Our purpose is to determine rigorously the amplitude and phase of the reflected propagating wave in the pipe and the amplitude of the diverging spherical wave at large distance from the mouth. The principal results are as follows.

With the end of the pipe chosen as a reference plane, the reflection coefficient for the dominant mode component of the velocity potential is given by

$$R=-|R|e^{2ikl},$$

where

$$|R|=\exp\left\{-\frac{2ka}{\pi}\int_0^{ka}\frac{\tan^{-1}(-J_1(x)/N_1(x))}{x[(ka)^2-x^2]^{\frac{1}{2}}}dx\right\},$$

and

$$\frac{l}{a}=\frac{1}{\pi}\int_0^{ka}\frac{\log\{\pi J_1(x)[(J_1(x))^2+(N_1(x))^2]^{\frac{1}{2}}\}}{x[(ka)^2-x^2]^{\frac{1}{2}}}dx+\frac{1}{\pi}\int_0^{\infty}\frac{\log[1/(2I_1(x)K_1(x))]}{x[x^2+(ka)^2]^{\frac{1}{2}}}dx.$$

Here and in the following a denotes the radius of the pipe, $k=2\pi/\lambda$ the propagation constant of sound waves in free space, and λ the associated wave-length. J_1, N_1 and I_1, K_1 designate the first-order cylinder functions of real and imaginary argument (Appendix A).

In the long wave-length (or low frequency) limit, $ka \ll 1$, the reflection coefficient assumes the form

$$R=-e^{2ikl},$$

where

$$\frac{l}{a}=\frac{1}{\pi}\int_0^\infty \frac{1}{x^2}\log\frac{1}{2I_1(x)K_1(x)}dx=0.6133$$

is the exact value of the end correction, to be compared with experimental determinations ranging from 0.58 to 0.66.

The angular distribution of the emitted radiation, which is symmetrical about the axis of the pipe, is described by the power-gain function

$$\mathcal{G}(\vartheta)=\frac{4}{\pi\sin^2\vartheta}\frac{J_1(ka\sin\vartheta)}{[(J_1(ka\sin\vartheta)^2+(N_1(ka\sin\vartheta))^2]^{\frac{1}{2}}}\times\frac{|R|}{1-|R|^2}\exp\left[\frac{2ka\cos\vartheta}{\pi}P\times\int_0^{ka}\frac{x\tan^{-1}(-J_1(x)/N_1(x))dx}{[x^2-(ka\sin\vartheta)^2][x^2+(ka)^2]^{\frac{1}{2}}}\right],$$

defined relative to an isotropically radiating point source. The angle ϑ is measured from the axis of the pipe, and P signifies that the integral is to be understood as a principal value. The gain does not vanish for any direction in space; null directions and secondary maxima appear in the radiation pattern when the pipe sustains more than one propagating mode.

The maximum value of the gain occurs in the forward direction, and is simply

$$\mathcal{G}(0)=(ka)^2/(1-|R|^2),$$

a monotonically increasing function of frequency. Another indication of the greater directivity in the radiation pattern at high frequencies is found in the ratio

$$\mathcal{G}(\pi)/\mathcal{G}(0)=|R|^2.$$

The gain in the direction at right angles to the axis of the pipe also assumes a relatively simple form,

$$\mathcal{G}(\pi/2)=\frac{4}{\pi}\frac{J_1(ka)}{[(J_1(ka))^2+(N_1(ka))^2]^{\frac{1}{2}}}\frac{|R|}{1-|R|^2}.$$

These analytical expressions have been obtained from the solution of an integral equation by a Fourier transform method, and are rigorously correct provided that only dominant

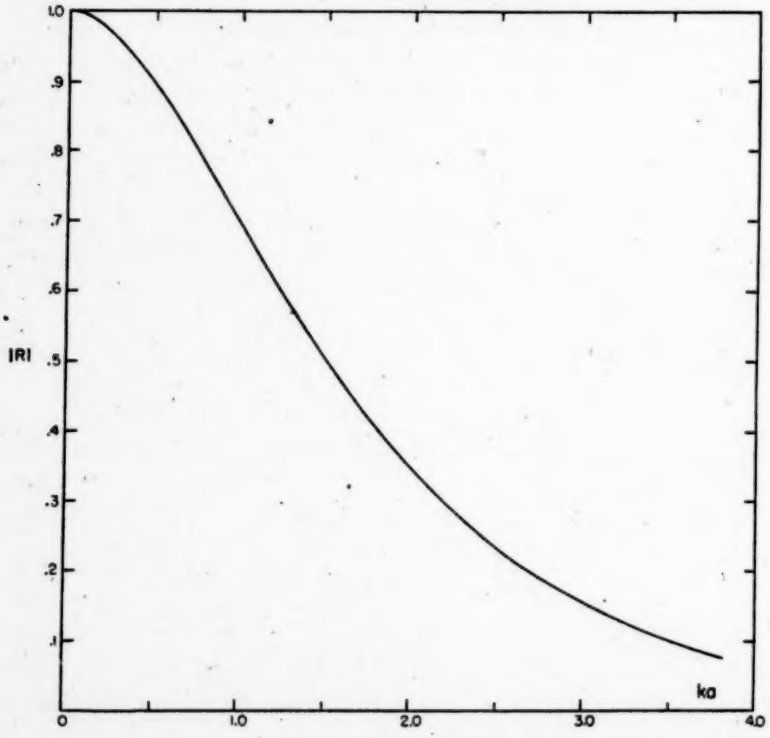

FIG. 1. Magnitude of the velocity potential reflection coefficient as a function of $ka=2\pi a/\lambda$.

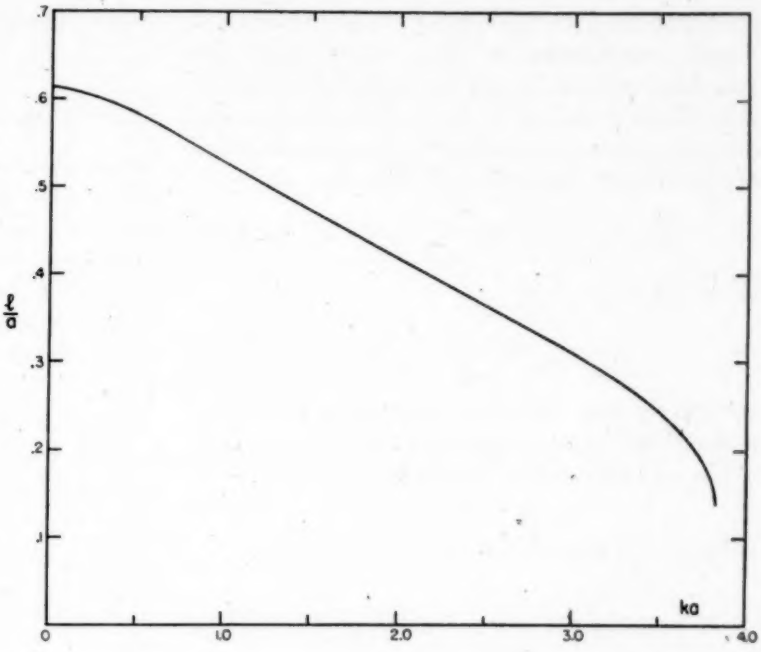

FIG. 2. End correction, in units of the pipe radius, as a function of ka.

mode propagation occurs in the pipe. This condition is realized by restricting values of the characteristic parameter, ka, in accordance with the inequality $0<ka<3.832$.[7] There is no essential difficulty in extending the results to a larger frequency range where reflected waves of several propagating modes are generated by the incident dominant mode waves. On the other hand, this method is not simply adapted to the problem of a flanged pipe.

The results of numerical calculation are displayed in the curves of Figs. 1–4.

The known radiation characteristics of the pipe determine the absorption of energy from an externally incident plane wave. This type of reciprocity is familiar in electromagnetic theory, for the intensity of radiation emitted by an antenna in a given direction is proportional to the absorption of radiation arriving from the same direction.

The absorption cross section, obtained on dividing the power transmitted into the pipe by the power incident per unit area, is

$$\sigma(\vartheta)=\pi a^2(\mathcal{G}(\vartheta)/\mathcal{G}(0)),$$

where ϑ denotes the angle between the direction of incidence of the plane wave and the axis of the pipe. This result is also rigorous in the wave-length range of the dominant mode. The range is reduced, however, to $0<ka<1.841$, in the case of oblique incidence ($\vartheta\neq 0$), owing to the excitation of all modes, including non-symmetric, at the mouth of the pipe.

The absorption cross section for normal incidence ($\vartheta=0$) is just the area of the mouth, independent of the wave-length, in the range $0<ka<3.832$.

III. DESCRIPTION OF PHYSICAL QUANTITIES

A well-known existence theorem states that the electromagnetic fields within a region are uniquely determined by the values of the tangential components of the electric or magnetic fields on the bounding surface of the region. Similarly, in the problem under consideration, the entire acoustic field can be derived from its boundary values on the surface of the pipe, regarded as an obstacle imbedded in free space. In this section we shall obtain the dependence of the physical quantities on these (as yet unknown) boundary values.

The fundamental field variable is the scalar velocity potential $\psi(\mathbf{r})$, which satisfies the wave equation

$$(\nabla^2+k^2)\psi(\mathbf{r})=0 \qquad \text{(III. 1)}$$

[7] The cut-off frequencies of the various modes are determined by the zeros of the derivative of integral order Bessel functions; for the symmetric modes these are identical with the zeros of the first-order Bessel function.

for harmonic time variation e^{-ikct} (c = velocity of sound propagation in free space), and has vanishing normal derivative on the surface of the pipe. If the pipe is excited internally, and sustains only the dominant mode, the asymptotic forms of the velocity potential are (Fig. 5)

$$\psi(\mathbf{r}) \sim Ae^{ikz}+Be^{-ikz}, \quad z\to-\infty \qquad \text{(III. 2a)}$$

within the pipe, and

$$\psi(\mathbf{r}) \sim f(\vartheta)e^{ikr}/r, \quad r\to\infty \qquad \text{(III. 2b)}$$

outside the pipe. With this type of excitation, the entire field is axially symmetric.

Let us apply Green's theorem in the form

$$\int[\psi(\mathbf{r})(\nabla^2+k^2)\phi(\mathbf{r})-\phi(\mathbf{r})(\nabla^2+k^2)\psi(\mathbf{r})]d\tau$$
$$=\int[\psi(\mathbf{r})\mathbf{n}\cdot\nabla\phi(\mathbf{r})-\phi(\mathbf{r})\mathbf{n}\cdot\nabla\psi(\mathbf{r})]dS \qquad \text{(III. 3)}$$

to the velocity potential $\psi(\mathbf{r})$ and the plane wave

$$\phi(\mathbf{r})=e^{-i\mathbf{k}\cdot\mathbf{r}}=e^{-ikr\cos\Theta},$$
$$\cos\Theta=\cos\vartheta\cos\vartheta'+\sin\vartheta\sin\vartheta'\cos(\varphi-\varphi'), \qquad \text{(III. 4)}$$

whose direction of propagation is specified by the angles (ϑ', φ'). The domain of integration, indicated in Fig. 5, is bounded by surfaces inside and outside the pipe; $\mathbf{n}$ is a unit vector which is normal to the bounding surface at each point and is directed outwards from the region. The length L is chosen sufficiently large so that the asymptotic forms (2) may be employed on the surfaces S_1, S_2.

The volume integral in (3) vanishes since $\psi(\mathbf{r})$ and $\phi(\mathbf{r})$ are solutions of the homogeneous wave Eq. (1). Separating the various parts of the surface integral, we find, with the use of (2) and the boundary condition for the radial derivative of the velocity potential at the surface of the pipe,

$$\int_{S_1}\left[f(\vartheta)\frac{e^{ikr}}{r}\frac{\partial}{\partial r}e^{-ikr\cos\Theta}-e^{-ikr\cos\Theta}\frac{\partial}{\partial r}f(\vartheta)\frac{e^{ikr}}{r}\right]dS$$
$$-\int_{S_3}\Big\{(Ae^{-ikL}+Be^{ikL})\frac{\partial}{\partial z}[\exp(-ikz\cos\vartheta'-ik\rho\sin\vartheta'\cos(\varphi-\varphi')]_{z=-L}$$
$$-\exp(ikL\cos\vartheta'-ik\rho\sin\vartheta'\cos(\varphi-\varphi'))\frac{\partial}{\partial z}(Ae^{ikz}+Be^{-ikz})_{z=-L}\Big\}dS$$
$$-\int_{S_2}[\psi(\mathbf{r})_{\rho=a+0}-\psi(\mathbf{r})_{\rho=a-0}]\frac{\partial}{\partial\rho}[\exp(-ikz\cos\vartheta'-ik\rho\sin\vartheta'\cos(\varphi-\varphi'))]_{\rho=a}dS=0. \qquad \text{(III. 5)}$$

The difference of the velocity potential on inner and outer surfaces of the pipe, which appears in the integral S_3, is a consequence of the oppositely directed normals at these surfaces.

The integration on the surface S_1 is effected by choosing the direction (ϑ', φ') as the polar axis; thus

$$\int_{S_1}\left[f(\vartheta)\frac{e^{ikr}}{r}\frac{\partial}{\partial r}e^{-ikr\cos\Theta}-e^{-ikr\cos\Theta}\frac{\partial}{\partial r}f(\vartheta)\frac{e^{ikr}}{r}\right]dS$$
$$=-ik\int_0^{2\pi}\int_0^{\pi}(1+\cos\Theta)f(\vartheta)e^{ikr(1-\cos\Theta)}r\sin\Theta d\Theta d\Phi+\int_0^{2\pi}\int_0^{\pi}f(\vartheta)e^{ikr(1-\cos\Theta)}\sin\Theta d\Theta d\Phi$$
$$=-\int_0^{2\pi}\int_0^{\pi}(1+\cos\Theta)f(\vartheta)\left[\frac{d}{d\Theta}e^{ikr(1-\cos\Theta)}\right]d\Theta d\Phi+\int_0^{2\pi}\int_0^{\pi}f(\vartheta)e^{ikr(1-\cos\Theta)}\sin\Theta d\Theta d\Phi$$
$$=-4\pi f(\vartheta')+\int_0^{2\pi}\int_0^{\pi}e^{ikr(1-\cos\Theta)}\frac{d}{d\Theta}f(\vartheta)d\Theta d\Phi.$$

If the integration by parts is continued, the integral is developed in a series of inverse powers of r. Consequently,

$$\operatorname*{Lim}_{r\to\infty}\int_{S_1}\left[f(\vartheta)\frac{e^{ikr}}{r}\frac{\partial}{\partial r}e^{-ikr\cos\Theta}-e^{-ikr\cos\Theta}\frac{\partial}{\partial r}f(\vartheta)\frac{e^{ikr}}{r}\right]dS=-4\pi f(\vartheta'). \tag{III. 6}$$

If we return to (5) and perform some of the remaining integrations it follows that (dropping the primes on the angle ϑ)

$$f(\vartheta)=\operatorname*{Lim}_{L\to\infty}\left[\frac{ka}{2}\sin\vartheta J_1(ka\sin\vartheta)\int_{-L}^{0}H(z)e^{-ikz\cos\vartheta}dz\right.$$
$$\left.+i\frac{a}{2}\frac{J_1(ka\sin\vartheta)}{\sin\vartheta}\{A(1+\cos\vartheta)e^{-ikL(1-\cos\vartheta)}-B(1-\cos\vartheta)e^{ikL(1+\cos\vartheta)}\}\right], \tag{III. 7}$$

where $H(z)$ is the discontinuity of the velocity potential on crossing the surface of the pipe

$$H(z)=\psi(\mathbf{r})_{\rho=a+0}-\psi(\mathbf{r})_{\rho=a-0}.$$

If we define a function of the complex variable ζ by

$$F(\zeta)=\operatorname*{Lim}_{L\to\infty}\left[\frac{a}{2}(k^2-\zeta^2)^{\frac{1}{2}}J_1((k^2-\zeta^2)^{\frac{1}{2}}a)\int_{-L}^{0}H(z)e^{-i\zeta z}dz\right.$$
$$\left.+i\frac{a}{2}\frac{J_1((k^2-\zeta^2)^{\frac{1}{2}}a)}{(k^2-\zeta^2)^{\frac{1}{2}}}\{A(k+\zeta)e^{-iL(k-\zeta)}-B(k-\zeta)e^{iL(k+\zeta)}\}\right], \tag{III. 8}$$

it follows that when $Im\,\zeta>0$ (or $>|Im\,k|$) the terms involving A and B vanish in the limit $L\to\infty$, and

$$F(\zeta)=\frac{a}{2}(k^2-\zeta^2)^{\frac{1}{2}}J_1((k^2-\zeta^2)^{\frac{1}{2}}a)\times\int_{-\infty}^{0}H(z)e^{-i\zeta z}dz. \tag{III. 9}$$

Equation (7) may now be regarded as the analytic continuation of this function on the line $Im\,\zeta=0$ (or in the strip $-|Im\,k|\leqslant Im\,\zeta\leqslant|Im\,k|$), at the point $\zeta=k\cos\vartheta$:

$$F(k\cos\vartheta)=f(\vartheta)=\frac{ka}{2}\sin\vartheta J_1(ka\sin\vartheta)\times\int_{-\infty}^{0}H(z)e^{-ikz\cos\vartheta}dz. \tag{III. 10}$$

The integral

$$H(\zeta)=\int_{-\infty}^{0}H(z)e^{-i\zeta z}dz \tag{III. 11}$$

defines the Fourier transform of a function $H(z)$ which vanishes for positive z. $H(z)$ has the same asymptotic form as the velocity potential on the inner surface of the pipe (since the field outside decreases in magnitude with the nature of a spherical wave), and we infer from (2a) and (11) that the transform $H(\zeta)$ has simple poles at $\zeta=\pm k$.

Using (7) and (9), we find

$$f(0)=i\tfrac{1}{2}ka^2A=-\tfrac{1}{2}ka^2\operatorname*{Lim}_{\zeta\to k}(\zeta-k)H(\zeta)$$
$$=-\tfrac{1}{2}ka^2\operatorname{Res}_{\zeta=k}H(\zeta), \tag{III. 12}$$

$$f(\pi)=-i\tfrac{1}{2}ka^2B=\tfrac{1}{2}ka^2\operatorname*{Lim}_{\zeta\to-k}(\zeta+k)H(\zeta)$$
$$=\tfrac{1}{2}ka^2\operatorname{Res}_{\zeta=-k}H(\zeta), \tag{III. 13}$$

where $\operatorname{Res}_{\zeta=\pm k}H(\zeta)$ denotes the residue of the function $H(\zeta)$ at the poles $\zeta=\pm k$, respectively.

Thus

$$A=i\operatorname{Res}_{\zeta=k}H(\zeta),$$
$$B=i\operatorname{Res}_{\zeta=-k}H(\zeta), \tag{III. 14}$$

and the reflection coefficient for the dominant mode component of the velocity potential takes the form

$$R=\frac{B}{A}=\frac{\operatorname{Res}_{\zeta=-k}H(\zeta)}{\operatorname{Res}_{\zeta=k}H(\zeta)}. \tag{III. 15}$$

To describe the radiation characteristics of the pipe, we calculate the power-gain function, which compares the intensity of radiation in a given direction with that of an isotropically radiating point source of equal power output.

We assume as the expression for the time average energy flow per unit area

$$\mathbf{S}=Re\frac{1}{ik}\psi^*(\mathbf{r})\nabla\psi(\mathbf{r}), \qquad \text{(III. 16)}$$

and verify that this corresponds to dissipationless transport of energy by the sound waves in free space, for

$$\nabla\cdot\mathbf{S}=Re\nabla\cdot\left(\frac{1}{ik}\psi^*(\mathbf{r})\nabla\psi(\mathbf{r})\right)$$
$$=Re\frac{1}{ik}(|\nabla\psi(\mathbf{r})|^2-k^2|\psi(\mathbf{r})|^2)=0.$$

Through (16), the average power incident on the mouth of the pipe is found to be

$$P_{\text{inc}}=\pi a^2|A|^2, \qquad \text{(III. 17)}$$

and therefore the power leaving the end of the pipe for external space is

$$P_{\text{rad}}=\pi a^2(|A|^2-|B|^2)$$
$$=\pi a^2|A|^2(1-|R|^2). \qquad \text{(III. 18)}$$

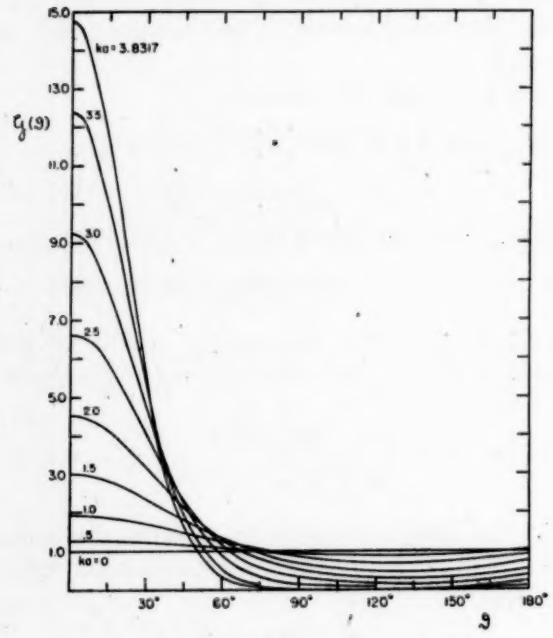

FIG. 3. The dependence of the power-gain function on angle for various values of ka.

Since $\nabla_r\psi(\mathbf{r})\sim ik\psi(\mathbf{r})$, $r\to\infty$, the average power radiated into unit solid angle about the direction (ϑ, φ) is given by

$$P(\vartheta)=\text{Lim}_{r\to\infty}r^2|\psi(\mathbf{r})|^2=|f(\vartheta)|^2; \qquad \text{(III.19)}$$

thus the power-gain function becomes

$$\mathcal{G}(\vartheta)=\frac{P(\vartheta)}{P_{\text{rad}}/4\pi}=\frac{4}{a^2}\frac{|f(\vartheta)|^2}{|A|^2(1-|R|^2)}. \qquad \text{(III. 20)}$$

Using the connections between the incident and reflected amplitudes A, B and the radiated amplitudes $f(0)$, $f(\pi)$ provided in (12) and (13), we find

$$\mathcal{G}(\vartheta)=\frac{(ka)^2}{1-|R|^2}\frac{|f(\vartheta)|^2}{|f(0)|^2}. \qquad \text{(III. 21)}$$

It follows readily that

$$\mathcal{G}(0)=\frac{(ka)^2}{1-|R|^2}, \qquad \text{(III. 22)}$$

and

$$\frac{\mathcal{G}(\pi)}{\mathcal{G}(0)}=\frac{|f(\pi)|^2}{|f(0)|^2}=|R|^2. \qquad \text{(III. 23)}$$

Using (10), (12), and (15), the gain function (21) takes the form

$$\mathcal{G}(\vartheta)=\frac{(k\sin\vartheta J_1(ka\sin\vartheta))^2|H(k\cos\vartheta)|^2}{|\text{Res}_{\zeta=k}H(\zeta)|^2-|\text{Res}_{\zeta=-k}H(\zeta)|^2}. \qquad \text{(III. 24)}$$

Equations (15) and (24) provide the dependence of the important physical quantities on the transform $H(\zeta)$. We note that these expressions are independent of any constant multiplying $H(\zeta)$.

As the final task of this section we shall derive the reciprocity relation between emission and absorption of energy by the pipe. For this purpose, we consider the independent situations in which plane waves are incident on the mouth from within and outside the pipe. The velocity potentials for the two fields $\psi_a(\mathbf{r})$, $\psi_b(\mathbf{r})$ have the asymptotic forms

$$\left.\begin{aligned}&\psi_a(\mathbf{r})\sim Ae^{ikz}+Be^{-ikz}\\&\psi_b(\mathbf{r})\sim Ce^{-ikz}\end{aligned}\right\}\begin{matrix}z\to-\infty,\\ \text{inside the pipe}\end{matrix}$$

and (III. 25)

$$\left.\begin{aligned}&\psi_a(\mathbf{r})\sim f(\vartheta)\frac{e^{ikr}}{r}\\&\psi_b(\mathbf{r})\sim e^{-ikr\cos\Theta}+g(\vartheta,\varphi)\frac{e^{ikr}}{r}\end{aligned}\right\}\begin{matrix}r\to\infty,\\ \text{outside the pipe.}\end{matrix}$$

Applying Green's theorem (3) to the functions $\psi_a(\mathbf{r})$, $\psi_b(\mathbf{r})$ in the closed region indicated in Fig. 5, we find that the integral over the bounding surface vanishes. There is no contribution to this integral from the inner and outer surfaces of the pipe, in consequence of the boundary condition for the velocity potentials, and thus

$$\int_{S_1}\left[\psi_a(\mathbf{r})\frac{\partial}{\partial r}\psi_b(\mathbf{r})-\psi_b(\mathbf{r})\frac{\partial}{\partial r}\psi_a(\mathbf{r})\right]dS = \int_{S_2}\left[\psi_a(\mathbf{r})\frac{\partial}{\partial z}\psi_b(\mathbf{r})-\psi_b(\mathbf{r})\frac{\partial}{\partial z}\psi_a(\mathbf{r})\right]dS.$$

Inserting the forms (25), and following the procedure used in the derivation of (6), we find that

$$C=2f(\vartheta')/ika^2A.$$

Using (20) and (22), it follows that

$$|C|^2=\mathcal{G}(\vartheta')/\mathcal{G}(0),$$

and thus the absorption cross section of the pipe for a plane wave incident in the direction specified by the angles (ϑ, φ) is

$$\sigma(\vartheta)=\pi a^2|C|^2 = \pi a^2\mathcal{G}(\vartheta)/\mathcal{G}(0). \qquad \text{(III. 26)}$$

IV. INTEGRAL EQUATION FORMULATION

To proceed with the evaluation of the reflection coefficient and power-gain function, it is necessary to calculate the Fourier transform of the discontinuity of the velocity potential at the surface of the pipe. In this section we shall obtain an integral equation for the determination of the transform.

We begin by deriving a general expression for the velocity potential at an arbitrary point in space, in terms of its discontinuity at the surface of the pipe. The mathematical medium for this purpose is provided by the free space scalar Green's function

$$G(\mathbf{r}, \mathbf{r}')=\frac{e^{ik|\mathbf{r}-\mathbf{r}'|}}{4\pi|\mathbf{r}-\mathbf{r}'|}, \qquad \text{(IV. 1)}$$

which satisfies the inhomogeneous wave equation

$$(\nabla^2+k^2)G(\mathbf{r}, \mathbf{r}')=-\delta(\mathbf{r}-\mathbf{r}'). \qquad \text{(IV. 2)}$$

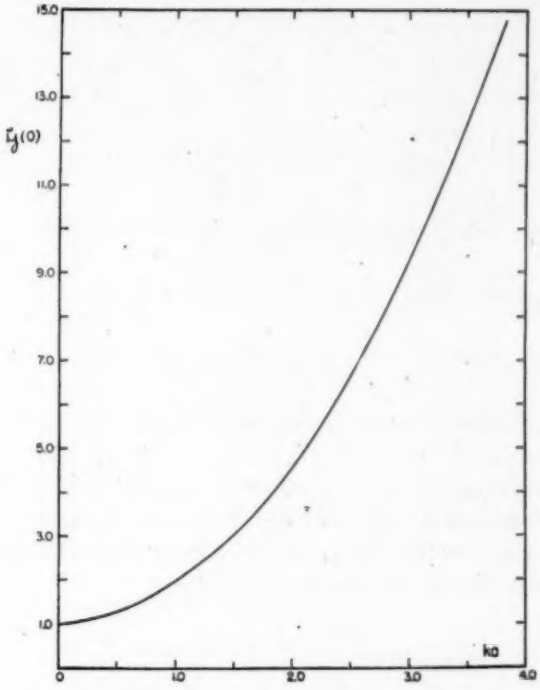

FIG. 4. The gain in the forward direction as a function of ka.

Upon applying Green's theorem in the form

$$\int[G(\mathbf{r}', \mathbf{r})(\nabla'^2+k^2)\psi(\mathbf{r}') -\psi(\mathbf{r}')(\nabla'^2+k^2)G(\mathbf{r}', \mathbf{r})]d\tau' = \int[G(\mathbf{r}', \mathbf{r})\mathbf{n}\cdot\nabla'\psi(\mathbf{r}') -\psi(\mathbf{r}')\mathbf{n}\cdot\nabla'G(\mathbf{r}', \mathbf{r})]dS', \qquad \text{(IV. 3)}$$

where the integration is extended over all space and the boundary includes the inner and outer surfaces of the pipe, we find, using the boundary condition for the velocity potential at the surface of the pipe,

$$\psi(\mathbf{r})=a\int_0^{2\pi}d\varphi'\int_{-\infty}^{0}\Psi(\varphi', z')\frac{\partial}{\partial\rho'}G(\mathbf{r}', \mathbf{r})_{\rho'=a}dz', \qquad \text{(IV. 4)}$$

$$\Psi(\varphi, z)=\psi(\mathbf{r})_{\rho=a+0}-\psi(\mathbf{r})_{\rho=a-0}.$$

As the notation indicates, the formulation is not restricted to the case of an axially symmetric field.

It should be noted that there is no contribution to (3) from that part of the surface which spans the interior of the pipe, since the magnitude of the Green's function decreases inversely as the

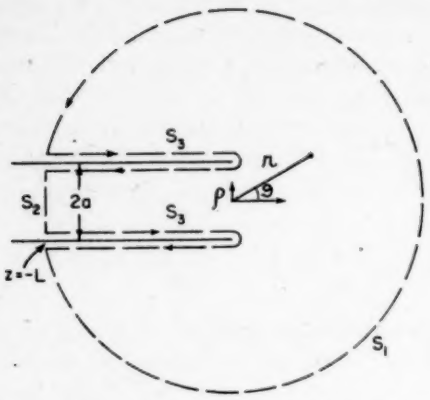

FIG. 5. Domain of integration for Eq. (III. 3).

distance between the points $\mathbf{r}$, $\mathbf{r}'$, and the velocity potential is bounded. The surface integral exterior to the pipe also vanishes, for, in consequence of the asymptotic forms

$$\psi(\mathbf{r})\sim f(\mathbf{n})\frac{e^{ikr}}{r},$$

$$G(\mathbf{r},\mathbf{r}')\sim\frac{\exp[ik(r-\mathbf{n}\cdot\mathbf{r}')]}{4\pi r},\qquad \mathbf{n}=\mathbf{r}/r,\ r\to\infty$$

it follows that

$$\lim_{r\to\infty} r^2\left[G(\mathbf{r},\mathbf{r}')\frac{\partial}{\partial r}\psi(\mathbf{r})-\psi(\mathbf{r})\frac{\partial}{\partial r}G(\mathbf{r},\mathbf{r}')\right]=0.$$

Equation (4) provides confirmation of the assertion that the entire field is determined by its boundary values at the surface of the pipe.

Upon requiring that the velocity potential (4) satisfy the boundary condition at the surface of the pipe, we are provided with the integral equation

$$\int^{2\pi}d\varphi'\int_{-\infty}^{0}\Psi(\varphi',z')\frac{\partial}{\partial\rho}\frac{\partial}{\partial\rho'}\times G(\mathbf{r},\mathbf{r}')_{\rho,\,\rho'=a}dz'=0,\quad z<0 \qquad \text{(IV. 5)}$$

for the determination of $\Psi(\varphi, z)$.

To effect the angular integration in (5), it is convenient to express the Green's function as a Fourier series in the angular variable $(\varphi-\varphi')$. For this purpose, we rewrite (2) in the form[8]

$$\left(\frac{1}{\rho}\frac{\partial}{\partial\rho}\left(\rho\frac{\partial}{\partial\rho}\right)+\frac{1}{\rho^2}\frac{\partial^2}{\partial\varphi^2}+\frac{\partial^2}{\partial z^2}+k^2\right)\times G(\rho,\rho',\varphi-\varphi',z-z')=-\frac{\delta(\rho-\rho')}{\rho}\delta(\varphi-\varphi')\delta(z-z'); \qquad \text{(IV. 6)}$$

that the Green's function depends on the difference of the coordinates φ, φ' and z, z' is evident from (1).

Multiplying (6) by $e^{-i\zeta z}$ and integrating over all values of z, we find

$$\left(\frac{1}{\rho}\frac{\partial}{\partial\rho}\left(\rho\frac{\partial}{\partial\rho}\right)+\frac{1}{\rho^2}\frac{\partial^2}{\partial\varphi^2}+k^2-\zeta^2\right)G(\rho,\rho',\varphi-\varphi',\zeta)=-\frac{\delta(\rho-\rho')}{\rho}\delta(\varphi-\varphi'). \qquad \text{(IV. 7)}$$

Here

$$G(\rho,\rho',\varphi-\varphi',\zeta)=\int_{-\infty}^{\infty}G(\rho,\rho',\varphi-\varphi',z)e^{-i\zeta z}dz$$

$$=\int_{-\infty}^{\infty}\frac{\exp[ik(\rho^2+\rho'^2-2\rho\rho'\cos(\phi-\phi')+z^2)^{\frac{1}{2}}]}{4\pi(\rho^2+\rho'^2-2\rho\rho'\cos(\phi-\phi')+z^2)^{\frac{1}{2}}}e^{-i\zeta z}dz \qquad \text{(IV. 8)}$$

is the Fourier transform of the Green's function with respect to z.

Introducing coordinates in the ζ-plane,

$$\zeta=\xi+i\eta,$$

it follows that

$$|G(\rho,\rho',\varphi-\varphi',\zeta)|\leqslant\int_{-\infty}^{\infty}|G(\rho,\rho',\varphi-\varphi',z)|e^{\eta z}dz.$$

Assuming the propagation constant k to have an arbitrarily small positive imaginary part[9] (which is eventually set equal to zero), we find,

[8] The three-dimensional representation of the delta-function satisfies the conditions $\delta(\mathbf{r}-\mathbf{r}')=0$, $\mathbf{r}\neq\mathbf{r}'$ and $\int\delta(\mathbf{r}-\mathbf{r}')d\tau=1$, where $d\tau=\rho d\rho d\varphi dz$ is the volume element in cylindrical coordinates.

[9] This corresponds to a small attenuation of sound waves traveling in free space.

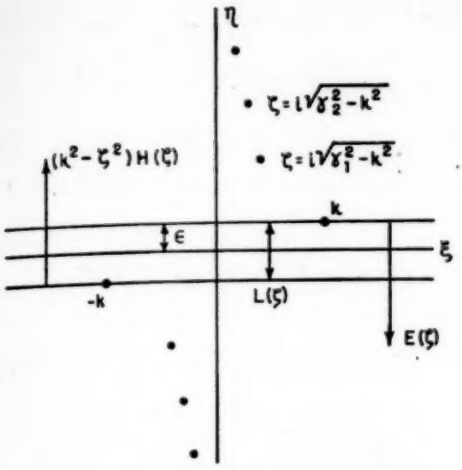

FIG. 6. Regions of regularity of transforms.

in consequence of the asymptotic form

$$G(\rho, \rho', \varphi-\varphi', z)\sim e^{ik|z|}/z, \quad |z|\to\infty,$$

that the transform $G(\rho, \rho', \varphi-\varphi', \zeta)$ is regular in the strip $|\eta|<\epsilon(=Im\ k)$. The operation of integration by parts twice, with discard of the integrated terms, in the derivation of the equation

$$\int_{-\infty}^{\infty}\frac{\partial^2}{\partial z^2}G(\rho, \rho', \varphi-\varphi', z)e^{-i\zeta z}dz = \int_{-\infty}^{\infty}G(\rho, \rho', \varphi-\varphi', z)\frac{\partial^2}{\partial z^2}e^{-i\zeta z}dz = -\zeta^2 G(\rho, \rho', \varphi-\varphi', \zeta)$$

is justified if ζ lies in the strip.

Introducing the expansion

$$G(\rho, \rho', \varphi-\varphi', \zeta)=\frac{1}{2\pi}\sum_{m=-\infty}^{\infty}e^{im(\varphi-\varphi')}G_m(\rho, \rho', \zeta) \tag{IV. 9}$$

in (7), and multiplying through by $e^{-im\varphi}$, we find, after integrating over the range of the angle φ,

$$\left(\frac{1}{\rho}\frac{d}{d\rho}\left(\rho\frac{d}{d\rho}\right)+k^2-\zeta^2-\frac{m^2}{\rho^2}\right)G_m(\rho, \rho', \zeta) = -\frac{\delta(\rho-\rho')}{\rho}. \tag{IV. 10}$$

When $\rho\neq\rho'$, the right-hand member of (10) vanishes, and we arrive at Bessel's differential equation.

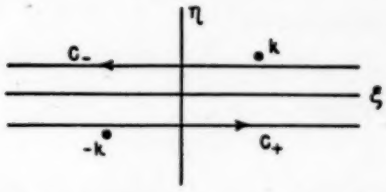

FIG. 7. Integration contours for $L_+(\zeta)$, $L_-(\zeta)$.

Since the Green's function (1) describes the propagation of a spherical wave from the source point $\mathbf{r}=\mathbf{r}'$, we look for a solution of (10) which involves cylindrical wave propagation outwards along the radius ρ. In view of the regularity of $G_m(\rho, \rho', \zeta)$ when either ρ or ρ' vanishes, and its symmetry in these coordinates, we write

$$\begin{aligned} G_m(\rho, \rho', \zeta) &= A_m H_m^{(1)}((k^2-\zeta^2)^{\frac{1}{2}}\rho) \\ &\quad\times J_m((k^2-\zeta^2)^{\frac{1}{2}}\rho'), \quad \rho>\rho', \\ G_m(\rho, \rho', \zeta) &= A_m H_m^{(1)}((k^2-\zeta^2)^{\frac{1}{2}}\rho') \\ &\quad\times J_m((k^2-\zeta^2)^{\frac{1}{2}}\rho), \quad \rho<\rho'. \end{aligned} \tag{IV. 11}$$

J_m is the mth order Bessel function, and $H_m^{(1)}=J_m+iN_m$ is the mth order Hankel function of the first kind.

To insure the proper sense of cylindrical wave propagation, it is necessary to specify the phases of the radical in (11): this we do on the real axis of the ζ-plane, adopting the values 0, $\pi/2$ for the phase in the sections $|\zeta|<k$, $>k$, respectively.

The same coefficient A_m occurs in the expressions (11), owing to the continuity of the function $G_m(\rho, \rho', \zeta)$ at $\rho=\rho'$. The value of A_m is obtained from the inhomogeneous term of the differential Eq. (10) on multiplying both sides by ρ and integrating in a small interval about ρ':

$$\rho\frac{d}{d\rho}G_m(\rho, \rho', \zeta)\Big|_{\rho=\rho'-\Delta}^{\rho=\rho'+\Delta}+\int_{\rho'-\Delta}^{\rho'+\Delta}\left(k^2-\zeta^2-\frac{m^2}{\rho^2}\right)\rho \times G_m(\rho, \rho', \zeta)d\rho=-1.$$

Recalling the continuity of the terms in the integrand, and passing to the limit $\Delta\to 0$, we find

$$\rho\frac{d}{d\rho}G_m(\rho, \rho', \zeta)\Big|_{\rho=\rho'-0}^{\rho=\rho'+0}=-1.$$

Introducing the expressions (11), and em-

ploying the relation

$$H_m^{(1)\prime}(z)J_m(z)-J_m'(z)H_m^{(1)}(z)=2i/\pi z,$$

it follows that

$$A_m=\tfrac{1}{2}\pi i.$$

Thus, using $\rho_>$, $\rho_<$ to denote the larger and smaller of the coordinates ρ, ρ' respectively,

$$G_m(\rho,\rho',\zeta)=\frac{\pi i}{2}H_m^{(1)}((k^2-\zeta^2)^{\frac{1}{2}}\rho_>)\times J_m((k^2-\zeta^2)^{\frac{1}{2}}\rho_<), \quad \text{(IV. 12)}$$

and by the Fourier inversion formula,

$$G(\rho,\rho',\varphi-\varphi',z-z')=\frac{i}{8\pi}\int_{-\infty+i\eta}^{\infty+i\eta}\sum_{m=-\infty}^{\infty}e^{im(\varphi-\varphi')}H_m^{(1)}((k^2-\zeta^2)^{\frac{1}{2}}\rho_>)J_m((k^2-\zeta^2)^{\frac{1}{2}}\rho_<)e^{i\zeta(z-z')}d\zeta$$

$$=\frac{i}{8\pi}\int_{-\infty+i\eta}^{\infty+i\eta}H_0^{(1)}[(k^2-\zeta^2)^{\frac{1}{2}}(\rho^2+\rho'^2-2\rho\rho'\cos(\varphi-\varphi'))^{\frac{1}{2}}]e^{i\zeta(z-z')}d\zeta. \quad \text{(IV. 13)}$$

The integration contour in (13) is a straight line in the region of regularity of the Green's function transform.

Returning to the integral Eq. (5), and assuming

$$\Psi(\varphi,z)=e^{im\varphi}H_m(z), \quad \text{(IV. 14)}$$

we find

$$\int_{-\infty}^{0}H_m(z')K_m(z-z')dz'=0, \quad z<0, \quad \text{(IV. 15)}$$

where

$$K_m(z)=\int_0^{2\pi}e^{im\varphi'}\frac{\partial}{\partial\rho}\frac{\partial}{\partial\rho'}\times G(\rho,\rho',\varphi-\varphi',z)_{\rho,\rho'=a}d\varphi'. \quad \text{(IV. 16)}$$

Thus, using the Green's function representation

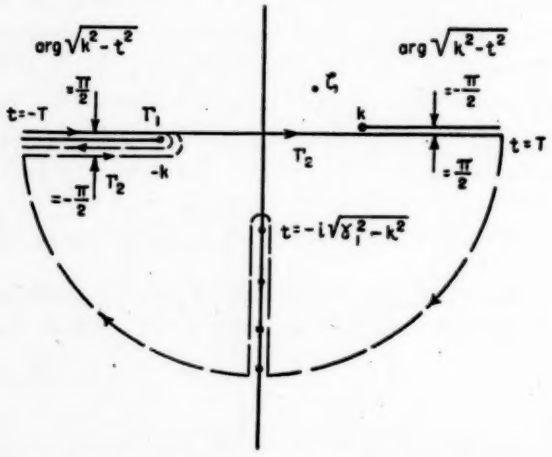

FIG. 8. Integration contours for Eq. (V. 17).

(13), it follows that

$$K_m(z)=\frac{1}{2\pi}\int_{-\infty+i\eta}^{\infty+i\eta}K_m(\zeta)e^{i\zeta z}d\zeta, \quad \text{(IV. 17)}$$

with

$$K_m(\zeta)=\tfrac{1}{2}\pi i(k^2-\zeta^2)H_m^{(1)\prime}((k^2-\zeta^2)^{\frac{1}{2}}a)\times J_m'((k^2-\zeta^2)^{\frac{1}{2}}a). \quad \text{(IV. 18)}$$

The primes in (18) denote differentiations with respect to the argument of the cylinder functions.

The integral Eq. (15) resembles the Wiener-Hopf type,[10] and may be solved by application of a Fourier transform method. In the course of solution, we use the fact that the asymptotic form of $H_m(z)$, for large negative values of z, is the same as that of the velocity potential on the inner surface of the pipe (see remarks following (III. 11)).

The formulation thus far is completely general and applies directly if the pipe is excited in any set of modes with a common angular dependence of the type (14). This generality is not required for present purposes since our interest relates only to the case of symmetric excitation ($m=0$) in accordance with the program outlined in the preceding sections.

With wave-lengths permitting only dominant mode propagation, our problem therefore is to

[10] R. E. A. C. Paley and N. Wiener, *Fourier Transforms in the Complex Domain* (Am. Math. Soc. Colloquium Publications, New York, 1934), Vol. XIX; E. C. Titchmarsh, *Introduction to the Theory of Fourier Integrals* (Oxford University Press, London, 1937), Chapter IV, p. 339; E. Reissner, J. Math. and Phys. M. I. T. (20) 5, 219 (1941).

obtain a solution $H_0(z)$ of the integral equation

$$\int_{-\infty}^{0} H_0(z')K_0(z-z')dz'=0, \quad z<0, \quad \text{(IV. 19)}$$

with the asymptotic form (omitting an unessential constant factor)

$$H_0(z)\sim Ae^{ikz}+Be^{-ikz}, \quad z\to-\infty. \quad \text{(IV. 20)}$$

For an extended frequency interval, we must include in (20) additional reflected waves of the higher symmetric modes, with appropriate propagation constants.

In concluding this section we note an alternative integral equation formulation of the problem, originating with the division of space into the two regions $\rho\gtrless a$. Using (3) in conjunction with appropriate Green's functions, the velocity potential in each region is expressed in terms of its radial derivative on the surface $\rho=a$, $z>0$. The requirement of continuity for the velocity potential on crossing this surface provides an inhomogeneous integral equation of the Wiener-Hopf type for the determination of the common radial derivative.

The transform of the radial derivative allows a simple calculation of the physical quantities; the results are identical with those obtained from the formulation in terms of the discontinuity of the velocity potential at the surface of the pipe.

If an infinite flange is fitted to the open end of the pipe, the new formulation requires modification only in the construction of the Green's function for the region $\rho>a$. Using the method of images, the new Green's function is obtained by adding to (1) a similar expression in which the sign of z' is reversed. The kernel of the resulting inhomogeneous integral equation thus includes a term depending on $z+z'$, which considerably complicates the Fourier transform solution.

V. FOURIER TRANSFORM SOLUTION OF THE INTEGRAL EQUATION

In preparation for the Fourier transform solution of (IV. 19), we consider an extended integral equation (in which subscripts are omitted):

$$\int_{-\infty}^{\infty} H(z')K(z-z')dz'=\begin{cases}E(z), & z\geqslant 0\\ 0, & z<0,\end{cases}$$

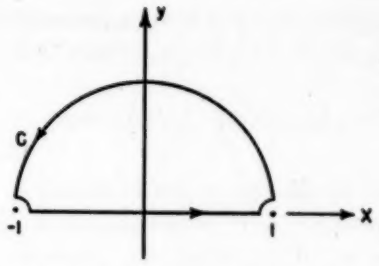

FIG. 9. Integration contour for Eq. (VI. 11).

where

$$H(z)=\begin{cases}0, & z>0\\ H_0(z), & z\leqslant 0,\end{cases} \quad \text{(V. 1)}$$

and

$$K(z)=\int_0^{2\pi}\frac{\partial}{\partial\rho}\frac{\partial}{\partial\rho'}G(\rho,\rho',\varphi-\varphi',z)_{\rho,\rho'=a}d\varphi'.$$

By construction, the integral Eq. (1) is equivalent to (IV. 19), for $z<0$; the function $E(z)$ is defined by (1) for $z\geqslant 0$.

Multiplying (1) by $e^{-i\zeta z}$ and integrating over all values of z,

$$\int_{-\infty}^{\infty}\left(\int_{-\infty}^{\infty}H(z')K(z-z')dz'\right)e^{i\zeta z}=\int_0^{\infty}E(z)e^{-i\zeta z}dz;$$

thus, with a change of variable, we have

$$\int_{-\infty}^{0}H(z')e^{-i\zeta z'}dz'\int_{-\infty}^{\infty}K(t)e^{-i\zeta t}dt=\int_0^{\infty}E(z)e^{-i\zeta z}dz,$$

and

$$H(\zeta)K(\zeta)=E(\zeta), \quad \text{(V. 2)}$$

where $H(\zeta)$, $K(\zeta)$, and $E(\zeta)$ denote the Fourier transforms of the respective functions.

The transform Eq. (2) has significance if both members are regular in a common domain of the ζ-plane. To verify the existence of such a domain we examine the nature of the individual transforms.

From the discussion following (III. 11), we recall that the transform

$$H(\zeta)=\int_{-\infty}^{0}H(z)e^{-i\zeta z}dz=\int_{-\infty}^{0}H(z)e^{-i\xi z+\eta z}dz \quad \text{(V. 3)}$$

has simple poles at $\zeta = \pm k$. In consequence of the asymptotic form (IV. 20), it follows that

$$|H(\zeta)| \leqslant \int_{-\infty}^{0} |H(z)| e^{\eta z} dz$$

is bounded in the region $\eta > \epsilon$ $(= Im\ k)$.

The transform $K(\zeta)$ is obtained from (IV. 18) by setting $m=0$ and using the relations (A. 4), (A. 5) of the Appendix:

$$K(\zeta) = \tfrac{1}{2}\pi i(k^2-\zeta^2) \times H_1^{(1)}((k^2-\zeta^2)^{\frac{1}{2}}a) J_1((k^2-\zeta^2)^{\frac{1}{2}}a). \quad \text{(V. 4)}$$

Inserting the explicit form (IV. 1) of the Green's function in (1), and performing the indicated differentiations, we find

$$K(z) \sim e^{ik|z|}/z^3, \quad |z| \to \infty;$$

thus the transform $K(\zeta)$ is regular in the strip $|\eta| < \epsilon$.

Although $K(\zeta)$ vanishes at $\zeta = \pm k$, these are branch points of the function. If we write

$$K(\zeta) = \tfrac{1}{2}(k^2-\zeta^2)L(\zeta),$$
$$L(\zeta) = \pi i H_1^{(1)}((k^2-\zeta^2)^{\frac{1}{2}}a) J_1((k^2-\zeta^2)^{\frac{1}{2}}a), \quad \text{(V. 5)}$$

the function $L(\zeta)$ is regular in the strip $|\eta| < \epsilon$, and has the value unity at the branch points.

We next establish the important result that $L(\zeta)$ does not vanish in this strip. To do so, we note first that $H_1^{(1)}(z)$ has no zeros for which $-\pi/2 \leqslant \arg z \leqslant 3\pi/2$.[11] Since this phase interval contains all the values appropriate to the function $(k^2-\zeta^2)^{\frac{1}{2}}$ in the ζ-plane, we conclude that $H_1^{(1)}((k^2-\zeta^2)^{\frac{1}{2}}a)$ has no zeros. The zeros of $J_1((k^2-\zeta^2)^{\frac{1}{2}}a)$ occur at $\zeta = \pm k$,[12] and at $\zeta = \pm(\gamma_n^2-k^2)^{\frac{1}{2}}$, where $J_1(\gamma_n a)=0$. However, the latter set, comprising the attenuation constants for the non-propagating symmetric modes of the pipe, have imaginary parts with magnitudes in excess of ϵ, and lie outside the strip.

The results show that $H(\zeta)$ and $K(\zeta)$ are regular in separate domains of the ζ-plane. However, the product $H(\zeta)K(\zeta)$ may be separated into a pair of factors which are regular in a common domain. This is accomplished by writing $K(\zeta)$ in the form (5), and associating the factor $(k^2-\zeta^2)/2$ with $H(\zeta)$. The function $(k^2-\zeta^2)H(\zeta)$ is regular for $\eta \geqslant -\epsilon$, and thus has a common domain of regularity with $L(\zeta)$.

A discussion of the transform $E(\zeta)$ is based on (1); inserting the asymptotic form of the kernel, we find

$$E(z) \sim e^{ikz} \int_{-\infty}^{0} H(z') \frac{e^{-ikz'}}{(z-z')^3} dz', \quad z \to \infty.$$

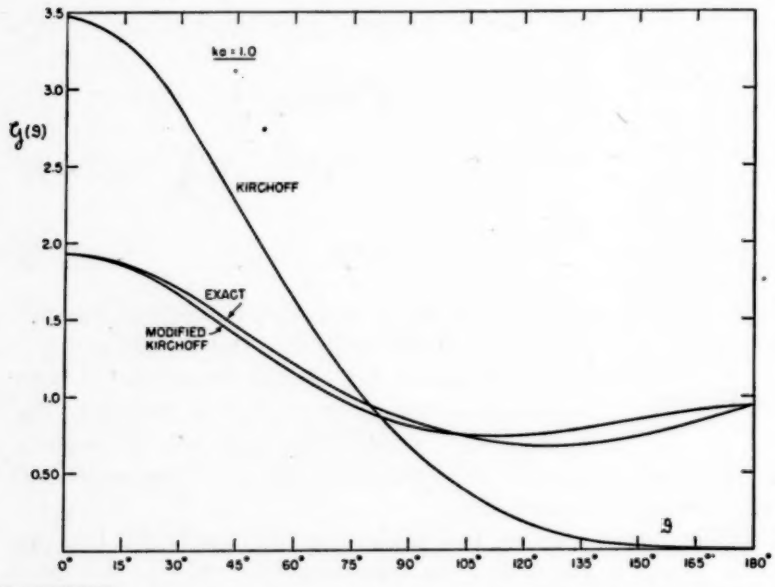

FIG. 10. Comparison of exact and approximate gain functions.

[11] This follows from an investigation of the zeros of $K_1(z) = -(\pi/2)H_1^{(1)}(iz)$; G. N. Watson, *A Treatise on the Theory of Bessel Functions* (Cambridge University Press, Teddington, England, 1945), p. 511.

[12] The zeros of $J_1((k^2-\zeta^2)^{\frac{1}{2}}a)$ at $\zeta = \pm k$ are compensated by the singulartities of $H_1^{(1)}((k^2-\zeta^2)^{\frac{1}{2}}a)$, resulting in a finite value for $L(\zeta)$.

In estimating the z dependence of the integral, it is not permissible to neglect z' in the denominator; if this is done, the integral has the value of the transform $H(\zeta)$ at the pole $\zeta=k$ (corresponding to the incident wave Ae^{ikz}). However, if we replace $H(z)$ by e^{ikz}, it follows that

$$E(z)\sim e^{ikz}/z^2, \quad z\to\infty.$$

This result may be verified by noting that $E(z)$ is proportional to the ρ-derivative of the velocity potential on the surface $\rho=a$ and utilizing the asymptotic form (III. 2b).

The transform

$$E(\zeta)=\int_0^\infty E(z)e^{-i\zeta z}dz=\int_0^\infty E(z)e^{-i\xi z+\eta z}dz \quad \text{(V. 6)}$$

is thus regular in the region $\eta\leqslant\epsilon$.

Collecting results, we find that the strip $|\eta|<\epsilon$ is a common region of regularity for the functions $(k^2-\zeta^2)H(\zeta)$, $L(\zeta)$, and $E(\zeta)$, appearing in the modified form of the transform Eq. (2):

$$(k^2-\zeta^2)H(\zeta)L(\zeta)=2E(\zeta). \quad \text{(V. 7)}$$

It is convenient to designate the regions $\eta>-\epsilon$, $\eta<\epsilon$ as the upper and lower half-planes, respectively (Fig. 6).

In order to solve the transform Eq. (7), we represent $L(\zeta)$ as a quotient of functions $L_+(\zeta)$, $L_-(\zeta)$, which are regular (and not zero) in the upper and lower half-planes, respectively. If the expression

$$L(\zeta)=L_+(\zeta)/L_-(\zeta) \quad \text{(V. 8)}$$

is inserted in (7), it follows that

$$(k^2-\zeta^2)H(\zeta)L_+(\zeta)=2E(\zeta)L_-(\zeta). \quad \text{(V. 9)}$$

The left-hand side of (9) is regular in the upper half-plane and the right-hand side in the lower half-plane. Both are regular in the strip $|\eta|<\epsilon$ and may be considered as analytic continuations of each other; together they define an integral function throughout the finite ζ-plane.

It turns out that the integral function has algebraic behavior at infinity in the respective half-planes and is in fact, a constant. Thus, the transforms $H(\zeta)$, $E(\zeta)$ bear a simple relation to $L_+(\zeta)$, $L_-(\zeta)$, respectively.

We next consider the explicit determination of $L_+(\zeta)$, $L_-(\zeta)$. The function $\log L(\zeta)$ is regular in the strip $|\eta|<\epsilon$, on the branch for which $\log 1=0$. Applying Cauchy's integral formula to a rectangular domain (with sides parallel to the coordinate axes) within the strip, we have

$$\log L(\zeta)=\frac{1}{2\pi i}\oint\frac{\log L(t)}{t-\zeta}dt$$

$$=\frac{1}{2\pi i}\oint\frac{\log\{\pi i H_1^{(1)}[(k^2-t^2)^{\frac{1}{2}}a]J_1[(k^2-t^2)^{\frac{1}{2}}a]\}}{t-\zeta}dt, \quad \text{(V. 10)}$$

where ζ is an internal point.

As $|t|\to\infty$, $\arg(k^2-t^2)^{\frac{1}{2}}=\pi/2$ within the strip, and we find with the help of (A. 11),

$$\log L(t)\sim\log|t|, \quad |t|\to\infty, \quad |Im\, t|<\epsilon.$$

Thus, there are vanishing contributions to the integral (10) from the vertical sections of the rectangular contour as these are displaced to infinity.

Consequently,

$$\log L(\zeta)=\log L_+(\zeta)-\log L_-(\zeta)$$

$$=\frac{1}{2\pi i}\int_{C_+}\frac{\log L(t)}{t-\zeta}dt+\frac{1}{2\pi i}\int_{C_-}\frac{\log L(t)}{t-\zeta}dt, \quad \text{(V. 11)}$$

where C_+, C_- designate infinite straight line contours in the strip $|Im\, t|<\epsilon$ (Fig. 7).

The function

$$L_+(\zeta)=\exp\left[\frac{1}{2\pi i}\int_{C_+}\frac{\log\{\pi i H_1^{(1)}[(k^2-t^2)^{\frac{1}{2}}a]J_1[(k^2-t^2)^{\frac{1}{2}}a]\}}{t-\zeta}dt\right] \quad \text{(V. 12)}$$

is regular and different from zero in the upper half-plane provided ζ does not lie on the contour C_+.

Similarly,

$$L_-(\zeta)=\exp\left[-\frac{1}{2\pi i}\int_{C_-}\frac{\log\{\pi i H_1^{(1)}[(k^2-t^2)^{\frac{1}{2}}a]J_1[(k^2-t^2)^{\frac{1}{2}}a]\}}{t-\zeta}dt\right] \tag{V. 13}$$

defines a non-vanishing regular function in the lower half-plane if ζ does lie on the contour C_-.

First Evaluation of $L_+(\zeta)$, $L_-(\zeta)$

The conversion of (12) and (13) into forms suitable for analytical and numerical manipulation is based on certain deformations of the contours C_+, C_-.

First, we note that in the limit $\epsilon\to 0$ the contours C_+, C_- coincide with the real axis of the t-plane, except for indentations at the points $t=\pm k$ and $t=\zeta$, if ζ is real. The contours are indented above $t=-k$, below $t=k$, and oppositely with respect to $t=\zeta$ (C_+ below, C_- above), thus preserving the correspondence of points in the ζ-plane with the regions of regularity of the functions $L_+(\zeta)$, $L_-(\zeta)$.

Actually, the logarithmic functions in (12) and (13) vanish at $t=\pm k$, so that the integrations are conducted entirely along the real axis with an indentation only if ζ is real.

Inserting the phase of the radical appropriate to the sections of the real axis $|t|<k$, $|t|>k$, and using (A. 6), (A. 7), we find

$$\left\{\begin{matrix}L_+(\zeta)\\ L_-(\zeta)\end{matrix}\right\}=\exp\left[\frac{1}{2\pi i}\int_{-k}^{k}\frac{\log\{\pi i H_1^{(1)}[(k^2-t^2)^{\frac{1}{2}}a]J_1[(k^2-t^2)^{\frac{1}{2}}a]\}}{t-\zeta}dt\right.$$
$$\left.+\frac{\zeta}{\pi i}\int_k^\infty\frac{\log\{2K_1[(t^2-k^2)^{\frac{1}{2}}a]I_1[(t^2-k^2)^{\frac{1}{2}}a]\}}{t^2-\zeta^2}dt\right], \tag{V. 14}$$
$$L_+(-\zeta)=1/L_-(\zeta).$$

We note, on referring to (A. 12), that the integrals along the sections $t>k$, $t<-k$ are individually non-convergent.

When ζ is real, the singular integral of (14) is calculated as the principal value $\pm\pi i$ (residue of the integrand at the pole $t=\zeta$). The choice of sign corresponds to the sense of deformation of the contour, being positive for $L_+(\zeta)$ and negative for $L_-(\zeta)$.

Accordingly, we find

$$L_+(k\cos\vartheta)=[\pi i H_1^{(1)}(ka\sin\vartheta)J_1(ka\sin\vartheta)]^{\frac{1}{2}}\cdot\exp\left[i\frac{ka\cos\vartheta}{\pi}P\int_0^{ka}\frac{x\log[\pi i H_1^{(1)}(x)J_1(x)]}{[x^2-(ka\sin\vartheta)^2][(ka)^2-x^2]^{\frac{1}{2}}}dx\right.$$
$$\left.+i\frac{ka\cos\vartheta}{\pi}\int_0^\infty\frac{x\log[1/2I_1(x)K_1(x)]}{[x^2+(ka\sin\vartheta)^2][x^2+(ka)^2]^{\frac{1}{2}}}dx\right], \tag{V. 15}$$

where P designates the principal value.

The principal value is not required if ζ coincides with either of the branch points $\pm k$, and it turns out that

$$L_+(k)=\frac{1}{L_+(-k)}=\exp\left[i\frac{ka}{\pi}\int_0^{ka}\frac{\log[\pi i H_1^{(1)}(x)J_1(x)]}{x[(ka)^2-x^2]^{\frac{1}{2}}}dx+i\frac{ka}{\pi}\int_0^\infty\frac{\log[1/(2I_1(x)K_1(x))]}{x[x^2+(ka)^2]^{\frac{1}{2}}}dx\right]. \tag{V. 16}$$

Second Evaluation of $L_+(\zeta)$, $L_-(\zeta)$

To avoid questions of convergence with those parts of the integrals (12) and (13) for which $|Re\,t|>Re\,k$, we begin with sections of the contours C_+, C_- extending from $t=-T$ to $t=T$. Later we proceed to the limit $T\to\infty$.

The abbreviated contour C_+' may be replaced by the contours Γ_1, Γ_2 shown in Fig. 8. Γ_1 is extended along the sides of a horizontal branch cut which is drawn from the point $t=-k$, and Γ_2 proceeds along the under side of the branch cut on to the point $t=T$ of the original contour C_+.

In this discussion, we employ the logarithmic derivative

$$\frac{d}{d\zeta}\log L_+(\zeta)=\frac{1}{2\pi i}\int_{C_+'}\frac{\log\{\pi i H_1^{(1)}[(k^2-t^2)^{\frac{1}{2}}a]J_1[(k^2-t^2)^{\frac{1}{2}}a]\}}{(t-\zeta)^2}dt, \tag{V. 17}$$

from which $L_+(\zeta)$ is determined, exclusive of a multiplicative constant, by a single integration. If the point $t=\zeta$ is located in the upper half-plane, C_+' or any equivalent contours may be freely deformed in the lower half-plane provided we do not pass through singularities of the logarithm in the integrand of (17).

Combining the integrands of (17) on the upper and lower sections of Γ_1 we find, using (A. 6)–(A. 9),

$$\frac{d}{d\zeta}\log L_+(\zeta)\bigg|_{\Gamma_1}=-\frac{1}{2\pi i}\int_k^T\log\left\{\frac{K_1([t^2-k^2]^{\frac{1}{2}}a)+\pi e^{-i\pi/2}I_1([t^2-k^2]^{\frac{1}{2}}a)}{K_1[(t^2-k^2)^{\frac{1}{2}}a]}\right\}\frac{dt}{(t+\zeta)^2}. \tag{V. 18}$$

It follows from (A. 13) that (18) diverges logarithmically in the limit $T\to\infty$; if we supply the factor $\exp[i(\pi/2)-2a(t^2-k^2)^{\frac{1}{2}}]$ to the argument of the logarithm, the singular dependence may be isolated, with the result

$$\frac{d}{d\zeta}\log L_+(\zeta)\bigg|_{\Gamma_1}=\frac{ia}{\pi}\lim_{T\to\infty}\left\{\log\frac{2T}{k}+\frac{1}{4}\frac{1}{k+\zeta}-\frac{ia}{\pi}\left[1+\frac{2\zeta}{(k^2-\zeta^2)^{\frac{1}{2}}}\tan^{-1}\left(\frac{k-\zeta}{k+\zeta}\right)^{\frac{1}{2}}\right]\right.$$
$$\left.-\frac{1}{2\pi i}\int_k^\infty\log\left\{\frac{e^{i\pi/2}K_1[(t^2-k^2)^{\frac{1}{2}}a]+\pi I_1[(t^2-k^2)^{\frac{1}{2}}a]}{K_1[(t^2-k^2)^{\frac{1}{2}}a]}\exp[-2a(t^2-k^2)^{\frac{1}{2}}]\right\}\frac{dt}{(t+\zeta)^2}\right\}. \tag{V. 19}$$

Next, we close the contour Γ_2 as shown in Fig. 8, proceeding along circular arcs in the lower half-plane and on opposite sides of a branch cut along the negative imaginary axis (which is drawn through the zeros $t=-i(\gamma_n^2-k^2)^{\frac{1}{2}}$ of the Bessel function $J_1[(k^2-t^2)^{\frac{1}{2}}a]$). On this complete contour (17) vanishes since the integrand is analytic at all interior points. Thus the integral along Γ_2 may be expressed in terms of integrals along the remainder of the closed contour; if these be traversed in the same sense, we have

$$\int_{\Gamma_2}=-\int_{\text{arcs}}-\int_{\text{branch cut}}. \tag{V. 20}$$

Referring to (A. 11), it follows that the integral (17) along a circular arc in the third quadrant, on which $-\pi/2<\arg(k^2-t^2)^{\frac{1}{2}}<0$, takes the constant value

$$\frac{1}{2\pi i}\int_{\text{arc}}\frac{dt}{t^2}(2i)(ita)=\frac{a}{2} \tag{V. 21}$$

in the limit $T\to\infty$. The integral along a circular arc in the fourth quadrant, on which $0<\arg(k^2-t^2)^{\frac{1}{2}}<\pi/2$, vanishes in this limit.

The value of the remaining integral in (20) depends upon the difference in phase of the integrand on opposite sides of the branch cut along the negative imaginary axis.

Using the asymptotic expansion

$$\gamma_n a\sim(n+\tfrac{1}{4})\pi+0\left(\frac{1}{n}\right),\quad n\gg 1, \tag{V. 22}$$

we find that the number of zeros of $J_1[(k^2-t^2)^{\frac{1}{2}}a]$ contained on the section of the negative imaginary

axis $|Im\, t| < T$, is

$$n_T \sim [\gamma_n a/\pi] = [Ta/\pi], \quad Ta/\pi \gg 1;$$

here $[Ta/\pi]$ is the largest integer not exceeding Ta/π.

Thus, since the functions $H_1^{(1)}([k^2-t^2]^{\frac{1}{2}}a)$ and

$$J_1([k^2-t^2]^{\frac{1}{2}}a) \Big/ \prod_{n=1}^{[Ta/\pi]} [t+i(\gamma_n{}^2-k^2)^{\frac{1}{2}}]$$

have the same phase on opposite sides of the branch cut, the integral becomes

$$\frac{1}{2\pi i}\int_{\text{branch cut}} \log \prod_{n=1}^{[Ta/\pi]} [t+i(\gamma_n{}^2-k^2)^{\frac{1}{2}}] \frac{dt}{(t-\zeta)^2} = \sum_{n=1}^{[Ta/\pi]} \int_{t=-i(\gamma_n{}^2-k^2)^{\frac{1}{2}}}^{-iT} \frac{dt}{(t-\zeta)^2}$$

$$= \sum_{n=1}^{[Ta/\pi]} \left(\frac{1}{\zeta+iT} - \frac{1}{\zeta+i[\gamma_n{}^2-k^2]^{\frac{1}{2}}} \right). \quad \text{(V. 23)}$$

Further, since

$$\lim_{m\to\infty} \left[\sum_{n=1}^{m} \frac{1}{n} - \log m \right] = \log \gamma = 0.5772,$$

we have

$$\lim_{T\to\infty} \sum_{n=1}^{[Ta/\pi]} \left[\frac{1}{\zeta+iT} - \frac{1}{\zeta+(\gamma_n{}^2-k^2)^{\frac{1}{2}}} \right] = \frac{ia}{\pi} \lim_{T\to\infty} \log \frac{Ta\gamma}{\pi} - \frac{ia}{\pi} - \sum_{n=1}^{\infty} \left[\frac{1}{\zeta+i(\gamma_n{}^2-k^2)^{\frac{1}{2}}} + \frac{ia}{n\pi} \right]. \quad \text{(V. 24)}$$

Collecting the results (21) and (24) for use in (20), we find

$$\frac{d}{d\zeta} \log L_+(\zeta) \Big|_{\Gamma_2} = -\frac{ia}{\pi} \lim_{T\to\infty} \log \frac{Ta\gamma}{\pi} + \frac{ia}{\pi} - \frac{a}{2} + \sum_{n=1}^{\infty} \left[\frac{1}{\zeta+i(\gamma_n{}^2-k^2)^{\frac{1}{2}}} + \frac{ia}{n\pi} \right]. \quad \text{(V. 25)}$$

When (19) and (25) are combined, the arbitrary parameter T conveniently disappears and we have

$$\frac{d}{d\zeta} \log L_+(\zeta) = \frac{1}{4(k+\zeta)} + \frac{ia}{\pi} \log \frac{2\pi i}{\gamma k a} - \frac{2i\zeta a}{\pi(k^2-\zeta^2)^{\frac{1}{2}}} \tan^{-1}\left(\frac{k-\zeta}{k+\zeta} \right)^{\frac{1}{2}} + \sum_{n=1}^{\infty} \left[\frac{1}{\zeta+i(\gamma_n{}^2-k^2)^{\frac{1}{2}}} + \frac{ia}{n\pi} \right]$$

$$- \frac{1}{2\pi i} \int_k^{\infty} \log \left\{ \frac{e^{i\pi/2} K_1([t^2-k^2]^{\frac{1}{2}}a) + \pi I_1([t^2-k^2]^{\frac{1}{2}}a)}{K_1[(t^2-k^2)^{\frac{1}{2}}a]} \right.$$

$$\left. \times \exp[-2a(t^2-k^2)^{\frac{1}{2}}] \right\} \frac{dt}{(t+\zeta)^2}. \quad \text{(V. 26)}$$

Integrating with respect to ζ and supplying an integration constant, it follows that

$$L_+(\zeta) = C((k+\zeta)a)^{\frac{1}{2}} F_+(\zeta) \prod_{n=1}^{\infty} \left\{ \left[1 - \left(\frac{k}{\gamma_n} \right)^2 \right]^{\frac{1}{2}} - \frac{i\zeta}{\gamma_n} \right\} e^{i\zeta a/n\pi}$$

$$\cdot \exp\left[\frac{i\zeta a}{\pi} \left(\log \frac{2\pi i}{\gamma k a} + 1 \right) + \frac{2ia}{\pi} (k^2-\zeta^2)^{\frac{1}{2}} \tan^{-1}\left(\frac{k-\zeta}{k+\zeta} \right)^{\frac{1}{2}} \right], \quad \text{(V. 27)}$$

where

$$F_+(\zeta) = \exp\left[\frac{1}{2\pi i} \int_k^{\infty} \log \left\{ \frac{e^{i\pi/2} K_1[(t^2-k^2)^{\frac{1}{2}}a] + \pi I_1[(t^2-k^2)^{\frac{1}{2}}a]}{K_1[(t^2-k^2)^{\frac{1}{2}}a]} \exp[-2a(t^2-k^2)^{\frac{1}{2}}] \right\} \frac{dt}{t+\zeta} \right]. \quad \text{(V. 28)}$$

The infinite product in (27) converges uniformly in the upper half-plane. This result follows from (22) since for any value of ζ

$$\{[1-(k/\gamma_n)^2]^{\frac{1}{2}}-i\zeta/\gamma_n\}e^{i\zeta a/n\pi}\sim 1+a_n(\zeta),\quad a_n(\zeta)=O(1/n^2),\quad Im\,\zeta>0,\quad n\gg\max([ka],[|\zeta a|]).^{13}$$

On deforming the contour C_- in the upper half-plane, and employing similar procedures, we find (in view of the symmetry of $L(\zeta)$ with regard to ζ)

$$\frac{1}{L_-(\zeta)}=L_+(-\zeta)=C((k-\zeta)a)^{\frac{1}{2}}\frac{1}{F_-(\zeta)}\prod_{n=1}^{\infty}\left\{\left[1-\left(\frac{k}{\gamma_n}\right)^2\right]^{\frac{1}{2}}+\frac{i\zeta}{\gamma_n}\right\}e^{-i\zeta a/n\pi}\cdot$$

$$\cdot\exp\left[-\frac{i\zeta a}{\pi}\log\left(\frac{2\pi i}{\gamma ka}+1\right)+\frac{2ia}{\pi}(k^2-\zeta^2)^{\frac{1}{2}}\tan^{-1}\left(\frac{k+\zeta}{k-\zeta}\right)^{\frac{1}{2}}\right],\quad (V.29)$$

(V. 23) where

$$F_-(\zeta)=\frac{1}{F_+(-\zeta)}=\exp\left[-\frac{1}{2\pi i}\int_k^{\infty}\log\left\{\frac{e^{i\pi/2}K_1[(t^2-k^2)^{\frac{1}{2}}a]+\pi I_1[(t^2-k^2)^{\frac{1}{2}}a]}{K_1[(t^2-k^2)^{\frac{1}{2}}a]}\right.\right.$$

$$\left.\left.\times\exp[-2a(t^2-k^2)^{\frac{1}{2}}]\right\}\frac{dt}{t-\zeta}\right].\quad (V.30)$$

(V. 24) To determine the constant C we multiply (27) and (29) and obtain, on referring to (8),

$$\pi iH_1^{(1)}[(k^2-\zeta^2)^{\frac{1}{2}}a]J_1[(k^2-\zeta^2)^{\frac{1}{2}}a]$$

$$=C^2((k^2-\zeta^2)a^2)^{\frac{1}{2}}F_+(\zeta)F_+(-\zeta)\exp[ia(k^2-\zeta^2)^{\frac{1}{2}}]\prod_{n=1}^{\infty}\left(1-\frac{k^2-\zeta^2}{\gamma_n^2}\right).\quad (V.31)$$

(V. 25) Introducing the product representation

$$J_1(za)=\frac{za}{2}\prod_{n=1}^{\infty}\left(1-\frac{z^2}{\gamma_n^2}\right)$$

in (31), it follows that

$$C^2F_+(\zeta)F_+(-\zeta)=\frac{\pi i}{2}((k^2-\zeta^2)a^2)^{\frac{1}{2}}H_1^{(1)}([k^2-\zeta^2]^{\frac{1}{2}}a)\exp[-ia(k^2-\zeta^2)^{\frac{1}{2}}].\quad (V.32)$$

(V. 26) We next examine the form of this equation as $|\zeta|\to\infty$ within the strip $|\eta|<\epsilon$. Employing the asymptotic expressions (A. 10) and

$$F_+(\pm\zeta)\sim\exp\left[\pm\frac{1}{2\pi i}\frac{1}{\zeta a}\int_0^{\infty}\log\left\{\frac{e^{i\pi/2}K_1(x)+\pi I_1(x)}{k_1(x)}e^{-2x}\right\}\frac{xdx}{(x^2+(ka)^2)^{\frac{1}{2}}}\right]\to 1,\quad |\zeta|\to\infty$$

(V. 27) we find

$$C^2=(\tfrac{1}{2}\pi)^{\frac{1}{2}}e^{-i\pi/4}.\quad (V.33)$$

(V. 28)

[13] The condition for uniform convergence is stated in E. T. Whittaker and G. N. Watson, *A Course of Modern Analysis* (Cambridge University Press, Teddington, 1944), p. 49.

Consequently,

$$L_+(k\cos\vartheta)=\left\{\frac{\pi ka}{2}(1+\cos\vartheta)\right\}^{\frac{1}{4}}\left\{\frac{2J_1(ka\sin\vartheta)}{ka\sin\vartheta}\right\}^{\frac{1}{2}}\exp\left[-\frac{i\pi}{8}+\frac{ika\cos\vartheta}{\pi}\left(\log\frac{2\pi i}{\gamma ka}+1\right)+i\vartheta\frac{ka\sin\vartheta}{\pi}\right.$$
$$\left.-i\sum_{n=1}^{\infty}\left(\sin^{-1}\frac{k\cos\vartheta}{(\gamma_n^2-k^2\sin^2\vartheta)^{\frac{1}{2}}}-\frac{ka\cos\vartheta}{n\pi}\right)\right.$$
$$\left.+\frac{1}{2\pi i}\int_0\frac{\log\left\{\dfrac{e^{i\pi/2}K_1(x)+\pi I_1(x)}{K_1(x)}e^{-2x}\right\}}{(x^2+(ka)^2)^{\frac{1}{2}}+ka\cos\vartheta}\frac{xdx}{(x^2+(ka)^2)^{\frac{1}{2}}}\right]. \quad (V.34)$$

Equation (32) allows a simple determination of the behavior of $F_+(\zeta)$ near the point $\zeta=-k$. On approximating the Hankel function of small argument by means of (A. 1)–(A. 3) and using (33), it follows that

$$F_+(\zeta)\sim\left(\frac{2}{\pi}\right)^{\frac{1}{2}}e^{i\pi/4}\frac{(2ka)^{-\frac{1}{2}}((k+\zeta)a)^{-\frac{1}{2}}}{F_+(k)}, \quad \zeta\to-k. \quad (V.35)$$

Combining (35) with (27) and (28), we find

$$L_+(k)=\frac{1}{L_+(-k)}=(\pi ka)^{\frac{1}{4}}\exp\left[-\frac{i\pi}{8}+\frac{ika}{\pi}\left(\log\frac{2\pi i}{\gamma ka}+1\right)-i\sum_{n=1}^{\infty}\left(\sin^{-1}\frac{k}{\gamma_n}-\frac{ka}{n\pi}\right)\right.$$
$$\left.+\frac{1}{2\pi i}\int_0^{\infty}\frac{\log\left\{\dfrac{e^{i\pi/2}K_1(x)+\pi I_1(x)}{K_1(x)}e^{-2x}\right\}}{(x^2+(ka)^2)^{\frac{1}{2}}+ka}\frac{xdx}{(x^2+(ka)^2)^{\frac{1}{2}}}\right]. \quad (V.36)$$

Further, on inserting the value of C in (32), and setting $\zeta=0$, it follows that

$$\int_0^{\infty}\log\left\{\frac{e^{i\pi/2}K_1(x)+\pi I_1(x)}{K_1(x)}e^{-2x}\right\}\frac{xdx}{x^2+(ka)^2}=\pi i\log\left\{\left(\frac{\pi ka}{2}\right)^{\frac{1}{2}}\exp[i(\tfrac{3}{4}\pi-ka)]H_1^{(1)}(ka)\right\}; \quad (V.37)$$

finally, on extracting the real part of this integral, and proceeding to the limit $ka\to0$, we find

$$\int_0^{\infty}\log\left\{\left[1+\left(\frac{\pi I_1(x)}{K_1(x)}\right)^2\right]^{\frac{1}{2}}e^{-2x}\right\}\frac{dx}{x}$$
$$=\lim_{ka\to0}Re\left[\pi i\log\left\{\left(\frac{\pi ka}{2}\right)^{\frac{1}{2}}\exp[i(\tfrac{3}{4}\pi-ka)]H_1^{(1)}(ka)\right\}\right]=-\pi^2/4. \quad (V.38)$$

Having completed the decomposition of $L(\zeta)$, we return to the transform Eq. (9). In order to determine the nature of the integral function defined by this equation, we examine the form of both members as $|\zeta|\to\infty$ in their respective half-planes of regularity.

According to (3), the order of magnitude of $H(\zeta)$ in the upper half-plane is determined by the behavior of $H(z)$ for small negative values of z. The velocity potentials on inner and outer surfaces of the pipe are continuous functions of z which assume equal values on the surface $\rho=a$, $z>0$. Therefore, $H(z)$ is a continuous function of z which vanishes for positive z, and we may write

$$H(z)\sim z^{\alpha}, \quad \alpha>0, \quad z\to0^-. \quad (V.39)$$

We thus deduce from (3)

$$H(\zeta)\sim(-i\zeta)^{-\alpha-1}, \quad |\zeta|\to\infty, \quad Im\ \zeta>0. \tag{V. 40}$$

Similarly, the order of magnitude of $E(\zeta)$ in the lower half-plane is determined by the behavior of $E(z)$ for small positive values of z. $E(z)$ has an integrable singularity at $z=0$ (being related to the component of the particle velocity along the cylindrical radius, at the periphery of the pipe), and we write

$$E(z)\sim z^{-\beta}, \quad \beta<1, \quad z\to 0^+. \tag{V. 41}$$

We thus deduce from (6),

$$E(\zeta)\sim(i\zeta)^{\beta-1}, \quad |\zeta|\to\infty, \quad Im\ \zeta<0. \tag{V. 42}$$

The asymptotic forms of $L_+(\zeta)$, $L_-(\zeta)$ are given in Appendix B; combining these with (40) and (42), we find:

$$\begin{aligned} \text{integral function} &= (k^2-\zeta^2)H(\zeta)L_+(\zeta)\sim(-i\zeta)^{\frac{1}{2}-\alpha} && \text{upper half-plane} \\ &= 2E(\zeta)L_-(\zeta)\sim(i\zeta)^{\beta-\frac{1}{2}}, \quad |\zeta|\to\infty && \text{lower half-plane.} \end{aligned}$$

In view of the bounds on α, β it follows that the integral function cannot become infinite, in the upper and lower half-planes, as rapidly as the square root of ζ. Such an integral function is a polynomial of degree less than $\frac{1}{2}$, i.e., a constant. Consequently, the values of α, β are each $\frac{1}{2}$, and $H(\zeta)$, $E(\zeta)$ are specified by the known functions $L_+(\zeta)$, $L_-(\zeta)$ in accordance with the equations

$$H(\zeta)=C/[(k^2-\zeta^2)L_+(\zeta)], \quad E(\zeta)=C/[2L_-(\zeta)], \tag{V. 43}$$

in which C is a constant.

VI. EVALUATION OF PHYSICAL QUANTITIES

It is a simple matter now to evaluate the physical quantities by means of the formulation developed in Section III.

To obtain the velocity potential reflection coefficient, we insert the values (compare (V. 43))

$$\mathrm{Res}_{\zeta=\pm k}H(\zeta)=\mp C/2kL_+(\pm k)$$

in (III. 15), and find

$$R=-L_+(k)/L_+(-k). \tag{VI. 1}$$

Employing (V. 16), it follows that

$$R=-|R|e^{2ikl}=-(L_+(k))^2, \tag{VI. 2}$$

where

$$|R|=|L_+(k)|^2=\exp\left\{-\frac{2ka}{\pi}\int_0^{ka}\frac{\tan^{-1}(-J_1(x)/N_1(x))}{x[(ka)^2-x^2]^{\frac{1}{2}}}dx,\right\} \tag{VI. 3}$$

and

$$\frac{l}{a}=\frac{1}{\pi}\int_0^{ka}\frac{\log\{\pi J_1(x)[(J_1(x))^2+(N_1(x))^2]^{\frac{1}{2}}\}}{x[(ka)^2-x^2]^{\frac{1}{2}}}dx+\frac{1}{\pi}\int_0^{\infty}\frac{\log\{1/[2I_1(x)K_1(x)]\}}{x(x^2+(ka)^2)^{\frac{1}{2}}}dx. \tag{VI. 4}$$

Alternatively, using (V. 36), (V. 38), we find

$$|R|=(\pi ka)^{\frac{1}{2}}\exp\left[-ka+\frac{1}{\pi}\int_0^{\infty}\tan^{-1}\left(\frac{K_1(x)}{\pi I_1(x)}\right)\left(1-\frac{ka}{(x^2+(ka)^2)^{\frac{1}{2}}}\right)\frac{dx}{x}\right], \tag{VI. 5}$$

and

$$\frac{l}{a}=\frac{1}{\pi}\left(\log\frac{2\pi}{\gamma ka}+1\right)-\frac{1}{ka}\sum_{n=1}^{\infty}\left(\sin^{-1}\frac{k}{\gamma_n}-\frac{ka}{n\pi}\right)+\frac{1}{2\pi}\int_0^{\infty}\log\left\{\left[1+\left(\frac{\pi I_1(x)}{K_1(x)}\right)^2\right]^{\frac{1}{2}}e^{-2x}\right\}\frac{dx}{x(x^2+(ka)^2)^{\frac{1}{2}}}. \tag{VI. 6}$$

To obtain the power-gain function, we insert the expression

$$H(k\cos\vartheta) = C/[(k\sin\vartheta)^2 L_+(k\cos\vartheta)]$$

in (III. 25), and find, with reference to (1), (3),

$$\mathcal{G}(\vartheta) = \left(\frac{2J_1(ka\sin\vartheta)}{\sin\vartheta}\right)^2 \frac{|R|}{1-|R|^2} \frac{1}{|L_+(k\cos\vartheta)|^2}. \tag{VI. 7}$$

Employing (V. 15), it follows that

$$\mathcal{G}(\vartheta) = \frac{4}{\pi\sin^2\vartheta} \frac{J_1(ka\sin\vartheta)}{[(J_1(ka\sin\vartheta))^2+(N_1(ka\sin\vartheta))^2]^{\frac{1}{2}}} \frac{|R|}{1-|R|^2}$$

$$\times\exp\left[\frac{2ka\cos\vartheta}{\pi} P\int_0^{ka} \frac{x\tan^{-1}(-J_1(x)/N_1(x))dx}{[x^2-(ka\sin\vartheta)^2][x^2+(ka)^2]^{\frac{1}{2}}}\right]. \tag{VI. 8}$$

From (3) and (8) we may readily verify the simple forms of the gain function appropriate to the directions $\vartheta = 0, \pi/2, \pi$, as given in Section I.

Alternatively, using (V. 34) in conjunction with (7), we find

$$\mathcal{G}(\vartheta) = 2\left(\frac{2ka}{\pi}\right)^{\frac{1}{2}} \frac{J_1(ka\sin\vartheta)}{\sin\vartheta(1+\cos\vartheta)^{\frac{1}{2}}} \frac{|R|}{1-|R|^2}$$

$$\times\exp\left[ka\cos\vartheta - \frac{1}{\pi}\int_0^{\infty} \frac{\tan^{-1}(K_1(x)/\pi I_1(x))}{(x^2+(ka)^2)^{\frac{1}{2}}+ka\cos\vartheta} \frac{xdx}{(x^2+(ka)^2)^{\frac{1}{2}}}\right]. \tag{VI. 9}$$

The identical simplification of (9), for the special directions considered above, may be confirmed with the use of (V. 37) and (5).

It remains to be shown that the gain function is correctly normalized. According to the definition (III. 20), this implies that the result of integrating (8) or (9) over the complete solid angle subtended at the mouth of the pipe is 4π. Since the gain function is symmetric about the axis of the pipe, this condition may be stated as

$$\int_0^{\pi} \mathcal{G}(\vartheta)\sin\vartheta d\vartheta = 2. \tag{VI. 10}$$

We now verify (10) for the first form of the gain function. Let us consider the integral

$$I = \int_C \exp\left[-\frac{1}{\pi}\int_{-1}^{1} \tan^{-1}\left\{-\frac{J_1[(1-t^2)^{\frac{1}{2}}ka]}{N_1[(1-t^2)^{\frac{1}{2}}ka]}\right\} \frac{dt}{t-\frac{1}{2}(z+(1/z))}\right] \frac{dz}{z^2-1}, \tag{VI. 11}$$

extended over the contour shown in Fig. 9. If z lies on the arc of the unit circle, the t integration contour is indented above the pole $t = \frac{1}{2}(z+1/z) = \cos\vartheta$. This pole disappears if z is located on the section of the real axis, $|z|<1$, since $|\frac{1}{2}(z+(1/z))|>1$ and thus lies outside the range of the t integral. Furthermore, the integrand of (11) is analytic on the indentations at $z=\pm 1$ (of radius δ) and everywhere within the contour since $Im\, t = 0$, and $Im\, \frac{1}{2}(z+1/z) = -\frac{1}{2}(1/|z| - |z|)\sin\vartheta < 0$.

Thus the integral I vanishes, and we deduce that the result of integrating along the arc of the unit circle and the section of the real axis is $\pi i/2$ (sum of residues of the integrand at the poles

$z=\pm 1$). Using (3), we find

$$\int_0^{\pi-\delta} \exp\left[-\frac{1}{\pi}\int_{-1}^{1}\tan^{-1}\left\{-\frac{J_1[(1-t^2)^{\frac{1}{2}}ka]}{N_1[(1-t^2)^{\frac{1}{2}}ka]}\right\}\frac{dt}{t-\cos\vartheta}\right]\frac{d\vartheta}{2\sin\vartheta}$$

$$+\int_{-1+\delta}^{1-\delta}\exp\left[-\frac{1}{\pi}\int_{-1}^{1}\tan^{-1}\left\{-\frac{J_1[(1-t^2)^{\frac{1}{2}}ka]}{N_1[(1-t^2)^{\frac{1}{2}}ka]}\right\}\frac{dt}{t-\frac{1}{2}(x+1/x)}\right]\frac{dx}{x^2-1}$$

$$=\frac{\pi i}{2}\frac{1}{2}\left(\exp\left[-\frac{1}{\pi}\int_{-1}^{1}\tan^{-1}\left\{-\frac{J_1[(1-t^2)^{\frac{1}{2}}ka]}{N_1[(1-t^2)^{\frac{1}{2}}ka]}\right\}\frac{dt}{t-1}\right]\right.$$

$$\left.-\exp\left[-\frac{1}{\pi}\int_{-1}^{1}\tan^{-1}\left\{-\frac{J_1[(1-t^2)^{\frac{1}{2}}ka]}{N_1[(1-t^2)^{\frac{1}{2}}ka]}\right\}\frac{dt}{t+1}\right]\right)=\frac{\pi i}{4}\left(\frac{1}{|R|}-|R|\right). \quad \text{(VI. 12)}$$

Since

$$Im\exp\left\{i\tan^{-1}\left(-\frac{J_1(ka\sin\vartheta)}{N_1(ka\sin\vartheta)}\right)\right\}=\frac{J_1(ka\sin\vartheta)}{[(J_1(ka\sin\vartheta))^2+(N_1(ka\sin\vartheta))^2]^{\frac{1}{2}}},$$

it follows that

$$Im\exp\left\{-\frac{1}{\pi}\int_{-1}^{1}\tan^{-1}\left\{-\frac{J_1[(1-t^2)^{\frac{1}{2}}ka]}{N_1[(1-t^2)^{\frac{1}{2}}ka]}\right\}\frac{dt}{t-\cos\vartheta}\right\}$$

$$=\frac{J_1(ka\sin\vartheta)\exp\left\{-\frac{1}{\pi}P\int_{-1}^{1}\tan^{-1}\left\{-\frac{J_1[(1-t^2)^{\frac{1}{2}}ka]}{N_1[(1-t^2)^{\frac{1}{2}}ka]}\right\}\frac{dt}{t-\cos\vartheta}\right\}}{[(J_1(ka\sin\vartheta))^2+(N_1(ka\sin\vartheta))^2]^{\frac{1}{2}}}. \quad \text{(VI. 13)}$$

The contour of integration in (13) is indented above the point $t=\cos\vartheta$, and P designates the principal value.

On extracting the imaginary part of (12), we find by referring to (8) and (13) and passing to the limit $\delta\to 0$,

$$\int_0^{\pi}\frac{J_1(ka\sin\vartheta)}{[(J_1(ka\sin\vartheta))^2+(N_1(ka\sin\vartheta))^2]^{\frac{1}{2}}}\exp\left\{-\frac{1}{\pi}P\int_{-1}^{1}\tan^{-1}\left\{-\frac{J_1[(1-t^2)^{\frac{1}{2}}ka]}{N_1[(1-t^2)^{\frac{1}{2}}ka]}\right\}\frac{dt}{t-\cos\vartheta}\right\}$$

$$=\frac{\pi}{8}\frac{1-|R|^2}{|R|}\int_0^{\pi}\mathfrak{S}(\vartheta)\sin\vartheta d\vartheta=\frac{\pi}{4}\frac{1-|R|^2}{|R|},$$

or,

$$\int_0^{\pi}\mathfrak{S}(\vartheta)\sin\vartheta d\vartheta=2.$$

VII. APPROXIMATION FORMULAS AND METHODS

The exact formulas for the magnitude of the reflection coefficient admit simple approximations when suitable restrictions are imposed on the values of ka.

Equation (VI. 3) provides a convenient basis for approximation in the range $ka<1$; this range corresponds to low frequency sound vibrations or wave-lengths large compared to the diameter of the pipe. On expanding the arc tangent in ascending powers of the argument, and employing the corresponding series representations of the Bessel and Neumann functions, (A. 1), (A. 2), we find

$$|R|\doteq\exp[-(ka)^2/2]\left(1+\tfrac{1}{8}(ka)^4\left[\log\frac{1}{\gamma ka}+\frac{19}{12}\right]\right), \quad ka<1. \quad \text{(VII. 1)}$$

At $ka=1$, the value of $|R|$ computed from (1) is in excess of the correct value by less than 3 percent; the deviations decrease with smaller values of ka.

An approximation for l/a in this range is more difficult to obtain; Fig. 2 indicates, however, that here the deviations from the static value ($l/a=0.6133$, $ka=0$) are small.

For values of ka greater than unity, we use (VI. 5) as the basis for approximation. The result of expanding the integrand in inverse powers of ka is

$$\int_0^\infty \tan^{-1}\left(\frac{K_1(x)}{\pi I_1(x)}\right)\left(1-\frac{ka}{(x^2+(ka)^2)^{\frac{1}{2}}}\right)\frac{dx}{x}$$
$$=\frac{1}{2(ka)^2}\int_0^\infty x\tan^{-1}\left(\frac{K_1(x)}{\pi I_1(x)}\right)dx+O\left(\frac{1}{(ka)^4}\right);$$

thus, on retaining only the first term of the expansion, and noting from (V. 37) that

$$\int_0^\infty x\tan^{-1}\left(\frac{K_1(x)}{\pi I_1(x)}\right)dx=\pi(ka)^2$$
$$\times\lim_{ka\to\infty}\left\{\left[\frac{\pi ka}{2}\{(J_1(ka))^2+(N_1(ka))^2\}\right]^{\frac{1}{2}}\right\}=\frac{3\pi}{16},$$

we find

$$|R|\doteq(\pi ka)^{\frac{1}{2}}e^{-ka}\left(1+\frac{3}{32}\frac{1}{(ka)^2}\right),\quad ka>1. \quad \text{(VII. 2)}$$

At $ka=1$, Eq. (2) yields a value smaller than the correct one by about 3 percent; the deviations are less than 1 percent for $ka>2$.

In consequence of the logarithmic singularity of the first integrand in (VI. 4) at the zeros of the Bessel function, the values of l/a abruptly decrease near $ka=3.832$.

It is of interest to compare the results of a rigorous formulation of the problem with those obtained by approximation methods; the comparison serves to determine the applicability of these methods in problems of a related nature, whose exact solution is difficult to obtain (e.g., for cylindrical pipes with different cross sections).

Approximation methods for the calculation of the reflection coefficient are not easily devised; however, it is possible to account in a simple manner for the directional properties of the radiation field. In the latter connection, we proceed via an assumed expression for the discontinuity of the velocity potential at the surface of the pipe. Representing this quantity as a combination of incident and reflected dominant mode waves,

$$H(z)=e^{ikz}+Re^{-ikz},\quad z\leqslant 0,$$
$$=0,\quad z>0, \quad \text{(VII. 3)}$$

where R is the reflection coefficient, it follows that

$$H(\zeta)=i\left(\frac{1}{\zeta-k}+\frac{R}{\zeta+k}\right). \quad \text{(VII. 4)}$$

Substituting from (4) in (III. 24), we find, after inserting a normalization factor,

$$\mathcal{G}(\vartheta)=\frac{1}{N}\left(\frac{J_1(ka\sin\vartheta)}{\sin\vartheta}\right)^2\frac{1}{1-|R|^2}[(1+\cos\vartheta)^2$$
$$-2\sin^2\vartheta Re\,R+(1-\cos^2\vartheta)|R|^2]. \quad \text{(VII. 5)}$$

We note that (5) has the correct functional dependence on $|R|$, when evaluated in the directions $\vartheta=0,\pi$. On imposing the normalization condition (VI. 10), we find

$$N=\frac{1+|R|^2}{1-|R|^2}-\frac{1}{2ka}\frac{|1+R|^2}{1-|R|^2}\int_0^{2ka}J_0(t)dt$$
$$+\frac{2}{ka}\frac{Re\,R}{1-|R|^2}J_1(2ka). \quad \text{(VII. 6)}$$

If the reflected wave is omitted in (3), we obtain, instead of (5),

$$\mathcal{G}(\vartheta)=\frac{1}{N}\left(\frac{1+\cos\vartheta}{\sin\vartheta}J_1(ka\sin\vartheta)\right)^2, \quad \text{(VII. 7)}$$

where the normalization factor is given by

$$N=1-\frac{1}{2ka}\int_0^{2ka}J_0(t)dt,$$
$$\doteq\tfrac{1}{3}(ka)^2,\quad ka\ll 1,$$
$$\doteq 1-1/2ka,\quad ka\gg 1. \quad \text{(VII. 8)}$$

Equation (7) corresponds to the result of the Kirchoff approximation, in which the radiation field is calculated from the incident field and its normal derivatives at the mouth of the pipe. The Kirchoff approximation is least accurate at low frequencies, predicting a non-isotropic gain function in the limit $ka \to 0$ (compare Fig. 3) which decreases from a value 3 in the forward direction to 0 in the backward direction.

A considerable improvement on the Kirchoff result is achieved by inserting the correct values of the reflection coefficient in (5) and (6). The accuracy of this modified Kirchoff formula is shown by the comparison curves of Fig. 10, calculated for the value $ka=1$. This feature is in accord with the fact that the radiation field is derived principally from the surface discontinuity of the velocity potential on a section of the pipe, terminating at the mouth, whose linear dimension is comparable to the wave-length. At low frequencies, the length of this section is large compared to the transverse dimension of the pipe, and the radiation field can be accurately derived from the asymptotic form of the velocity potential within the pipe.

Rigorous solutions have also been obtained for the problem of electromagnetic radiation from a semi-infinite circular wave guide. We expect to publish the details shortly.

ACKNOWLEDGMENT

The authors wish to thank Miss Barbara Siegle for carrying out the numerical calculations.

APPENDIX A

Summary of Formulas Involving First-Order Cylinder Functions

$$J_1(z)=\sum_{m=0}^{\infty}\frac{(-1)^m(z/2)^{2m+1}}{m!(m+1)!}, \tag{A. 1}$$

$$N_1(z)=\frac{2}{\pi}\log(z/2)\cdot J_1(z)-\frac{2}{\pi z}-\frac{1}{\pi}\sum_{m=0}^{\infty}\frac{(-1)^m(z/2)^{2m+1}}{m!(m+1)!}\times(\psi(m+1)+\psi(m+2)),$$

$$\psi(m+1)=\frac{1}{1}+\frac{1}{2}+\cdots+\frac{1}{m}-\log\gamma,$$

$$\log\gamma=0.5772, \tag{A. 2}$$

$$H_1^{(1)}(z)=J_1(z)+iN_1(z), \tag{A. 3}$$

$$J_1(z)=-dJ_0(z)/dz, \tag{A. 4}$$

$$H_1^{(1)}(z)=-dH_0^{(1)}(z)/dz, \tag{A. 5}$$

$$H_1^{(1)}(iz)=-2K_1(z)/\pi, \tag{A. 6}$$

$$J_1(iz)=iI_1(z), \tag{A. 7}$$

$$H_1^{(1)}(e^{-i\pi/2}z)=2K_1(z)/\pi+2e^{-i\pi/2}I_1(z), \tag{A. 8}$$

$$J_1(e^{-i\pi/2}z)=-e^{i\pi/2}I_1(z). \tag{A. 9}$$

The remaining formulas are asymptotic expansions valid when $|z|$ is large compared to unity.

$$H_1^{(1)}(z)\sim(2/\pi z)^{\frac{1}{2}}e^{i(z-3\pi/4)}\left(1-\frac{3}{8iz}+\cdots\right),\quad -\pi<\arg z<2\pi, \tag{A. 10}$$

$$H_1^{(1)}(z)J_1(z)\sim\frac{1}{\pi z}[1+e^{2i(z-3\pi/4)}]\left(1-\frac{3}{8iz}+\cdots\right)-\frac{i}{\pi z}[1-e^{2i(z-3\pi/4)}]\left(\frac{3}{8z}-\cdots\right),\quad |\arg z|<\pi \tag{A. 11}$$

$$I_1(z)K_1(z)\sim\frac{1}{2z}\left(1-\frac{15}{64z^2}+\cdots\right)+\frac{e^{-2z+3\pi i/2}}{2z}\left(1+\frac{3}{4z}-\cdots\right),\quad -\pi/2<\arg z<3\pi/2, \tag{A. 12}$$

$$\frac{I_1(z)}{K_1(z)}\sim\frac{1}{\pi}e^{2z}\left(1-\frac{3}{4z}+\cdots\right)+\frac{1}{\pi}e^{-2z+3\pi i/2},\quad -\pi/2<\arg z<3\pi/2. \tag{A. 13}$$

APPENDIX B

For the determination of the integral function defined by the transform Eq. (V. 9), we require the behavior of $L_+(\zeta)$, $L_-(\zeta)$ when $|\zeta|\to\infty$, in the upper and lower half-planes, respectively. Referring to (V. 14), we note first that

$$\int_{-k}^{k}\frac{\log[\pi i H_1^{(1)}((k^2-t^2)^{\frac{1}{2}}a)J_1((k^2-t^2)^{\frac{1}{2}}a)]}{t-\zeta}dt\sim-\frac{2}{\zeta a}\int_0^{ka}\frac{x\log[\pi i H_1^{(1)}(x)J_1(x)]}{((ka)^2-x^2)^{\frac{1}{2}}}dx=O(1/\zeta),$$

$$|\zeta|\to\infty,\quad Im\,\zeta>0.$$

Furthermore, using (A. 12),

$$\int_k^\infty\frac{\log[2K_1((t^2-k^2)^{\frac{1}{2}}a)I_1((t^2-k^2)^{\frac{1}{2}}a)]}{t^2-\zeta^2}dt=\int_k^\infty\frac{\log(1/ta)}{t^2-\zeta^2}dt+\int_k^\infty\frac{\log[2K_1((t^2-k^2)^{\frac{1}{2}}a)I_1((t^2-k^2)^{\frac{1}{2}}a)ta]}{t^2-\zeta^2}dt$$

$$\sim\frac{1}{i\zeta}\int_{k/-i\zeta}^\infty\frac{\log(1/-i\zeta av)}{v^2+1}dv-\frac{1}{\zeta^2 a}\int_0^\infty\frac{\log[2K_1(x)I_1(x)(x^2+(ka)^2)^{\frac{1}{2}}]}{(x^2+(ka)^2)^{\frac{1}{2}}}xdx$$

$$\sim(\pi/2i\zeta)\log(-i\zeta)+O(1/\zeta),\quad|\zeta|\to\infty,\quad Im\,\zeta>0.$$

Thus,

$$L_+(\zeta)\sim(-i\zeta)^{-\frac{1}{2}},\quad|\zeta|\to\infty,\quad Im\,\zeta>0,\tag{B. 1}$$

and by (V. 14),

$$L_-(\zeta)=(1/L_+(-\zeta))\sim(i\zeta)^{\frac{1}{2}},\quad|\zeta|\to\infty,\quad Im\,\zeta<0.\tag{B. 2}$$

On the Polarization of Fast Neutrons

JULIAN SCHWINGER
Harvard University, Cambridge, Massachusetts
(Received January 8, 1948)

ALTHOUGH the production of polarized thermal neutrons has long been an accomplished fact, no such success has been forthcoming with fast neutrons. Only one method for the polarization of fast neutrons has thus far been suggested,[1] of which the essential mechanism is the large, effective nuclear spin-orbit interaction present when neutrons are resonance scattered by helium and similar nuclei. It is the purpose of this note to suggest a second mechanism for polarizing fast neutrons—the spin-orbit interaction arising from the motion of the neutron magnetic moment in the nuclear Coulomb field. Despite the apparent small magnitude of this interaction, the long-range nature of the Coulomb field is such that the use of small scattering angles will produce almost complete polarization under ideal conditions. A closely related phenomenon produced by this electromagnetic interaction is an additional scattering of unpolarized neutrons which increases rapidly with decreasing scattering angle and is comparable with purely nuclear scattering at the small angles effective in producing polarized neutrons.

The energy of a neutron moving in an electric field, $\mathbf{E}=-\nabla\phi$, is described by the following contribution to the neutron Hamiltonian:

$$H'=\mu_n(eh/2M^2c^2)\boldsymbol{\sigma}\cdot\mathbf{E}\times\mathbf{p}, \tag{1}$$

where $\mu_n=1.91$ is the numerical value of the neutron moment in units of $eh/2Mc$, $\boldsymbol{\sigma}$ is the Pauli spin vector, and $\mathbf{p}$ is the momentum of the neutron. In order that the electric field be fully effective in producing spin-dependent scattering the major portion of this scattering should take place outside of the nucleus ($r\gg R$), but well within the screening radius of the atomic electrons ($r\ll a$). This restricts the range of useful scattering angles, since the waves scattered through an angle ϑ are primarily generated at a distance r from the nucleus, given by

$$2kr\sin\vartheta/2\sim 1, \tag{2}$$

where $k=p/\hbar$ is the neutron wave number. Hence, the unscreened Coulomb field of a point nucleus will be effective for scattering in the angular range:

$$1/ka\ll 2\sin\vartheta/2\ll 1/kR. \tag{3}$$

If the nuclear radius and atomic screening radius are taken to be

$$R=1.5\cdot 10^{-13}A^{\frac{1}{3}}\text{ cm} \quad\text{and}\quad a=0.53\cdot 10^{-8}Z^{-\frac{1}{3}}\text{ cm},$$

the angle restrictions for a 1-Mev neutron scattered in Pb, for example, are

$$4\cdot 10^{-4}\ll 2\sin\vartheta/2\ll\tfrac{1}{2}. \tag{4}$$

The electromagnetic scattering of a neutron under these conditions can be calculated with the plane wave Born approximation, for the nuclear scattered wave is negligible compared with the incident wave at the significant scattering distances. We denote the incident plane wave by

$$\psi_{\text{inc}}=e^{i\mathbf{k}_0\cdot\mathbf{r}}\chi, \tag{5}$$

where $\mathbf{k}_0$ is the initial propagation vector and χ is a spin function. The asymptotic form of the wave scattered in the direction of the propagation vector $\mathbf{k}$ is then

$$\psi_{sc}\sim(e^{ikr}/r)f(\vartheta)\chi, \tag{6}$$

with

$$f(\vartheta)=f_0(\vartheta)+\tfrac{1}{2}i\boldsymbol{\sigma}\cdot\mathbf{n}\cot\vartheta/2(\hbar/Mc)(Ze^2/\hbar c). \tag{7}$$

In this formula, $\mathbf{n}$ is the unit vector defined by

$$\mathbf{k}\times\mathbf{k}_0=\mathbf{n}k^2\sin\vartheta, \tag{8}$$

and $f_0(\vartheta)$ is the amplitude of the wave scattered by specifically nuclear forces. We assume the latter to be spin-independent and, further, ignore any inelastic nuclear scattering. Both of these assumptions are not unreasonable for neutron energies in the vicinity of 1 Mev.

The intensity of the scattered wave is determined by the following spin scalar product:

$$r^2(\psi_{sc},\psi_{sc})=(\chi, f^\dagger(\vartheta)f(\vartheta)\chi), \tag{9}$$

[1] J. Schwinger, Phys. Rev. 69, 681 (1946).

which yields

$$r^2(\psi_{sc}, \psi_{sc}) = |f_0(\vartheta)|^2 + \gamma^2 \cot^2\vartheta/2 + 2\gamma Im\, f_0(\vartheta)\, \cot\vartheta/2\, \mathbf{n}\cdot\mathbf{P}_{inc}, \quad (10)$$

in which

$$\gamma = \tfrac{1}{2}\mu_n(\hbar/Mc)(Ze^2/\hbar c) \quad (11)$$

and

$$\mathbf{P}_{inc} = (\chi, \sigma\chi) \quad (12)$$

is a vector describing the polarization state of the incident beam. The corresponding vector for the scattered wave is

$$\mathbf{P}_{sc} = (\psi_{sc}, \sigma\psi_{sc})/(\psi_{sc}, \psi_{sc}), \quad (13)$$

where

$$r^2(\psi_{sc}, \sigma\psi_{sc}) = \mathbf{n}2\gamma Im\, f_0(\vartheta)\, \cot\vartheta/2 + |f_0(\vartheta)|^2\mathbf{P}_{inc} + \gamma^2\cot^2\vartheta/2(2\mathbf{nn}\cdot\mathbf{P}_{inc} - \mathbf{P}_{inc}) - 2\gamma Re\, f_0(\vartheta)\, \cot\vartheta/2\mathbf{n}\times\mathbf{P}_{inc}. \quad (14)$$

For an initially unpolarized beam:

$$\mathbf{P}_{sc} = \mathbf{n}\frac{2Im\, f_0(\vartheta)\gamma\, \cot\vartheta/2}{|f_0(\vartheta)|^2 + \gamma^2\cot^2\vartheta/2} = \mathbf{n}P(\vartheta). \quad (15)$$

The discussion of the latter formula is greatly simplified by noting that, within the restricted angular range (3), the specifically nuclear scattering must be insensitive to angle and can be replaced by the value appropriate to forward scattering. Now, according to a well-known theorem, $Im\, f_0(0)$ is related to the total scattering cross section by

$$Im\, f_0(0) = (k/4\pi)\sigma, \quad (16)$$

while

$$|f_0(0)|^2 = (\sigma/4\pi)G \quad (17)$$

expresses the differential cross section for forward scattering in terms of the "gain," the ratio of the actual forward scattered intensity to that of an isotropic scatterer. It follows from the form of (15) that there is an optimum scattering angle, ϑ_0, for the production of polarized neutrons, namely,

$$\tan\vartheta_0/2 = \frac{\gamma}{|f_0(0)|} = \tfrac{1}{2}\mu_n\frac{Ze^2}{\hbar c}\left[\frac{4\pi(\hbar/Mc)^2}{\sigma G}\right]^{\frac{1}{2}}. \quad (18)$$

The maximum polarization is

$$P(\vartheta_0) = \frac{Im\, f_0(0)}{|f_0(0)|} = \left[\frac{k^2\sigma}{4\pi G}\right]^{\frac{1}{2}}. \quad (19)$$

In order to estimate the magnitudes of these quantities, it is necessary to have some knowledge of the energy dependence of σ and G. The model of an impenetrable sphere provides the following information in the limits $kR \ll 1$ and $kR \gg 1$:

$$\begin{aligned} kR \ll 1: &\quad \sigma = 4\pi R^2, \quad G = 1 \\ kR \gg 1: &\quad \sigma = 2\pi R^2, \quad G = \tfrac{1}{2}(kR)^2. \end{aligned} \quad (20)$$

The predicted limiting forms of the quantities (18) and (19) are then

$$\tan\vartheta_0/2 = \begin{cases} \tfrac{1}{2}\mu_n\dfrac{Ze^2}{\hbar c}\dfrac{\hbar/Mc}{R}, & kR \ll 1 \\ \mu_n\dfrac{Ze^2}{\hbar c}\dfrac{\hbar/Mc}{R}\dfrac{1}{kR}, & kR \gg 1 \end{cases} \quad (21)$$

and

$$P(\vartheta_0) = \begin{cases} kR, & kR \ll 1 \\ 1, & kR \gg 1. \end{cases} \quad (22)$$

It appears to be a reasonable interpolation to place

$$\tan\vartheta_0/2 \cong \tfrac{1}{2}\mu_n\frac{Ze^2}{\hbar c}\frac{\hbar/Mc}{R}, \qquad P(\vartheta_0) \cong 1 \quad (23)$$

for $kR \sim 2$, which is the value appropriate to 1-Mev neutrons scattered in Pb. Under these conditions, we expect practically complete polarization for a scattering angle of $\vartheta_0 = 1.5°$. In view of the stationary character of the polarization in the vicinity of this angle, somewhat larger angles can be employed without undue impairment of the degree of polarization. Thus, for $\vartheta = 3°$, $P = 0.80$; $\vartheta = 6°$, $P = 0.47$; $\vartheta = 9°$, $P = 0.32$.

To detect the polarization produced by scattering, it is necessary to subject the polarized neutrons to a second scattering process. If the two scattering angles are ϑ_1 and ϑ_2, with the normals to the two scattering planes being $\mathbf{n}_1$ and $\mathbf{n}_2$, respectively, the intensity after the second deflection is, according to (10) and (15), proportional to

$$1 + \mathbf{n}_1\cdot\mathbf{n}_2 P(\vartheta_1)P(\vartheta_2). \quad (24)$$

When both scattering events occur in the same plane, the intensity for the situation in which the two deflections occur in the same sense ex-

ceeds that for deflections in the opposite sense in the ratio:

$$R=\frac{1+P(\vartheta_1)P(\vartheta_2)}{1-P(\vartheta_1)P(\vartheta_2)}. \tag{25}$$

If both scattering angles equal the optimum angle ϑ_0, this ratio can be very large. Thus the experimental difficulties accompanying the small angles involved are ameliorated to some extent by the large effects under investigation. However, somewhat larger angles can be employed without destroying the experimental effect. For example, under the numerical conditions previously employed, $R=2.0$ for $\vartheta_1=1.5°$, $\vartheta_2=9°$, while $R=1.2$ for $\vartheta_1=\vartheta_2=9°$.

Finally, we note that the differential cross section for the scattering of an unpolarized neutron beam is modified at small angles. According to Eq. (10),

$$\sigma(\vartheta)=\sigma_0(\vartheta)+\gamma^2\cot^2\vartheta/2,$$

where $\sigma_0(\vartheta)$ is the specifically nuclear differential cross section, which assumes the value $(\sigma/4\pi)G$ at the small angles significant for the electromagnetic scattering. Thus the additional contribution to the scattering increases rapidly with diminishing angle and equals the purely nuclear scattering at precisely the angle ϑ_0 that is optimum for polarization. In view of the small angular range over which it is effective, the electromagnetic scattering provides a negligible contribution to the total cross section, namely,

$$\delta\sigma\sim 2\pi\gamma^2\log a/R=2\pi\mu_n^2(\hbar/Mc)^2 \times(Ze^2/\hbar c)^2\log 3.5\cdot 10^4(AZ)^{-\frac{1}{3}} \tag{26}$$

for $kR>1$, which has the value $\delta\sigma=2.6\cdot 10^{-26}$ cm^2 for Pb.

Letters to the Editor

PUBLICATION of brief reports of important discoveries in physics may be secured by addressing them to this department. The closing date for this department is five weeks prior to the date of issue. No proof will be sent to the authors. The Board of Editors does not hold itself responsible for the opinions expressed by the correspondents. Communications should not exceed 600 words in length.

The Disintegration Scheme of Cs^{134}

KAI SIEGBAHN
Nobel Institute for Physics, Academy of Science, Stockholm
AND
MARTIN DEUTSCH
Research Laboratory of Nuclear Science and Engineering, Massachusetts Institute of Technology, Cambridge, Massachusetts
December 26, 1947

ELLIOTT and Bell[1] have recently published a disintegration scheme for Cs^{134} which is more complete than the one proposed originally by the present authors.[2] Some time ago we obtained results very similar to those of Elliott and Bell, and we confirm their disintegration scheme in every detail. Additional support comes from measurements of gamma-gamma coincidences, using calibrated counters.[3] The coincidence rate per recorded gamma-ray of Cs^{134} was found to be 0.96 ± 0.04 times that obtained with Co^{60}. Using the general formula for the coincidence rate in a complex decay given in reference 3 (p. 272, footnote 11) and the counter calibration curve given in the same paper, we find that the original incomplete scheme[2] predicts a ratio of 0.71 for the fractional coincidence rate in Cs^{134} to that in Co^{60}, in disagreement with experiment. Assuming the new scheme, on the other hand, we can use the general formula to calculate, from the observed coincidence rate, the fraction of the disintegrations leading to the 1.97-Mev level in Ba^{134}. The result is 0.26 ± 0.08 in excellent agreement with the value proposed by Elliott and Bell from spectrometer measurements. From absorption measurements using a windowless counter, we estimate the abundance of the very soft beta-ray spectrum at 0.32 ± 0.08, again consistent with the other determinations. Failure to resolve the 0.57-Mev gamma-ray in our early measurements was apparently due to a slight error in alignment of the spectrometer at that time which also seems to have caused a minor shift in the energy calibration. Our best values for the gamma-ray energies are now 0.566 ± 0.01 Mev, 0.603 ± 0.01 Mev, and 0.798 ± 0.015 Mev, based on the photoelectron energies from a thin uranium radiator. These values are just outside our earlier probable errors but well within the combined errors of the two determinations. The energy of the 1.35-Mev gamma-ray is still too uncertain to permit definite assignment to one or the other of the two possible "cross-over" transitions. Internal conversion electrons have been observed in the beta-ray spectrometer. There is about 4.4×10^{-3} conversion electron per disintegration due to the 0.57-Mev and the 0.60-Mev gamma-ray combined and about 2.4×10^{-3} due to the 0.798-Mev gamma-ray. Comparison with the conversion coefficients observed for the gamma-rays of I^{130} (reference 3, Fig. 4B; the ordinates in this figure should be labeled 10^{-2}, not 10^{-3}) makes it appear probable that the multipole nature of the Cs^{134} gamma-rays is the same as that of the I^{130} gamma-rays. A search for Xe K-x-rays, using a krypton-filled counter, yielded negative results. This places an upper limit of 5 percent on the K electron capture by Cs^{134}.

Mr. A. E. Miller helped in taking data used in this work. This research was supported in part by the Office of Naval Research.

[1] L. G. Elliott and R. E. Bell, Phys. Rev. **72**, 979 (1947).
[2] K. Siegbahn and M. Deutsch, Phys. Rev. **71**, 483 (1947).
[3] A. Roberts, L. G. Elliott, J. R. Downing, W. C. Peacock, and M. Deutsch, Phys. Rev. **64**, 268 (1943).

Constant Temperature Operation of the Hot Wire Anemometer at High Frequencies

ELI OSSOFSKY*
Flight Propulsion Research Laboratory (NACA), Aberdeen Proving Ground, Maryland
November 14, 1947**

APPLICATION of the constant temperature hot wire anemometer to turbulence measurements presupposes successful design of an electronic amplifier for the instrument. The difficulty encountered has been spontaneous oscillation in the over-all system. From wire parameters, a "dynamic transresistance" is calculated for the wire in the bridge and inserted in the loop feed-back equation. Stability criteria then dictate a minimum allowable frequency range for the amplifier alone which depends on wire parameters and amplifier transconductance.

For a particular wire and a chosen anemometer frequency range the table shows the necessary amplifier transconductance and frequency range.

Instrument range kc	Amplifier g Mho	Amplifier range kc	% Turbulence constant temperature	% Turbulence constant current
31	20	110	0.5	0.0055
78	50	270	0.20	0.022
160	100	540	0.56	0.062

Besides increasing the difficulties of bridge and amplifier design, this comparatively wide frequency range emphasizes the problem of noise. Column 4 shows the percent turbulence whose signal equals the thermal noise voltage in the system arising from the wire. For comparison, column 5 shows the corresponding percent turbulence in an ideal constant current instrument. A more detailed account of this work will probably be published at a later date.

* Now at Ballistic Research Laboratories, Aberdeen Proving Ground, Maryland.
** This communication was submitted to the American Physical Society as an abstract for the New York meeting, but because of an oversight it was not included in the bulletin for that meeting.

On the Capture of Negative Mesons

O. PICCIONI
Massachusetts Institute of Technology, Cambridge, Massachusetts
January 8, 1948

WHILE nothing is known as yet about what happens after the capture of a normal negative meson (mass 100 Mev), it may be of some interest to report a few considerations regarding the end of the life of such a particle, when it is stopped in an element with relatively high Z. In such elements experimental evidence has shown that negative mesons do not undergo the normal decay process,[1-3] and therefore it seems reasonable to assume that they are captured by the nuclei. Now, from general considerations[4] one would expect a nuclear disruption after the meson capture. Assuming that this is the case, Heisenberg[5] has pointed out that it is surprising that no evidence of stars produced this way is as yet available from the cloud-chamber pictures taken for the purpose of photographing the decay process. We want to emphasize here that: (a) a star is easier to recognize than a decay electron, and can hardly be missed; (b) there are, up to now, four photographs of mesons stopped in gas and giving decay electrons, and several more photographs of mesons stopped in gas without indication of decay electrons; among them is one very clear photograph by T. H. Johnson and R. P. Shutt[6] in which a negative meson is shown to stop in the gas (argon) without giving any ionizing particle. It is also presumable that many pictures of the last kind were not published if they did not allow a good measure of the mass;* (c) many authors[6-9] worked with argon, with a magnetic field, or with high pressure. In argon[10] one would expect that negative mesons undergo capture with fairly high probability; on the other hand, the momentum-range relation, or the increase of ionization in a high pressure chamber, makes it unlikely to misinterpret a negative meson going toward the star for a particle coming out of the star. Therefore it seems unlikely that a negative meson produces a star after the capture. This is also compatible with the latest results of Lattes, Occhialini, and Powell.[11]

The recent result of Valley and Rossi[12] seems to indicate another possibility, suggesting that the capture actually is only an acceleration of the normal decay process. However, as the writer observed to the above-mentioned authors, this assumption is rather in disagreement with Rasetti's experiment on the decay electrons of mesons.[13] Rasetti had a narrow meson beam, and protected against side shower with lateral anticoincidence counters. In the path of the beam was an absorber (Fe or Al) beyond which an anticoincidence tray subtended the whole solid angle of the beam. The G-M counters E (Fig. 1, reference 13) which detected the decay electrons were entirely outside of the beam. From the delayed coincidences of the G-M counters E, with respect to the other trays, Rasetti obtained, by extrapolation, the total number of decay electrons $D2$, produced in the aluminum by normal (2.2 microsec. mean life) mesons, and detected by the G-M counters E. At the same time, the prompt coincidences (15 microsec. resolving time) of the counters E obviously comprised: decay electrons of 2.2 microsec. mean life $D2$, plus eventual decay electrons Dx of mean life less than 2 microsec. (which could not contribute to $D2$), plus some scattered mesons Sm and, perhaps, some residual showers Sh. In Fe the prompt coincidences of E were, in 100 hours, 45 ± 5 while $D2$ was 35 ± 7. We have then $Dx+Sm+Sh=(45\pm5)-(35\pm7)=10\pm8.6$. Even assuming $Sm+Sh=0$, we see that $Dx=10\pm8.6$ is too small, in comparison with 35 ± 7, to assume that each negative meson gives one electron. It is true that the low value of the mean life $\tau=2.2$ microsec. found by Rasetti seems to show a systematic error in the apparatus. However, $D2$ is not so closely correlated to τ as it is to the measured ratio η of decay electrons to stopped mesons. This ratio, measured for Al with the same apparatus, was found to be $\eta=0.4\pm0.15$. Now, from the results of Valley and Rossi η seems likely to be somewhat larger than 0.55. Since any systematic error of the apparatus would affect $D2$ exactly in the same proportion as η, it appears that the rate 35 ± 7 is not too large because of a systematic error.

With aluminum as absorber, Rasetti's data give $Dx\leqq10\pm8$ and $D2=20\pm6$. This comparison may be not as conclusive as the comparison between the number of mesons stopped (97 ± 15) and the prompt coincidences of E (30 ± 5), which again is equal to $D2+Dx+Sm+Sh$. This comparison can be done because for the aluminum absorber there is available the value of the total efficiency of the counters E for electrons of 40 Mev emerging from the Al (2.5 cm thick). This value was 0.5, taking into account the finite range of the electrons, since the geometrical efficiency was 0.56. Should every meson give one electron, the rate $(97\pm15)/2$ should be equal or less than 30 ± 5. We emphasize that in the last comparison only data obtained with a circuit of large resolving time (15 microsec.) are taken into account.

Therefore, we have to admit that so far both the cloud chamber and the G-M experiments failed to observe the event following the capture of a negative meson. To check another possibility, an experiment is now in progress at M.I.T.** the purpose of which is to find out whether or not one (or more) photon of energy about 40 Mev (or more) accompanies the stopping of a meson in Fe. Although the data do not have as yet a good accuracy, preliminary results seem to indicate a negative answer.

The writer wishes to thank Dr. Valley and Dr. Rossi for stimulating discussion on the subject of this letter.

* I am indebted to Dr. T. H. Johnson for having shown to me one of such unpublished photographs taken in a high pressure (argon) chamber.

** This experiment is being supported partially by Contract N5ori-78, U. S. Navy Department, Office of Naval Research.

[1] M. Conversi, E. Pancini, and O. Piccioni, Phys. Rev. **68**, 232 (1945); M. Conversi, E. Pancini, and O. Piccioni, Phys. Rev. **71**, 209 (1947); M. Conversi and O. Piccioni, Nuovo Cimento **2**, 71 (1944); *ibid.*, Phys. Rev. **70**, 859 (1946).
[2] T. Sigurgierson and A. Yamakama, Phys. Rev. **71**, 319 (1947).
[3] G. E. Valley, Phys. Rev. **72**, 772 (1947).
[4] J. A. Wheeler, Phys. Rev. **71**, 320 (1947).
[5] W. Heisenberg, *Vortrage über Kosmische Strahlung* (Berlin, 1943).
[6] S. H. Neddermeyer and C. D. Anderson, Phys. Rev. **54**, 88 (1938).
[7] E. J. Williams and G. R. Evans, Nature **145**, 818 (1940).
[8] T. H. Johnson and R. P. Shutt, Phys. Rev. **61**, 380 (1942).
[9] R. P. Shutt, S. De Benedetti, and T. H. Johnson, Phys. Rev. **62**, 552 (1942).
[10] E. Fermi and E. Teller, Phys. Rev. **72**, 399 (1947).
[11] C. M. G. Lattes, G. P. S. Occhialini, and C. F. Powell, Nature **160**, 453 (1947).
[12] I am indebted to Dr. Valley for preliminary communication of these results. G. E. Valley and B. Rossi, Phys. Rev. **73**, 177 (1948).
[13] F. Rasetti, Phys. Rev. **60**, 198 (1941).

On the Intrinsic Moment of the Electron*

H. M. FOLEY AND P. KUSCH
Columbia University, New York, New York
December 26, 1947

IN a previous letter[1] we have reported the observation that the ratio of the g_J values of the $^2P_{3/2}$ and $^2P_{\frac{1}{2}}$ states of gallium has the value 2.00344; the value 2 for this ratio follows from Russell-Saunders coupling and the conventional spin and orbital gyromagnetic ratios. If each of these states is exactly described by Russell-Saunders coupling, this observation can only be explained by setting $(\delta_S-2\delta_L)=0.00229\pm0.00008$, where the electron spin g value is $g_S=2+\delta_S$, and the orbital momentum g value is $g_L=1+\delta_L$. Since each of these atomic states may be separately subject to configuration interaction perturbations, the interpretation of this result was not entirely clear.

A determination has now been made of the ratio of the g_J values of Na in the $^2S_{\frac{1}{2}}$ state and of Ga in the $^2P_{\frac{1}{2}}$ state. The experimental procedure was similar to that previously described.[1] The known hyperfine interaction constants of gallium[2] and sodium[3] were employed in the analysis of the data. We find for this ratio the value 3.00732 ± 0.00018 instead of the value 3. This result can be explained by making $(\delta_S-2\delta_L)=0.00244\pm0.00006$.

The agreement between the values of $(\delta_S-2\delta_L)$ obtained by the two experiments makes it unlikely that one can account for the effect by perturbation of the states. The effect of configuration interaction on the g_J value of sodium is presumably negligible.[4] To explain our observed effect without modification of the conventional values of g_S or g_L introduces the rather unlikely requirement that both states of gallium be perturbed, and by amounts just great enough to give the agreement noted above.

From any experiment in which the ratio of the g_J values of atomic states is determined, it is possible to determine only the quantity $(\delta_S-2\delta_L)$. If, on the basis of the correspondence principle we set δ_L equal to zero, we may state the result of our first experiment as

$$g_S=2.00229\pm0.00008$$

and that of our recent experiment as

$$g_S=2.00244\pm0.00006.$$

It is not possible, at the present time, to state whether the apparent discrepancy between these values is real. It is conceivable that some small perturbation of the states would give rise to a discrepancy of the indicated magnitude.

These results are not in agreement with the recent suggestion by Breit[6] as to the magnitude of the intrinsic moment of the electron.

* Publication assisted by the Ernest Kempton Adams Fund for Physical Research of Columbia University.
[1] P. Kusch and H. M. Foley, Phys. Rev. 72, 1256 (1947).
[2] G. E. Becker and P. Kusch, to be published.
[3] S. Millman and P. Kusch, Phys. Rev. 58, 438 (1940).
[4] M. Phillips, Phys. Rev. 60, 100 (1941).
[5] Dr. J. Schwinger has very kindly informed us in advance of publication of his conclusion from theoretical studies that δ_L is zero whereas δ_S may not vanish.
[6] G. Breit, Phys. Rev. 72, 984 (1947).

The Thermal Diffusion Constant of Nitrogen

ALFRED K. MANN
University of Virginia, Charlottesville, Virginia†
January 5, 1948

IT is the purpose of this note to report the results of some two-bulb thermal diffusion experiments that have been performed with neon, argon, and nitrogen. Previously, two-bulb thermal diffusion experiments with isotopic mixtures have been performed by Nier[1] (methane and neon) and by Stier[2] (neon and argon).

The value of the thermal diffusion constant, α, can be computed from the observed data by means of the equation

$$\alpha=\frac{C_2^0-C_2}{nC_1C_2}\cdot\frac{1+\beta+T_1/T_0}{(1+\beta/2)\ln T_1/T_0},\qquad(1)\dagger\dagger$$

where C_2^0 is the concentration of the heavy isotope in the cold bulb;
(C_1), C_2 is the concentration of the (light) heavy isotope in normal material;
n is the number of repeated runs;
T_0 and T_1 are the temperatures of the cold and hot bulbs, respectively;
$\beta\equiv T_1V_c/T_cV_1$, is a small correction for the gas in the connecting tube between the bulbs.

Since α is a temperature dependent quantity, it is customary to specify the temperature at which measurements are made by a criterion due to Brown,[3] namely,

$$T=(T_1T_0/T_1-T_0)\ln T_1/T_0,\qquad(2)$$

where T is the temperature assigned to a measured value of α and T_0 and T_1 signify as before.

It is also convenient to refer to R_T, where R_T is defined as the ratio of the experimentally determined value of α to the value of α predicted on the basis of the elastic sphere molecular model.

The apparatus used in the experiments reported here was similar to that described by Nier and Stier. The high temperature was obtained by a specially constructed regulated furnace and the low temperature by a constant temperature bath.

The gas samples from the thermal diffusion experiments were analyzed with a Nier-type mass spectrometer.[4] The procedure was as follows. Six determinations of the ratio of the intensity of the heavy isotope to the intensity of the light isotope were made on the normal material. Then six determinations of the same ratio were made on the sample collected from a thermal diffusion experiment. The average of the six values from the normal material was compared with the average of the six values from the sample to obtain the quantity $(C_2^0-C_2)/C_2$, which can be substituted directly into (1).

In the case of neon, there was no background behind either the Ne^{20} or the Ne^{22} peak, and the two peaks were completely resolved in the mass spectrometer. With argon, the A^{36} and A^{40} peaks were completely resolved, but it was necessary to make a small correction for the background behind the A^{36} peak. With nitrogen, there was a background of approximately 0.05 times the intensity of the $N^{14}N^{15}$ peak in the valley between $N^{14}N^{15}$ and N_2^{14}. It was also

TABLE I.

Gas	Temp °K[d]	Separation %	α	R_T	R_T (Stier)
Neon	329	$Ne^{22}/Ne^{20}=4.48\pm0.27$[a]	$0.0273\pm6\%$	$0.65\pm6\%$	$0.63\pm5\%$
Argon	329	$A^{38}/A^{40}=2.24\pm0.22$[b]	$0.0164\pm10\%$	$0.35\pm10\%$	$0.33\pm5\%$
Nitrogen	329	$(N^{14}N^{15})/N_2^{14}=1.41\pm0.14$[c]	$0.0051\pm10\%$	$0.33\pm10\%$	—

[a] Average of four values from one sample. Seven repeated runs.
[b] Average of seven values from one sample. Five repeated runs.
[c] Average of fifteen values from three samples. Ten repeated runs.
[d] Computed from Eq. (2): $T_0=195°K$, $T_1=623°K$.

necessary to make small corrections for the background behind both peaks.

The results of the thermal diffusion experiments are shown in Table I where comparisons are made with Stier's values for neon and argon.

The value of R_T for nitrogen at 333°K has been computed from observed viscosity data assuming an inverse νth power collision law by Jones and Furry.[8] The value obtained in this way is $R_T=0.46$, which is to be compared with the value given in Table I. The discrepancy between the theoretical and experimental values is not unexpected in view of the simplified molecular model used in the calculations and of Nier's results with methane.

It would have been desirable to investigate the expected increase of α with increasing temperature, but in the case of nitrogen it seemed doubtful that any significant variation could be detected because of the lack of precision of the measurements.

It is a pleasure to acknowledge the continued interest and helpfulness of Professor E. P. Ney, under whose guidance this work was done, and the advice and encouragement of Professors J. W. Beams and L. B. Snoddy.

† Present address: Columbia University, New York 27, New York.
[1] A. O. Nier, Phys. Rev. **56**, 1009 (1939); A. O. Nier, Phys. Rev. **57**, 338(L) (1940).
[2] L. Stier, Phys. Rev. **62**, 548 (1942).
†† This equation holds for a gas sample collected from the cold bulb. A similar equation holds for a sample from the hot bulb.
[3] H. Brown, Phys. Rev. **58**, 661 (1940).
[4] E. P. Ney, Doctoral Dissertation, University of Virginia (1944).
[5] R. C. Jones and W. H. Furry, Rev. Mod. Phys. **18**, 151 (1946).

Statistical Theory of the Elementary Process of Plastic Deformation

W. JAMES LYONS
Chemical and Physical Research Laboratories, The Firestone Tire and Rubber Company, Akron, Ohio
December 18, 1947

BECAUSE of the physically significant relationship to which it leads, the theory presented in outline in the following paragraphs is of interest. While believed to be logically complete, the development is regarded as no more than a statistical framework into which a more descriptive theory of the elementary physical processes of creep, etc., possibly may be built. The reasoning follows the pattern of conventional physical statistics, though the reference of probabilities to unit time is somewhat of an innovation.

Let the element i (Fig. 1) be defined as a volume sufficiently small to enclose only a single *unit dislocation* which is not further divisible into smaller dislocations; N_k = number of such elements in the kth cross-sectional plane of the specimen, of area a; n = number of such cross-sectional planes per unit-length; and λ = average projection of each randomly directed unit dislocation in the stress direction. The definition of i implies that the projection of the unit dislocation on the kth plane occupies the whole cross-sectional area of i. Let $w_{i,k,f}$ = probability that a unit dislocation or jump will occur in a forward direction over the cross section of the ith element in the kth plane in unit time, and let $w_{i,k,b}$ = probability that a similar jump will occur in a backward direction in the same element in unit time.

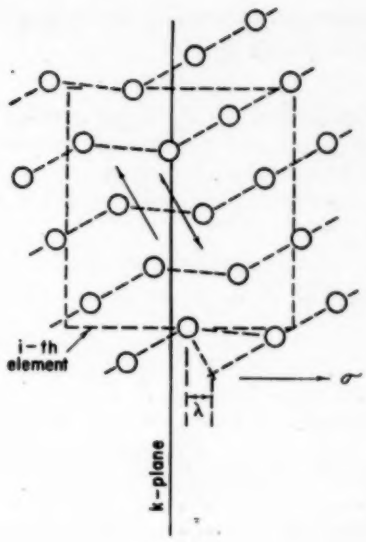

FIG. 1.

Now the probabilities $w_{k,f}$ and $w_{k,b}$ of forward and backward displacements λ, over the whole kth plane in unit time, are given by

$$\left.\begin{aligned} w_{k,f} &= \prod_{i=1}^{N_k} w_{i,k,f}, \\ \text{and} \qquad w_{k,b} &= \prod_{i=1}^{N_k} w_{i,k,b}. \end{aligned}\right\} \tag{1}$$

Evidently $w_{k,f}$ and $w_{k,b}$ are the probability that a forward jump will occur in *every* one of the elements i in the kth cross section in a particular unit of time, and the similar probability of a backward jump.

Assumption I. The probability of a forward or backward unit dislocation (jump) occurring over a given area of a cross-sectional plane per unit time is some function ϕ or ψ, respectively, of the force acting over that area.

Then for the ith element

$$w_{i,k,f}=\phi(f_{i,k}), \tag{2}$$

where $f_{i,k}$ = the component of force in the direction of the observed stress acting in the ith element of the kth plane. The implication of Assumption I is that the forms of the functions ϕ and ψ are the same whether the force acts on a

single element or on a group of elements, such as those comprising the kth plane. Thus

$$w_{k,f}=\phi(f_k), \tag{3}$$

where f_k = component of force in the direction of the observed stress acting over the *whole* kth cross section. Similarly, for a backward unit dislocation,

$$w_{i,k,b}=\psi(f_{i,k}), \tag{4}$$

and

$$w_{k,b}=\psi(f_k). \tag{5}$$

In view of Eqs. (1) to (5) we have

$$\left.\begin{aligned}\phi(f_k)&=\prod_{i=1}^{N_k}\phi(f_{i,k}),\\ \text{and}\qquad\\ \psi(f_k)&=\prod_{i=1}^{N_k}\psi(f_{i,k}).\end{aligned}\right\} \tag{6}$$

But, clearly,

$$f_k=\sum_{i=1}^{N_k} f_{i,k}. \tag{7}$$

In accordance with a proof frequently cited in thermodynamics,[1] Eqs. (6) and (7) define the exponential relations:

$$\left.\begin{aligned}w_{k,f}&=\phi(f_k)=\exp c_1 f_k,\\ \text{and}\qquad\\ w_{k,b}&=\psi(f_k)=\exp c_2 f_k,\end{aligned}\right\} \tag{8}$$

where c_1 and c_2 are parameters.

Assumption II. The probability of a unit dislocation per unit time in the direction of the force component (forward jump) is the same in either direction from the cross-sectional plane, i.e.,

$$\phi(f_k)=\psi(-f_k). \tag{9}$$

Now, since a forward jump and a backward jump are mutually exclusive events, the net probability of a forward jump per unit time is the difference $w_{k,f}-w_{k,b}$. The net strain in the direction of stress, occurring in time Δt, is evidently

$$\Delta\epsilon=n\lambda(w_{k,f}-w_{k,b})\Delta t. \tag{10}$$

From Eqs. (8) and (9) it follows that $c_1=-c_2$, and hence we have from Eqs. (8),

$$\left.\begin{aligned}w_{k,f}-w_{k,b}&=\exp c_1 f_k-\exp(-c_1 f_k)\\ &=2\sinh c_1 f_k.\end{aligned}\right\} \tag{11}$$

Thus,

$$\Delta\epsilon=n\lambda\times 2\sinh c_1 f_k\times\Delta t,$$

or

$$\lim_{\Delta t\to 0}\frac{\Delta\epsilon}{\Delta t}=\frac{d\epsilon}{dt}=2n\lambda\sinh c_1 f_k. \tag{12}$$

Placing $f_k=a\sigma$, $2n\lambda=A$, and $ac_1=B$, we finally obtain

$$d\epsilon/dt=A\sinh B\sigma, \tag{13}$$

where σ = the stress in the specimen in the neighborhood of the kth plane.

Equation (13) is of the form which has been proposed by several workers[2-4] for the description of plastic deformational phenomena in metals as well as high polymers. While the foregoing theory itself gives no description of the elementary mechanism of dislocation, Assumptions I and II may be regarded as establishing conditions which must be met by postulated molecular forces in a more detailed theory leading to Eq. (13).

[1] Cf., for example, Max Planck, *Theory of Heat* (MacMillan Company, Ltd., London, 1932), p. 227.
[2] A. Nadai, *Stephen Timoshenko Anniversary Volume* (MacMillan Company, Ltd., London, 1938), p. 155.
[3] A. Tobolsky and H. Eyring, J. Chem. Phys. 11, 125 (1943).
[4] A. V. Tobolsky and R. D. Andrews, J. Chem. Phys. 13, 3 (1945).

Discrete Space-Time and Integral Lorentz Transformations

A. SCHILD[1]
The Institute for Advanced Study, Princeton, New Jersey
December 22, 1947

THE idea of introducing discreteness into space and time has occasionally been considered[2] as a means of removing the "infinities" which trouble modern physical theory, both classical and quantal. The objection which is usually raised against such discrete schemes is that they are not invariant under the Lorentz group. The purpose of this investigation is to show that *there is a simple model of discrete space-time which, although not invariant under all Lorentz transformations, does admit a surprisingly large number of Lorentz transformations.* This group of transformations is, in fact, sufficiently large to make conceivable the use of this model as a background for physical theory.

Consider all events in Minkowski space-time whose four coordinates $x^r\equiv(t, x, y, z)$ are integers.[3] (The velocity of light is taken as unity.) We shall call the set of such events the "hypercubic lattice," or *cubic lattice*, for short. The proper homogeneous Lorentz transformations which leave the cubic lattice as a whole invariant will be called *integral Lorentz transformations*. A world vector whose four coordinates are integers will be called an *integral vector*; the adjective *primitive* will be added if the components of the vector have no common integer factor other than ± 1. Two integral vectors obtainable from one another by an integral Lorentz transformation will be called *integral transforms*. We now give a brief sketch of the principal results; a more detailed account will be published elsewhere.

The integral Lorentz transformations form a group. A Lorentz transformation $x'^r=L_s^r x_s$ is integral if and only if all its components L_s^r are integers. Thus the problem of finding all integral Lorentz transformations is equivalent to the solution of 10 quadratic Diophantine equations in 16 unknown integers L_s^r. This problem can be approached by means of the two-dimensional spinor calculus[4] and the elementary theory of Gaussian integers.[5]

With an integral vector (t, x, y, z) we associate a Hermitian spintensor $a^{\dot\alpha\beta}$ as follows:

$$\left.\begin{aligned}a^{\dot 1 1}&=t+z, \quad a^{\dot 1 2}=x-iy,\\ a^{\dot 2 1}&=x+iy, \quad a^{\dot 2 2}=t-z.\end{aligned}\right\} \tag{1}$$

It can be shown that all primitive integral null vectors

pointing into the future are represented by spinvectors c^α:

$$a^{\dot\alpha\beta}=c^{\dot\alpha}c^{\beta}, \tag{2}$$

where c^1, c^2 are Gaussian integers, so that c^1 and c^2 are relatively prime and neither is divisible by $1+i$, or else so that $1+i$ is the greatest common factor of c^1, c^2 and one of them is divisible by 2. Such spinvectors will be called *integral*.

As is well known, the spin transformations

$$c'^\alpha=\lambda_\beta{}^\alpha c^\beta, \quad c'^{\dot\alpha}=\bar\lambda_\beta{}^\alpha c^{\dot\beta}, \quad |det(\lambda_\beta{}^\alpha)|=1, \tag{3}$$

represent all proper homogeneous Lorentz transformations, $\lambda_\beta{}^\alpha$ being determined by $L_s{}^r$ to within an arbitrary phase factor $e^{i\delta}$. If this phase factor is chosen suitably, the integral Lorentz transformations are represented by exactly those spin transformations which, together with their inverse, map integral spinvectors into integral spinvectors. This theorem enables us to find the following spin representation of the integral Lorentz group:

$$\lambda_1{}^1\lambda_2{}^2-\lambda_2{}^1\lambda_1{}^2=1, \tag{4}$$

where one of the following cases applies: I. $\lambda_\beta{}^\alpha$ are Gaussian integers such that $\Sigma_{\alpha\beta}\lambda_\beta{}^\alpha$ is divisible by $1+i$. II. $\lambda_\beta{}^\alpha=\mu_\beta{}^\alpha/(1+i)$, where $\mu_\beta{}^\alpha$ are Gaussian integers not divisible by $1+i$. III. $\lambda_\beta{}^\alpha=2^{\frac{1}{2}}\mu_\beta{}^\alpha/(1+i)$, where $\mu_\beta{}^\alpha$ are Gaussian integers such that $\Sigma_{\alpha\beta}\,\mu_\beta{}^\alpha$ is divisible by $1+i$. IV. $\lambda_\beta{}^\alpha=\frac{1}{2}2^{\frac{1}{2}}\mu_\beta{}^\alpha$, where $\mu_\beta{}^\alpha$ are Gaussian integers not divisible by $1+i$. The theory of Gaussian integers shows immediately that each of the above cases includes an infinity of spin transformations. Thus, *the integral Lorentz group is infinite*, though discrete.

From the above it can be deduced that all primitive integral null vectors are equivalent, in the sense that any two of them are integral transforms of one another.

Consider any integral vector and form the set of all its integral transforms. Project each of these vectors onto the xyz space. Then the directions defined by these projections in 3-space are everywhere dense. This shows that our discrete space-time model possesses a large measure of *spatial isotropy*. It is obvious that our cubic lattice is invariant under all translations which map one lattice point into another. In this sense our discrete model is *homogeneous*.

Finally we must mention a property of our model which constitutes a drawback as far as hopes for physical application are concerned. The velocities associated with integral Lorentz transformations are given by the formula $v=(n^2-1)^{\frac{1}{2}}/n$, where n is any positive integer. The smallest non-zero velocity is $\frac{1}{2}3^{\frac{1}{2}}=0.866$ times the velocity of light.

[1] Frank B. Jewett Fellow, on leave from Carnegie Institute of Technology, Pittsburgh, Pennsylvania.
[2] V. Ambarzumian and D. Iwanenko, Zeits. f. Physik 64, 563 (1930); L. Silberstein, *Discrete Space-Time* (University of Toronto Studies, Physics Series, 1936).
[3] The coordinates are integral multiples of a "fundamental length" ϵ (probably of the order of nuclear dimensions). We choose ϵ as the unit of length.
[4] O. Laporte and G. E. Uhlenbeck, Phys. Rev. 37, 1381 (1931).
[5] G. H. Hardy and E. M. Wright, *An Introduction to the Theory of Numbers* (Oxford University Press, New York, 1908), Chapter XII.

Range and Energy of Beta-Radiation from Calcium 45

A. K. SOLOMON
Biophysical Laboratory, Harvard Medical School, Boston, Massachusetts
AND
L. E. GLENDENIN
Massachusetts Institute of Technology, Cambridge, Massachusetts
December 29, 1947

THE radiations given off by Ca^{45} have been investigated by Walke, Thompson, and Holt[1] who report beta-radiations of maximum energy 0.2 and 0.9 Mev, gamma-radiation of 0.7 Mev, and a half-life of 180 days. The energies of the radiation were determined by absorption measurements. In view of the importance of this isotope in biological research, it has seemed advisable to reinvestigate the radiation characteristics.

Experimental details.—Carrier-free Ca^{45}, produced by $n-p$ reaction on monoisotopic Sc^{45}, was obtained from the Atomic Energy Commission. The counting apparatus was the same as that previously described;[2] a thin-window (1.9 mg/cm²) Geiger counter was used. The source was essentially carrier-free, and was deposited in a thin (0.017-inch) aluminum stamping. The beta-radiation was measured by absorption in aluminum foils.

Results and discussion.—The method of Feather[3] was used in analyzing the results, as previously described.[2] The initial strength of the sources varied from 3000 to

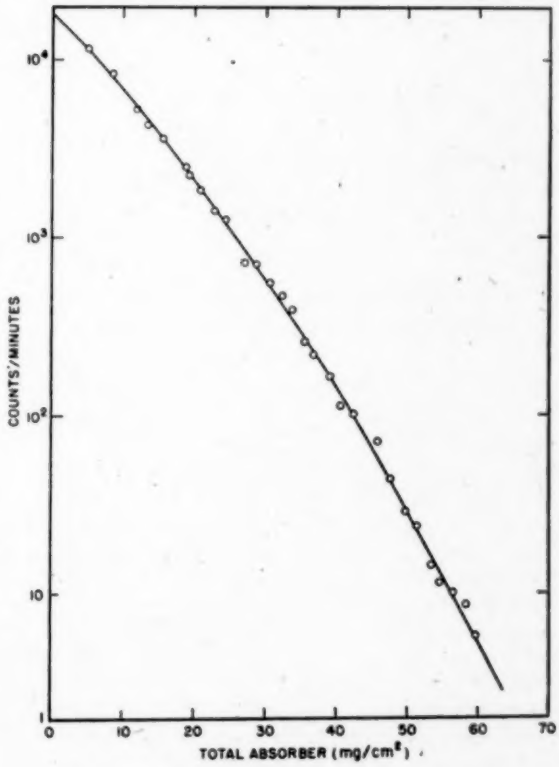

FIG. 1. Aluminum absorption curve of Ca^{45} β-radiation.

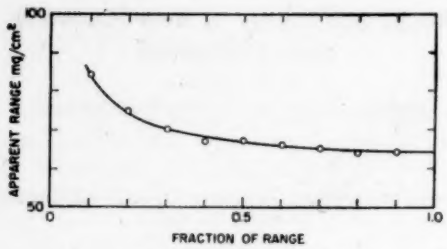

FIG. 2. Feather plot for Ca^{45}.

12,000 counts per minute, and the contribution due to gamma-rays and other unabsorbed contaminants was less than one part in 3000 with the strongest source, thus indicating the absence of any appreciable amount of gamma-radiation. The absorption curve obtained with the strongest source is shown in Fig. 1. The Feather plot, shown in Fig. 2, gives a range of 64 ± 1 mg/cm².

Glendenin[4] has shown that a reliable range-energy curve for the low energy region can be derived from the data of Marshall and Ward[5] for monoenergetic electrons and beta-ray spectrograph data on low energy beta-emitters. Glendenin's curve is identical with that of Marshall and Ward below 0.5 Mev. Using this range-energy curve, we have found that the Ca^{45} beta-radiation has a maximum energy of 260 ± 5 kev. We have found no evidence of any harder beta-radiation, or of any gamma-radiation at all in the course of this investigation.[6]

Acknowledgments.—This work has been supported with funds from the Office of Naval Research. The authors wish to express their appreciation to Miss Jacqueline Becker for her assistance in making the counts.

[1] Walke, Thompson, and Holt, Phys. Rev. **57**, 171 (1940).
[2] Solomon, Gould, and Anfinsen, Phys. Rev. **72**, 1097 (1947).
[3] Feather, Proc. Camb. Phil. Soc. **35**, 599 (1938).
[4] Glendenin, Nucleonics, in press for January, 1948.
[5] Marshall and Ward, Can. J. Research **15**, 29 (1939).
[6] This result is in good agreement with a value of 250 kev, given in *Radioisotopes, Catalog and Price List No. 2*, revised September, 1947, distributed by Isotopes Branch, United States Atomic Energy Commission. Unfortunately, the Atomic Energy Commission's result is not supported by any published experimental evidence.

On Quantum-Electrodynamics and the Magnetic Moment of the Electron

JULIAN SCHWINGER
Harvard University, Cambridge, Massachusetts
December 30, 1947

ATTEMPTS to evaluate radiative corrections to electron phenomena have heretofore been beset by divergence difficulties, attributable to self-energy and vacuum polarization effects. Electrodynamics unquestionably requires revision at ultra-relativistic energies, but is presumably accurate at moderate relativistic energies. It would be desirable, therefore, to isolate those aspects of the current theory that essentially involve high energies, and are subject to modification by a more satisfactory theory, from aspects that involve only moderate energies and are thus relatively trustworthy. This goal has been achieved by transforming the Hamiltonian of current hole theory electrodynamics to exhibit explicitly the logarithmically divergent self-energy of a free electron, which arises from the virtual emission and absorption of light quanta. The electromagnetic self-energy of a free electron can be ascribed to an electromagnetic mass, which must be added to the mechanical mass of the electron. Indeed, the only meaningful statements of the theory involve this combination of masses, which is the experimental mass of a free electron. It might appear, from this point of view, that the divergence of the electromagnetic mass is unobjectionable, since the individual contributions to the experimental mass are unobservable. However, the transformation of the Hamiltonian is based on the assumption of a weak interaction between matter and radiation, which requires that the electromagnetic mass be a small correction ($\sim(e^2/\hbar c)m_0$) to the mechanical mass m_0.

The new Hamiltonian is superior to the original one in essentially three ways: it involves the experimental electron mass, rather than the unobservable mechanical mass; an electron now interacts with the radiation field only in the presence of an external field, that is, only an accelerated electron can emit or absorb a light quantum;* the interaction energy of an electron with an external field is now subject to a *finite* radiative correction. In connection with the last point, it is important to note that the inclusion of the electromagnetic mass with the mechanical mass does not avoid all divergences; the polarization of the vacuum produces a logarithmically divergent term proportional to the interaction energy of the electron in an external field. However, it has long been recognized that such a term is equivalent to altering the value of the electron charge by a constant factor, only the final value being properly identified with the experimental charge. Thus the interaction between matter and radiation produces a renormalization of the electron charge and mass, all divergences being contained in the renormalization factors.

The simplest example of a radiative correction is that for the energy of an electron in an external magnetic field. The detailed application of the theory shows that the radiative correction to the magnetic interaction energy corresponds to an additional magnetic moment associated with the electron spin, of magnitude $\delta\mu/\mu=(\frac{1}{2}\pi)e^2/\hbar c=0.001162$. It is indeed gratifying that recently acquired experimental data confirm this prediction. Measurements on the hyperfine splitting of the ground states of atomic hydrogen and deuterium[1] have yielded values that are definitely larger than those to be expected from the directly measured nuclear moments and an electron moment of one Bohr magneton. These discrepancies can be accounted for by a small additional electron spin magnetic moment.[2] Recalling that the nuclear moments have been calibrated in terms of the electron moment, we find the additional moment necessary to account for the measured hydrogen and deuterium hyperfine structures to be $\delta\mu/\mu=0.00126\pm0.00019$ and $\delta\mu/\mu=0.00131\pm0.00025$, respectively. These values are not in disagreement with the theoretical prediction. More precise conformation is provided by measurement of the g values for the $^2S_{\frac{1}{2}}$, $^2P_{\frac{1}{2}}$, and $^2P_{3/2}$ states of sodium and gallium.[3] To account for these results, it is necessary to ascribe the following additional spin magnetic moment to the electron, $\delta\mu/\mu=0.00118\pm0.00003$.

The radiative correction to the energy of an electron in a Coulomb field will produce a shift in the energy levels of hydrogen-like atoms, and modify the scattering of electrons in a Coulomb field. Such energy level displacements have recently been observed in the fine structures of hydrogen,[4] deuterium, and ionized helium.[5] The values yielded by our theory differ only slightly from those conjectured by Bethe[6] on the basis of a non-relativistic calculation, and are, thus, in good accord with experiment. Finally, the finite radiative correction to the elastic scattering of electrons by a Coulomb field provides a satisfactory termination to a subject that has been beset with much confusion.

A paper dealing with the details of this theory and its applications is in course of preparation.

* A classical non-relativistic theory of this type was discussed by H. A. Kramers at the Shelter Island Conference, held in June 1947 under the auspices of the National Academy of Sciences.

[1] J. E. Nafe, E. B. Nelson, and I. I. Rabi, Phys. Rev. **71**, 914 (1947); D. E. Nagel, R. S. Julian, and J. R. Zacharias, Phys. Rev. **72**, 971 (1947).

[2] G. Breit, Phys. Rev. **71**, 984 (1947). However, Breit has not correctly drawn the consequences of his empirical hypothesis. The effects of a nuclear magnetic field and a constant magnetic field do not involve different combinations of μ and $\delta\mu$.

[3] P. Kusch and H. M. Foley, Phys. Rev. **72**, 1256 (1947), and further unpublished work.

[4] W. E. Lamb, Jr. and R. C. Retherford, Phys. Rev. **72**, 241 (1947).

[5] J. E. Mack and N. Austern, Phys. Rev. **72**, 972 (1947).

[6] H. A. Bethe, Phys. Rev. **72**, 339 (1947).

Excitation Curves of (α, n); $(\alpha, 2n)$; $(\alpha, 3n)$ Reactions on Silver

S. N. GHOSHAL
Department of Physics, University of California, Berkeley, California
January 5, 1948

SILVER bombarded with α-particles from the 60-in. cyclotron produces radioactive substances with the following three half-lifes: 65 min., 5.2 hr., and 2.7 d. All of these activities have been chemically attributed to indium and have been assigned by mass-spectrograph separation to In^{110}, In^{109}, and In^{111}, respectively. Tendam and Bradt[1] recently announced similar activities. Their assignment of 65-min. and 2.7-d activities agrees with ours. The 23-min. activity found by them was not looked for in the present experiment.

The excitation curves for the isotopes reported above have been determined for α-energies up to 37 Mev and are reproduced in Fig. 1. The abscissae give the energy in Mev, the ordinates the cross sections in arbitrary units. The ordinate units are, however, the same for reactions leading to the formation of the same isotope. Evaluation of absolute cross sections has not yet been possible due to lack of knowledge regarding the efficiencies of the different radiations for the ionization chamber used.

From the figure it is seen that the 65-min. activity belonging to In^{110} (emitting positrons of 1.7 Mev), a product of $Ag^{107}(\alpha, n)$ reaction, has a threshold of 11 Mev.* The yield after attaining a peak at 17.5 Mev drops rapidly to low values when the $(\alpha, 2n)$ process appears as a competing process. After attaining a minimum, the 65-min. activity again increases and does not reach saturation even at 37 Mev. Apparently this part of the curve is due to $Ag^{109}(\alpha, 3n)In^{110}$. The sharpness of the peak at 17.5 Mev is also interesting. The difference of 4 Mev between (α, n) and $(\alpha, 2n)$ thresholds is much smaller than that between $(\alpha, 2n)$ and $(\alpha, 3n)$ thresholds ($\sim$8 Mev). This difference seems to be due to the Coulomb barrier which cuts off the production of any alpha-reaction below 11 Mev.

The 2.7-d activity belonging to In^{111} has a threshold of about 15 Mev, which is in agreement with that found by Tendam and Bradt.[1] This activity is produced by the $Ag^{109}(\alpha, 2n)$ process, and emits a γ-ray of about 0.2 Mev (no positrons). After attaining a peak around 27 Mev, the yield begins to drop and reaches about 16 percent of maximum at 37 Mev.

The 5.2-hr. period is produced by $Ag^{107}(\alpha, 2n)In^{109}$ reaction. The excitation curve is similar to the excitation curve of In^{111}, as is expected, since both are products of $(\alpha, 2n)$ reactions. The threshold of In^{109} is about 13.5 Mev, slightly lower than that of In^{111}. At higher energies, however, the two curves differ widely. Instead of decreasing, the 5.2-hr. curve goes on increasing even beyond 30 Mev, after which it drops slightly, the yield at 37 Mev being 80 percent of the maximum.

This suggests the production of a different isotope at higher α-energies having a very similar half-life. A comparison with the $Ag^{109}(\alpha, 3n)In^{110}$ curve and with the $Ag^{109}(\alpha, 2n)In^{111}$ curve suggests that this new activity is probably due to $Ag^{107}(\alpha, 3n)In^{108}$. The possibility of its being due to $Ag^{109}(\alpha, 3n)In^{110}$ (an isomer of 65-min. period) is ruled out by the fact that the threshold and low energy part of the curve is similar to the other $(\alpha, 2n)$ curve and not to the (α, n) curve.

To verify this conclusion, two foils were bombarded, one with 37-Mev alphas (foil 1) and the other with 20-Mev alphas (foil 2). The latter is not likely to have any In^{108} in it, while the former should mostly contain In^{108} with little In^{109}. The absorption curves for the radiations from the two foils, corrected for In^{111}, showed marked differences. Foil 1 showed a γ-ray of about 0.65 Mev, while foil 2 showed a γ-ray of about 0.5 Mev. No positrons were detected. These conclusions were also corroborated by

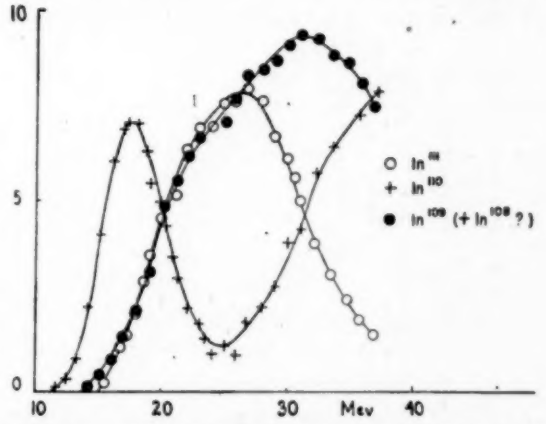

FIG. 1. The abscissa represents energy of the bombarding α-particles in Mev. The ordinate represents cross section in arbitrary units. The curve with open circles represents the cross section for the formation of In^{111}. The one with crosses represents the cross section for the formation of In^{110}, while the curve with solid circles represents the cross section for the formation of In^{109}, and at the higher energies probably of In^{108} also.

mass-spectrograph work, though the evidence is not yet conclusive.

It is a pleasure to thank Professor Emilio Segrè for suggesting the problem and for his kind interest and continued guidance during the progress of the work. Thanks are also due the 60-in. cyclotron crew for their valuable cooperation and to Dr. B. Moyer and his associates for the mass-spectrograph work.

* Tendam and Bradt[1] obtained a threshold of 12 Mev.
[1] D. J. Tendam and H. L. Bradt, Phys. Rev. 72, 1118 (1947).

High Altitude Measurements on Extensive Showers

ROLAND MAZE, ANDRÉ FRÉON, AND PIERRE AUGER
Laboratoire de physique, Ecole Normale Supérieure, Paris, France
December 19, 1947

AN apparatus was built in order to study extensive showers at high elevations. It is possible to discriminate all the coincidences, from threefold to ninefold, between nine counters.

The efficiency of such a disposition is 466 times greater than those of a conventional one, and about 10 times greater than Rogosinsky's "master group" apparatus.

A band of perforated paper is used to record the coincidences; a longitudinal line of dots corresponds to each counter. The transverse alignment of dots indicates the order of each coincidence, and identifies also the counters which have been operated. Two or three papers can be perforated at the same time in order to obtain duplicate records.

Experiments were carried out during the months of July and September, from sea level to 22,000 feet in a Halifax airplane.

Nine counters of 120-cm² effective area were put under the roof of the plane. For the narrow showers three of them were placed 12.5 cm from each other in the middle of the arrangement; the other counters were about two meters apart, the total width of the arrangement being 15 meters.

In the first part of the experiments counters were unshielded; in the second part, shells of 4 mm of lead were placed close to the counters in order to estimate the ratio between photons and electrons in the showers by means of the photon-electron transition effect.

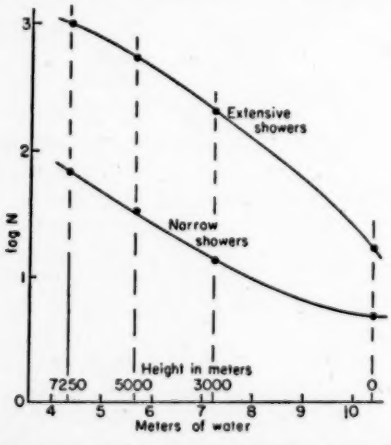

FIG. 1. Variation with altitude of the number of showers N per 100 minutes. The statistical error for extensive showers is 3 percent, for narrow showers, 10 percent.

The main features of the data are the following (see Fig. 1):

1. No striking change is to be observed in the structure of extensive showers between sea level and 22,000 ft.

2. Apart from an appreciable number of narrow showers at sea level, due to secondary effects from mesons, the relative increase of intensity for extensive and narrow showers is the same between sea level and 22,000 ft. The absolute intensity of big showers is 50 times greater, at this height, than at sea level.

3. The density δ of extensive showers increases with height. The number *versus* density curve can be represented by the empirical law $N=k\delta^{-\gamma-1}$; the integral exponent γ varies from 1.67 ± 0.1 at sea level to 1.41 ± 0.05 at 22,000 ft.

4. Many showers of weak density can be observed in altitude, giving threefold coincidences; this fact is in good agreement with Mr. Della Corte's experiments.

New experiments will be soon performed at higher altitudes and other ones with lead screens above the counters, in order to investigate penetrating rays in the showers.

More details concerning both the apparatus and the experimental results will be shortly published in the Journal de Physique.

Beta-Rays and Gamma-Rays from Arsenic (76)*

M. V. SCHERB AND C. E. MANDEVILLE
Bartol Research Foundation of the Franklin Institute, Swarthmore, Pennsylvania
January 2, 1948

THE 26-hour activity was induced in As_2O_3, irradiated by slow neutrons in the Clinton pile. The beta- and gamma-rays of this isotope have been investigated by absorption and coincidence methods.

By inserting thin aluminum foils before a single G-M counter, the absorption limit of the beta-rays was found to be 1.34 g/cm², 2.76 Mev as calculated by Feather's equation.[1] The beta-ray absorption curve is shown in Fig. 1.

Two G-M counters were placed in coincidence; a source of radioactive As^{76} was placed behind a thick aluminum radiator, and coincidences produced by the secondary electrons were observed as a function of the aluminum absorber thickness placed between the two counters. The coincidence absorption curve, given in Fig. 2, shows an end point at 0.84 g/cm². From an accurately constructed calibration curve for the G-M coincidence counting set, this absorber thickness was found to correspond to a quantum energy of 1.98 Mev. This calibration curve will soon be published in The Physical Review.

A thin source of As^{76} was placed between two counters in coincidence, and the beta-gamma coincidence rate was observed as a function of aluminum absorber thickness before the beta-ray counter. The curve of Fig. 3 was thus obtained. The coincidence rate is seen to decrease from an extrapolated value of 0.184×10^{-3} coincidence per beta-ray at zero absorber thickness to zero at 1.00 g/cm². One of the

inner beta-ray groups then has an end point at 2.16 Mev. The plateau-like structure of the curve between 0.35 g/cm² and 0.50 g/cm² may not be altogether justified on considering the statistical probable errors. At worst, however, it can be said that the curve experiences a change of slope at 0.35 g/cm². A third beta-ray group would then have an end point at 0.94 Mev. The curve of Fig. 3 was taken with a coincidence resolving time of 0.10 microsecond. Although the accidental rate was virtually eliminated, a strong gamma-gamma coincidence rate made high statistical accuracy impossible, except for very long time intervals. The region beyond 1.00 g/cm² was explored with the 0.10-microsecond resolving time for beta-gamma coincidences, and for counting rates as high as 35,000 single counts per minute in the beta-ray counter, no coincidences were found in excess of the gamma-gamma coincidence rate. *The beta-ray spectrum of energy 2.76 Mev then leads to the ground state of the* Se^{76} *residual nucleus.* The fact that the intense beta-rays of high energy are not coupled with gamma-radiation explains the low beta-gamma coincidence rate at zero absorber thickness observed in this experiment and previously.[3]

The gamma-gamma coincidence rate was $(0.31 \pm 0.02) \times 10^{-3}$ coincidence per gamma-ray recorded in the gamma-ray counter.

The coincidence absorption curve of Fig. 2 confirms the results of earlier investigators who reported gamma-rays of energy 2 Mev.[2,3] This line was not reported in the most recent spectrometric investigation.[4] The three spectra at 0.94, 2.16, and 2.76 Mev evidently correspond to those previously reported at 1.29, 2.49, and 3.04 Mev as measured by the lens-type spectrometer.[4]

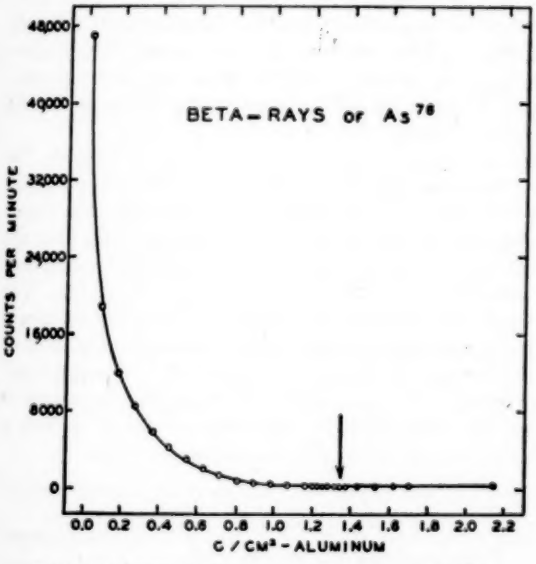

FIG. 1. Absorption in aluminum of the beta-rays of As^{76}.

The fact that the beta-rays of highest energy are associated with a ground state transition, as indicated by these coincidence experiments, is consistent with the proposed term diagram.[4]

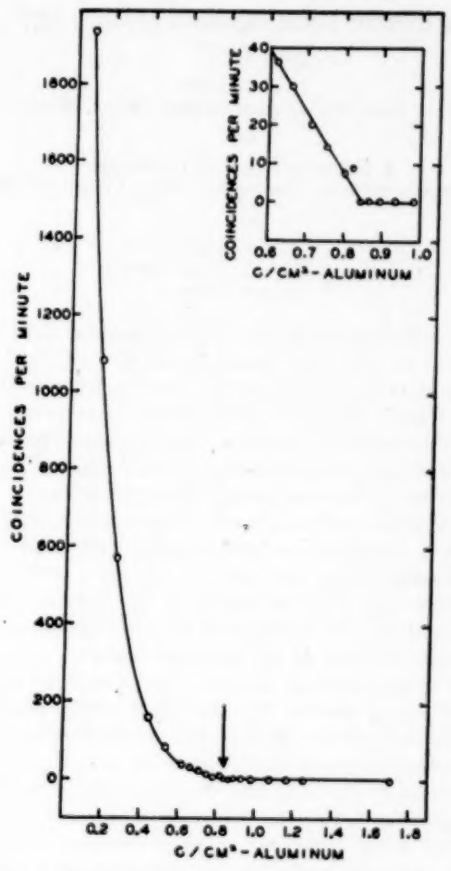

FIG. 2. Coincidence absorption of the secondary electrons of the gamma-rays of As^{76}.

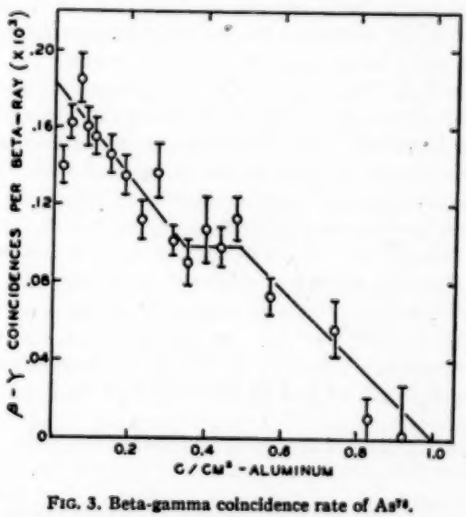

FIG. 3. Beta-gamma coincidence rate of As^{76}.

* Assisted by the Office of Naval Research.

[1] N. Feather, Proc. Camb. Phil. Soc. 34, 599 (1938).
[2] A. C. G. Mitchell, L. M. Langer, and P. W. McDaniel, Phys. Rev. 57, 1107 (1940).
[3] P. Harteck, F. Knouer, and W. Schaeffer, Zeits. f. Physik 109, 153 (1938); C. E. Mandeville, Phys. Rev. 63, 91 (1943); L. C. Miller and L. F. Curtiss, Phys. Rev. 70, 983 (1946).
[4] K. Siegbahn, Ark. f. Mat. Astr. o. Fys. 34(A), 9 (1947).

The Electro-Disintegration of Cu^{63}, Ag^{107}, and Ag^{109}*

L. S. SKAGGS**
Tumor Clinic, Michael Reese Hospital, Chicago, Illinois
AND
J. S. LAUGHLIN AND A. O. HANSON
Department of Physics, University of Illinois, Urbana, Illinois
AND
J. J. ORLIN**
Bergen's Museum, Bergen, Norway
January 8, 1948

THE electrons from the 22-Mev betatron have been used to study the disintegration of Cu^{63}, Ag^{107}, and Ag^{109} by the direct action of electrons having energies of 13 to 17½ Mev. This action gives rise to the same reactions as those produced by photons. The disintegration of Be^9 by direct electron bombardment has been reported and the cross section for electro-disintegration measured.[1]

The electrons are brought out of the donut by means of a magnetic shunt as a parallel monoenergetic beam.[2] The beam emerges from the donut through a 0.0015-inch Duralumin window. The current is of the order of 10^{-6} ampere and is concentrated in an area 5 cm wide and 2 cm high at a distance of 45 cm from the window.

A set of uniform foils placed in the path of an electron beam of energy greater than threshold energy should be activated due to both electro- and photo-disintegrations. If the total thickness of the foil assembly is small compared to the range of the electrons, then the number of electro-disintegrations will be approximately the same in each foil. Since the x-rays produced at these energies are almost entirely in the forward direction, the photo-disintegration in the assembly will increase linearly, to a first approximation, with foil position in the direction of the beam. The intercept of this linear increase of activity at the midpoint of the first foil represents the electro-disintegration effect plus the effect of any general x-ray background.

Sets of foils ¾ inch high and 1 inch wide were placed in the electron beam at a distance of 45 cm from the window of the donut. Additional single foils were placed just below the electron beam to measure the background x-ray effect. An open air ionization chamber placed just behind the foils measured the ionization produced by those electrons which passed through the foils. The electron current was determined from the ionization produced, assuming that electrons of this energy range give rise to 60 ion pairs per cm.[3]

In the case of Cu^{63} the reaction $Cu^{63}(e; n, e')Cu^{62}$ is expected above a threshold of 10.9 Mev.[4] Bombardments were made at 17½, 16, and 13 Mev with 0.005-inch foils and at 16 Mev with 0.002-inch foils. Ag^{107} and Ag^{109} have thresholds of 9.5 and 9.3 Mev, respectively. The activities induced in the foils were counted on thin-walled Geiger counters. Figure 1 shows a plot of the activity of Cu^{62} *versus* foil position for a set of 0.002-inch foils bombarded with 16-Mev electrons. The activities of Ag^{106} (24.5 min.) and Ag^{108} (2.3 min.) obtained by bombarding 0.001-inch foils with 16-Mev electrons are also shown. The electro-disintegration intercepts and the rate of increase of activity caused by the photo-effect were nearly the same for the two silver isotopes.

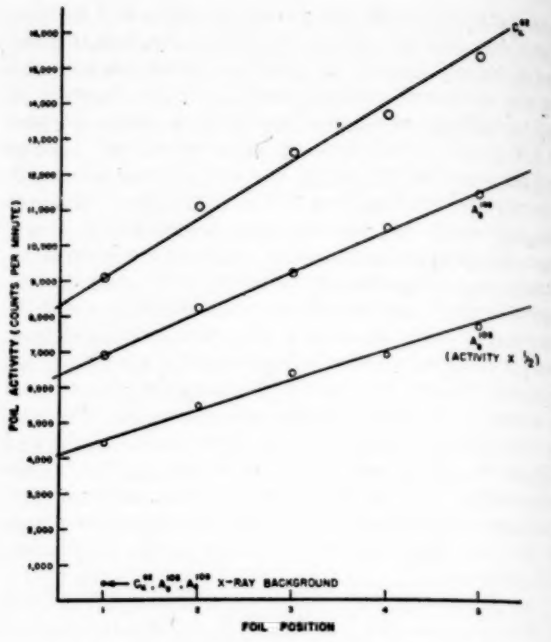

FIG. 1. The activity of Cu^{62}, Ag^{106}, and Ag^{108} as a function of foil position.

The calculated cross sections are given in Table I. The absolute values may be in error by a factor of two but the relative values are somewhat more accurate. The slopes of the lines in Fig. 1 with the theoretical value for the radiation cross section and the x-ray spectrum[5] can be used to estimate the photo-disintegration cross section. The average cross sections for photo-disintegration by x-rays above the threshold energy were consistently found to be 400 times that for electro-disintegration. This ratio is approximately that expected on the basis of calculations in which the interaction of the electron with a nucleus is represented entirely by its electromagnetic field.

TABLE I. Electro-disintegration cross sections in 10^{-29} cm².

Electron energy	Cu^{63}	Ag^{107}	Ag^{109}
13 Mev	1.4		
16 Mev	16	54	79
17½ Mev	32		

* This work was in part supported by ONR Contract N6ori-71, T. O. 1.
** Now on leave at the University of Illinois, Urbana, Illinois.
[1] G. B. Collins, B. Waldman, and E. Guth, Phys. Rev. **56**, 876 (1939); M. L. Wiedenbeck, Phys. Rev. **69**, 235 (1946).
[2] L. S. Skaggs, G. M. Almy, D. W. Kerst, and L. H. Lanzl, Phys. Rev. **70**, 95 (1946).
[3] R. B. Brode, Rev. Mod. Phys. **11**, 222 (1939).
[4] G. C. Baldwin and H. W. Koch, Phys. Rev. **67**, 1 (1945).
[5] W. Heitler, *The Quantum Theory of Radiation* (Oxford University Press, London 1944), pp. 170–173.